Investigating contributions of trisomy 21 in Down syndrome to Alzheimer disease phenotypes in a novel mouse cross

A thesis presented in partial fulfilment of the requirements for the degree of Doctor of Philosophy from University College London

Xun Yu Choong

Department of Neurodegenerative Disease
Institute of Neurology
University College London

2016

Declaration

I, Xun Yu Choong, confirm that the work presented in this thesis is my own. Where information has been derived from other sources, I confirm that this has been indicated in the thesis.

Acknowledgements

The work done in this project was only possible with the support of numerous friends and colleagues, with whom I have grown an incredible amount. Foremost thanks go to Prof. Elizabeth Fisher and Dr. Frances Wiseman, who have been inexhaustibly dedicated supervisors and inspirational figures. Special mention also goes to two unofficial mentors who have looked out for me throughout the PhD, Dr. Karen Cleverley and Dr. Sarah Mizielinska.

The Fisher and Isaacs groups have been a joy to work with and have always unhesitatingly offered time and help. Thank you to the Down syndrome group: Olivia Sheppard, Dr. Toby Collins, Dr. Suzanna Noy, Amy Nick, Laura Pulford, Justin Tosh, Matthew Rickman; other members of Lizzy's group: Dr. Anny Devoy, Dr. Rosie Bunton-Stasyshyn, Dr. Rachele Saccon, Julian Pietrzyk, Dr. Beverley Burke, Heesoon Park, Julian Jaeger; the Isaacs group: Dr. Adrian Isaacs, Dr. Emma Clayton, Dr. Roberto Simone, Charlotte Ridler, Frances Norona.

The PhD office has also been a second home in more ways than one, thanks to: Angelos Armen, Dr. Chris McKinnon, Dr. Billy West, Jamie "hypocorism Swag Villain" Miller, Lucianne Dobson, Lucy Sheytanova, Ruchi Kumari, and Alexandra Philiastides. Outside the PhD office, much support has come from Davor Ivankovic, Ania Graca, Andrianos Liavas, Stephanie Bowen, Ana Carolina Saraiva, Steven van de Pavert, James Fairney, Ylonna Kurtzke, Michelle Fong, Sherlynn Chan, Sua Ning, Lim Kang Hong, Pak Shu Hwa and Yarn Shih. Credit and commendation also go to The Espresso Room, for flat whites that never fail.

The support staff in the MRC Prion Unit have also played crucial roles. In Queen Square House: Kevin Williams, Ryan Peter, Rosie Baverstock-West, Nato Koiava, and others; in Wakefield Street: Emma Trice, Charlotte Bailey, Michael Brown, Craig Fitzhugh, Jayne Holby, Amanda Dickson, and many more; in the ION Education Unit: Daniela Warr Schori, David Blundred and co.

Much of this project has involved learning techniques outside those established in the group, and my gratitude goes to the following for allowing me their time: Prof. Victor Tybulewicz, Prof. Anne Stephenson, Dr. Silvia Purro, Dr. Marifé Cano, Dr. Pavlos Alifragis, Dr. Matthew Ellis, Dr. Daniah Trabzuni and Dr. Vincent Plagnol. In addition, I am hugely appreciative of Dr. Rohan de Silva and Dr. Abraham Acevedo Arozena for a memorable PhD viva.

Thank you to the Brain Research Trust for allowing me to embark on the 4-year PhD in Clinical Neuroscience, particularly as an Overseas student.

Finally, my greatest thanks go to Ba, Ma and Ning, for having given everything they can for me to be here today.

“Onwards and upwards!”

Abstract

Down syndrome (DS) is a common, complex disorder caused by having an extra copy of human chromosome 21 (trisomy 21). While clinical presentation varies extensively, Alzheimer disease (AD) pathology is found in brains of virtually all people with DS by 40 years. This increases their dementia risk such that one third of the DS population develops AD by 60 years. Therefore DS allows the investigation of pathogenetic mechanisms underlying its clear genetic form of early-onset AD.

To model DS in mice, a 'transchromosomic' model, Tc1, was generated carrying a freely segregating copy of human chromosome 21 (Hsa21), which is trisomic for ~75% of Hsa21 genes. However, Tc1 is not functionally trisomic for *APP*. By crossing Tc1 with the J20 model, a transgenic mouse overexpressing mutant human *APP* that models amyloid deposition, it is possible to compare contributions of trisomy 21 and APP/Aβ overexpression to phenotypes in the genotypically different offspring. The work presented in this thesis therefore characterises AD-related phenotypes in progeny of the Tc1xJ20 cross.

I first established a primary cortical culture model from early postnatal Tc1xJ20 pups, which would allow the *in vitro* observation and manipulation of cortical neurons in a more accessible system compared to *in vivo* study. To assess the validity and utility of these cultures, they were characterized for APP expression, Aβ production, proportion of neuronal cells in culture and levels of mosaicism for the Hsa21 chromosome. These *in vitro* phenotypes obtained were compared with relevant *in vivo* observations in Tc1xJ20 mice. Secondly, to study neuroinflammation and glial reactivity, I developed a digital analysis protocol to systematically quantify morphological characteristics of microglia and astrocytes visualized by immunohistochemistry in Tc1xJ20 brain sections. To further identify AD-related phenotypes that may be differentially influenced by genotype, I annotated data obtained from a pilot RNA sequencing study of Tc1xJ20 hippocampal tissues, identified gene candidates of interest, and explored functions that may be altered by genotype by clustering differentially expressed genes by associated functions.

These results therefore allow for discussion and evaluation of the novel Tc1xJ20 model for identifying novel genetic contributions of trisomy 21 on AD phenotypes, apart from *APP.*

Table of Contents

Declaration 2

Acknowledgements 3

Abstract 5

Table of Contents 6

List of Figures 11

List of Tables 14

List of Supplementary Tables 15

Abbreviations 16

Chapter 1. Introduction 20

1.1. Down syndrome 20

1.2. Alzheimer disease 21

1.2.1. Proteolytic processing of amyloid precursor protein (APP) 22

1.2.2. Genetics of AD 24

1.2.2.1. Familial AD (FAD) 24

1.2.2.2. Sporadic AD (SAD) 24

1.2.3. The amyloid cascade hypothesis 25

1.3. Alzheimer disease in Down syndrome 26

1.3.1. APP and Aβ phenotypes in DS and AD-DS 27

1.3.2. Features distinguishing AD-DS from other forms of AD 28

1.4. Mouse models of Down syndrome and Alzheimer disease 30

1.4.1. Mouse models of DS 30

1.4.2. The transchromosomic Tc1 mouse 34

1.4.3. Considerations when studying AD phenotypes in DS mouse models 38

1.5. Mouse models of AD 39

1.5.1. Transgenic models of AD 39

1.5.2. The J20 mouse model of APP/Aβ overexpression 40

1.6. The Tc1xJ20 model of trisomy 21 and APP/Aβ overexpression 44

1.6.1. Trisomy 21 exacerbates mortality associated with APP/Aβ overexpression 45

1.6.2. Trisomy 21 exacerbates behavioural deficits associated with APP/Aβ overexpression 45

1.6.3. Trisomy 21 accelerates Aβ accumulation 48

1.6.4. Which genes on Hsa21, other than *APP*, exacerbate APP/Aβ-related phenotypes? 50
1.6.5. What phenotypes may be studied to investigate the effects of trisomy 21 on age-dependent AD pathology? 50
1.6.6. How does trisomy 21 alter gene expression and what clues may this yield to pathophysiology? 51
1.7. Thesis aims 51
Chapter 2. Materials and methods 52
2.1. Mice 52
2.2. Housing and husbandry of mice 52
2.3. Culling of mice 52
2.4. Genotyping 53
2.4.1. DNA isolation 53
2.4.2. Polymerase chain reaction (PCR) for Tc1xJ20 genotyping 54
2.5. Agarose gel electrophoresis 55
2.6. Quantitative PCR (qPCR) for J20 *APP* transgene copy number 56
2.7. Primary cortical culture 57
2.7.1. Preparation of 13-mm coverslips and 12-well plates 57
2.7.2. Isolation and culture of primary cells 57
2.7.3. Collection of media and cell lysates 59
2.8. qPCR for Tc1 mosaicism 59
2.9. RNA extraction from adult mouse cortical tissue 61
2.10. Determining concentration and purity of nucleic acids 62
2.11. Reverse transcription with elimination of genomic DNA 62
2.12. Reverse transcription qPCR (qRT-PCR) 63
2.13. Protein extraction from adult mouse hippocampal and cortical tissue 64
2.14. Quantifying protein concentration in brain homogenates and cell lysates 65
2.15. Western blots 66
2.15.1. Sodium dodecyl sulphate-polyacrylamide gel electrophoresis (SDS-PAGE) 66
2.15.2. Transfer of proteins to membranes by electroblotting 66
2.15.3. Immunodetection 66
2.15.4. Visualisation and quantification of protein bands 68
2.15.5. Loading controls 68
2.16. Quantification of Aβ peptides 68
2.17. Immunostaining of cultured cells 69
2.17.1. Fixing of cells 69

2.17.2. Immunofluorescent staining 69
2.17.3. Visualisation and quantification 70
2.18. Histology 71
2.19. Image acquisition and processing 72
2.20. Two-dimensional fluorescence *in situ* hybridisation (2D-FISH) 74
2.21. RNA sequencing 75
2.22. Functional clustering of differential gene expression 76
2.23. Statistical analysis 76
Chapter 3. Development of an *in vitro* model for AD-DS 77
3.1. Introduction 77
3.1.1. The utility of an *in vitro* assay for AD-DS 77
3.2. Considerations in protocol design for Tc1xJ20 primary neuronal cultures 78
3.2.1. Use of early postnatal mice for culture 78
3.2.2. Standardising plating density 78
3.2.3. Mosaicism 79
3.3. APP and Aβ phenotypes in primary neurons 79
3.4. Aims 81
3.5. Results 81
3.5.1. Full-length human APP (hAPP) expression 81
3.5.2. Total full-length APP expression 84
3.5.3. APP C-terminal Fragment (CTF) expression 86
3.5.4. Human soluble Aβ38, Aβ40 and Aβ42 production 87
3.5.5. BACE1 expression 90
3.5.6. Proportion of neuronal cells *in vitro* 91
3.5.7. Hsa21 mosaicism in primary culture 93
3.6. Discussion 95
3.6.1. Validity of primary cortical culture model in studying APP/Aβ phenotypes 95
3.6.2. Investigating cell culture variability by assessing proportions of neuronal cells and levels of mosaicism 96
3.6.3. Recommendations for future primary neuronal culture 97
Chapter 4. Investigating gliosis in trisomy 21 and APP/Aβ overexpression 99
4.1. Introduction 99
4.1.1. Neuroinflammation in AD 100
4.1.2. Neuroinflammation in DS 104
4.1.3. Aims 106
4.2. Results 106

4.2.1. Identification and characterization of microglia 107
4.2.2. Identification and characterization of astrocytes..... 123
4.3. Discussion 142
4.3.1. Successful identification of discrete microglial cells 142
4.3.2. Increased microglial reactivity in APP/Aβ overexpression 142
4.3.3. Artefacts in astrocyte characterization due to variations in background staining intensity 144
4.3.4. Trisomy 21 does not significantly alter any glial phenotype when studied across the hippocampus 148
4.3.5. Conclusion..... 148
Chapter 5. Investigating effects of trisomy 21 and APP/Aβ overexpression on mRNA expression profiles..... 149
5.1. Introduction..... 149
5.1.1. Aims 151
5.2. Results 152
5.2.1. Differentially expressed genes identified between Tc1/Wt, Tc1;J20/J20 and J20/Wt..... 152
5.2.2. Identifying functional clusters from differentially expressed genes 154
5.2.3. Investigating the concordance of candidate gene expression between hippocampal and cortical samples 156
5.2.3.3. *App*..... 156
5.2.3.4. Immediate-Early Genes (IEGs): *Arc*, *Dusp1*, *Egr1*, *Fos* 157
5.2.3.5. *Per1*..... 162
5.2.3.6. *Chrm4* 163
5.2.3.7. *Snx27* 164
5.3. Discussion 165
5.3.1. Functional clustering identifies effect of trisomy on hippocampal transcription relating to cytoplasmic vesicles 165
5.3.2. Effects of genotype on gene expression differ in cortical and hippocampal tissue 167
5.3.2.1. *App*..... 167
5.3.2.2. Immediate-Early Genes 168
5.3.2.3. *Per1*..... 169
5.3.2.4. *Chrm4* 169
5.3.2.5. *Snx27* 170
5.3.3. Discordance between hippocampal and cortical RNA expression..... 170
5.3.4. Future work 171

Chapter 6. Discussion 173
6.1. *In vitro* modelling of APP/Aβ phenotypes influenced by trisomy 21 173
6.2. Investigate cytoplasmic vesicular phenotypes 174
6.3. Emerging focus on neuroinflammation in trisomy 21 in AD-DS 175
6.4. Discordant phenotypes between cortex and hippocampus 176
6.5. The value of DS mouse models in future AD-DS research 176
Supplementary Tables 178
References 202

List of Figures

Figure 1.1 APP processing and cleavage products 22
Figure 1.2 Amyloid plaques and neurofibrillary tangles in the brain of a 65-year old DS individual 26
Figure 1.3 Human chromosome 21 (Hsa21), orthologous mouse chromosomes (Mmu) and key mouse models of Down syndrome. 32
Figure 1.4 Proposed structure of Hsa21 in Tc1 35
Figure 1.5 Specificity of PDGF-β immunostaining in hippocampus of nonhuman primates 41
Figure 1.6 *Pdgfb* expression in mouse brain structures as illustrated by the Allen Mouse Brain Atlas 41
Figure 1.7 Map of the *APP* construct used to generate J20 mice 41
Figure 1.8 Trisomy 21 exacerbates mortality associated with APP/Aβ overexpression 45
Figure 1.9 Trisomy 21 exacerbates spatial short-term memory deficits. 46
Figure 1.10 Trisomy 21 exacerbates non-spatial short-term memory deficits 46
Figure 1.11 Trisomy 21 exacerbates hyperactivity and failure to habituate to a novel environment. 47
Figure 1.12 Trisomy 21 significantly increases Aβ plaque deposition in the hippocampus of mice 48
Figure 1.13 Hippocampal sections demonstrating increased Aβ plaque deposition by trisomy 21. 49
Figure 3.1 Human APP (hAPP) protein expression in primary cortical culture. 82
Figure 3.2 hAPP protein expression in 3-month old Tc1xJ20 cortical homogenate. 83
Figure 3.3 Human and mouse total APP protein expression in primary cortical culture. 84
Figure 3.4 Human and mouse total APP protein expression in 3-month Tc1xJ20 cortical homogenate. 85
Figure 3.5 α- and β-CTF expression in primary cortical culture. 86
Figure 3.6 α- and β-CTF expression in 3-month old Tc1xJ20 cortical homogenate. 87
Figure 3.7 Human Aβ production in primary cortical culture. 88
Figure 3.8 Human Aβ in Tris-soluble fraction of 3-month old hippocampal tissue. 89
Figure 3.9 BACE1 protein expression in primary cortical culture. 90
Figure 3.10 BACE1 protein expression in 3-month old Tc1xJ20 cortical homogenate. 91
Figure 3.11 Influence of genotype on the proportion of neurons in culture. 92
Figure 3.12 Proportion of primary cortical cells retaining the Hsa21 chromosome. 93

Figure 3.13 Proportion of cells retaining the Hsa21 chromosome in adult Tc1 hippocampus. 94
Figure 4.1 Identification and characterisation of microglial cells. 109
Figure 4.2. Increased microglial numbers and size with APP/Aβ overexpression in hippocampal sections from Tc1xJ20 mice..... 110
Figure 4.3 Total hippocampal surface area covered by microglia significantly increases with APP/Aβ overexpression. 118
Figure 4.4 Hippocampal microglial density significantly increases with age and *APP* overexpression. 119
Figure 4.5 Area of microglial 'inseparable clusters' significantly increases with APP/Aβ overexpression. 120
Figure 4.6 Average total area, and area of processes, per microglial cell increases with APP/Aβ overexpression. 121
Figure 4.7 No significant differences in average number of branches, length of main line and area of cell body in microglial cells. 122
Figure 4.8 Identification and characterization of astrocytes (GFAP+). 123
Figure 4.9 Area covered by astrocytes increases with age, but density of astrocytes reduces with age..... 125
Figure 4.10 Total hippocampal surface area covered by astrocytes significantly increases with age. 133
Figure 4.11 Astrocyte density in hippocampal sections significantly decreases with age and APP/Aβ overexpression. 134
Figure 4.12 Area of astrocytic 'inseparable clusters' significantly increases with age. 135
Figure 4.13 Average area per astrocyte increases with age. 136
Figure 4.14 Average astrocyte cell body area is not altered by age, trisomy 21 or APP/Aβ overexpression. 136
Figure 4.15 Average area of astrocyte processes increases with age, together with increased length of the main line and number of branches per astrocyte. 137
Figure 4.16 β3T and GFAP protein expression in hippocampal homogenate from 3-month old mice 138
Figure 4.17 β3T and GFAP protein expression in hippocampal homogenate from 3-month old mice 139
Figure 4.18 Trisomy 21 increases hippocampal S100β protein expression in 3-month old mice 140
Figure 4.19 Trisomy 21 increases cortical S100β protein expression in 3-month old mice, which is further increased with APP/Aβ overexpression 141

Figure 4.20. Increased microglial activation with APP/Aβ overexpression and age, based on the nominal scoring of morphology class. 144
Figure 4.21 Aβ plaque deposition in 10-month old J20 hippocampal section, showing intense staining around the dentate gyrus. 145
Figure 5.1 Comparison of *App* hippocampal RNA-seq results with hippocampal and cortical *App* RNA expression quantified by qRT-PCR. 157
Figure 5.2 Comparison of *Arc* hippocampal RNA-seq results with cortical *Arc* RNA expression by qRT-PCR 159
Figure 5.3 Comparison of *Dusp1* hippocampal RNA-seq results with cortical *Dusp1* RNA expression by qRT-PCR. 160
Figure 5.4 Comparison of *Egr1* hippocampal RNA-seq results with cortical *Egr1* RNA expression by qRT-PCR. 160
Figure 5.5 Comparison of *Fos* hippocampal RNA-seq results with cortical *Fos* RNA expression by qRT-PCR. 161
Figure 5.6 Comparison of *Per1* hippocampal RNA-seq results with cortical *Per1* RNA expression by qRT-PCR. 162
Figure 5.7 Comparison of *Chrm4* hippocampal RNA-seq results with cortical *Chrm4* RNA expression by qRT-PCR. 163
Figure 5.8 Comparison of *Snx27* hippocampal RNA-seq results with cortical *Snx27* RNA expression by qRT-PCR. 164

List of Tables

Table 1.1 Trisomic regions and triplicated gene content in Down syndrome mouse models 33
Table 1.2 RefSeq Hsa21 genes not functionally trisomic in Tc1 36
Table 1.3 Neurological and non-neurological deficits characterized in Tc1 mice 37
Table 1.4 Phenotype timeline and summary of J20 phenotypes 43
Table 1.5 Possible genotypes in Tc1xJ20 progeny 44
Table 2.1 Reagents for DNA isolation 53
Table 2.2 Genotyping primer sequences and volumes used in stock primer mixes 54
Table 2.3 Thermal cycling programme for Tc1 and J20 genotyping 55
Table 2.4 Primers and probes for J20 *APP* transgene copy number qPCR 56
Table 2.5 Master mix (per well) for J20 *APP* transgene copy number qPCR 56
Table 2.6 Thermal cycling programme for J20 *APP* transgene copy number qPCR 57
Table 2.7 Primary cortical culture media 57
Table 2.8 *CLDN8* primers and probe 60
Table 2.9 Master mix (per well) for mosaicism qPCR 61
Table 2.10 Master mixes for reverse transcription and “no amplification controls” 63
Table 2.11 Primers and probes for qRT-PCR 64
Table 2.12 Master mix (per well) for qRT-PCR 64
Table 2.13 Primary and secondary antibodies used for western blots 67
Table 2.14 Primary and secondary antibodies used for immunofluorescent staining 70
Table 2.15 Parameters to count objects using ITCN in ImageJ 70
Table 2.16 Processes used to quantify GFAP (astrocytes) and Iba1 (microglia) area of staining and individual cell morphology in hippocampal sections 73
Table 4.1 Samples used for digital immunohistochemical analysis of microglia and astrocytes 107
Table 5.1 Effect of trisomy 21 on differential gene expression in Tc1/Wt and Tc1;J20/J20. 153
Table 5.2 Functional clusters associated with the differentially expressed genes identified between each pair of genotypes. 155

List of Supplementary Tables

Supplementary Table 1 Differential gene expression identified between 3-month Tc1;J20 and J20 mice following RNA-seq of hippocampal tissue..... 178
Supplementary Table 2 Differential gene expression identified between 3-month Tc1 and Wt mice following RNA-seq of hippocampal tissue..... 179
Supplementary Table 3 Differential gene expression identified between 3-month J20 and Wt mice following RNA-seq of hippocampal tissue..... 180
Supplementary Table 4 Functional Annotation Clustering by DAVID for significantly differentially expressed genes between Tc1;J20 and J20 (14 out of 28 genes not included in clustering) 182
Supplementary Table 5 Functional Annotation Clustering by DAVID for differentially expressed genes between Tc1 and Wt (45 out of 64 genes not included in analysis) 185
Supplementary Table 6 Functional Annotation Clustering by DAVID for differentially expressed genes between J20 and Wt (10 out of 24 genes not included in analysis) 197

Abbreviations

Aβ	β-amyloid
ACTB	β-actin
AD	Alzheimer disease
ADAM	A disintegrin and metalloprotein
AD-DS	Alzheimer disease in Down syndrome
AICD	APP intracellular domain
AKT	Protein kinase B
ALS2CL	ALS2 C-Terminal Like
AMPAR	α-amino-3-hydroxy-5-methyl-4-isoxazolepropionic acid receptor
AP1G2	Adaptor-Related Protein Complex 1, Gamma 2 Subunit
APH1	Anterior pharynx defective
APOB	Apolipoprotein B
APOE	Apolipoprotein E
APP	Amyloid precursor protein
AraC	Cytosine arabinofuranoside
ARC	Activity-regulated cytoskeleton-associated protein
β3T	β3-tubulin
BACE1	β-secretase 1
BFCN	Basal forebrain cholinergic neurons
BPSD	Behavioral and psychological symptoms of dementia
BSA	Bovine serum albumin
CA1	Cornus ammonis 1
CAA	Cerebral amyloid angiopathy
Cas9	CRISPR associated protein 9
CDK5	Cyclin-Dependent Kinase 5
cDNA	Complementary DNA
CHRM4	Cholinergic Receptor, Muscarinic 4
CLDN8	Claudin 8
CLU	Clusterin
CNS	Central nervous system
CO2	Carbon dioxide
CR1	Complement receptor 1
CRISPR	Clustered regularly interspaced short palindromic repeats
CSF	Cerebrospinal fluid

CSTB	Cystatin B
C_T	Threshold cycle
CTF	C-terminal fragment
CXADR	Coxsackie Virus And Adenovirus Receptor
DAPI	4',6-diamidino-2-phenylindole
DAVID	Database for Annotation, Visualization and Integrated Discovery
ddH2O	Double-distilled water
DEGs	Differentially expressed genes
DIV	Days *in vitro*
DMEM	Dulbecco's Modified Eagle's Medium
DOPEY2	Dopey Family Member 2
DS	Down syndrome
DSCR1	Down syndrome critical region gene 1
DUSP1	Dual specificity phosphatase 1
DYRK1A	Dual-specificity tyrosine-(Y)-phosphorylation regulated kinase 1A
EDTA	Ethylenediaminetetraacetic acid
EGR1	Early growth response protein 1
EPHB2	EPH receptor B2
FAD	Familial Alzheimer disease
FBS	Foetal bovine serum
FDR	False discovery rate
FISH	Fluorescence *in situ* hybridisation
FITC	Fluorescein isothiocyanate
FOS	FBJ murine osteosarcoma
GABA	Gamma-aminobutyric acid
GAD2	Glutamate decarboxylase 2
GAPDH	Glyceraldehyde-3-phosphate dehydrogenase
GFAP	Glial fibrillary acid protein
GluR1	Glutamate receptor 1
GRIN2B	Glutamate receptor ionotropic, NMDA 2B
GSK-3β	Glycogen synthase kinase 3-β
HBSS	Hanks' Balanced Salt Solution
HCl	Hydrochloric acid
HEPES	4-(2-hydroxyethyl)-1-piperazineethanesulfonic acid
HRP	Horseradish peroxidase
Hsa21	Human chromosome 21

Iba1	Ionized calcium-binding adapter molecule 1
IEGs	Immediate-early genes
IFNAR	Interferon (Alpha, Beta And Omega) Receptor
IL-1	Interleukin-1
iPSC	Induced pluripotent stem cells
ITSN1	Intersectin-1
JAK-STAT	Janus kinase - Signal transducer and activator of transcription
LTD	Long term depression
LTP	Long term potentiation
MAP2	Microtubule-associated protein 2
MES	2-(N-morpholino)ethanesulfonic acid
MML	Middle molecular layer
Mmu	Mouse chromosome
mRNA	Messenger RNA
NaOH	Sodium hydroxide
NeuN	Feminizing locus on X-3
NFT	Neurofibrillary tangle
NFκB	Nuclear factor kappa-light-chain-enhancer of activated B cells
NG2	Neural/glial antigen 2
NMDA	N-Methyl-D-aspartic acid
NP-40	Tergitol-type NP-40
PBS	Phosphate buffered saline
PCR	Polymerase chain reaction
PDGF-β	Platelet-derived growth factor beta
PDL	Poly-D-lysine
PEN2	Presenilin enhancer
PER1	Period1
PFA	Paraformaldehyde
PI	Protease inhibitor
PRMT2	Protein arginine methyltransferase 2
PSEN	Presenilin
PVDF	Polyvinylidene fluoride
qPCR	Quantitative polymerase chain reaction
qRT-PCR	Reverse transcription quantitative polymerase chain reaction
Rab5	Ras-related protein 5
RCAN1	Regulator of calcineurin 1

RIPA	Radioimmunoprecipitation assay buffer
RIPK4	Receptor-interacting serine-threonine kinase 4
RNA	Ribonucleic acid
RNAi	RNA interference
RNA-seq	RNA sequencing
RT	Room temperature
S100B	S100 calcium-binding protein B
SAD	Sporadic Alzheimer disease
sAPP	Soluble APP fragment
SDS-PAGE	Sodium dodecyl sulphate-polyacrylamide gel electrophoresis
SEM	Standard error of the mean
shRNA	Short hairpin RNA
SLC17A8	Solute carrier family 17 (vesicular glutamate transporter), member 8
SNX27	Sorting nexin 27
SOD1	Superoxide dismutase 1
SSC	Saline-sodium citrate buffer
SYNJ1	Synaptojanin 1
TBE	Tris/Borate/EDTA buffer
TGF-β	Transforming growth factor β
TIAM	T-cell lymphoma invasion and metastasis
TNFR	Tumor necrosis factor receptor
TREM2	Triggering receptor expressed on myeloid cells 2

Chapter 1. Introduction

1.1. Down syndrome

Down syndrome (DS) is a complex, heterogeneous disorder caused by the total or partial trisomy of human chromosome 21 (Hsa21) (Lejeune et al. 1959). 95% of trisomy 21 is caused by the improper segregation of Hsa21 due to non-disjunction at meiosis I, with errors occurring primarily during maternal meiosis (S. L. Sherman et al. 2007; Antonarakis 1991). In addition, about 4% of cases are each due to Robertsonian translocations of Hsa21, or somatic mosaicism (Flores-Ramírez et al. 2015; Petersen and Mikkelsen 2000). DS is a common condition, with an incidence of 1 in 800 live births (de Graaf et al. 2015). Despite the increased availability of prenatal diagnosis and options for termination, DS prevalence is growing due to increasing maternal age, the greatest risk factor for DS (Loane et al. 2013), together with rises in DS life expectancy (Bittles and Glasson 2004; Yang et al. 2002). In Northern Europe, for example, numbers of people with DS over 40 years old have doubled since 1990, and in the UK this age group accounts for a third of the estimated 40,000 people with DS (Wu and Morris 2013).

Clinical presentation of DS is complex, with a wide range of phenotypic variability between individuals (Jensen and Bulova 2014; Zigman 2013). A few features occur ubiquitously, including intellectual disability, muscle hypotonia and characteristic facial dysmorphology. Significantly for this project, Alzheimer disease (AD) neuropathology is also pervasive in individuals with DS after 35 years of age, who are also at an increased risk for dementia (McCarron et al. 2014). Other DS-associated phenotypes manifest with varying levels of penetrance and severity, such as congenital heart malformations in 40% of individuals, and increased risks for different forms of leukaemia (Freeman et al. 2008).

The dosage imbalance of Hsa21, which carries 233 coding genes, 299 long non-coding genes (Ensembl release 78) and 29 microRNAs (miRBase release 21) (Griffiths-Jones 2004), is likely to underlie phenotypes relating to DS (Lyle et al. 2009; Korenberg et al. 1994). However, triplication of these genes does not inevitably lead to the expected 1.5-fold levels of overexpression compared to euploid individuals, due to mechanisms of gene regulation and homeostasis, which often depend on environmental context. An illustration of this is shown in studies of DS fetal cortical tissue, which revealed that multiple Hsa21 proteins are expressed at lower or similar levels to disomic controls

(Cheon, Kim, Yaspo, et al. 2003; Cheon, Bajo, et al. 2003; Cheon, Kim, Ovod, et al. 2003; Cheon, Shim, et al. 2003). Furthermore, trisomy 21 is associated with widespread transcriptional dysregulation, such as through epigenetic modifications of chromosomal domains, which may be the direct result of aneuploidy rather than triplication of a specific gene (Letourneau et al. 2014). Finally, DS brain gene expression is also characterized by accelerated epigenetic changes associated with aging which may exert effects on gene regulation (Horvath et al. 2015). Therefore, it is necessary to verify the effect of trisomy on candidate gene expression, in relevant tissues and contexts, before inferences can be made on whether overexpression of candidate Hsa21 genes in trisomy may be responsible for phenotypes associated with DS. This will be facilitated by characterization studies at transcriptomic and proteomic levels, together with meta-analyses, which provide powerful tools for understanding global patterns of alterations in gene expression (for example, Vilardell et al. 2011).

As further elaborated below, the DS population has the most common genetic form of early-onset AD, caused by trisomy 21. This project therefore focuses on understanding how trisomy 21 may influence AD phenotypes in DS (AD-DS), allowing investigation of initial pathogenic events leading to AD and dementia, which will be relevant both to people with DS and the general population.

1.2. Alzheimer disease

AD is a neurodegenerative disorder characterized by the chronic progression of cognitive dysfunction from memory loss to dementia, non-cognitive psychiatric symptoms and behavioural disturbances, together with difficulties in performing basic activities of daily living (Ballard et al. 2011; Burns and Iliffe 2009). AD accounts for 50-60% of all cases of dementia (Blennow et al. 2006), which together with a globally aging population poses a pressing public health problem. In 2013, the worldwide prevalence of AD was recorded at 5 million people over the age of 65, which is projected to increase to 13.8 million in 2050 (Hebert et al. 2013; Thies and Bleiler 2013). In the UK, this manifests as a prevalence of 7.1% in people over 65 years of age, or about 80,000 people, which is forecast to increase to over 1 million by 2025 (Prince et al. 2014).

Currently, post-mortem histological examination remains the definitive method of diagnosing AD, which exhibits classical pathological hallmarks such as amyloid pathology, including amyloid plaque deposition and cerebral amyloid angiopathy, and

neurofibrillary tangles (NFTs); these features are associated with glial responses, neuronal and synaptic loss (Serrano-Pozo et al. 2011). Amyloid plaques are formed as a result of the extracellular accumulation primarily of β-amyloid (Aβ) peptides with 40 (Aβ40) or 42 (Aβ42) residues, which are products formed during the metabolism of amyloid precursor protein (APP). NFTs are comprised of paired helical filaments and other assembled forms of the protein tau, a microtubule-associated protein that becomes aberrantly folded and hyperphosphorylated in AD (Iqbal et al. 2005). However, the relationship between the histopathological features of AD and dementia is not yet clear (Castellani and Perry 2014).

1.2.1. Proteolytic processing of amyloid precursor protein (APP)

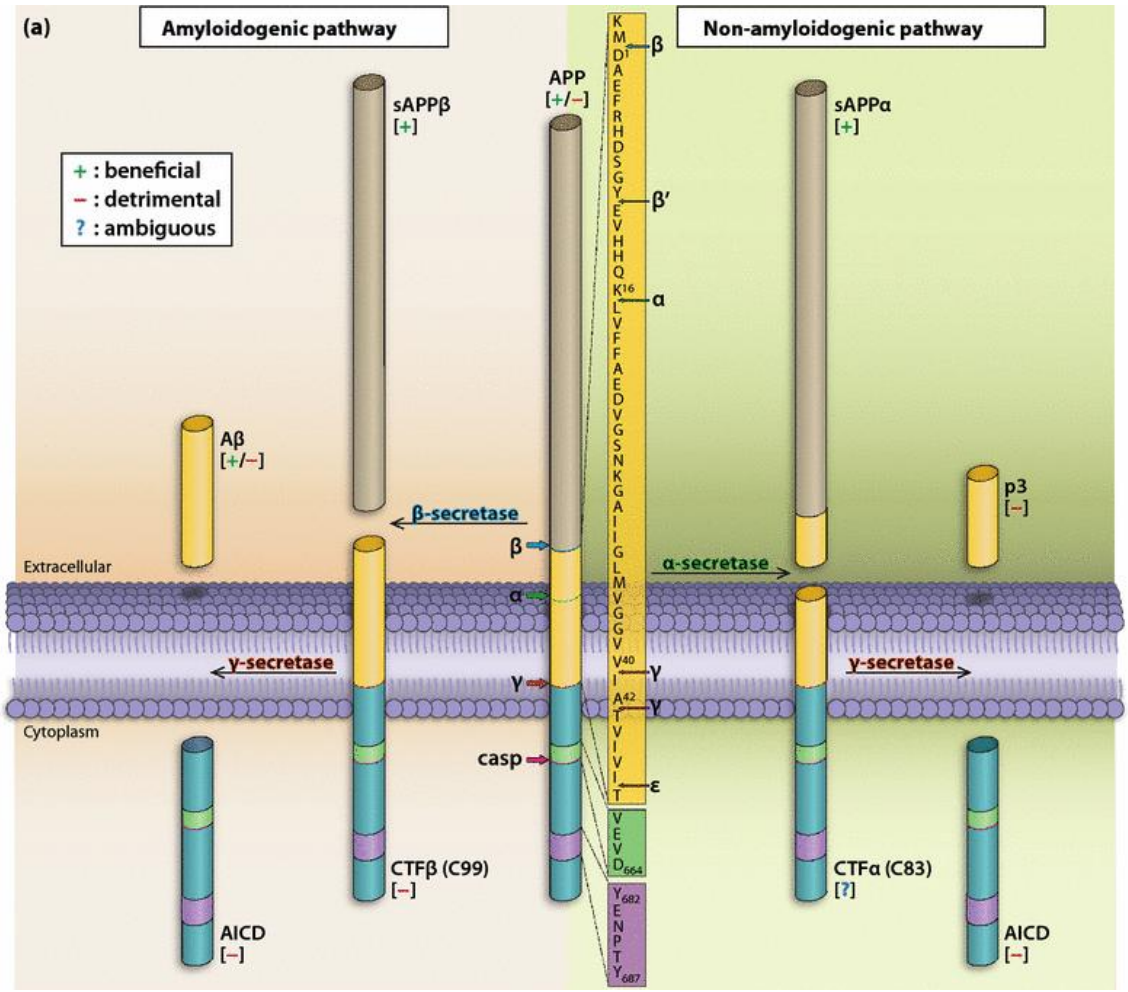

Figure 1.1 APP processing and cleavage products

The amyloidogenic processing pathway is illustrated on the left, while the non-amyloidogenic processing pathway is depicted on the right. APP amino acid sequences for 3 domains are detailed in the yellow, green and purple boxes with numbering based on the APP695 isoform. The Aβ42 domain is detailed in the yellow box, and begins from D^{1} to A^{42}. Adapted from Nhan et al. 2014.

APP, encoded by the *APP* gene located on Hsa21, is a type I integral membrane protein with its amino terminus in extracellular space and its carboxyl terminus within the cytosol (Dyrks et al. 1988; Kang et al. 1987). Different APP isoforms are generated through alternative splicing. The APP695 isoform is the most abundant isoform in the brain and primarily expressed in neurons, while two longer APP751 and APP770 isoforms are expressed in other cell types. Additional isoforms, have also been identified although their physiological roles remain unclear (van der Kant and Goldstein 2015).

Aβ peptides found deposited in amyloid plaques are products formed during the proteolytic processing of APP as summarized in Figure 1.1 (Nhan et al. 2014). APP is processed down two principal pathways, the amyloidogenic (which generates Aβ) and non-amyloidogenic pathways. The non-amyloidogenic pathway commences with cleavage by α-secretase, comprising members of the ADAM (a disintegrin and metalloprotein) family, releasing sAPPα, a soluble ectodomain of APP, and a membrane-tethered intracellular C-terminal fragment, called α-CTF or C83. In the amyloidogenic pathway, cleavage by β-secretase (BACE1) yields a shorter soluble APPβ fragment (sAPPβ) and a longer CTFβ or C99. Following cleavage by α-secretase or β-secretase, γ-secretase cleaves CTFs within the transmembrane domain. In the amyloidogenic pathway, cleavage of β-CTF yields Aβ and an APP intracellular domain (AICD) fragment; in the non-amyloidogenic pathway, cleavage of α-CTF releases a 3-kDa peptide named p3, and an identical AICD fragment. γ-secretase is a complex consisting of presenilin (PSEN), nicastrin, anterior pharynx defective (APH1) and presenilin enhancer (PEN2). Unusually, γ-secretase is capable of step-wise cleavage at multiple sites within the CTF, and in Aβ production this results in the generation of Aβ peptides from 39-43 amino acids in length (Morishima-Kawashima 2014). Besides cleavage by α-, β-, and γ-secretases, other N-terminal fragments (NTFs) of APP have been found in human and rodent tissues that are produced by unknown proteases (Vella and Cappai 2012; Portelius et al. 2010; De Chiara et al. 2010).

1.2.2. Genetics of AD

1.2.2.1. Familial AD (FAD)

FAD can be caused by the autosomal dominant inheritance of genetic mutations, which collectively account for only 0.5% of all AD cases (Ryan and Rossor 2010). These mutations are found in three genes – *APP*, Presenilin-1 (*PSEN1*) and *PSEN2* – which result in early-onset AD compared to sporadic AD (SAD), with an age of onset of 35-55 years for individuals with *PSEN1* mutations, and 40-70 years for *APP* and *PSEN2*-affected individuals. Mutations relating to FAD largely increase the production of Aβ, and/or alter the ratio of Aβ42/Aβ40 towards Aβ42, perceived to be the more neurotoxic species due to its increased propensity to aggregate (Mucke and Selkoe 2012). The clustering of FAD mutations in the presenilin genes, as well as regions of *APP* close to secretase cleavage sites, has therefore pointed towards the importance of Aβ in AD pathogenesis.

In addition to the point mutations described above, duplication of the wildtype *APP* locus alone ('Dup-APP') is also sufficient to cause a highly penetrant form of early-onset AD (Swaminathan, Huentelman, et al. 2012; Hooli et al. 2012; McNaughton et al. 2012; Thonberg et al. 2011; Kasuga et al. 2009; Rovelet-Lecrux et al. 2007; Rovelet-Lecrux et al. 2006; Sleegers et al. 2006). As discussed below in Section 1.3, this is especially important for understanding links between AD and DS, as three copies of *APP* are also present in DS.

1.2.2.2. Sporadic AD (SAD)

The vast majority of AD cases are idiopathic, with SAD accounting for more than 99% of affected individuals. Though twin studies have shown that SAD exhibits strong heritability (Gatz et al. 2006), this genetic component is complex and heterogeneous. The strongest genetic risk factor for SAD is *APOE* (Saunders et al. 1993; Corder et al. 1993), which accounts for 27.3% of the 80% estimated disease heritability (Lambert et al. 2013), and is determined by the presence of three major allelic variants (ε2, ε3 and ε4). The continued search for other risk loci explaining the remaining genetic heritability has been driven by large collaborative genome-wide association studies, which have identified more than 20 different risk loci to date (Van Cauwenberghe et al. 2015). None of these, however, exert an effect on AD risk close in magnitude to *APOE* ε4*,* but have pointed towards three functional clusters that may highlight mechanisms

underlying AD pathophysiology – cholesterol and lipid metabolism, immune system and inflammatory response, and endosomal vesicle cycling (Van Cauwenberghe et al. 2015). Further efforts are currently underway to identify more rare variants, employing advances in massive parallel sequencing technologies (Del-Aguila et al. 2015).

1.2.3. The amyloid cascade hypothesis

Mutations leading to alterations in Aβ production are causative of FAD, lending support to the idea that amyloid may be pathogenic for AD. This forms the basis for the amyloid cascade hypothesis, which posits that Aβ is the causative agent in AD, triggering a series of events leading to other pathological features downstream, including the formation of NFTs, cell loss and eventually dementia (Hardy and Selkoe 2002; Hardy and Higgins 1992). However, while FAD mutations bring forward the age of onset of AD, they do not appear to accelerate disease progression (Ryman et al. 2014), suggesting that Aβ may be a trigger for AD pathogenesis but is not a mediator of downstream mechanisms underlying neurodegeneration. This is also supported by the poor correlation between amyloid pathology with neuronal loss and clinical symptoms in SAD; tau pathology is the closest neuropathological correlate with these features of neurodegeneration (Serrano-Pozo et al. 2011). Though the amyloid cascade hypothesis is currently the most widely accepted paradigm guiding investigations of AD pathogenesis, it has become clear that Aβ does not cause AD via a simple linear toxicity pathway, but involves a complex network of pathological developments. These potentially include features such as neuroinflammation and oxidative stress relevant to aging, which remains the greatest risk factor for AD and numerous other neurodegenerative diseases (Abner et al. 2015). The main dispute between proponents of and detractors from the amyloid cascade hypothesis therefore centres on the necessity of Aβ toxicity as an initial pathogenic event, amid difficulties hitherto in identifying Aβ forms, models, mechanisms, and relevant time points to address this question (Musiek and Holtzman 2015; Herrup 2015). Nonetheless, Aβ plaque pathology is indicative of the AD clinical syndrome, and the ability to study its effects and interactions with other pathological features will aid our understanding of their relative contributions to neurodegeneration, and identify areas for therapeutic targeting.

1.3. Alzheimer disease in Down syndrome

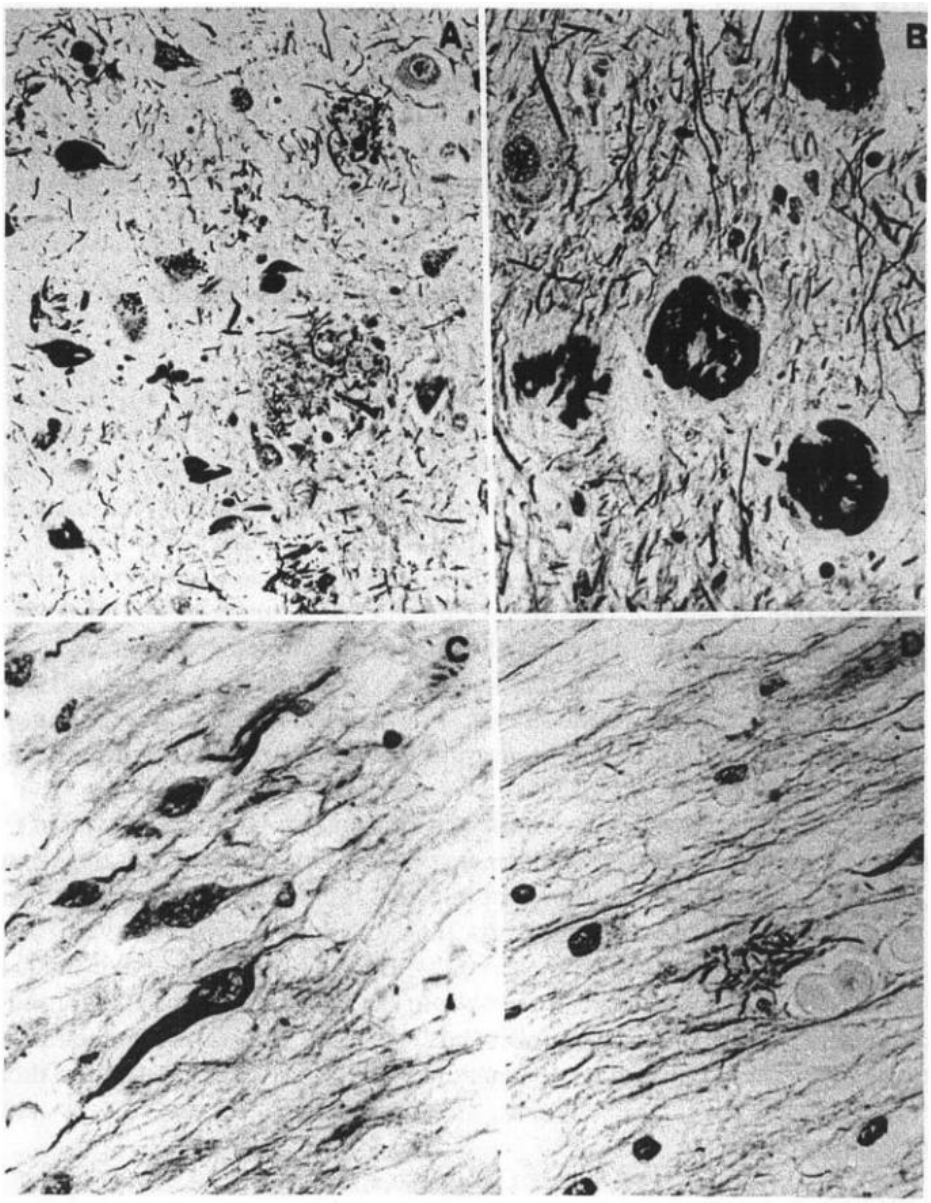

Figure 1.2 Amyloid plaques and neurofibrillary tangles in the brain of a 65-year old DS individual

Figure A shows plaques and NFTs in the corticomedial nucleus of the amygdala (x300). Figure B shows NFTs in nerve cells of the locus coeruleus. Figure C displays NFTs in a nerve cell of the olfactory tract. Figure D shows a plaque in the olfactory tract (Figures B to D are at x510). Adapted from Mann 1988a.

As depicted above in, AD pathology is found in brains of virtually all individuals with DS by 40 years of age (Mann and Esiri 1989; Wisniewski et al. 1985). This corresponds with an increased risk of dementia, with dementia rates approximately doubling every 5 years from <5% under the age of 40, to 68-80% of DS individuals over 65 years of age (McCarron et al. 2014; Margallo-Lana et al. 2007; Coppus et al. 2006; Tyrrell et al.

2001; Holland et al. 1998; Prasher and Krishnan 1993). Aging, as in SAD, therefore remains one of the most important risk factors for AD-DS, though variable patterns of onset have been observed, partially influenced by variations in survey methodology and diagnostic variability due to premorbid deficits (McCarron et al. 2014; Strydom et al. 2010). However, not all individuals convert to dementia, even by 70 years of age (Ghezzo et al. 2014; Krinsky-McHale et al. 2008). Sex does not influence the incidence of AD-DS (Coppus et al. 2006; Tyrrell et al. 2001), possibly due to changes in hormonal or cardiovascular biology that alter AD risk in DS, although further study is required to understand this (Wiseman et al. 2015). Overall, the DS population exhibits the most common genetic form of early-onset AD, caused by trisomy 21. Studying AD-DS therefore allows investigations into the initial pathogenic events leading to AD and dementia, relevant to both people with DS and to the general population.

One of the first relationships between DS and AD was established in 1984 when amyloid deposits isolated from DS and AD brains were shown to be homologous in protein sequence (Glenner and Wong 1984a), even before a missense mutation in *APP* was identified in two families with early-onset AD (Goate et al. 1991). As illustrated above**,** *APP* duplications are sufficient to cause early-onset FAD (Swaminathan, Huentelman, et al. 2012; Hooli et al. 2012; McNaughton et al. 2012; Thonberg et al. 2011; Kasuga et al. 2009; Rovelet-Lecrux et al. 2007; Rovelet-Lecrux et al. 2006; Sleegers et al. 2006). Furthermore, in a rare case of partial Hsa21 trisomy without the duplication of *APP*, no evidence of AD presentation was found in multiple assessments (Korbel et al. 2009). Therefore it is unsurprising that individuals with DS face a significantly increased risk of AD, since three copies of *APP* are expressed. However, the variable penetrance of dementia suggests that other genetic factors on Hsa21, and elsewhere in the genome, modulate the risk of developing AD.

1.3.1. APP and Aβ phenotypes in DS and AD-DS

In adults with DS, APP protein (Cheon et al. 2008; Rumble et al. 1989) and mRNA levels (Oyama et al. 1994) have been shown to be increased compared to controls in the cortex, generally close to the 1.5-fold levels expected with its trisomic gene dosage. Although not all studies have agreed on the presence of *APP* overexpression in DS (Argellati et al. 2006; Lockstone et al. 2007), a large meta-analysis of heterogeneous DS data sets has concluded that *APP* does display a gene dosage increase (Vilardell et al. 2011). However, in studies performed on fetal DS brains, investigations into *APP* mRNA (Argellati et al. 2006; Mao et al. 2005) and protein (Cheon et al. 2008) levels have suggested that there is no significant increase in expression levels at 18-19

weeks. This suggests a possible age-dependent increase in *APP* expression in DS individuals throughout life.

Studies of DS Aβ levels in brain and plasma have reported increases in both Aβ40 and Aβ42 in DS compared to controls (Head et al. 2011; Conti et al. 2010; Schupf et al. 2001; Mehta et al. 1998; Tokuda et al. 1997; Teller et al. 1996), of which high Aβ42 levels are associated with increased AD risk (Coppus et al. 2012; Head et al. 2011; Jones et al. 2009; Matsuoka et al.; Schupf et al. 2007). Consistent with this, increased Aβ production has been reported in DS induced pluripotent stem cell (iPSC) models (Murray et al. 2015; Shi et al. 2012). However, like the variable age of onset of AD-DS, there is wide variation in Aβ peptide levels in DS, which together with the possible age-dependent increase in *APP* expression suggests a complex underlying regulatory mechanism for Aβ-mediated pathology.

1.3.2. Features distinguishing AD-DS from other forms of AD

The highly variable age of onset of dementia in AD-DS supports the notion that trisomy 21 modulates dementia risk, as dementia in Dup-*APP* demonstrates complete penetrance by the age of 65 (Wiseman et al. 2015). People with AD-DS also present behavioural and psychological symptoms (BPSDs) prominently in early stages of disease, such as apathy, stubbornness or increased behavioural excesses, associated with impaired executive functioning and frontal lobe dysfunction (Oliver et al. 2011; Adams and Oliver 2010; Ball et al. 2008; Ball et al. 2006; Holland et al. 2000). These BPSDs present at higher rates than in early stages of FAD and SAD (Masters et al. 2015; Wallon et al. 2012).

While the overall distribution and composition of Aβ plaques and NFTs in DS, FAD and SAD are largely similar (Goedert et al. 1992; Mann 1988a; Wisniewski and Rabe 1986; Glenner and Wong 1984b), subtle differences may occur in the spatio-temporal development of Aβ deposition. Histological studies suggest that Aβ deposition is observed earliest in the hippocampus in AD-DS (Leverenz and Raskind 1998), while in SAD this occurs in the basal cortex (Braak and Braak 1991); at later stages, it further appears that AD-DS, compared to SAD, exhibits greater plaque deposition in the hippocampus (Mann 1988b), and less deposition in the cortex (Egensperger et al. 1999; Mann 1988b; Mann et al. 1987). This may be partially accounted for by the larger average plaque size in AD-DS compared to SAD, although it is unclear why this is the case – possible reasons include altered Aβ aggregation kinetics due to overproduction

in *APP* trisomy, and altered neurodevelopment in DS resulting in changes to synaptic activity influencing Aβ production (Wiseman et al. 2015). On the other hand, NFT development in AD-DS mirrors observations in SAD, where increases in NFT density correlate well with cognitive decline (Margallo-Lana et al. 2007; Wisniewski et al. 1985). However, it has been suggested that the cortex and locus coeruleus in AD-DS may be less susceptible to NFT-associated pathology, including reduced cell loss and smaller decreases in nucleolar volume. Together, these histopathological differences suggest that regions of the trisomic brain may be differentially responsive to similar pathological hallmarks observed in AD.

Vascular dementia and cerebral infarcts appear to be rare in AD-DS, compared to SAD (Evenhuis 1990; Mann 1988b), though cerebral haemorrhage cases relating to cerebral amyloid angiopathy (CAA) have been described in AD-DS (Mendel et al. 2010; Naito et al. 2008; Donahue et al. 1998; McCarron et al. 1998). This is particularly interesting considering that 20-50% of Dup-*APP* patients exhibit intracerebral haemorrhages (Lladó et al. 2014; Wallon et al. 2012; Swaminathan, Huentelman, et al. 2012; McNaughton et al. 2012; Kasuga et al. 2009; Rovelet-Lecrux et al. 2007; Sleegers et al. 2006; Rovelet-Lecrux et al. 2006), suggesting that trisomy of other regions on Hsa21 in DS may serve to protect against this form of pathology.

Seizure susceptibility in adulthood appears heightened by *APP* duplication, as both AD-DS (84%) and Dup-*APP* (57%) exhibit significantly higher rates of seizures than SAD (<5-20%) (De Simone et al. 2010; Rovelet-Lecrux et al. 2006; Mendez and Lim 2003). This suggests that duplication of *APP* (and of genes in adjacent loci) may be epileptogenic, contributing to the complex relationship between Aβ neurotoxicity and hyperexcitability, which remains a poorly understood subject (Noebels 2011).

Given the universal triplication of *APP* in trisomy 21, and AD neuropathology from 40 years of age, the DS population presents the largest genetic population for studying AD, particularly through the lens of the amyloid cascade hypothesis. Understanding the factors underlying why not every DS individual with early extensive amyloid deposition converts to dementia is a key research challenge, which will provide mechanistic insights to inform our understanding across all genetic forms of AD.

1.4. Mouse models of Down syndrome and Alzheimer disease

1.4.1. Mouse models of DS

Hsa21 has synteny with the mouse genome, such that its orthologous genes are distributed in three segments, with conserved order and gene orientation, on mouse chromosomes 10 (Mmu10), Mmu16 and Mmu17 (Dierssen et al. 2009; Hattori et al. 2000); the mouse *App* gene lies on Mmu16. To mimic the effects of trisomy 21, several mouse models with precisely defined trisomies, now usually targeted by chromosome engineering (Tybulewicz and Fisher 2006; Brault et al. 2006), have been generated to provide a set of models segmentally trisomic for regions orthologous to Hsa21 (Davisson et al. 1993; Sago et al. 1998; Olson et al. 2004; Li et al. 2007; Pereira et al. 2009; Herault et al. 2009; Yu, Li, et al. 2010; Liu et al. 2011; Liu et al. 2014; Brault et al. 2015).

Generating a series of models with different partial trisomies creates a mapping panel in which individual phenotypes may be assessed in several strains, and so assigned to specific trisomic chromosomal region(s). As DS phenotypes likely arise from abnormal gene dosage, candidate genes can be chosen from the trisomic critical region, that when present in three copies give rise to phenotypes of interest. Individual candidate genes can then be studied, for example, in overexpression or knockout models, to assess the effects of different copy numbers of the gene

Figure 1.3 provides an overview of DS mouse models and the chromosomal segments for which they are trisomic. Table 1.1 details the gene content for each DS mouse model shown, including protein-coding and non-coding genes relevant to human trisomy 21.

While numerous DS mouse models have been published, there is no single complete model, and the usefulness of multiple strains lies in their comparative and complementary use in studying genotype-phenotype relationships. DS models are also more advantageous than the use of transgenic mice due to the likely expression of trisomic genes at endogenous levels, mimicking human DS transcription. We can also study the interactions of Hsa21 dosage-sensitive genes with the rest of the genome (Hsa21 and non-Hsa21), as well as effects exerted by the presence of aneuploidy.

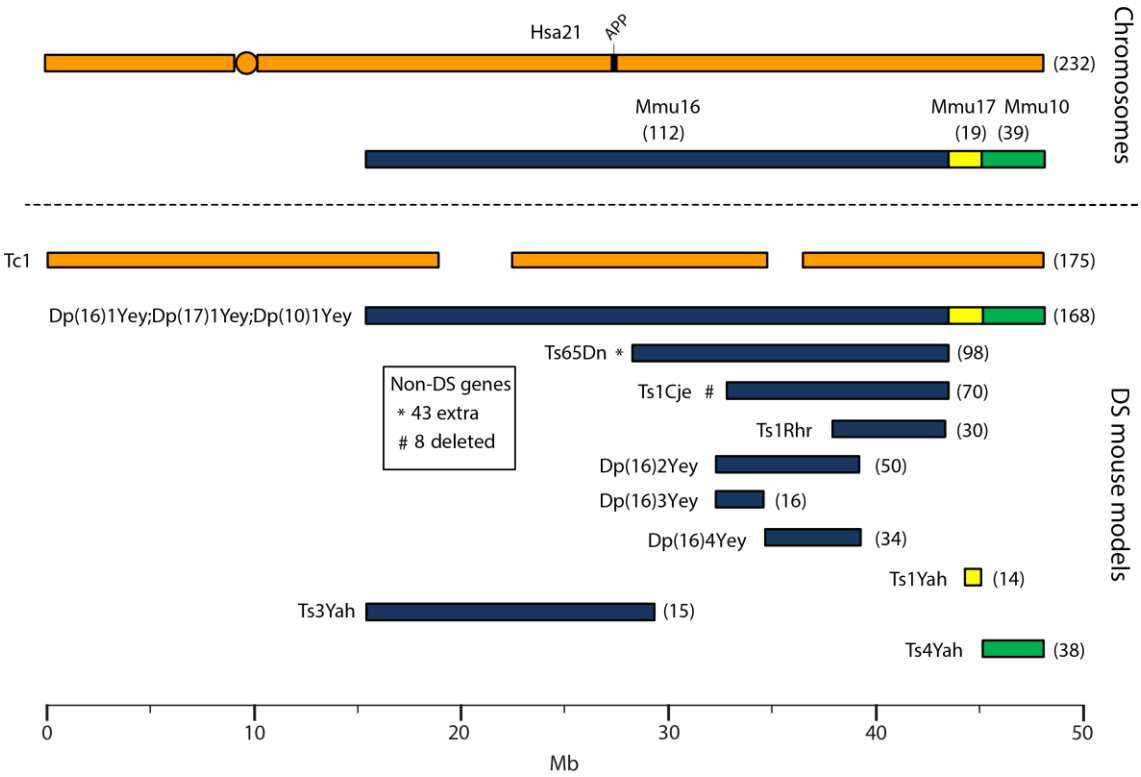

Figure 1.3 Human chromosome 21 (Hsa21), orthologous mouse chromosomes (Mmu) and key mouse models of Down syndrome.

Figure from Choong et al. 2015. Diagram representing Hsa21 and its alignment with syntenic regions on Mmus 16, 17 and 10. The orange circle represents the human centromere and mouse models are colour-coded and aligned according to the chromosomal segment for which they are trisomic. Numbers in brackets represent the number of protein-coding Hsa21 orthologous genes within each region or mouse model, according to Ensembl release 79 and the breakpoints published in papers referenced here. The Tc1 mouse is the only model which carries Hsa21, though genomic rearrangements and deletions (indicated by breaks in the chromosome) mean the mouse is functionally trisomic for only ~75% of Hsa21 genes (Gribble et al. 2013). All other mouse models carry duplications of mouse orthologues. The Dp1(16)Yey; Dp1(17)Yey;Dp1(10)Yey (or Ts1Yey;Ts3Yey;Ts2Yey) mouse was generated by crossing together 3 partial trisomy models (Yu, Li, et al. 2010) and spans the entirety of the Hsa21-syntenic regions. The Ts65Dn mouse (Davisson et al. 1993) contains a freely segregating segment of Mmu16, however it is also trisomic for 43 extra protein-coding genes on the centromeric section of Mmu17 that are not relevant to DS (indicated in the by an asterisk (*) and accompanying text box; Duchon et al. 2011; Reinholdt et al. 2011). The Ts1Cje mouse (Sago et al. 1998) also contains a monosomy of 8 protein-coding genes on Mmu12, irrelevant to the DS phenotype (indicated by "#" and accompanying text box. Gene numbers are based on Ensembl release 79, compared to the original 7 monosomic genes detailed in Duchon et al. 2011). Other mice are Ts1Rhr or Dp1(16)Rhr mice (Olson et al. 2004); Ts1Yah mice (Pereira et al. 2009); Ts3Yah (previously published as Ts2Yah) (Brault et al. 2015) and Ts4Yah mice (previously published as Ts3Yah mice) (Herault et al. 2009). Other useful examples of mouse models include the Ts43H model (not shown) which is partially trisomic for Mmu17 including some genes with orthologues on Hsa21 (Vacík et al. 2005). The scale is in megabase pairs (Mb).

Table 1.1 Trisomic regions and triplicated gene content in Down syndrome mouse models

Models are shown in Figure 1 and compared to Hsa21 (Ensembl release 79). Table compiled by Laura Pulford (Choong et al. 2015).

		Protein-coding genes		Non-protein-coding genes		Total genes		% Protein-coding genes from Hsa21
Hsa21		232		648		880		
DS mouse model	**Official MGI name***	**Mouse genes**	**Hsa21 genes**	**Mouse genes**	**Hsa21 genes**	**Mouse genes**	**Hsa21 genes**	
Tc1	B6;129S-Tc(Hsa21)1TybEmcf/J	-	175	-	Undetermined	-	N/A	75
Dp(16)1Yey	B6.129S7-Dp(16Lipi-Zbtb21)1Yey/J	149	112	112	6	261	118	48
Dp(17)1Yey	B6;129S7-Dp(17Abcg1-Rrp1b)3Yey/J	19	18	6	0	25	18	8
Dp(10)1Yey	B6;129S7-Dp(10Prmt2-Pdxk)2Yey/J	55	39	20	1	75	40	17
Ts65Dn**	B6EiC3Sn a/A-Ts(1716)65Dn	133	98	71	3	204	101	42
Ts1Cje***	B6.Cg-T(12;16)1Cje/CjeDnJ	76	70	51	1	127	71	30
Ts1Rhr	B6.129S6-Dp(16Cbr1-Fam3b)1Rhr/J	32	30	20	0	52	30	13
Dp(16)2Yey	129-Dp(16Tiam1-Kcnj6)6Yey/J	53	50	37	1	90	51	22
Dp(16)3Yey	129-Dp(16Tiam1-Il10rb)8Yey/J	18	16	12	0	30	16	7
Dp(16)4Yey	129-Dp(16Ifnar1-Kcnj6)10Yey/J	35	34	24	1	59	35	15
Ts1Yah	B6;129P2-Dp(17Abcg1-Cbs)1Yah/Orl	15	14	4	0	19	14	6
Ts3Yah (previously Ts2Yah)	B6;129P2-Dp(16Hspa13-App)2Yah/Orl	19	15	45	5	64	20	6
Ts4Yah (previously Ts3Yah)	B6.Cg-Dp(10Prmt2-Cstb)3Yah/Orl	54	38	20	1	74	39	16
Trisomic/monosomic regions and gene content irrelevant to Hsa21 and its syntenic regions in mice								
Ts65Dn**	B6EiC3Sn a/A-Ts(1716)65Dn	43	-	36	-	79	-	
Ts1Cje***	B6.Cg-T(12;16)1Cje/CjeDnJ	8	-	4	-	12	-	

*Mouse genome informatics site that includes the official mouse strain names www.informatics.jax.org; the shaded line shows number of Hsa21 genes.

**indicates gene content of Ts65Dn and ***indicates gene content of Ts1Cje mice.

The most complete mouse model to date, *Dp(10)1Yey/+;Dp(16)1Yey/+;Dp(17)1Yey/+*, is trisomic for all Hsa21 syntenic regions and was generated by crossing three DS models segmentally trisomic for the respective Hsa21 orthologous regions on Mmu10, Mmu16 and Mmu17 (Yu, Li, et al. 2010; Yu, Liu, et al. 2010; Li et al. 2007). However, the vast majority of studies relating to AD-DS have been performed on the Ts65Dn mouse, which has been a 'standard model' of DS for many years, prior to the development of newer strains by chromosome engineering (Davisson et al. 1993; Reeves et al. 1995). Ts65Dn carries a reciprocal translocation between Mmu16 and Mmu17, resulting in trisomy of ~42% of the protein-coding genes orthologous to Hsa21. As this product contains a fusion of the distal end of Mmu16 with a small centromeric section of Mmu17, it also contains 79 additional genes (including long non-coding sequences) from Mmu17 outside the Hsa21 region of synteny, which need to be taken into account when analysing phenotypes (Duchon et al. 2011; Reinholdt et al. 2011). The extra triplicated genes irrelevant to DS include non-Hsa21 genes, such as *SYNJ2* and *TIAM2* that have Hsa21/Mmu16 paralogues (*SYNJ1*, *TIAM1*), which may complicate phenotype-genotype correlations (Duchon et al. 2011). Other triplicated genes in Ts65Dn irrelevant to DS include several genes encoding dynein light chains that may influence endosomal trafficking, and so potentially affect neuronal phenotypes (Hartley et al. 2015).

1.4.2. The transchromosomic Tc1 mouse

In 2005, the Tc1 mouse was generated, which carries a freely segregating, almost complete copy of Hsa21 (O'Doherty et al. 2005). This was possible through irradiation microcell-mediated chromosome transfer, a process that involves gamma irradiation to transfer Hsa21 into mouse embryonic stem cells. However, the irradiation also resulted in the generation of 41 rearrangement breakpoints, as revealed by massively parallel sequencing (Gribble et al. 2013). As illustrated in Table 1.4**,** the Hsa21 chromosome in Tc1 is rearranged, including a change in the position of the centromere such that the chromosome becomes metacentric. This also exerts effects on the expression of Hsa21 genes, as summarized in Table 1.2. Tc1 mice are functionally trisomic for ~75% of Hsa21 genes, with 9 duplicated and 50 disrupted or deleted genes (Gribble et al. 2013). Crucially for this project, Tc1 is not functionally trisomic for *APP*, due to a rearrangement that affected the genomic position of its final coding exon on the Hsa21 chromosome (Gribble et al. 2013; Sheppard et al. 2012). Furthermore, the Hsa21 chromosome is lost stochastically at different rates in different mouse tissues – thus, Tc1 mice are mosaic for the human chromosome.

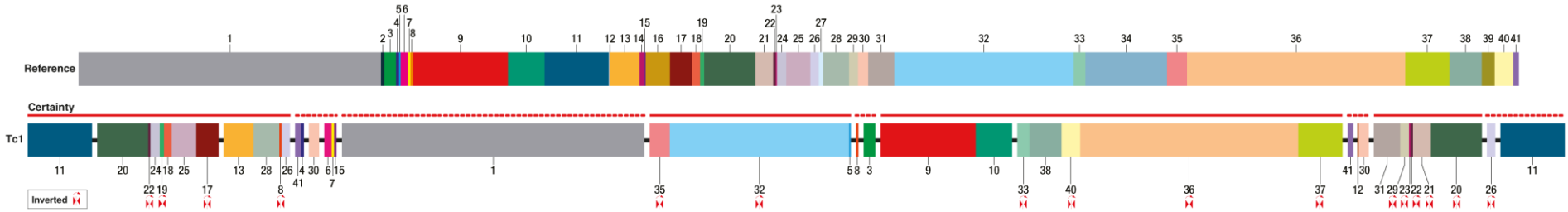

Figure 1.4 Proposed structure of Hsa21 in Tc1

Regions 1-41 were determined based on FISH mapping data, and are depicted in the original Hsa21 sequence in the top row ("Reference"). In the Tc1 Hsa21 chromosome, these regions have been rearranged as indicated. A solid red line indicates strong certainty of the rearrangement, while the dotted red line represents a suggested rearrangement. Red arrows indicate inverted chromosome regions. Region 12 is triplicated but the position of the other two copies is unknown. Position of region 27 is unknown. The positions of acrocentric regions 1, 2, 3, 7 and 8 are unknown and are placed arbitrarily. Regions 26, 30 and 41 are duplications and their positions are suggested by FISH within the resolution of the technique. Regions 14, 16, 34 and 39 are deleted. Figure from Gribble et al. 2013.

Table 1.2 RefSeq Hsa21 genes not functionally trisomic in Tc1

Adapted from Supplementary Table 4 from Gribble et al. 2013.

Deleted	BTG3, ATP5O, C21orf119, C21orf45, C21orf49, C21orf54, C21orf59, C21orf62, C21orf63, C21orf82, C21orf91, CHODL, CLIC6, CRYZL1, DNAJC28, DONSON, FAM165B, GART, GCFC1, IFNAR1, IFNAR2, IFNGR2, IL10RB, ITSN1, KCNE1, KCNE2, MRAP, MRPS6, NCRNA00157, NCRNA00160, OLIG1, OLIG2, RCAN1, SLC19A1, SLC5A3, SNORA80, SON, SYNJ1, TCP10L, TMEM50B, URB1
Partially deleted and rearranged	COL18A1, PCBP3, RUNX1, TMPRSS15,
Duplicated	ABCC13, C21orf131, HSPA13, NRIP1, PRMT2, RBM11, S100B, SAMSN1, USP25,
Duplicated and rearranged	BAGE, BAGE2, BAGE3, BAGE4, BAGE5
Partially duplicated	LIPI
Partially duplicated and rearranged	C21orf34, DIP2A, NCAM2
Rearranged	APP, NDUFV3, TRPM2

Despite these caveats, Tc1 mice recapitulate a wide range of phenotypes relevant to DS, as summarised in Table 1.3. Of particular relevance to AD pathology, age-dependent increases in phosphorylated tau and altered regulation of tau phosphorylation have been observed in Tc1 mice (Sheppard et al. 2012).

Table 1.3 Neurological and non-neurological deficits characterized in Tc1 mice

Neurological phenotypes		
Phenotype	**Deficits observed**	**References**
Behavioural deficits	Deficits in short term memory but preserved long term memory in novel objection recognition task	Morice et al. 2008; O'Doherty et al. 2005
	Impaired spatial working memory but spared long-term spatial reference memory in Morris water maze	Morice et al. 2008
	Hyperactivity, abnormal exploratory behaviour and impaired habituation to environment open field test	Galante et al. 2009; O'Doherty et al. 2005
	Severe deficits in motor skills and learning on static road and rotarod tests	Galante et al. 2009
Synaptic plasticity	Reduced hippocampal early long-term potentiation (1 h) but normal late LTP (24 h and 48 h)	Morice et al. 2008; O'Doherty et al. 2005
	Normal basal synaptic transmission and inhibitory tone	O'Doherty et al. 2005
	Impaired short-term plasticity at dentate gyrus-CA3 excitatory synapses	Witton et al. 2015
	No reduction in cerebellar long-term depression at parallel fibre-Purkinje cell synapse	Galante et al. 2009
Synaptic architecture	Reduced hippocampal surface membrane expression of the AMPAR subunit GluR1	Morice et al. 2008
	Loss of postsynaptic thorny excrescences from hippocampal CA3 dendrites	Witton et al. 2015
	Reduced dentate gyrus middle molecular layer (MML) synaptic density	
	In MML, no alterations in synapse morphology classifications (thin, stubby, mushroom and axo-dendritic)	
	In cortical projection neurons, fewer mushroom spines (associated with established synaptic inputs) and increased stubby spines	Haas et al. 2013
Cerebellar phenotypes	Decreased density of cerebellar granule neurons	O'Doherty et al. 2005

Table continued on the next page

Altered regulation of tau phosphorylation	Tau aberrantly phosphorylated at threonine 212 in hippocampus and cortex of aged (20 months) but not young (2 months) Tc1 mice	Sheppard et al. 2012
	Increased protein expression of DYRK1A, a kinase that phosphorylates tau at threonine 212, in both young and old Tc1 mice. *DYRK1A* is trisomic in Tc1	
	Aberrant phosphorylation of kinases GSK-3β and AKT in old but not young Tc1 mice. GSK-3β is capable of phosphorylating tau while AKT regulates GSK-3β activity	
	No change in protein expression of CDK5 and its regulators p35/p25 in hippocampus and cortex of both old and young Tc1 mice	
Sleep	Fragmented patterns of sleep-like behaviour in light phase of a 12:12-h light/dark cycle, and continuous wakefulness at beginning of dark phase	Heise et al. 2015
	Poorer induction of sleep-like behaviour by acute light pulse at night	
Non-neurological phenotypes		
Phenotype	**Deficits observed**	**References**
Cardiac malformations	Atrioventricular septal defects observed	Dunlevy et al. 2010; O'Doherty et al. 2005
Craniofacial morphology	No obvious differences in overall facial bone morphology and skull dimensions measured by CT scans, with a decrease observed in one measurement of mandible size	O'Doherty et al. 2005
Immune response	Reduced T lymphocyte activation measured by CD25 and CD69 upregulation in the spleen and lymph nodes, following stimulation of T cell receptors or costimulatory receptor CD28	O'Doherty et al. 2005
Cancer	Macrocytic anaemia and increased extramedullary haematopoiesis observed	Alford et al. 2010
	Reduced growth of transplanted lung carcinoma cells and repressed tumour angiogenesis	Reynolds et al. 2010
Sterility	Male Tc1 mice are usually sterile	Reeves 2006
Hearing	Normal hearing sensitivity and gross ear anatomy	Kuhn et al. 2012

1.4.3. Considerations when studying AD phenotypes in DS mouse models

In studying mouse phenotypes to understand AD-DS, two key issues are presented. Firstly, there is a need to longitudinally test DS models to identify changes in older mice that are not apparent at younger ages, which may indicate aging or neurodegenerative processes rather than neurodevelopmental deficits. Secondly, normal aging processes in DS need to be separated from those connected specifically to AD-DS. A study that has addressed both (1) neurodegenerative versus

neurodevelopmental and (2) normal aging versus AD phenotypes has been performed in the Ts65Dn mouse. This study concerned the loss of basal forebrain cholinergic neurons (BFCNs), and was carried out through an experimental design involving optimal crossing of different mouse models and assessment of the genetically distinct progeny (Salehi et al. 2006). Firstly, Salehi and colleagues quantified the known loss of BFCNs in Ts65Dn mice, and showed this loss to be age-dependent. The authors then compared BFCN loss between Ts65Dn and Ts1Cje mice: Ts65Dn mice lost BFCNs but Ts1Cje mice turned out to have no loss compared to wildtype mice. Therefore this mapped a dosage-sensitive critical region that had to contain a candidate gene relevant to phenotype. A key candidate in this region was *App*. By crossing Ts65Dn mice to heterozygous *App* knockout mice, the authors generated progeny that carried the trisomic region with either two or three copies of wildtype *App*. BFCN loss was subsequently shown to arise mainly from having three copies of *App* and, further associated with impairments in retrograde transport of nerve growth factor, linked to enlarged early endosomes (Salehi et al. 2006). These have also been observed in individuals with DS and early AD (Cataldo et al. 2000).

1.5. Mouse models of AD

1.5.1. Transgenic models of AD

As the etiology of SAD is unknown, mouse models have primarily employed genetic mutations associated with FAD to model the disease, with the assumption that downstream events in familial and sporadic AD are sufficiently similar for comparison (LaFerla and Green 2012). AD models are primarily transgenic lines that overexpress one or more of the human mutant genes that cause FAD (Webster et al. 2014; Braidy et al. 2012). These transgenes usually insert in the genome at random sites and may be driven by artificial promoters, which vary in terms of their spatial and temporal expression patterns, usually resulting in expression at 5-10 fold levels compared to endogenous mouse orthologues (Hall and Roberson 2012; Balducci and Forloni 2011). Overexpressing wildtype human *APP* or mouse *App* does not result in amyloid deposition (Elder et al. 2010), hence known FAD-causing mutations in human *APP* need to be employed. However, the expression of wildtype mouse APP, or wildtype or mutant human APP protein can influence amyloid pathology (Kokjohn and Roher 2009). For example, mouse APP may be processed with little BACE1 cleavage due to amino acid differences between the two APP species, which may consequently yield three times less Aβ than wildtype human APP (De Strooper et al. 1995). In addition,

the genetic background of AD mouse strains affects a range of APP/Aβ phenotypes, including plaque deposition, APP metabolism, survival and seizure rates (Jackson et al. 2015; Rustay et al. 2010; Lassalle et al. 2008; Krezowski et al. 2004; Lehman et al. 2003; Carlson et al. 1997).

In general, while mutant *APP* transgenic mice develop robust amyloid deposition, synaptotoxic features and memory impairments, none of them reproduces tau-containing neurofibrillary tangles, the hallmark pathology of AD which most closely correlates with dementia (Hall and Roberson 2012). The combined overexpression of mutant *APP* and mutant human tau is required to reproduce both amyloid and tau pathology, although tau mutations in humans do not alone cause AD, but frontotemporal dementia. Therefore mutant *APP* and presenilin transgenics may be best considered models of APP/Aβ overexpression than full AD.

1.5.2. The J20 mouse model of APP/Aβ overexpression

In this project, the B6.Cg-Tg(PDGFB-APPSwInd)20Lms/2Mmjax (J20) model is used (Mucke et al. 2000). J20 mice express a mutant human *APP* transgene (Figure 1.5) which includes introns 6-8 allowing for the expression of all three major APP isoforms: APP695, APP751 and APP770 (Games et al. 1995; Rockenstein et al. 1995). Expression is directed by the PDGF-β promoter (Sasahara et al. 1991), which is neuron-specific (Figure 1.6) and expressed in the isocortex, olfactory areas, hippocampal formation, cortical subplate, medulla and cerebellum (Figure 1.7). The *APP* gene bears two sets of mutations, the Swedish (K670N/M671L) and Indiana mutations (V717F), which were previously discovered in separate families with FAD (Mullan et al. 1992; Murrell et al. 1991). The Swedish mutation increases Aβ production by β-secretase cleavage (Haass et al. 1995; Johnston et al. 1994; Cai et al. 1993; Citron et al. 1992), while the Indiana mutation promotes the production of Aβ42 over Aβ40 (Suzuki et al. 1994; Tamaoka et al. 1994). Incorporating both mutations therefore allows studying the effects of APP/Aβ overexpression with a greater Aβ42/Aβ40 ratio.

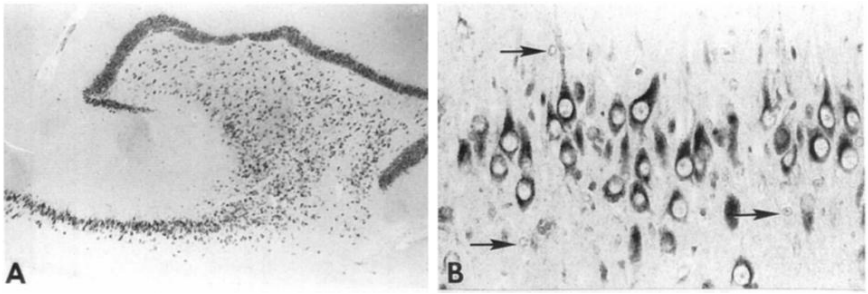

Figure 1.5 Specificity of PDGF-β immunostaining in hippocampus of nonhuman primates

Figures A and B demonstrate strong PDGF-β immunoreactivity in neurons of (A) the hippocampal formation and (B) CA2 region, with arrows in Figure B indicating a lack of immunoreactivity in glial cells (Games et al. 1995).

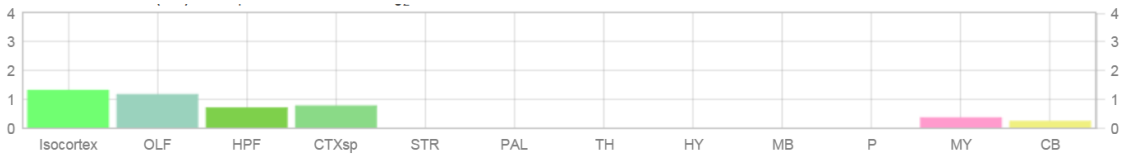

Figure 1.6 *Pdgfb* expression in mouse brain structures as illustrated by the Allen Mouse Brain Atlas

The histogram represents expression energy in each brain region, which reflects the intensity of expressing pixels normalized to the sum of all pixels. *Pdgfb* expression in a sagittal section of C57BL/6J mouse brain is detected in the isocortex, olfactory areas, hippocampal formation, cortical subplate, medulla and cerebellum. Expression is not detected in striatum, pallidum, thalamus, hypothalamus, midbrain and pons.

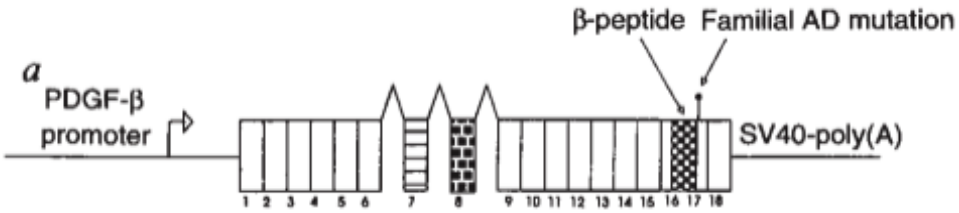

Figure 1.7 Map of the *APP* construct used to generate J20 mice

Adapted from Games et al. 1995. The original construct contains a PDGF-β promoter, full-length human APP cDNA encoding the Indiana mutation (V717F), and includes genomic sequences for for *APP* introns 6-8. The Swedish mutation (K670N/M671L) was introduced into the transgene by PCR primer modification (Hsia et al. 1999).

A list of phenotypes observed in J20 mice is presented in Table 1.4 (adapted from Alzforum.org). Diffuse plaque deposition is observed from 5-7 months, which becomes widespread by 8-10 months (Mucke et al. 2000); at the latter age, synaptic loss is observed as detected by synaptophysin staining, although this does not correlate with plaque load (Wright et al. 2013). Neuronal loss in the hippocampal CA1 region is observed beginning from 12 weeks (Wright et al. 2013), together with impairments in basal synaptic transmission, long-term potentiation at the Schaffer collateral to CA1 synapse (Saganich et al. 2006) and spatial memory deficits (Wright et al. 2013). Alterations in glial volume and density are observed from 3 months at pre-plaque stages in J20 hippocampal regions (Pomilio et al. 2015; Beauquis et al. 2014), with significant increases in reactive glial numbers from 6 months (Wright et al. 2013). These phenotypes allow the J20 mouse to be used for the study of pathogenic APP/Aβ overexpression and its consequences, including effects on neural network excitability (Bomben et al. 2014; Rubio et al. 2012; Cissé, Sanchez, et al. 2011) and the toxicity of Aβ oligomers (Mably et al. 2015). However, as seen in all *APP* single transgenic models, no NFTs are observed. J20 mice are therefore primarily models of amyloidosis rather than complete models of AD pathology.

Table 1.4 Phenotype timeline and summary of J20 phenotypes

Adapted from Alzforum.org (http://www.alzforum.org/research-models/j20-pdgf-appswind). The figure below illustrates the onset of phenotypes colour-coded accordingly in the table below.

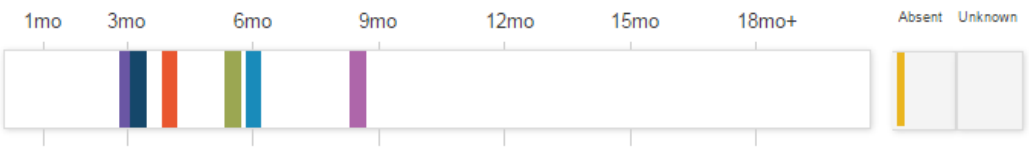

Phenotype	Details
Plaques	5-7 months: diffuse amyloid-β plaques deposit in the dentate gyrus and neocortex 8-10 months: widespread amyloid deposition observed by this age
NFTs	Absent
Neuronal loss	Neuronal loss varies by brain region. In the hippocampal CA3 region, no neuronal loss observed up to 36 weeks In the hippocampal CA1 region, neuronal loss is observed at 12, 24, and 36 weeks, but none at 6 weeks (Wright et al. 2013)
Gliosis	2-3 months: significant increase in the number of reactive GFAP+ astrocytes and CD68+ microglia in hippocampus No significant difference observed at 6 and 12 weeks (Wright et al. 2013)
Synaptic loss	8-10 months: age-dependent loss of synaptophysin immunoreactivity in presynaptic terminals observed but does not correlate with plaque load (Mucke et al. 2000)
Changes in LTP/LTD	3-6 months: significant deficits in LTP at the Schaffer collateral–CA1 synapse compared with control mice at 3-6 months (Saganich et al. 2006)
Cognitive impairment	Deficits in spatial memory and learning appear as the mice age. 16 weeks: spatial reference memory deficits measured by the radial arm maze (Wright et al. 2013) 6-7 months: spatial memory retention and acquisition deficits in the Morris water maze (Palop et al. 2003)

1.6. The Tc1xJ20 model of trisomy 21 and APP/Aβ overexpression

Table 1.5 Possible genotypes in Tc1xJ20 progeny

As Tc1 mice are not functionally trisomic for *APP*, crossing Tc1 with the J20 model of APP/Aβ overexpression allows the study of how trisomy 21 may influence AD-related phenotypes in Tc1;J20 compared to J20, due to genetic factors other than *APP* trisomy.

Female / Male	Wt	Tc1
Wt	**Wt** (Wildtype)	**Tc1** (Trisomy 21)
J20	**J20** (APP/Aβ overexpression)	**Tc1;J20** (Trisomy 21 and APP/Aβ overexpression)

The Tc1 mouse model is trisomic for ~75% of genes on Hsa21, but is not functionally trisomic for *APP* (Gribble et al. 2013; Sheppard et al. 2012). Therefore, by crossing the Tc1 model of trisomy 21 to the J20 model of APP/Aβ overexpression, we can investigate if trisomy 21 influences amyloidosis-related phenotypes observed in J20 mice, due to genetic factors other than *APP* trisomy. This is possible by characterizing and comparing phenotypes between the progeny produced by Tc1xJ20 mice (Table 1.5). The colour codes in Table 1.5 will be used to represent mice of each respective genotype in the rest of this thesis.

Studies undertaken by Dr. Frances Wiseman below have demonstrated pathological phenotypes observed in J20 mice that are exacerbated by trisomy 21 in Tc1;J20 mice.

1.6.1. Trisomy 21 exacerbates mortality associated with APP/Aβ overexpression

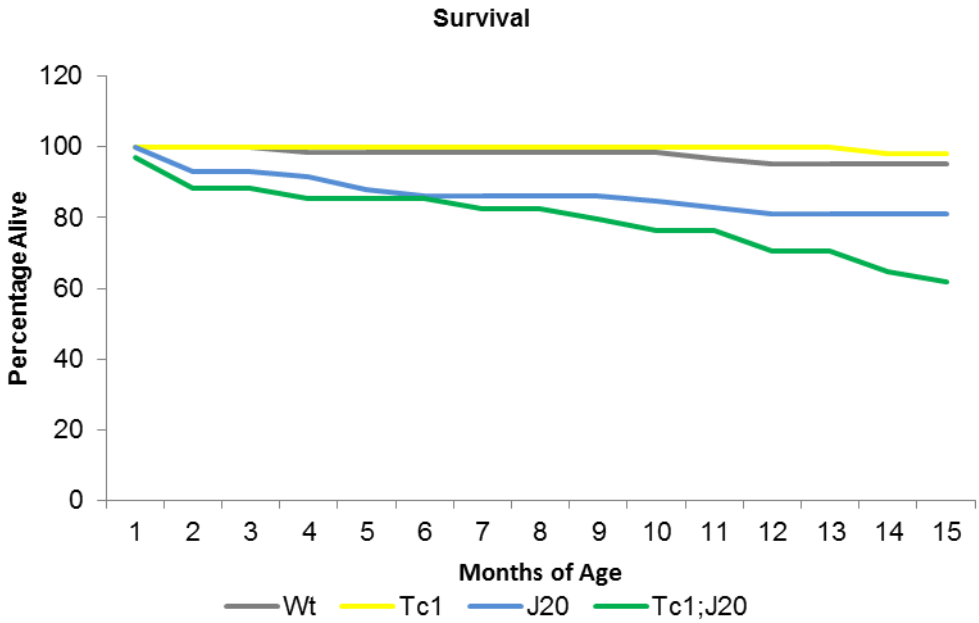

Figure 1.8 Trisomy 21 exacerbates mortality associated with APP/Aβ overexpression
Survival is significantly decreased between Tc1;J20 and J20 up to 15 months of age (X^2 = 3.88 p = 0.048).

As shown in Figure 1.8 Trisomy 21 exacerbates mortality associated with APP/Aβ overexpression, the increased mortality associated with APP/Aβ overexpression in J20 mice is worsened by the presence of trisomy 21 in Tc1;J20 mice, though trisomy 21 alone does not increase mortality in Wt mice. This suggests that trisomy 21 specifically exacerbates pathological effects of APP/Aβ overexpression, which appears to take effect throughout the lifespan.

1.6.2. Trisomy 21 exacerbates behavioural deficits associated with APP/Aβ overexpression

Trisomy 21 impairs both spatial and non-spatial short term memory deficits in Tc1;J20 compared to J20 mice, as measured respectively by novelty preference in the Sanderson Y-maze (Sanderson et al. 2009) and spontaneous alternation in a T-maze (Deacon and Rawlins 2006). In the spatial novelty preference task, the novelty

preference ratio was calculated based on time spent in a novel arm compared to a control arm to which the mouse was previously exposed to, with 1 min inter-trial intervals. Tc1;J20 mice displayed deficits in short-term spatial memory as indicated by reduced novelty preference ratios (Figure 1.9).

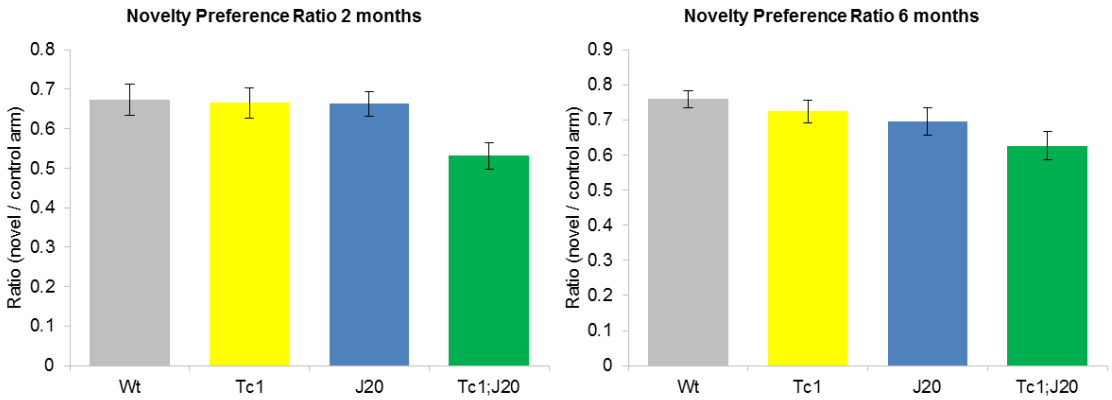

Figure 1.9 Trisomy 21 exacerbates spatial short-term memory deficits.

In a spatial novelty preference task using the Sanderson Y-maze at 1 min inter-trial intervals, the novelty preference ratio (ratio of time spent in the novel arm / control arm) was specifically reduced in Tc1;J20 mice (2-way ANOVA trisomy 21**APP* overexpression $F(1,89) = 5.736$ $p = 0.019$).

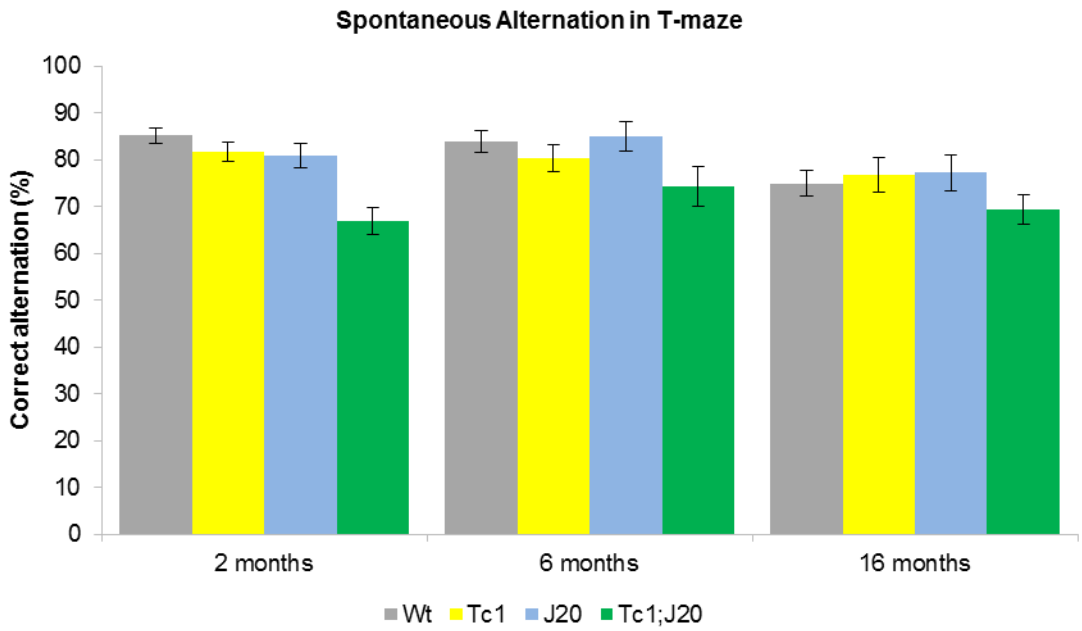

Figure 1.10 Trisomy 21 exacerbates non-spatial short-term memory deficits

In a longitudinal spontaneous alternation task, trisomy 21 significantly worsened performance in Tc1;J20 mice (2-way ANOVA trisomy 21**APP* overexpression $F(1,67) = 4.706$ $p = 0.034$).

On the other hand, spontaneous alternation in a T-maze measures non-spatial short term memory using exploratory behaviour in mice, based on the willingness to explore new environments. With repeated trials, mice should demonstrate a reduced tendency to visit a previously visited arm. In Tc1;J20 mice, deficits in short term memory were demonstrated by reduced frequencies of visiting the less familiar arm (Figure 1.10).

Trisomy 21 also aggravated hyperactive behaviour and failure to habituate to a new environment associated with APP/Aβ overexpression, as indicated by an open field test (Wright et al. 2013). Failure to habituate was demonstrated by measurement of total distance travelled in a novel open field, which mice were exposed to for 10 min on 3 consecutive days. As shown in Figure 1.11, distance travelled by Tc1;J20 mice did not decline with exposure and remained active throughout the 3 days of testing. The open field total distance travelled was significantly increased by APP/Aβ overexpression ($F(1,78) = 26.250$ $p<0.001$), trisomy 21 ($F(1,78) = 9.246$ $p=0.003$), and with a significant interaction between trisomy 21*APP/Aβ overexpression($F(1,78) = 7.818$ $p=0.007$), indicating that the hyperactivity caused by either trisomy 21 and APP/Aβ overexpression is further worsened in the presence of both conditions.

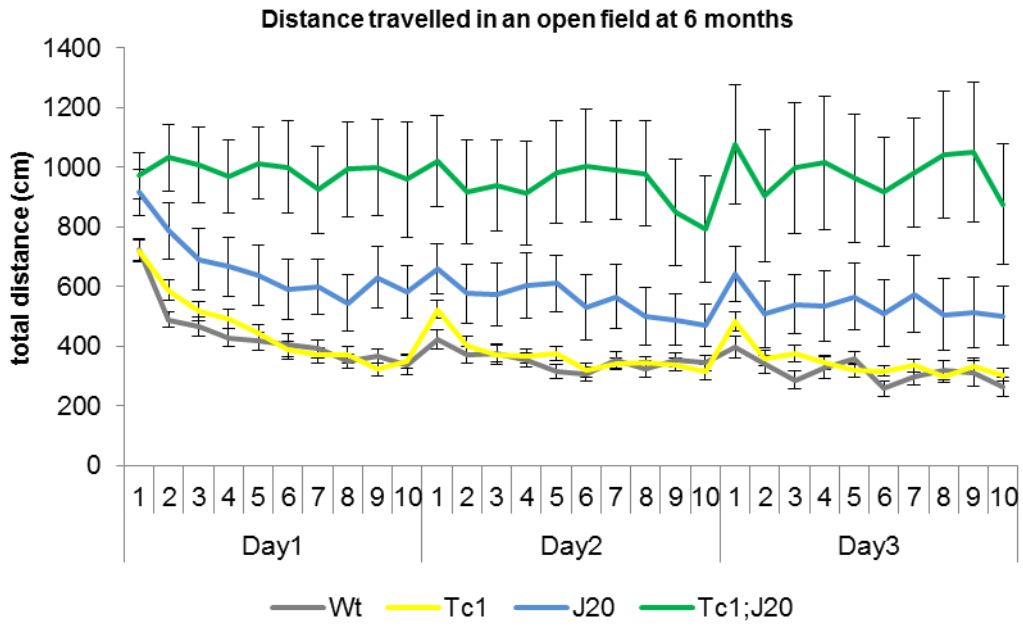

Figure 1.11 Trisomy 21 exacerbates hyperactivity and failure to habituate to a novel environment.

Total distance moved declined with exposure (exposure time in min ($F(9,702) = 20.742$ $p<0.001$), but Tc1;J20 did not show this effect with time and remained active throughout the task (2-way ANOVA time*APP/Aβ overexpression*trisomy 21 $F(9,702) = 3.436$ $p < 0.001$).

1.6.3. Trisomy 21 accelerates Aβ accumulation

Trisomy 21 strikingly accelerates Aβ deposition, as illustrated by an increase in Aβ plaque deposition in the hippocampus and cortex, in 6- and 16-month old Tc1;J20 mice compared to J20 mice. This is demonstrated by an increase in plaque number (Figure 1.12-Figure 1.13) and plaque area (data not shown), following immunohistochemistry using Aβ antibody 6F/3D.

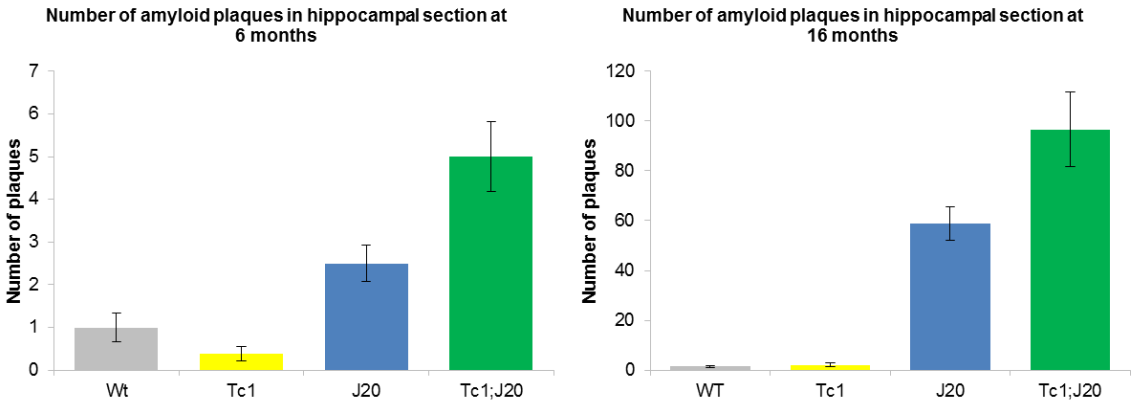

Figure 1.12 Trisomy 21 significantly increases Aβ plaque deposition in the hippocampus of mice

Trisomy 21 increases total plaque number at both 6 and 16 months (2-way ANOVA trisomy 21* APP/Aβ overexpression $F(1,77) = 6.744$ $p = 0.011$).

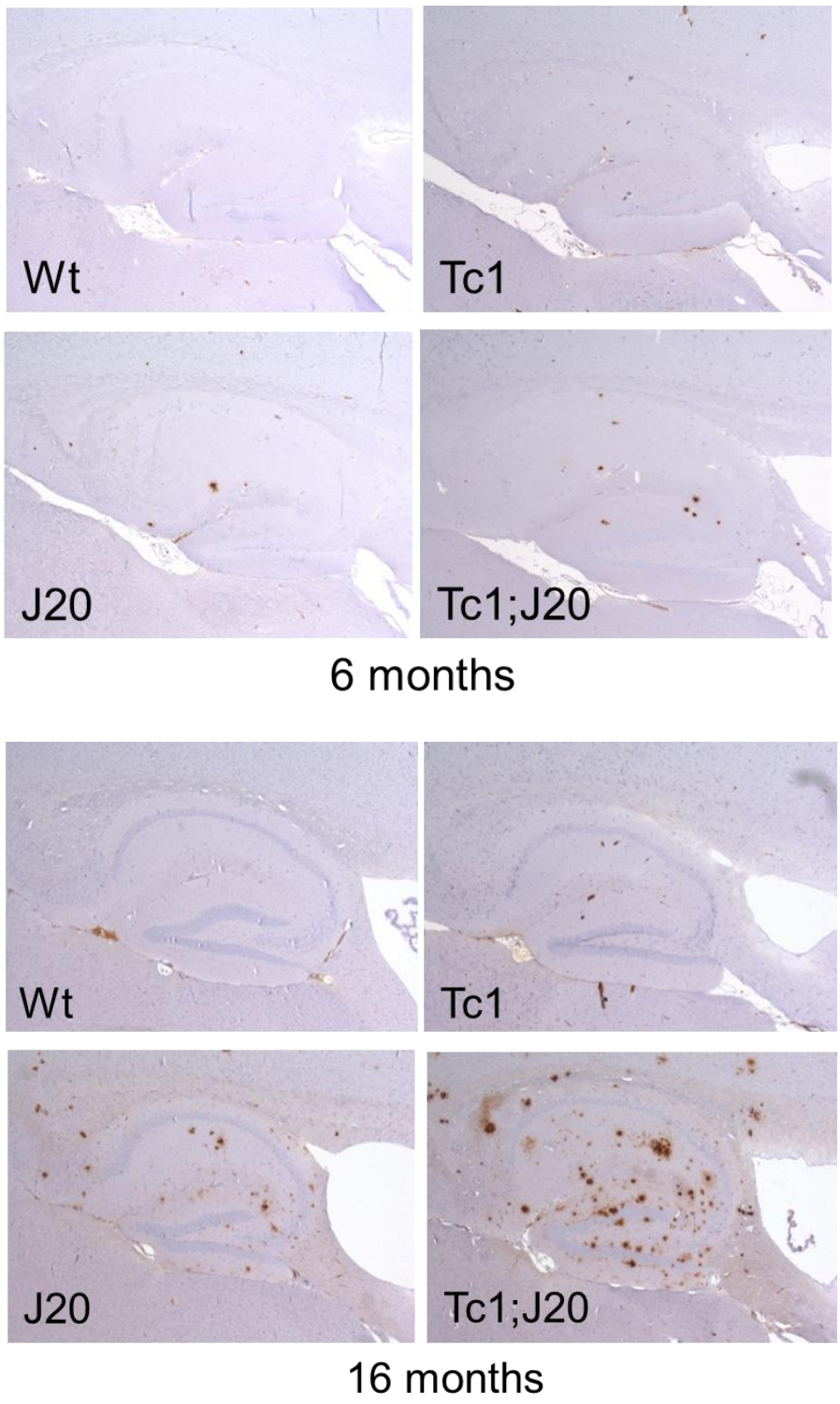

Figure 1.13 Hippocampal sections demonstrating increased Aβ plaque deposition by trisomy 21.

Only mice expressing the *APP* transgene develop plaques, therefore no Aβ deposition was observed in Wt and Tc1 mice. The number of plaques was increased in Tc1;J20 compared to J20 mice at both 6 and 16 months of age.

1.6.4. Which genes on Hsa21, other than *APP*, exacerbate APP/Aβ-related phenotypes?

As illustrated above, trisomy 21 is capable of exacerbating mortality, behavioural deficits and plaque deposition caused by APP/Aβ overexpression. Much attention in the group therefore has been focused on investigating the mechanisms that may underlie this exacerbation of Aβ accumulation, by characterizing features of Aβ production, clearance and aggregation, which are all factors that potentially influence the degree of plaque deposition.

Apart from this mechanism-driven approach, the use of DS mouse models offers the option of mapping phenotypes to dosage-sensitive regions on Hsa21. As introduced in Section 1.4.3, this has been performed by reducing the expression of trisomic candidate genes in DS models to disomic levels by crossing DS models with mice heterozygous for the candidate gene. However, this approach is unfeasible for the high-throughput screening of candidate genes, given its demands on funding, time and animal use. Chapter 3 therefore describes the development of an *in vitro* primary cortical culture model for the quicker study of AD phenotypes *in vitro* and potential use in modulating candidate gene expression for mapping purposes.

1.6.5. What phenotypes may be studied to investigate the effects of trisomy 21 on age-dependent AD pathology?

Age remains the greatest risk factor for AD and dementia, while DS has been characterized as a syndrome of accelerated aging in both epigenetic and clinical terms (Horvath et al. 2015; Zigman 2013). As Tc1xJ20 mice age, the difference in mortality rates between J20 and Tc1;J20 mice shows a trend of increasing from 12 months (Figure 1.8), although it has been difficult to demonstrate further deficits in behaviour at older ages due to a high floor effect in the tests performed (data not shown). While amyloid deposition is increased with age, amyloid burden in both patients with AD and AD mouse models has shown poor correlation with cognitive impairment and clinical progression; NFTs are the closest pathological correlate with disease. However, single *APP* transgenic models including J20 mice do not develop NFT pathology. Chapter 4 introduces a way to systematically examine glial morphological phenotypes in Tc1xJ20 mice with age, to contribute to future assessments of whether neuroinflammation may differ and interact in trisomy 21 and APP/Aβ overexpression.

1.6.6. How does trisomy 21 alter gene expression and what clues may this yield to pathophysiology?

Trisomy 21 does not only alter the expression of genes on Hsa21, but influences gene regulation on a genome-wide scale (Letourneau et al. 2014). Following RNA sequencing of 3-month old Tc1xJ20 hippocampal tissue, Chapter 5 explores how genes are differentially expressed by trisomy 21 and/or APP/Aβ overexpression, which functional changes these may be associated with and the generalizability of these results to cortical tissues affected by similar pathology.

1.7. Thesis aims

This project therefore explores complementary methods to our group's *in vivo* and *ex vivo* dissection of mechanisms underlying the exacerbation of amyloidosis by trisomy 21, with the following aims:

1. Develop an *in vitro* primary cortical cell model of AD-DS and evaluate its utility and limitations
2. Systematically quantify glial morphological phenotypes across age and genotype
3. Examine hippocampal RNA sequencing data to identify differentially expressed genes and associated functional clusters, and assess their relevance to cortical gene expression

Chapter 2. Materials and methods

Unless otherwise stated, all reagents were obtained from Thermo Fisher Scientific (including Life Technologies Corporation). Double-distilled water (ddH_2O) was obtained from a Barnstead™ Nanopure™ water purification system.

2.1. Mice

Maintenance of animals and all procedures performed were in accordance with the Animals (Scientific Procedures) Act 1986 and Home Office Project Licence number 30/2758.

2.2. Housing and husbandry of mice

Mice were housed in individually ventilated cages (Techniplast) with grade 5 dust-free autoclaved wood bedding, paper bedding and a translucent red “mouse house”. Free access to food and water was provided. The animal facility was maintained at a constant temperature of 19-23°C with 55 ± 10% humidity in a 12 h light/dark cycle. After pups were weaned at 21 days, they were moved to standardized group housing of 5 mice per cage. For breeding, mating cages set up contained two female Tc1 mice and one male J20 mouse.

2.3. Culling of mice

Pups aged 0-1 days (P0-1) used for primary cortical culture were culled via neonatal decapitation with a sharp pair of dissecting scissors. Adult mice were culled via rising levels of carbon dioxide followed by confirmation of death by cervical dislocation.

2.4. Genotyping

2.4.1. DNA isolation

Table 2.1 Reagents for DNA isolation

NaOH extraction solution			Tris neutralization buffer		
Stock	Vol. added	Final conc.	Stock	Vol. added	Final conc.
2M NaOH	187.5 µl	25 mM	1M Tris-HCl pH 5.5	600 µl	40 mM
0.5M EDTA pH 8.0	6 µl	0.2mM	ddH_2O	14.4 ml	
ddH_2O	14.8 ml				

The protocol for DNA isolation was adapted from The Jackson Laboratory (http://jaxmice.jax.org/support/genotyping/dna-isolation-protocols.html) and Truett et al. 2000. ~1 mm of tissue from tail biopsies was incubated in 75 µl NaOH extraction solution (Table 2.1) for 1 h at 98°C on a hot block. Following brief centrifugation in a microcentrifuge to collect condensation, 75 µl Tris Neutralization Buffer (Table 2.1) was added, and mixed by brief vortex. Samples were centrifuged at 21130 x g for 10 min at room temperature (RT) to pellet tissue debris. Supernatant, containing soluble DNA, was removed for use in subsequent genotyping steps, while the pellet was discarded.

2.4.2. Polymerase chain reaction (PCR) for Tc1xJ20 genotyping

Table 2.2 Genotyping primer sequences and volumes used in stock primer mixes

Tc1 primer mix

Primer name	Sequence (5' → 3')	Vol 5µM stock	Vol ddH_2O
D21S55F	GGTTTGAGGGAACACAAAGCTTAACTCCCA	20 µl	140 µl
D21S55R	CAGAGCTACAGCCTCTGACACTATGAACT	20 µl	
MyoF	TTACGTCCATCGTGGACAGCAT	10 µl	
MyoB	TGGGCTGGGTGTTAGTCTTAT	10 µl	

J20 primer mix

Primer name	Sequence (5' → 3')	Vol 5µM stock	Vol ddH_2O
IMR2044	GGTGAGTTTGTAAGTGATGCC	10 µl	140 µl
IMR2045	TCTTCTTCTTCCACCTCAGC	10 µl	
IMR0015	CAAATGTTGCTTGTCTGGTG	20 µl	
IMR0016	GTCAGTCGAGTGCACAGTTT	20 µl	

All genotyping primers were purchased from Eurofins as desalted lyophilised pellets. These were reconstituted in ddH_2O to 100 µM and stored at -20°C. Working dilutions were made to 5 µM with ddH_2O and stored at -20°C.

Genotyping for Tc1 and J20 genotypes was performed in separate parallel assays. Together with samples to be genotyped, a positive control (Tc1 or J20 DNA), negative control (Wt DNA) and no-amplification control (ddH_2O instead of DNA) were included in each assay. Supernatant obtained from the DNA isolation step (Section 2.4.1) was diluted 1:5 in ddH_2O. A PCR master mix was prepared on ice: for each sample, 8 µl Megamix-Blue (Microzone) was mixed with 1 µl Tc1 or J20 primer mix (Table 2.2). 9 µl PCR master mix and 1 µl diluted DNA were loaded into PCR tubes (Starlab), and placed in a thermal cycler with conditions defined in Table 2.3. Samples were subsequently used for agarose gel electrophoresis (Section 2.5).

Table 2.3 Thermal cycling programme for Tc1 and J20 genotyping

Tc1 programme			
Step	Temperature	Duration (min:s)	Cycles
Initial denaturation	95ºC	3:00	-
Denaturation	95ºC	0:30	35
Annealing	62ºC	1:00	
Extension	72ºC	0:45	
Reaction stop	72ºC	10:00	-
J20 programme			
Step	Temperature	Duration (min:s)	Cycles
Initial denaturation	95ºC	3:00	-
Denaturation	94ºC	0:30	30
Annealing	65ºC	1:00	
Extension	72ºC	0:45	
Reaction stop	72ºC	10:00	-

2.5. Agarose gel electrophoresis

2% agarose gels were prepared by heating 2 g UltraPure™ agarose in 100 ml 1x TBE buffer in a microwave oven until the agarose was fully dissolved. Once cooled enough to handle, 5 µl 500 µg/ml ethidium bromide (Sigma-Aldrich) was added and gently swirled to mix. The mixture was poured into a gel casting tray and allowed to set, before being submerged in 1x TBE buffer in a Horizon 11·14 Gel Casting System (Thistle Scientific). 3 µl HyperLadder IV DNA ladder (Bioline) was loaded into the first well followed by each sample. DNA fragments were electrophoresed at 130 V for 70 min, and digitally photographed under ultraviolet light using the Bio-Rad Gel Doc XR system with Quantity One software (version 4.5.1, Bio-Rad).

In Tc1 genotyping, observation of a 208 bp PCR product (D21S55F/R) together with a 245 bp product (MyoF/R) indicated a Tc1-positive genotype; the presence of the 245 bp product alone indicated a Tc1-negative genotype. For J20 genotyping, observation of a 360 bp PCR product (IMR2044/5) together with a 200 bp product (IMR0015/6) indicated a J20-positive genotype; the presence of the 200 bp product alone indicated a Tc1-negative genotype.

2.6. Quantitative PCR (qPCR) for J20 *APP* transgene copy number

Table 2.4 Primers and probes for J20 *APP* transgene copy number qPCR

Primer/Probe	Detects	5' probe label	Sequence (5' → 3')	3' probe label
oIMR1544	*APP* transgene		CACGTCGGCTCCAGCATT	
oIMR1545			TCACCAGTCATTTCTGCCTTTG	
TmoIMR0076		6-FAM	TGGGTTCAAACAAAGGTGCAA	TAMRA
oIMR5260	Endogenous *Apob*		GATGAAGATCACTGTCGCTATGAC	
oIMR5261			CATTGGACTCATGGTGGGCGGTG	
TmoIMR0107		VIC	CCAATGGTCGGGCACTGCTCAA	TAMRA

Table 2.5 Master mix (per well) for J20 *APP* transgene copy number qPCR

Component	Volume (µl) per well	Working conc. (µM)
oIMR1544	0.25	0.40
oIMR1545	0.25	0.40
TmoIMR0076	0.75	0.15
oIMR5260	0.25	0.40
oIMR5261	0.25	0.40
TmoIMR0107	0.75	0.15
ddH2O	2.5	-
TaqMan Universal PCR Master Mix	10	1x
Total volume	15	-

This protocol was adapted from that published by Jackson Laboratory (http://jaxmice.jax.org/protocolsdb/f?p=116:2:0::NO:2:P2_MASTER_PROTOCOL_ID,P2_JRS_CODE:16584,006293), and relies on the relative quantification of the *APP* transgene to internal endogenous control, *Apob,* in multiplex reactions.

DNA isolated from tail biopsies (Section 2.4.1) was diluted 1:20 in ddH_2O prior to use. As a positive control, J20 DNA with known copy number levels was obtained from Jackson Laboratory. A blank control was also included, where DNA was replaced with ddH_2O. A master mix was made up comprising TaqMan Universal PCR Master Mix, primers and probes for *Apob* and the J20 *APP* transgene as detailed in Table 2.5. 5 µl of each diluted DNA sample was run in triplicate in a 96-well plate for qPCR (Starlab). 7500 Software v2.0.1 was used to set up a standard (2 h) run, using default baseline and threshold settings and the following cycling conditions (Table 2.6).

Table 2.6 Thermal cycling programme for J20 *APP* transgene copy number qPCR

Step	Temperature	Duration (min:s)	Cycles
1	50ºC	2:00	-
2	95ºC	10:00	-
3	95ºC	00:15	40
4	60ºC	1:00	

To determine *APP* transgene copy number levels relative to *Apob*, average C_T values for *Apob* were subtracted from those of the *APP* transgene. This was expressed as a percentage of the normalised *APP* C_T observed in the positive control DNA. Tail biopsies expressing average *APP* C_T levels lower than 80% of positive control were re-tested, and the mouse was excluded from further experiments if *APP* transgene expression was shown repeatedly to be lower than 80% of positive control.

2.7. Primary cortical culture

2.7.1. Preparation of 13-mm coverslips and 12-well plates

12-well plates (SLS) and autoclaved 13-mm glass coverslips (VWR International), individually contained in 24-well plates (Appleton Woods), were coated with 30 μg/ml poly-D-lysine (PDL) in sterile distilled water for 2 h in a 37°C, 5% CO_2 incubator. These were washed three times with sterile distilled water and air-dried in a sterile cell culture laminar flow hood before use.

2.7.2. Isolation and culture of primary cells

Table 2.7 Primary cortical culture media

Dissection Medium	Plating Medium	Maintenance Medium
500 ml HBSS 5 ml HEPES 5 ml GlutaMAX™ 5 ml Sodium pyruvate 5 ml Penicillin-Streptomycin	500 ml DMEM 50 ml FBS 5 ml GlutaMAX™ 5 ml Sodium pyruvate 1 ml Penicillin-Streptomycin	500 ml Neurobasal®-A 10 ml B-27® 5 ml GlutaMAX™ 1 ml Penicillin-Streptomycin

Primary cortical cultures were prepared from pups culled by decapitation at post-natal day 0-1 (P0-1, within 48 h of birth). Heads were briefly rinsed in 70% ethanol/ddH_2O before being transferred to Dissection Medium, which was kept cold on ice prior to dissection. Tail biopsies were obtained for genotyping. As litters from the Tc1xJ20 colony result in offspring with four potential genotypes, each mouse brain was processed independently during primary culture, before their genotypes were identified.

A maximum of eight pups was used per culture to minimise cell stress due to long processing times.

Under a stereoscopic microscope, mouse brains were removed from skulls and transferred to new 6-cm petri dishes (Scientific Laboratory Supplies Ltd) with ice-cold Dissection Medium (Table 2.7). Using #5 and #5/45 forceps (Fine Science Tools), brains were divided into sagittal halves before overlying meninges were carefully removed as completely as possible. The hippocampus was dissected out, followed by cortical tissue. Cortical tissue was then cut into segments of ~1 mm in length. After three washes in 1 ml ice-cold Dissection Medium, cortical segments were incubated in 0.25% trypsin and 0.02% DNAse I in 1 ml Dissection Medium for 10-15 min in a 37ºC water bath. Each tube was inverted at 5-7 min of incubation to ensure mixing. Digested tissue was then washed three times in 1 ml Plating Medium (Table 2.7) pre-warmed to 37°C.

Tissues were subsequently dissociated by gentle trituration through autoclaved fire-polished glass pipettes (Sigma-Aldrich), with 8-10 passages up and down each pipette. Care was taken not to produce air bubbles. Samples in queue were stored in an incubator at 37°C, 5% CO_2. The crude suspension was left standing until visible tissue debris had settled.

To quantify the number of viable cells in the suspension, 10 µl 0.4% Trypan Blue (Sigma-Aldrich) was added to an equivalent volume of cell suspension, gently mixed by pipetting and loaded onto a c-chip haemocytometer (INCYTO). Under 10x magnification on a bright field microscope, the total number of white, intact cells in the 4 corner grids of 16 squares was counted. As each corner grid is equivalent to the number of cells x 10,000/ml, the total number of viable cells per ml of suspension was calculated by averaging the 4 corner grids and multiplying by 2 to account for the 1:2 dilution factor.

The cell suspension was seeded at the following concentrations, to ensure similar plating densities across both PDL-coated 12-well plates and 13-mm coverslips. In 12-well plates, 60,000 cells were seeded per well in 1 ml of Plating Medium. For 13-mm coverslips placed in a 24-well plate, a stock solution was first made at a density of 25,000 cells/100 µl Plating Medium per coverslip. 100 µl of this stock was then seeded per coverslip as a bubble. Cultures were incubated at 37ºC, 5% CO_2 for 2 h to ensure cell adherence. In 12-well plates, the Plating Medium was replaced with 2 ml

Maintenance Medium (Table 2.7) pre-warmed to 37°C. In the 24-well plate containing coverslips, 1 ml of Maintenance Medium was direct supplemented into each well. Cultures were maintained at 37ºC, 5% CO_2 and used for experiments from 14 days in vitro (DIV). At 7 DIV, 50% of the initial volume of Maintenance Medium used was supplemented to each well.

2.7.3. Collection of media and cell lysates

At 14 DIV, media was collected in 1 ml aliquots from 24-well plates containing seeded coverslips, and kept on ice. Tubes were centrifuged at 5525 x g at 4°C for 5 min to pellet cell debris. Supernatant was transferred into fresh tubes and flash frozen in dry ice, before storage at -70 °C.

Cells were lysed and harvested for DNA or protein analysis from 12-well plates. Following the removal of cell media, each well was rinsed once with sterile PBS. To harvest cells for protein analysis, cells with ice-cold RIPA buffer (150 mM sodium chloride, 50 mM Tris, 1% NP-40, 0.5% sodium deoxycholate, 0.1% sodium dodecyl sulphate) supplemented with Protease Inhibitor Cocktail Set I (PI, Merck Millipore) and removed using a cell scraper. To concentrate cell lysates obtained, 80 µl RIPA+PI buffer was shared between three wells in 12-well plates; RIPA+PI buffer used in the first well was scraped, pipetted into a second well, scraped and transferred for a third well, before being pooled together in an Eppendorf tube on ice. To reduce viscosity, lysates were treated with 1 µl Benzonase® (Novagen) for 15 min on ice, with inversion at 7-8 min. Lysates were centrifuged at 21130 x g for 15 min at 4°C to pellet cell debris. The supernatant was transferred to a new tube, flash-frozen in dry ice and stored at -70°C.

To harvest cells for DNA analysis, 75 µl of NaOH extraction buffer (Table 2.1) was used in place of RIPA buffer to lyse and scrape cells for collection. DNA extraction was subsequently performed as described in Section 2.4.1.

2.8. qPCR for Tc1 mosaicism

qPCR was used to compare relative expression of Hsa21- and mouse-specific genes in Tc1-positive cells, which are mosaic for the human chromosome. The genomic expression of human *CLDN8,* an Hsa21-encoded gene, was quantified by standard curve and expressed as a proportion of a mouse gene, *Apob*. Primer and probe

sequences were designed using Primer Express 3.0.1 software across exon-intron boundaries, against a series of Hsa21 genes intact in the Tc1 chromosome (Gribble et al. 2013). The specificity of these sequences for human and not mouse DNA was tested *in silico* using Electronic PCR (NCBI). *CLDN8* was subsequently selected for this assay due to its specificity for human DNA and acceptable primer and probe properties for qPCR (Table 2.8). Primers for *CLDN8* were obtained from Eurofins, while the probe was obtained from Life Technologies**.**

Table 2.8 *CLDN8* primers and probe

Primer /Probe	Sequence	T_M (ºC)	%GC	Length
Forward primer	GCTTCCCAGGTAAAAGCAATCTT	58.8	43	23
Reverse primer	TGGGACCAAGGGATAAAATAAATTAT	58.2	31	26
Probe	AATCCCCTACTCTCGTTTCACTTTGGCATTTC	69.4	44	32

To confirm the specificities of the primer and probe sequences for *CLDN8* and *Apob* to human and mouse DNA respectively, human genomic DNA (kindly provided by Gary Adamson) and DNA from wildtype mouse tail biopsies were used across concentrations ranging from 1.56-100 ηg/µl in multiplex qPCR. A confirmed human-specific qPCR primer and probe mix for Rnase P was used as a positive control for human DNA. qPCR cycle conditions used were identical to those described in Table 2.6.

To quantify mosaicism in DNA obtained from primary cortical cells, an eight-point standard curve was created for each assay plate using a mixture of human DNA and mouse DNA. The standard curve for human DNA included concentrations at 10, 7.5, 5, 2.5, 1.25, 0.625, 0.313 and 0.156 ηg/µl, while those for mouse DNA were 60, 40, 20, 10, 5, 2.5, 1.25 and 0.625 ηg/µl. Each standard and cell DNA sample was performed in triplicate. A master mix was made comprising TaqMan Universal PCR Master Mix, primers and probes for *CLDN8, and Apob or RNASEP* (Table 2.9). qPCR cycle conditions used were identical to those described in Table 2.6.

Table 2.9 Master mix (per well) for mosaicism qPCR

Component	Volume (µl) per well	Dye and Quencher
CLDN8 forward primer	0.1875	
CLDN8 reverse primer	0.1875	
CLDN8 probe	0.5625	FAM and TAMRA
Apob forward primer	0.1875	
Apob reverse primer	0.1875	
Apob probe	0.5625	VIC and TAMRA
ddH2O	4.625	
TaqMan Universal PCR Master Mix	7.5	
Total volume	14	

Standard curves for both human and mouse genomic expression were presented as semi-log regression line plots of C_T values against log concentration of standards. The accuracy of standard curves was only acceptable if the correlation coefficient (R^2) of regression lines was >0.99. C_T values were first checked to ensure they fell within the range of the standard curve. The concentrations of *CLDN8* and *Apob* gene content were then calculated from the equation of the regression line plot.

2.9. RNA extraction from adult mouse cortical tissue

RNA extraction was performed on cortical tissue in a fume hood decontaminated with *RNaseZap*® to remove RNases. Frozen cortical tissue (not allowed to thaw) from one hemisphere per mouse was homogenised using a TissueRuptor homogenizer (QIAGEN) in 700 µl QIAzol Lysis Reagent (QIAGEN), in 15 ml Falcon tubes. Homogenised tissue was allowed to stand at RT for 5 min to promote the dissociation of nucleoprotein complexes, before removing 300 µl to be flash-frozen and kept as stock at -70ºC. 80 µl chloroform was added to the remaining 400 µl homogenate, vigorously shaken by hand for 15 s, and left to stand for 3 min at RT. To separate the mixture into phases, homogenates were centrifuged at 6000 x g for 45 min at 4°C. The uppermost layer containing a colourless aqueous phase was transferred to a new collection tube, avoiding contamination by the lower phases. 1.5 volumes of 100% ethanol was added to each tube, and mixed by pipetting. This mixture was used for total RNA purification in subsequent steps.

Total RNA purification was performed with the miRNeasy Mini Kit (QIAGEN), which allowed the purification of total RNA of ~18 nucleotides and above. Centrifugation steps were modified from the manufacturer's protocol. Samples obtained from RNA extraction were loaded onto spin columns provided in the kit and centrifuged at 5600 x g for 2 min at RT. 700 µl RWT Buffer was loaded into the spin columns and centrifuged

at 10,000 x g for 15 s at RT. This was repeated with 500 µl RPE Buffer. A second wash with 500 µl RPE Buffer was performed with centrifugation at 10,000 x g for 2 min at RT. Spin columns were transferred to a new collection tube. RNA was eluted by the addition of 50 µl RNase-free water and centrifugation at 10000 x g for 1 min at RT. Freshly-eluted RNA was kept on ice for further use, or flash-frozen in dry ice for storage at -70 °C.

2.10. Determining concentration and purity of nucleic acids

Nucleic acid concentration was determined by measuring absorbance at 260 nm (A_{260}) using a NanoDrop™ ND-1000 spectrophotometer (NanoDrop Technologies). The ratio of absorbance at 260 nm and 280 nm was used to assess the purity of DNA and RNA. For pure DNA and RNA, the A_{260}/A_{280} ratio was expected to be ~1.8 and ~2.0 respectively.

2.11. Reverse transcription with elimination of genomic DNA

Reverse transcription of RNA was performed with the QuantiTect® Reverse Transcription Kit (QIAGEN), on bench space decontaminated with *RNaseZap*® to remove RNases. To control for potential genomic DNA contamination, “no amplification controls” were carried out in parallel with all reverse transcription RNA samples; these controls replaced reverse transcriptase with RNase-free water in assays.

All steps were performed according to the manufacturer’s protocol. RNA samples were thawed on ice and aliquots were diluted with RNase-free water to make 2 µg in 24 µl. To eliminate genomic DNA, 4 µl gDNA Wipeout Buffer was added to each aliquot of diluted RNA, incubated for 2 min at 42°C, before being held on ice. Two sets of master mixes were made for reverse transcription and for “no amplification controls”, comprising Quantiscript reverse Transcription buffer, reverse transcription primer mix, and either Quantiscript reverse transcriptase or RNase-free water respectively (Table 2.10). 14 µl RNA samples were incubated with 6 µl of their respective master mixes for 15 min at 42°C for reverse transcription, followed by 3 min at 95°C to inactivate reverse transcriptase. cDNA obtained was used directly for qPCR or stored at -20°C.

Table 2.10 Master mixes for reverse transcription and "no amplification controls"

Component	Reverse transcription master mix / sample (µl)	"No amplification control" master mix / sample (µl)
Quantiscript reverse transcriptase	1	0
RNase-free water	0	1
5x Quantiscript reverse transcription buffer	4	4
Reverse transcription primer mix	1	1
Total volume	6	6

2.12. Reverse transcription qPCR (qRT-PCR)

Cortical and hippocampal cDNA obtained following reverse transcription (Section 2.11) was used to quantify candidate gene RNA expression. cDNA was diluted 1:10 in ddH_2O for initial experiments, though the assays for *Arc* required the use of more concentrated cDNA. An eight-point standard was created for each assay plate using wildtype cortical or hippocampal cDNA accordingly, starting from 50 ηg/µl to 0.39 ηg/µl in 1:2 serial dilutions in ddH_2O. All cDNA samples were run with no amplification controls, with all samples, controls and standards in triplicate.

All mouse primer/probe sets for genes of interest, apart from *App*, were obtained from Life Technologies. Mouse *Gapdh* and *Actb* were used as endogenous reference genes. Details for primers and probes used are listed in Table 2.11. Master mixes for qPCR reactions are listed in Table 2.12. qPCR cycle conditions used were identical to those described in Table 2.6.

Table 2.11 Primers and probes for qRT-PCR

Primer/Probe	5' probe label	Sequence (5' → 3')	3' probe label
App forward primer	-	CTCCAGCCGTGGCACC	-
App reverse primer	-	AGTCCTCGGTCAGCAGCG	-
App probe	FAM	ACTCTGTGCCAGCCAATACCGAAAATGA	TAMRA
Gene	5' probe label	Product number (Life Technologies)	3' probe label
Actb	VIC	4352341E	MGB
Arc	FAM	Mm01204954_g1	MGB
Chrm4	FAM	Mm00432514_s1	MGB
Dusp1	FAM	Mm00457274_g1	MGB
Egr1	FAM	Mm00656724_m1	MGB
Fos	FAM	Mm00487425_m1	MGB
Gapdh	VIC	4352339E	MGB
Per1	FAM	Mm00501813_m1	MGB
Snx27	FAM	Mm01261511_mH	MGB

Table 2.12 Master mix (per well) for qRT-PCR

Component	Volume (µl) per well	Final conc.
TaqMan Universal PCR Master Mix	7.5	1x
Gapdh/Actb assay (20x)	0.3	0.4 µM
Candidate gene assay (20x)	0.3	0.4 µM
ddH_2O	0.4	-
Total volume	14	-

2.13. Protein extraction from adult mouse hippocampal and cortical tissue

Frozen cortical and hippocampal tissue were thawed on ice. Tissues were homogenised using a TissueRuptor homogenizer (QIAGEN) in RIPA buffer with protease inhibitor cocktail I (Section 2.13). Hippocampal tissue was lysed in 100 µl RIPA+PI buffer, while cortical tissue was lysed in 500 µl. Homogenates were aliquoted and kept on ice for subsequent use, or flash-frozen in dry ice for storage at -70 °C.

2.14. Quantifying protein concentration in brain homogenates and cell lysates

To determine total protein concentration in brain homogenate, Bio-Rad protein assay dye reagent concentrate was used (Bio-Rad). For cell lysates, the more sensitive QuantiPro™ BCA Assay Kit (Sigma-Aldrich) was used. Both methods were compatible with RIPA as the lysis buffer.

The Bio-Rad microassay procedure was used according to manufacturer's protocol. BSA standards in PBS were made up at 1000, 500, 400, 300, 200, 100, 50, 25 and 0 mg/ml. Brain homogenates in RIPA buffer were completely thawed on ice, and thoroughly mixed by vortex. The Bio-Rad reagent was diluted 1:5 in ddH_2O, while homogenate samples were diluted 1:5 in RIPA. 5 µl of diluted samples or standards were mixed with 200 µl of diluted reagent per well in a clear 96-well plate (Greiner Bio-one), with each sample or standard in triplicate. The plate was incubated for 10-15 min at RT, with gentle agitation on a platform shaker. Absorbance at 595 nm was measured in a TECAN plate reader (Sunrise).

To determine cell lysate protein concentration, the QuantiPro™ BCA Assay Kit was used as it was a more sensitive assay allowing the dilution of cell lysates at 1:200. Cell lysates were diluted 1:200 in ddH_2O prior to use (2.5 µl sample, 497.5 µl ddH_2O), and the assay was performed according to the manufacturer's protocol. Standards were made using the protein standard provided (Sigma-Aldrich P0914, 1.0 mg/ml BSA in 0.15 M sodium chloride, 0.05% sodium azide) at concentrations of 300, 200, 100, 50, 5 and 0 µg/ml. 150 µl of diluted sample or standard and 150 µl Working Reagent were mixed per well in a clear 96-well plate, in triplicate. Plates were sealed and placed on a hot block at 60°C for 1 h. After cooling to room temperature, plates were briefly centrifuged to collect condensation, and absorbance at 562 nm was measured in a TECAN plate reader (Sunrise).

In both protein quantification assays, protein concentration was calculated from the regression line plot obtained by plotting standards against absorbance signal. Standards were only deemed accurate enough if correlation coefficients (R^2) exceeded 0.99.

2.15. Western blots

2.15.1. Sodium dodecyl sulphate-polyacrylamide gel electrophoresis (SDS-PAGE)

Samples for protein analysis were prepared by the addition of LDS Sample Buffer (final dilution 1:4) and β-mercaptoethanol (final dilution 1:10) to working concentrations, generally 2 µg/µl. Prior to SDS-PAGE, samples were boiled for 10 min at 100°C on a hot block. Following brief centrifugation to collect condensation, samples were loaded onto pre-cast NuPAGE Novex 4-12% Bis-Tris 1.0 mm protein gels, in an XCell Surelock™ Mini-Cell Electrophoresis System, containing 1x MES SDS running buffer. SeeBlue® Plus2 pre-stained protein standard was used as a molecular weight marker. Gels were electrophoresed at 130 V for 90 min.

2.15.2. Transfer of proteins to membranes by electroblotting

Following SDS-PAGE, proteins separated down the gel were electroblotted onto PVDF or nitrocellulose (Pall) membranes. PVDF membranes were pretreated by soaking in 100% methanol for 30 s, ddH_2O for 5 min and left to equilibrate in Tris-Glycine Transfer Buffer (100 µl 10x Tris-Glycine Transfer Buffer (Geneflow), 200 µl methanol, 700 µl ddH_2O) for 5 min. No pretreatment was necessary for nitrocellulose membranes. Six sponge pads and four pieces of filter paper (Sigma-Aldrich) in matching sizes were also soaked in Transfer Buffer prior to use. The gels, sponges and filter paper were assembled in the electrophoresis system with care to remove air bubbles that would interfere with electroblotting. The system was rinsed with ddH_2O to remove excess MES buffer prior to inserting the blot module. Transfer Buffer was poured into the blot module, checked for leakage, before the rest of the tank surrounding the module was filled with ddH_2O. Electrophoresis was performed at 35 V for 2 h at RT.

2.15.3. Immunodetection

Membranes were removed from the electrophoresis system and placed into separate square petri dishes. To reduce non-specific antibody binding, membranes were blocked with 5% skim milk powder or 5% BSA, both diluted in PBS-T (100 ml 10x PBS, 900 ml ddH_2O, 500 µl Tween® 20 (Acros Organics))**,** for 1 h at RT with gentle agitation on a platform shaker. Membranes were rinsed in PBS-T before being divided into strips

across appropriate molecular weight markers. Incubation was performed with primary antibodies (Table 2.13) diluted in 1% BSA/PBS-T overnight at 4°C, with gentle agitation. At RT, membranes were then washed three times in PBS-T over 45 min, before incubation with secondary antibodies (Table 2.13) in 1% BSA/PBS-T for 1 h at RT. Infrared dye-conjugated secondary antibodies (LI-COR) were protected from light during incubation by wrapping dishes with aluminium foil. This was followed by a further three washes in PBS-T over 45 min, and one wash with ddH_2O.

Table 2.13 Primary and secondary antibodies used for western blots

Primary antibodies					
Antibody/Antigen	Host	Dilution	Supplier	Product no.	Remarks
APP (C-terminal)	Rabbit	1:5000 (cells)	Sigma-Aldrich	A8717	Polyclonal
BACE1	Rabbit	1:5000 (cells)	Abcam	Ab108394	Polyclonal
β3-tubulin	Mouse	1:5000 (cells, homogenate)	DSHB	E7-c	Monoclonal
β-Actin	Mouse	1:80000 (cells, homogenate)	Sigma-Aldrich	A5441	Monoclonal
β-Amyloid 1-16 (6E10)	Mouse	1:1000 (cells)	Covance	SIG-39320	Monoclonal, detects human APP
GAPDH	Rabbit	1:50000 (cells, homogenate)	Abcam	Ab9485	Polyclonal
GFAP	Rabbit	1:5000 (cells, homogenate)	Dako	Z0334	Polyclonal
S100β	Rabbit	1:5000 (homogenate)	Abcam	Ab52642	Monoclonal
Secondary antibodies					
Antibody/antigen	Conjugate	Dilution	Supplier	Product no.	Remarks
Anti-mouse	HRP	1:10000	Dako	P0260	
Anti-rabbit	HRP	1:10000	Dako	P0448	
Anti-mouse	IRDye 800CW	1:10000	LI-COR	926-32210	
Anti-mouse	IRDye 680LT	1:10000	LI-COR	926-68020	
Anti-rabbit	IRDye 800CW	1:10000	LI-COR	926-32211	
Anti-rabbit	IRDye 680RD	1:10000	LI-COR	926-68071	

2.15.4. Visualisation and quantification of protein bands

Proteins incubated with secondary antibodies conjugated to infrared dyes (IRDye, LI-COR) were visualized using the Odyssey Infrared Imaging System (LI-COR), at medium scanning quality. Intensity settings for the 700 nm and 800 nm channels were adjusted accordingly for optimal signal. Images were directly acquired and saved using the Odyssey software. Densitometric analysis of protein bands of interest was performed by encompassing bands of interest and background signal in selection rectangles of the same size. Background signal was then subtracted from signal obtained from each protein band.

Proteins incubated with secondary antibodies conjugated to horseradish peroxidase (HRP) were visualised using SuperSignal™ West Pico Chemiluminescent Substrate to produce a chemiluminescent signal, exposed to X-ray film (General Electric), and developed and fixed with an Xograph Imaging Machine (Xograph Imaging Systems). Developed blots were scanned for digital analysis using an HP Scanjet N6350 scanner. After importing into ImageJ software (National Institutes of Health, USA) and converting into 8-bit images, densitometric analysis was performed using the same principles as those described in Odyssey.

2.15.5. Loading controls

In all western blots, variations in amount of protein loaded were controlled for by normalising signals obtained from protein bands of interest to endogenous housekeeping proteins, β-Actin or GAPDH.

2.16. Quantification of Aβ peptides

To quantify Aβ38, Aβ40 and Aβ42 peptide levels, the V-PLEX Aβ Peptide Panel 1 (6E10) Kit (Meso Scale Diagnostics) was used according to the manufacturer's protocol. Conditioned media collected from primary cortical cultures was thawed completely in ice and mixed by vortex. 1000 ml wash buffer (PBS-T) was made comprising 1x PBS and 0.05% Tween-20, and dispensed into a squeeze bottle. 8-point calibrator standards for each of the three peptides were made up as 1:2 serial dilutions in Diluent 35. Conditioned media samples were also diluted 1:2 in Diluent 35, making up 200 µl per sample. Detection antibody solution and read buffer were also diluted according to manufacturer's protocol.

150 µl Diluent 35 was added per well for blocking, and incubated for 1 h at RT with agitation on a platform shaker. Wells were subsequently washed three times in wash buffer. 25 µl detection antibody solution was added to each well, followed by standards or samples, in triplicate. This was left to incubate for 2 h at RT on a shaker. During this time, concentration values for each Aβ standard, as well as the layout of samples, were programmed into the MSD Discovery Workbench® analysis software (Meso Scale Discovery). After incubation, wells were washed three times in wash buffer. 150 µl 2x Read Buffer T was added quickly but carefully to avoid air bubbles, and the plate was immediately read by the MSD imager.

2.17. Immunostaining of cultured cells

2.17.1. Fixing of cells

Primary cortical cultures were grown on PDL-coated 13 mm coverslips, each contained in a well of 24-well plates, as described in Section 2.7. To fix cells, culture media was removed and wells were washed once with sterile PBS (Sigma-Aldrich). Coverslips were then fixed in 4% paraformaldehyde (6 ml 10% PFA, 1.5 ml 10x PBS, 7.5 ml ddH_2O) for 10 min at RT. Cells were washed three times in PBS to remove excess fixative solution, before immediate subsequent use for immunofluorescent staining, or storage at 4°C.

2.17.2. Immunofluorescent staining

To permeabilise cells, coverslips were incubated with 0.1% Triton X-100/PBS for 5 min at RT, followed by one wash with PBS. Cells were then blocked with 5% BSA/PBS for 30 min at RT. This was followed by incubation with primary antibodies (Table 2.14) diluted in PBS, for 1 h at RT. Coverslips were washed three times with PBS, before incubation with Alexa® fluorescent dye-conjugated secondary antibodies (Table 2.14) diluted in PBS, for 1 h at RT, protected from light. Coverslips were washed three times in PBS, before being mounted on SuperFrost® microscope slides in ProLong® Gold Antifade Mountant. This mountant contains DAPI as a nuclear stain. Immunofluorescent staining was visualised by an Axioplan Imagine 2 upright microscope (Zeiss) within 48 h. Prior to visualization, slides were stored in 4°C protected from light.

To control for possible non-specific background from secondary antibodies, one coverslip per genotype per culture was treated as above but without incubation with NeuN primary antibody. At the same time, to control for background from non-specific immunoglobulin binding, a negative isotype control was also included where the NeuN primary antibody was replaced with a rabbit IgG antibody (Vector) at the same concentration (Table 2.14).

Table 2.14 Primary and secondary antibodies used for immunofluorescent staining

Primary antibodies					
Antibody/Antigen	Host	Dilution	Supplier	Product no.	Remarks
NeuN	Rabbit	1:500	Abcam	ABN78	
Rabbit IgG	Rabbit	1:500	Millipore	X0720	
Secondary antibodies					
Antibody/antigen	Conjugate	Dilution	Supplier	Product no.	Remarks
Anti-rabbit	Alexa Fluor® 488	1:1000	Abcam	Ab150077	

2.17.3. Visualisation and quantification

NeuN- and DAPI-stained cells were visualised using an Axioplan 2 Imaging upright microscope (Zeiss). Image acquisition was performed with AxioVision SE64 software (release 4.9.1, Zeiss). As NeuN-positive neurons tended to cluster toward the centre of the coverslip, becoming radially more infrequent, five fields of view were acquired to include as many NeuN-positive cells as possible on the coverslip for analysis. These included the field of view at the centre of the cluster, as well as the fields of view immediately adjacent to the left, right, top and bottom of the centre field.

To quantify the number of NeuN- and DAPI-positive cells, the Image-based Tool for Counting Nuclei (ITCN) plugin (UC Santa Barbara) was used in ImageJ. Parameters used for successfully separating and identifying NeuN and DAPI-positive cells are listed in Table 2.15.

Table 2.15 Parameters to count objects using ITCN in ImageJ

	DAPI	NeuN
Width	12 pixels	12 pixels
Minimum distance	6 pixels	6 pixels
Threshold	0.3	0.5

2.18. Histology

Brains were processed and labelled by Dr. Frances Wiseman and the MRC Prion Unit Histology department. Half brains were fixed by immersion in 10% buffered formal saline. Fixed brains were processed with increasing concentrations of industrial methylated spirits (1 x 70% and 5 x 100%, 1 h each), cleared with xylene (3 x 1 h) to complete dehydration and immersed through three wax changes. Molten paraffin wax was prepared and used to embed brains in sagittal orientation. Sections were cut using a Leica RM2135 microtome (Milton Keynes, UK) to a thickness of 5-10 µm. Serial sections were mounted on Superfrost™ microscope slides and air-dried for 2 h at 37ºC, and for 16 h at 60ºC.

Tissues were incubated in primary antibodies using the automated Ventana Discovery immunohistochemical staining machine (Ventana Medical Systems) and proprietary reagents (Roche). Tissues were placed in the Ventana machine and dewaxed automatically. For antigen retrieval Iba1 slides received standard cell conditioning heat treatment, and GFAP slides were incubated with proprietary Protease 1 for 4 min. Non-specific binding was inhibited by incubating sections with Superblock for 8 min. Sections were incubated with anti-Iba1 for 4 h (DAKO 019-19741, 1:250), and in parallel sections incubated with anti-GFAP for 32 min (DAKO clone Z0334, 1:1000). Sections were washed in Reaction Buffer to remove excess primary antibody. This was followed with incubation in swine anti-rabbit secondary antibody for 32 min (DAKO E0353, 1:200). To visualise antibody labels, sections were incubated with the DABMap kit and counterstained using haematoxylin and Bluing Reagent. Slides were then washed in hot soapy water to remove proprietary reagents and manually rehydrated through a series of alcohols and xylene, before mounting with coverslips using an automated system (Diapath automated coverslipper, Martinengo, Italy).

2.19. Image acquisition and processing

To systematically quantify the area of staining and morphological properties of astrocytes (labelled with GFAP) and microglia (labelled with Iba1), a digital analysis protocol was developed with Dr. Matthew Ellis, with assistance from Matthew Rickman in segmenting cortical and hippocampal regions of interest (Department of Neurodegenerative Disease, UCL Institute of Neurology). Histology slides were digitally acquired using a Leica SCN400F Slide Scanner (Leica Microsystems) at 40x magnification and 65% image compression during export. Images of slides were stored on Leica Slidepath (Leica Microsystems). Digital image analysis and protocol development was performed using Definiens Developer 2.3 (Definiens). The methods below describe the general processes and parameters used to achieve each objective during the development of the protocol; the full source code for the protocol can be found on the Definiens directory > Ruleset > Choong.X. The protocol for Iba1 is named “Iba1.v1.5.5-final.dcp”, while the one for GFAP is “GFAP.v1.5.5-final.dcp”. All imaging and quantification experiments were performed blinded to genotype to eliminate experimenter bias.

The protocol was initially developed using a GFAP image from a 16-month old mouse from Tc1xJ20, which featured the most extensive astrogliosis, including broad regions where astrocytic processes overlapped. As one of our objectives was to systematically identify individual astrocytes within clusters of cells, we used this image to ensure our selection parameters were sufficiently stringent to be applied uniformly to all samples.

Table 2.16 below summarises the flow of the processes in the digital protocol, together with the objectives and general parameters used for each step.

Table 2.16 Processes used to quantify GFAP (astrocytes) and Iba1 (microglia) area of staining and individual cell morphology in hippocampal sections

Process	Objective	Parameters
Identify cortical and hippocampal tissues	Segment cortical and hippocampal tissues	Outlines were traced by Matthew Rickman
	Exclude artefacts due to damage during histology processing	Outlines of damaged regions were traced by Matthew Rickman and excluded from analysis
Distinguish "true" brown staining from background	Identify dark brown stain	5^{th} centile of brown staining intensity was calculated to identify top 5% of stained tissue + 0.5 of remaining brown staining used as threshold following sampling
	Identify medium and light brown staining	By dividing the image into 5-pixel "chess board" pieces, within each piece top 80% x 2 = medium brown; top 80% = light brown
	Exclude background signal	The mean brightness of the homogenous white region and the periphery of the slide was used to exclude background
		Remove brown stains that have more dark blue than brown
Identify individual cell bodies, separate overlapping processes, remove inseparable clusters	Separate cells with overlapping processes	Shrink dark brown staining by 1 pixel, to identify break points for individual cells, and then grow back into area shrunk, extending into medium and light brown area. Further steps taken to grow dark brown areas into larger dark brown areas with even brown staining.
	Identify cell bodies	Identified using a "rolling ball" of different diameters to "roll" within cell bodies
	Exclude capillaries and other artefacts	Exclude brown objects > 200 μm^2, or >100 μm^2 and length/width > 2.5,
	Identify inseparable clusters	Brown areas >2000 μm^2 continuous area, or >1000 μm^2 AND > 3 cell bodies
	For microglia: remove false positive cell bodies	Cell bodies <40 μm^2, or with elliptic fit <0.65
Output phenotypes	Area of staining	Values of brown for cell bodies, processes and inseparable clusters summed up
	Number of astrocytes	Number of cell bodies was counted
	Length of midline	Distance was measured between the two longest processes
	Number of branches per astrocyte	Number of branches per astrocyte was calculated from the midline, not the cell body, due to technical limitations
	Length and width of astrocytes	These were calculated from the shape that was used to 'box in' the edges of an astrocyte
	Size of cell bodies	Area of cell bodies
	Staining intensity of cell bodies	Staining intensity of cell bodies was normalized to background by subtracting the mean signal for the unstained region

2.20. Two-dimensional fluorescence *in situ* hybridisation (2D-FISH)

The 2D-FISH protocol below was performed by Dr. Frances Wiseman.

Paraffin-embedded tissue sections were heated for 20 min at 60°C to dewax, and placed into xylene for 4 x 10 min. Sections were rehydrated through a series of alcohol dilutions, from 100% ethanol for 4 x 10 min, 95% ethanol for 2 x 5 min, 70% ethanol for 2 x 5 min, before being placed into water. Sections were transferred to 0.1 M citrate buffer (pH 6) and heated in a microwave oven for 20 min, allowed to cool for 20 min in citrate buffer, washed and stored in ddH_2O.

To prepare probe and hybridisation mix for later use, 100 ηg of probe for genomic DNA was dispensed per slide, together with 5 µg sonicated salmon sperm and CotI DNA per slide. 2 volumes of 100% ethanol were added followed by centrifugation in a centrifugal evaporator to pellet and dry the probe. Hybridization mix was prepared as follows for every 100 µl hybridization mix: 50 µl deionized formamide, 20 µl 50% dextran sulphate, 10 µl 20x saline-sodium citrate buffer (SSC), 1µl Tween-20 and 19 µl ddH_2O. 10 µl of hybridization mix was added to probe per slide. This was mixed well and briefly centrifuged. Probes were left to dissolve in hybridisation mix for 1 h.

To prepare for FISH, sections were aged for at least 2 days, before incubation in 2x SSC and 100 µl/ml RNase for 1 h at 37°C. This was followed by a quick wash in 2x SSC. Sections were dehydrated through 70%, 90% and 100% ethanol for 2 min each, before being air dried. An oven was warmed up to 70°C in the meantime, and sections were placed at 70°C for 5 min. Sections were then denatured in 70% formamide/2x SSC (pH 7.5) for 90 s at 75°C, before being placed in ice-cold 70% ethanol for 2 min. These were dehydrated through 90% and 100% ethanol for 2 min each, before being air dried.

As sections were drying, probe and competitor DNA in hybridisation mix was denatured at 70 ºC for 5 min. This was transferred to a 37°C water bath to preanneal for 15 min. Sections were also moved to warm on a 37°C hot block. 10 µl of preannealed probe and hybridisation mix were loaded onto a coverslip and placed over the section, with care taken to avoid formation of air bubbles. Coverslips were sealed rubber cement and incubated in a covered tray overnight at 37°C in a water bath.

Blocking buffer was made containing 5% skim milk powder in 4x SSC, warmed up to 37°C in a water bath to dissolve milk powder before storage on ice. This blocking buffer was used to dilute primary antibodies (FITC anti-digoxigenin at 1:30, FITC anti-sheep at 1:100). Antibody mixtures were centrifuged for 15 min at 4°C to precipitate clumps and kept on ice.

Following overnight incubation, rubber sealant was peeled off the slides, which were washed 4 times in 2x SSC at 45°C for 3 min each. This was followed by 4 washes in 0.1x SSC at 60°C for 3 min each, before being transferred to 4x SSC with 0.1% Tween-20. Each section was incubated with 40 μl blocking buffer under a coverslip, for 5 min at RT. The coverslip was removed, and primary antibody solutions were added to each slide, before incubation in a moistened chamber for 30-60 min at 37°C. Excess fluid was drained, sections were mounted in 25 μl Vectashield mountant containing DAPI, and sealed with rubber cement.

2.21. RNA sequencing

Extraction and purification of RNA was performed by Dr. Frances Wiseman as described in Section 2.9 before being transferred to UCL Genomics for further processing**.** RNA samples were checked for quality using a Bioanalyzer (Agilent). RNA was prepared for sequencing from 500 ηg of total RNA, following the Illumina TruSeq RNA v2 LS protocol (Illumina). Sequencing was performed on an Illumina Nextseq 500 sequencer at a read depth of approximately 30 million reads. Analysis of sequencing reads was subsequently performed by Dr. Manuela Zanda and Dr. Vincent Plagnol of the UCL Genetics Institute. Sequencing reads were aligned to a custom Tc1 mouse reference genome, which combined the full mouse genome and human chromosome 21 (both from NCBI build 37.2), using tophat v2.0.13. GTF files describing genes features were obtained from Ensembl (http://www.ensembl.org/info/data/ftp/index.html), while read count normalisation and differential expression analysis were performed by python scripts as part of the DEseq package. The set of scripts used are freely available from the Plagnol group at https://github.com/plagnollab/RNASeq_pipeline.

2.22. Functional clustering of differential gene expression

Differentially expressed genes with FDR-adjusted p-values < 0.05 were classified into functional clusters using the Database for Annotation, Visualization and Integrated Discovery (DAVID) v6.7 (National Institute of Allergy and Infectious Diseases (NIAID), National Institutes of Health, USA) (Huang et al. 2009). Gene lists were entered using official gene symbols as the identifier, with annotations limited to *Mus musculus*, and at lowest classification stringency.

2.23. Statistical analysis

Statistical analysis was performed using SPSS Statistics version 22 (IBM).

Chapter 3. Development of an *in vitro* model for AD-DS

3.1. Introduction

3.1.1. The utility of an *in vitro* assay for AD-DS

As described in Chapter 1, one of the greatest strengths in DS mouse models lies in their complementary use in mapping phenotypes to specific genes or chromosome regions on Hsa21. This has been successfully performed, for example, in demonstrating the necessity of *App* triplication to basal forebrain cholinergic neuron (BFCN) loss in Ts65Dn mice (Salehi et al. 2006). *App* was first identified as a candidate gene following the comparison of BFCN phenotypes between Ts65Dn with Ts1Cje mice, which did not demonstrate BFCN loss; this indicated the presence of a dosage-sensitive region triplicated in Ts65Dn, but not in Ts1Cje, that was causative for this phenotype. To investigate if *App* trisomy was responsible for BFCN loss, *App* expression was reduced to disomic levels by crossing Ts65Dn mice with heterozygous *App* knockout mice. This successfully demonstrated that disomic *App* expression was sufficient to prevent BFCN loss in Ts65Dn.

While this was an elegantly performed study, the *in vivo* and *ex vivo* examination of neuronal phenotypes is heavily taxing on resources and time, and may not offer a pragmatic system for the assessment of numerous candidate genes. The use of primary cell culture therefore offers a number of advantages as a routine and relatively high-throughput system: 1) it enables access to living neurons in a far less complex environment than neural tissue; 2) it is more amenable to genetic manipulation including the reduction of trisomic gene expression levels; 3) it allows the characterization of key neuronal phenotypes that are not recapitulated in other neuronal cell lines. These features include the ability to develop axons, dendrites and synapses, allowing for their functional study (Kaech and Banker 2006).

This approach has been successfully used to demonstrate the significance of candidate genes to AD phenotypes. For instance, lentiviral shRNA-mediated knockdown of *Ephb2* expression was performed in primary cortical and hippocampal neurons, to investigate the potential effects of *Ephb2* depletion by Aβ42. This was shown to impair NMDA-receptor-dependent gene expression *in vitro*, paving the way for further experiments into effects on long-term potentiation, synaptic plasticity and cognitive deficits (Cissé, Halabisky, et al. 2011). In another study, the knockdown of

Cdk5 expression in primary hippocampal neurons resulted in a reduction in phosphorylated tau, priming further *in vivo* work in an AD mouse model illustrating the potential of targeting *Cdk5* to ameliorate tau pathology (Piedrahita et al. 2010). While the knockdown of candidate gene expression has not yet been published in DS neuronal cultures, this approach has been performed in other DS cell types, such as primary fibroblasts. For instance, reducing the expression of the Hsa21-encoded phosphatase *SYNJ1* partially rescued endosomal abnormalities, including endosomal enlargement, in fibroblasts from humans with DS or AD (Cossec et al. 2012).

We therefore sought to design a protocol that allowed the potential use of RNA interference (RNAi) techniques (Seyhan 2011) to stably reduce the expression of Hsa21 candidate genes from trisomic to disomic levels, to identify genes influencing AD-related phenotypes in trisomic cells. The following section details parameters considered while developing the protocol.

3.2. Considerations in protocol design for Tc1xJ20 primary neuronal cultures

3.2.1. Use of early postnatal mice for culture

Primary cultures could be obtained either from embryonic mice or postnatal pups. While embryonic neurons are less susceptible to damage during culture preparation due to their simpler neuronal processes (Banker and Cowan 1979; Banker and Cowan 1977), and yield a greater proportion of neuronal cell types, using postnatal pups allows the continuous use of the same female mice for breeding, as the mothers need not be culled to obtain pups (Beaudoin et al. 2012). We therefore decided on using postnatal pups (within 48 h of birth) to minimise animal use and reduce variation introduced due to the use of different mothers. The use of pups is also suitable for studying *APP* expression from the J20 transgene, as its PDGF-β promoter has been shown to be expressed in cortical tissue from embryonic day 15 in mice (Sasahara et al. 1991) and J20 forebrain primary neurons have been shown to produce human Aβ (Vingtdeux et al. 2010).

3.2.2. Standardising plating density

Neuronal density has been systematically demonstrated to influence electrical activity during the maturation of primary neuronal cultures (Biffi et al. 2013). For instance,

sparse cultures (600 cells/mm^2) required a longer development time to achieve half the peak firing rate and network bursts compared to denser cultures (1600 cells/mm^2) (Biffi et al. 2013; Wagenaar et al. 2006). In addition, neuronal density influences other functional properties, including synaptic density (Cullen et al. 2010), dendrite morphology (Previtera et al. 2010; Ivenshitz and Segal 2010) and patterns of spontaneous network activity (Ivenshitz and Segal 2010; Cohen et al. 2008). The density of plated glial cells also influences their rate of proliferation and consequently the size of any effects contributed by glial function (Hartikka and Hefti 1988). There was a need therefore to select and standardize an appropriate plating density across wells and coverslips of different diameters.

The aim of developing the primary neuronal culture system was to reduce Hsa21 candidate gene expression, via lentiviral shRNA-mediated techniques. We therefore decided that a minimum of 8 wells was needed per culture, to allow for aspects of future work such as the titration of lentiviral concentrations needed in optimizing levels of knockdown.

3.2.3. Mosaicism

The freely-segregating Hsa21 chromosome in Tc1 mice is stochastically lost at different rates in different tissues, and will be a source of variability between each culture. Significantly for cell culture, aneuploidy (regardless of the chromosome involved) impairs proliferation and slows growth, as demonstrated in mouse embryonic fibroblasts trisomic for four different chromosomes (Williams et al. 2008), and in yeast (Pavelka et al. 2010; Torres et al. 2007; Niwa et al. 2006). In addition, aneuploid cells exhibit a range of phenotypes constituting an “aneuploidy stress response”, including altered metabolism, proteotoxic stress and increased genomic instability (reviewed in Siegel and Amon 2012). It is therefore important to understand the degree to which euploid cells may be outgrowing their less fit trisomic counterparts in a mosaic cortical culture.

3.3. APP and Aβ phenotypes in primary neurons

As introduced in Chapter 1, trisomy 21 was sufficient to exacerbate Aβ accumulation in Tc1;J20 mice, as demonstrated by increased plaque deposition in the Tc1;J20 cortex and hippocampus at 6 and 16 months. To assess the validity of using primary cortical neurons to model amyloid-related phenotypes in Tc1xJ20, it is necessary to

characterize baseline APP expression and metabolism *in vitro* before corroboration with *ex vivo* data. We chose to compare results from primary cortical culture with cortical tissue obtained from 3-month old Tc1xJ20 mice, to compare if *in vitro* APP/Aβ phenotypes may be used to model phenotypes present in young mice prior to observable plaque deposition.

This corroboration was necessary because variations in amyloid phenotypes could be introduced by the *in vitro* system. One source of variation arises from the increased proliferation of glial cells in culture, potentially altering the overall profile of APP metabolism *in vitro* compared to *ex vivo* (Annaert and De Strooper 2000). For instance, neurons are more likely than non-neuronal cells to process APP down the β-secretase pathway (Simons et al. 1996; Hung et al. 1992), while glial cells tend to drive APP processing down the α-secretase pathway (Wertkin et al. 1993; Haass et al. 1991). To investigate this, one could investigate levels of β-CTF and α-CTF in culture, which are products from β-secretase and α-secretase cleavage respectively.

The use of cortical cells at developmental stages may also further augment any effects relating to the proportions of neuronal and non-neuronal cells in culture. DS demonstrates a developmental shift towards increased gliogenesis and reduced neuronogenesis, as observed in morphological and histopathological studies of DS brains from fetal to adult ages (Guidi et al. 2011; Guidi et al. 2008; Griffin et al. 1998; Mito and Becker 1993). The overexpression of *S100B* and *APP* in DS has been shown to promote gliocentric differentiation in DS neural progenitors (Lu et al., 2011), while triplicated *App* impairs neuronal precursor differentiation and neurite development in Ts65Dn mice (Trazzi et al., 2013). Finally, neural progenitors derived from a monozygotic twin with Hsa21 trisomy displayed reduced neurogenesis and neurite branching, together with an increased tendency to differentiate into astroglial and oligodendroglial cells, compared to the twin without trisomy (Hibaoui et al., 2014).

Finally, any effect of trisomy on APP or Aβ phenotypes will also be influenced by variations in levels of Hsa21 mosaicism.

With these considerations in mind, we aimed to develop a primary cortical culture using early postnatal Tc1xJ20 mice, before validating APP/Aβ phenotypes *in vitro* with *ex vivo* results from 3-month old mice.

3.4. Aims

1. Measure APP/Aβ expression *in vitro* and compare with data from cortical homogenates
2. Determine proportion of neuronal cells present in primary cortical culture
3. Investigate the variability in levels of mosaicism in primary culture

3.5. Results

Primary cortical cultures were prepared from postnatal pups aged less than 48 h (postnatal day 0-1), seeded at 150 cells/mm^2 and allowed to differentiate for 14 days *in vitro* prior to use in experiments. For western blots and qPCR analysis, cortical cells were plated on PDL-coated 12-well plates, while cells to be used for immunofluorescent staining were plated on PDL-coated 13-mm coverslips.

For the study of protein expression, primary cortical cells were lysed in RIPA buffer with protease inhibitors, and cell lysate concentration was determined using a highly-sensitive protein quantitation assay, to facilitate accurate and consistent protein loading in western blots.

3.5.1. Full-length human APP (hAPP) expression

Full-length hAPP was detected using the 6E10 antibody (Covance), which is reactive to N-terminal amino acid residues 1-16 of Aβ, and hence specific to human Aβ. The epitope lies within amino acids 3-8 of Aβ (EFRHDS) which differs from the corresponding mouse sequence (EFGHDS). Western blotting was performed on primary cortical lysates and cortical homogenate from 3-month old Tc1xJ20 mice. Tc1 and Wt samples were run as negative controls. As the protein yield from primary cells was low compared to homogenate, cell samples were loaded in randomized order to minimize variation caused by lane effects; we noticed that samples running in the first and last lanes tended to separate more erratically.

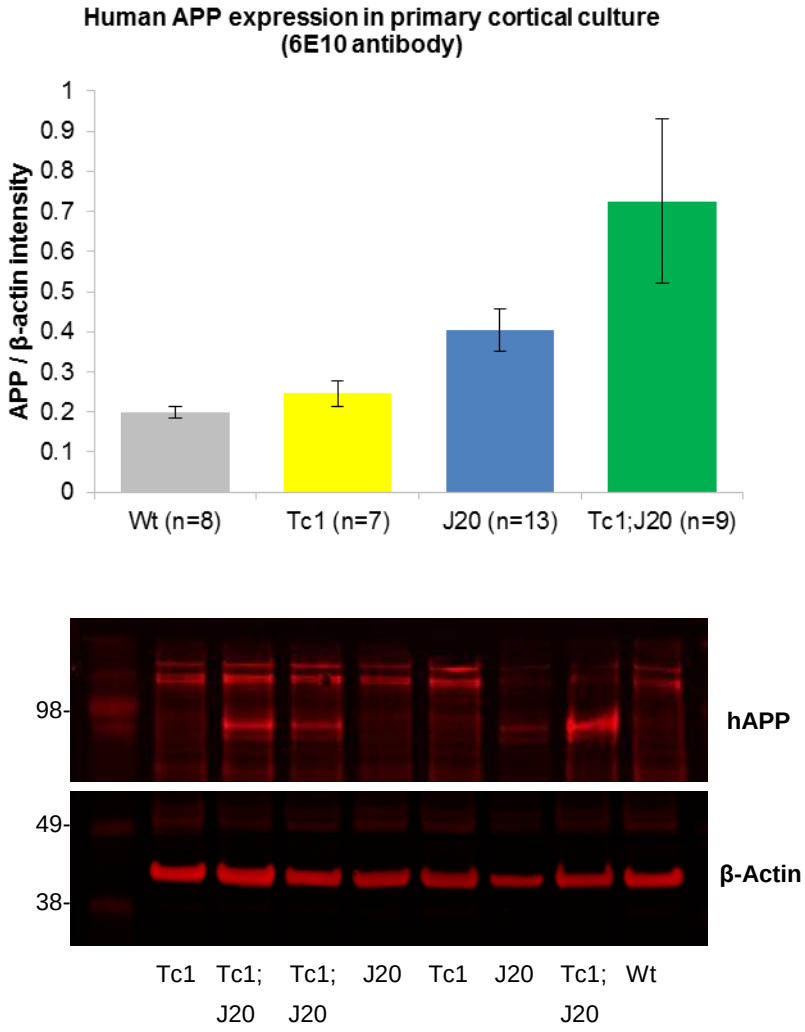

Figure 3.1 Human APP (hAPP) protein expression in primary cortical culture.

APP overexpression significantly increased hAPP levels, but there was no significant effect of trisomy 21 on hAPP expression. Graph shows mean values while error bars indicate SEM. Samples were loaded in randomized order to minimize variation caused by lane effects**.**

In primary cortical cells, *APP* overexpression significantly increased the expression of hAPP (2-way ANOVA $F(1,33) = 9.611$, $p = 0.004$). However there was no significant effect of trisomy 21 on hAPP expression ($F(1,33) = 2.802$, $p = 0.104$) and no interaction between trisomy 21**APP* overexpression ($F(1,33) = 1.547$, $p = 0.222$). In comparing means only between J20 and Tc1;J20, there was a non-significant trend towards increased hAPP in Tc1;J20 compared to J20 (independent samples t-test $F(1,20) = -1.781$, $p = 0.090$).

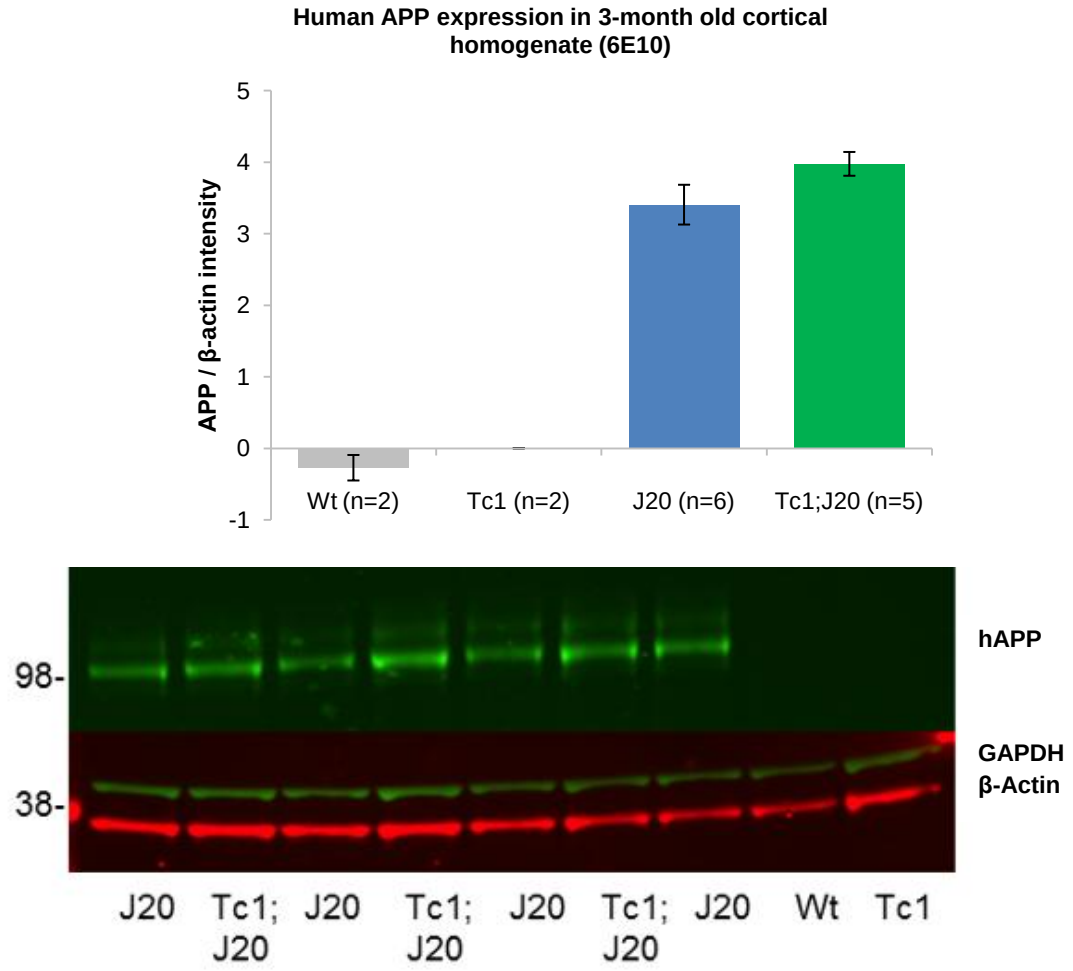

Figure 3.2 hAPP protein expression in 3-month old Tc1xJ20 cortical homogenate. There was no significant difference in hAPP expression between J20 and Tc1;J20. Graph shows mean values (labelled) while error bars indicate SEM. Experiments performed by Frances Wiseman.

In cortical homogenate from 3-month old Tc1xJ20 mice, there was no significant difference in hAPP expression between J20 and Tc1;J20 (independent samples t-test $F(1,9) = -1.666$, $p = 0.130$).

3.5.2. Total full-length APP expression

Total full-length APP was detected by the Sigma-Aldrich A8717 antibody (Sigma-Aldrich), reactive to both mouse and human APP. A8717 therefore is suitable for detecting APP expressed both from the J20 transgene and endogenous *App*, as well as β-CTFs and α-CTFs produced from cleavage of APP by β- and α-secretase respectively.

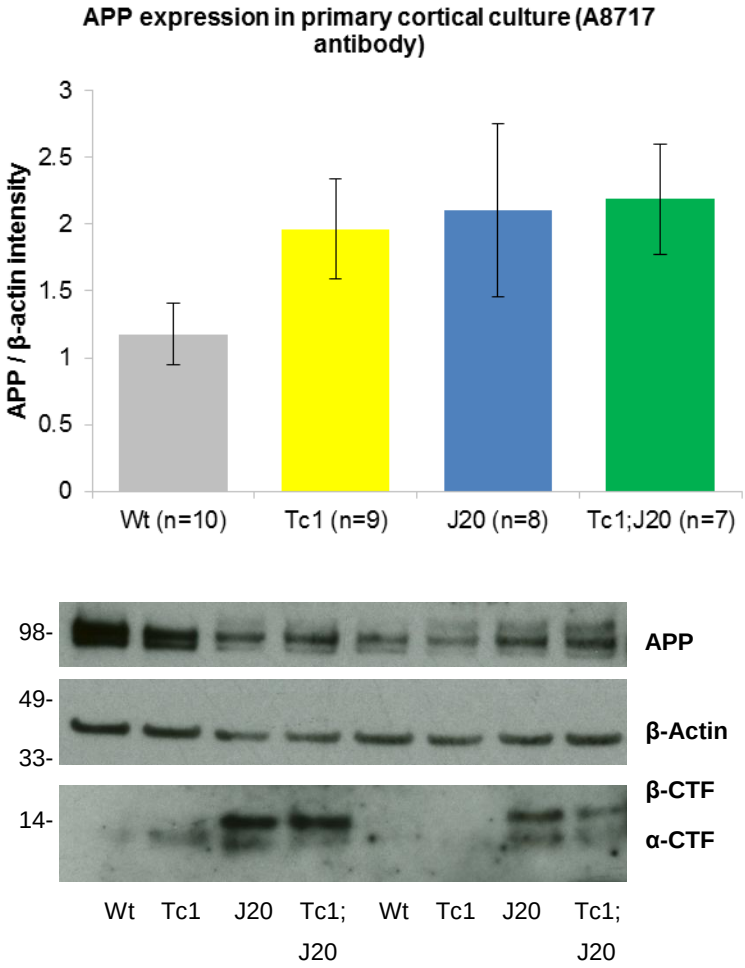

Figure 3.3 Human and mouse total APP protein expression in primary cortical culture. There was no significant effect of trisomy 21 or *APP* overexpression on total full-length APP expression. Graph shows mean values while error bars indicate SEM.

In primary cortical cells, there was no significant effect of trisomy 21 or *APP* overexpression on APP expression (2-way ANOVA Tc1 status ($F(1,29) = 0.949$, $p = 0.338$); J20 status ($F(1,29) = 1.680$, $p = 0.205$); Tc1*J20 interaction ($F(1,29) = 0.633$, $p = 0.433$)).

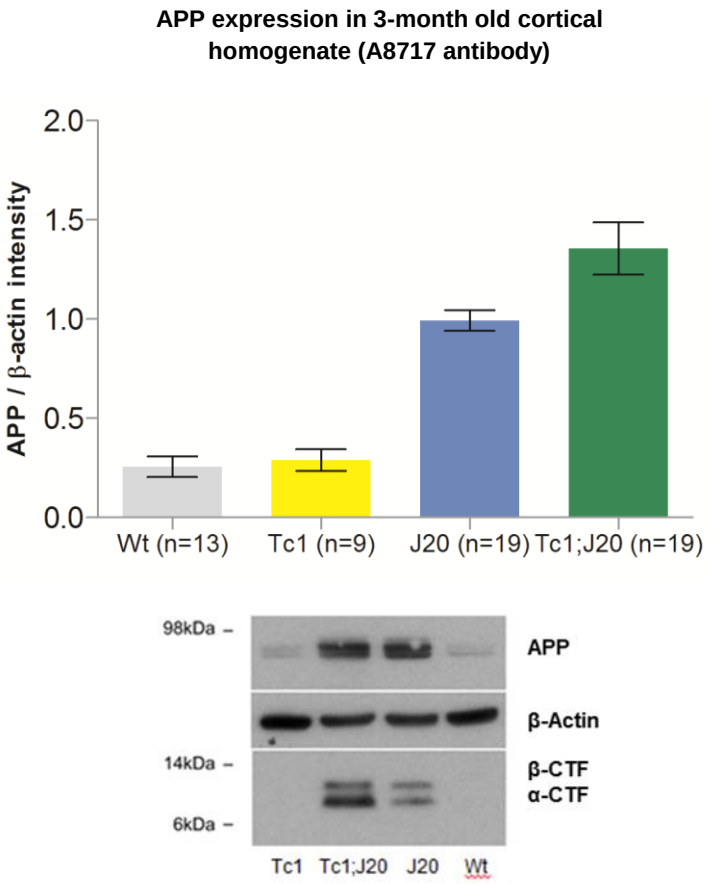

Figure 3.4 Human and mouse total APP protein expression in 3-month Tc1xJ20 cortical homogenate.

Trisomy 21 and *APP* overexpression both significantly increased total APP expression. There was a trend towards a significant effect between trisomy 21 and *APP* overexpression (p=0.08). Graph shows mean values while error bars indicate SEM. Experiments performed by Laura Pulford.

In cortical homogenate from 3-month old Tc1xJ20 mice, trisomy 21 and APP/Aβ overexpression both significantly increased APP expression, with a trend to significance in the interaction between both genotypes (2-way ANOVA Tc1 status ($F(1,52) = 4.158$, $p = 0.047$); J20 status ($F(1,52) = 89.924$, $p < 0.0001$); Tc1*J20 interaction ($F(1,52) = 3.178$, $p = 0.080$))

3.5.3. APP C-terminal Fragment (CTF) expression

As described in Section 3.5.2, the same A8717 polyclonal antibody was used to detect CTFs produced by the first cleavage step of APP; β-secretase generates β-CTFs (C99) in the amyloidogenic pathway, while α-secretase generates α-CTFs (C83) in the non-amyloidogenic pathway. Only J20 and Tc1;J20 results were used for analysis as CTF bands in Wt and Tc1 samples were very faint and infrequently observed.

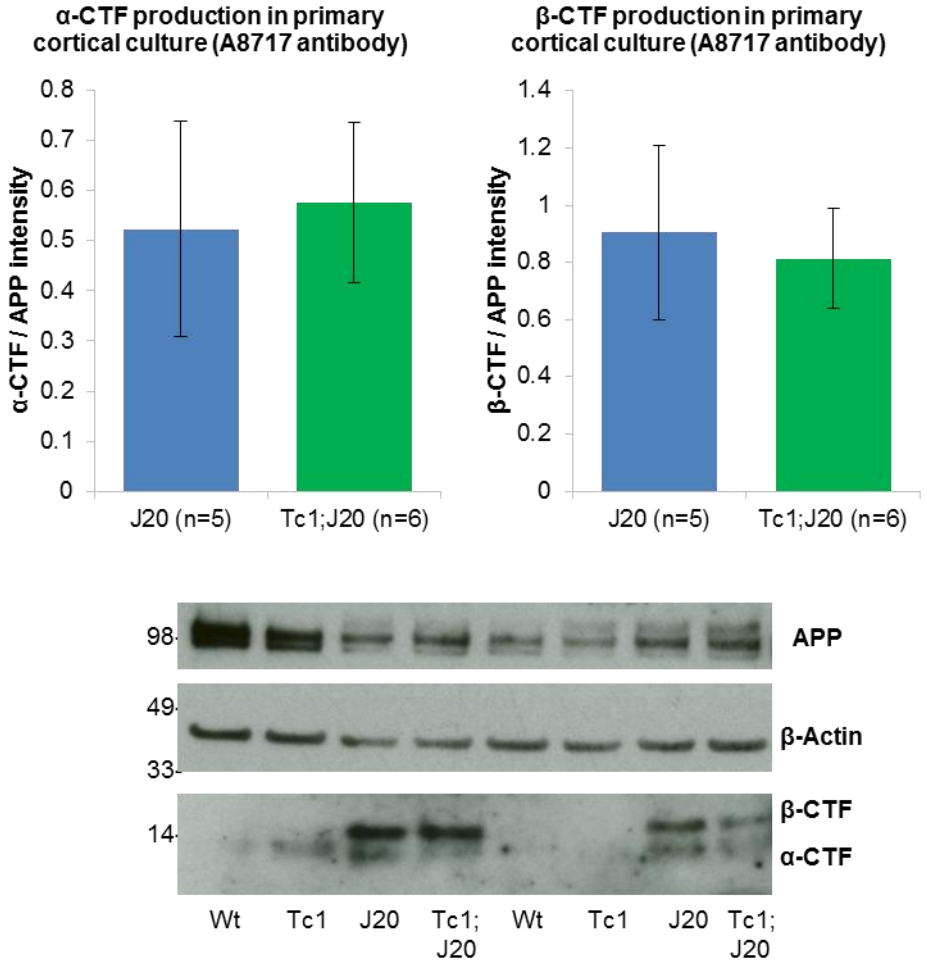

Figure 3.5 α- and β-CTF expression in primary cortical culture.

There was no significant effect of trisomy 21 or *APP* overexpression on β-CTF or α-CTF expression. Graph shows mean values while error bars indicate SEM.

In primary cortical cells, no significant difference was observed in both α-CTF and β-CTF production, between J20 and Tc1;J20 mice (α-CTF independent samples t-test ($t(9) = -0.202$, $p = 0.844$; β-CTF independent samples t-test $t(9) = 0.269$, $p = 0.794$).

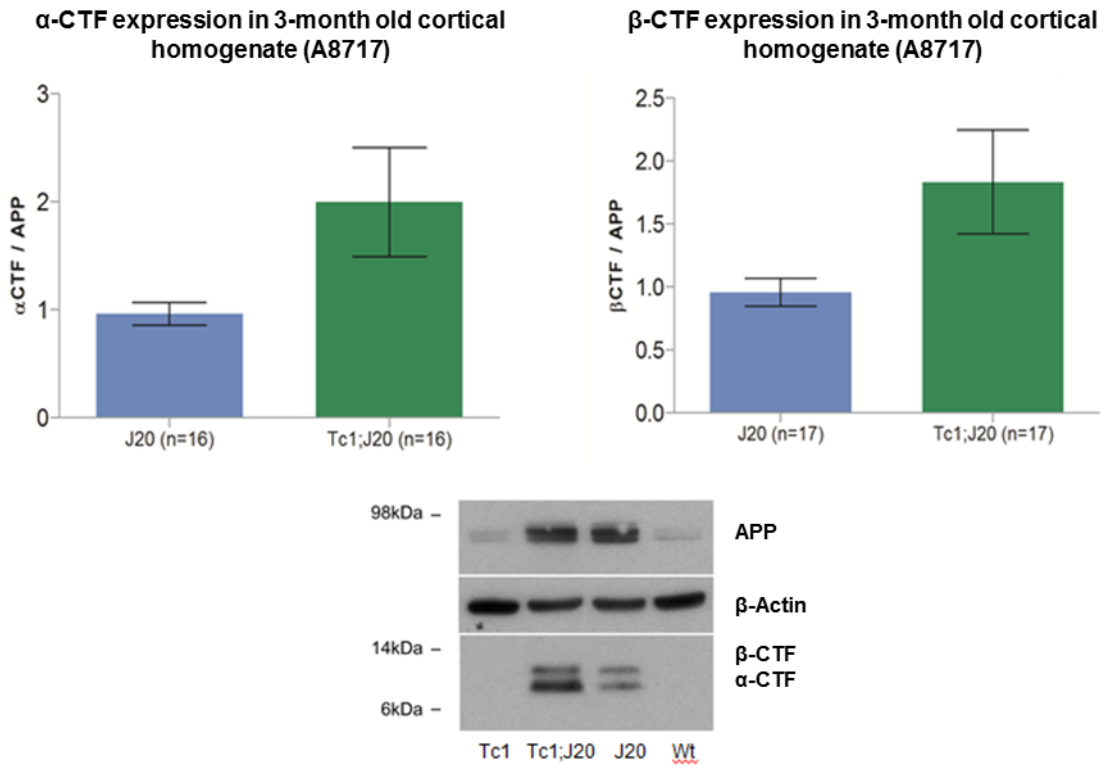

Figure 3.6 α- and β-CTF expression in 3-month old Tc1xJ20 cortical homogenate. Trisomy 21 significantly increases both α-CTF and β-CTF expression in Tc1;J20 compared to J20. Graph shows mean values while error bars indicate SEM. Experiments performed by Laura Pulford.

In 3-month old cortical homogenate, trisomy 21 in Tc1;J20 significant increased expression of both β-CTF and α-CTF compared to J20 (α-CTF independent samples t-test ($F(9) = -0.202$, $p = 0.844$); β-CTF $t(9) = 0.269$, $p = 0.794$).

3.5.4. Human soluble Aβ38, Aβ40 and Aβ42 production

To quantify levels of secreted Aβ38, Aβ40 and Aβ42 from primary cortical neurons, a sandwich immunoassay was used which detects all three Aβ species from samples in the same well using peptide-specific capture antibodies. As these Aβ antibodies were developed using 6E10, only human Aβ peptides were detected in this assay; Tc1 and Wt hence served as negative controls. Following the binding of Aβ from samples to the capture antibodies immobilized in the well, a buffer is added containing detection antibodies which emit light following the application of voltage through the plate electrodes. The intensity of emitted light was used to quantify Aβ.

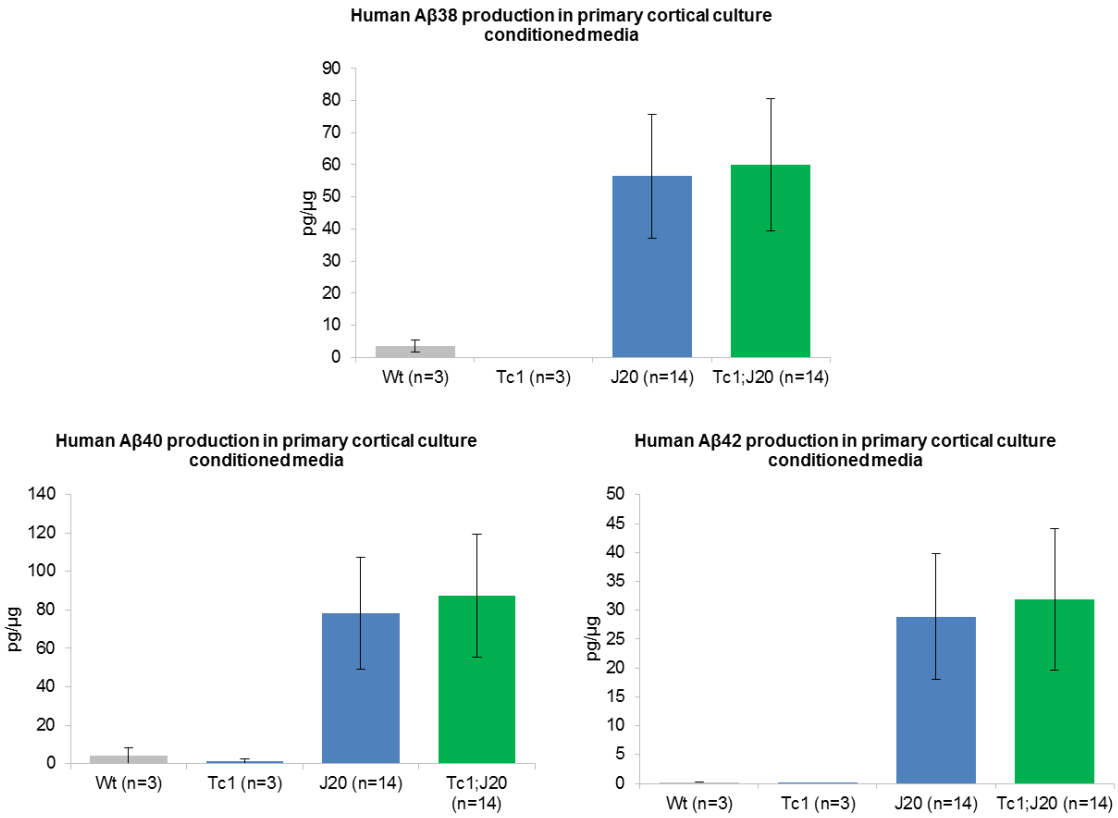

Figure 3.7 Human Aβ production in primary cortical culture.

There was no significant effect of trisomy 21 or *APP* overexpression on Aβ38, Aβ40 or Aβ42 levels in conditioned media. Graph shows mean values (labelled) while error bars indicate SEM.

In primary cortical cells, conditioned medium was collected from cultures after 14 DIV. There was no significant difference in any of the secreted human Aβ38, Aβ40 and Aβ42 levels between J20 and Tc1;J20 cultures (independent samples t-test Aβ38 $t(26) = -0.129$, $p = 0.899$; Aβ40 $t(26) = -0.210$, $p = 0.836$; Aβ42 $t(26) = -0.184$, $p = 0.856$.

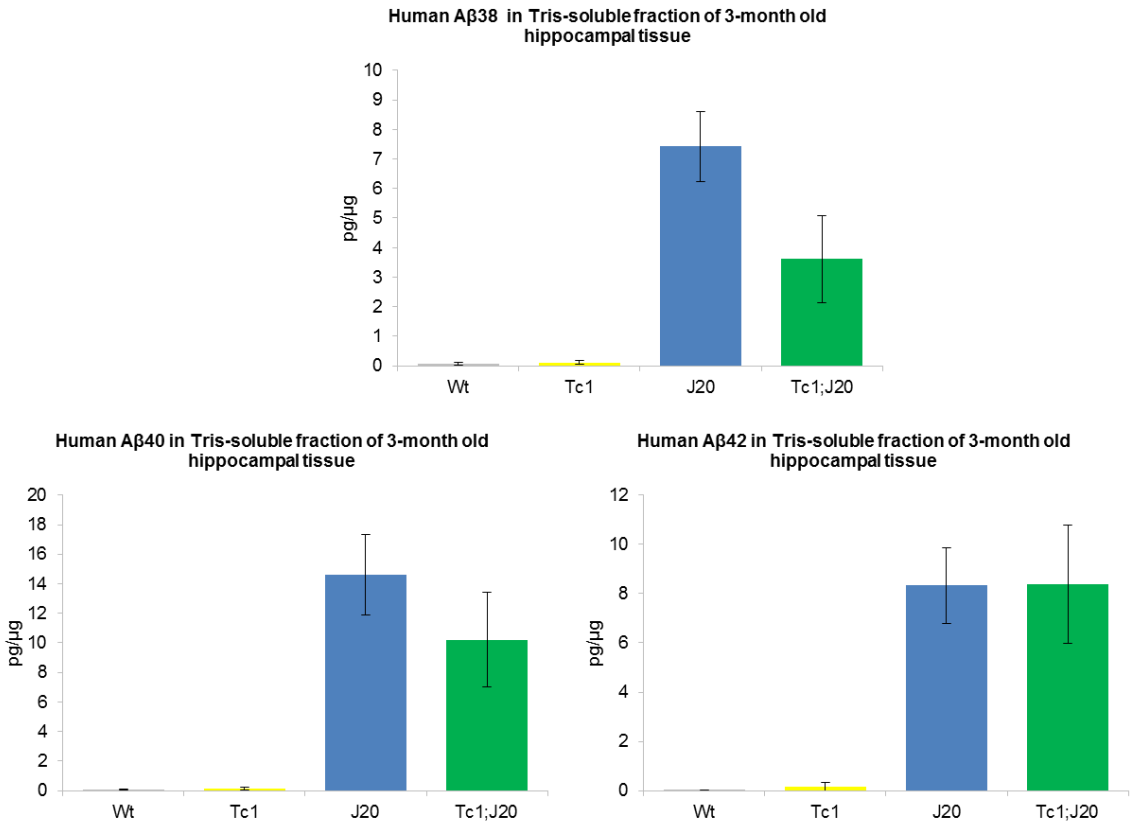

Figure 3.8 Human Aβ in Tris-soluble fraction of 3-month old hippocampal tissue.

Trisomy 21 decreased the abundance of Tris-soluble Aβ38 and Aβ40, without a significant difference in levels of Aβ42. Graph shows mean values while error bars indicate SEM. Experiments were performed by Frances Wiseman.

Following homogenization in Tris buffer and preparation as according to Holtta et al. 2013, the Tris-soluble fraction of 3-month old hippocampal homogenate was used to study small soluble forms of Aβ. Trisomy 21 decreased the abundance of Tris-soluble human Aβ38 ($F(1,7) = 15.126$ $p = 0.006$), Aβ40 ($F(1,11) = 6.359$ $p = 0.028$), but no change in levels of Aβ42 ($F(1,11) = 0.663$ $p = 0.433$). This resulted in an alteration of the Aβ38/42 Tris-soluble ratio ($F(1,5) = 6.667$ $p = 0.049$) between J20 and Tc1;J20.

3.5.5. BACE1 expression

To investigate if the difference in CTF profiles in primary cortical culture and cortical homogenate was due to differences in secretase expression, western blots for BACE1 (β-secretase) were performed. β-secretase cleaves APP in the first step of the amyloidogenic APP processing pathway to generate sAPPβ and β-CTF (Figure 1.1).

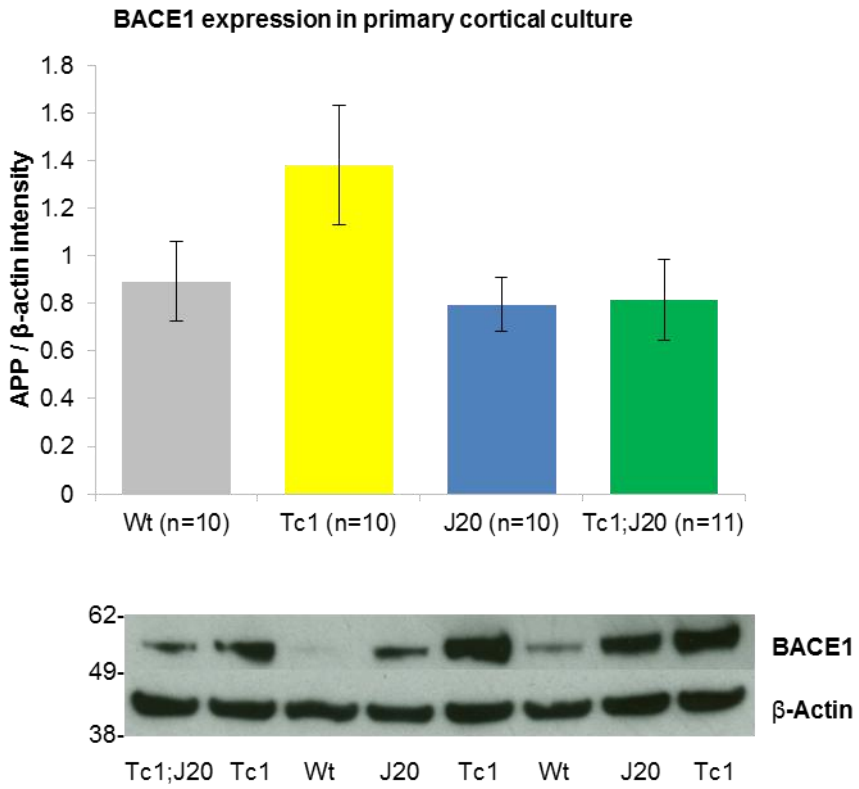

Figure 3.9 BACE1 protein expression in primary cortical culture.

There was no significant effect of trisomy 21 or *APP* overexpression on BACE1 expression. Graph shows mean values (labelled) while error bars indicate SEM.

In primary cortical cells, there was no significant effect of trisomy 21 or *APP* overexpression on BACE1 expression (ANOVA Tc1 status ($F(1,37) = 1.960$, $p = 0.170$); J20 status ($F(1,37) = 3.340$, $p = 0.076$); Tc1*J20 interaction ($F(1,37) = 1.669$, $p = 0.204$).

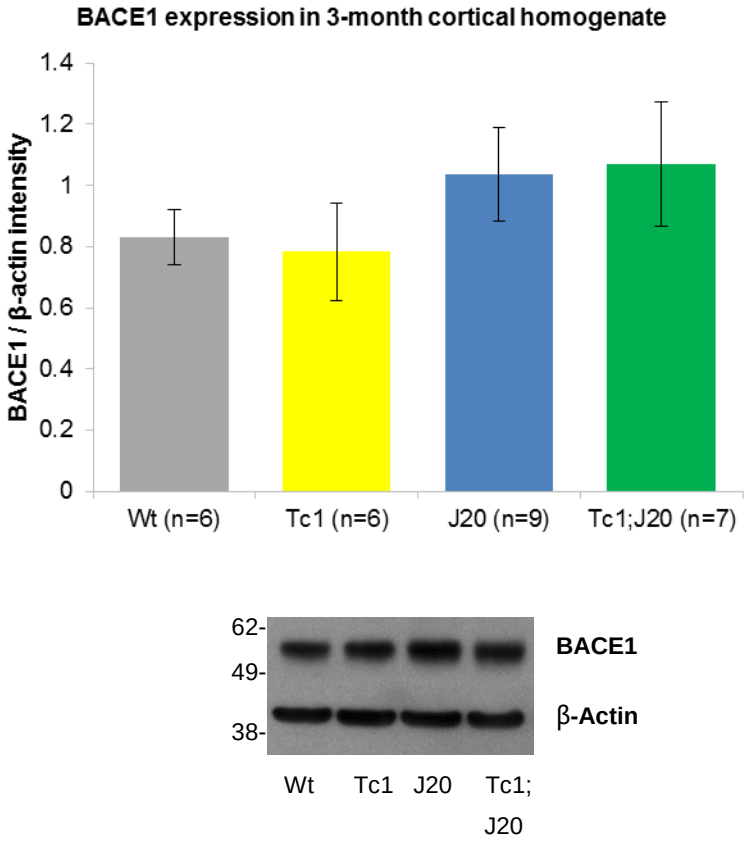

Figure 3.10 BACE1 protein expression in 3-month old Tc1xJ20 cortical homogenate. There was no significant effect of trisomy 21 or *APP* overexpression on BACE1 expression. Graph shows mean values while error bars indicate SEM. Experiments performed by Dr. Karen Cleverley.

Similarly in 3-month old Tc1xJ20 cortical homogenate, there was no significant effect of trisomy 21 or *APP* overexpression on BACE1 expression (ANOVA Tc1 status ($F(1,24) = 0.002$, $p = 0.963$); J20 status ($F(1,24) = 2.573$, $p = 0.122$); Tc1*J20 interaction ($F(1,24) = 0.071$, $p = 0.792$).

3.5.6. Proportion of neuronal cells *in vitro*

To quantify the proportion of neuronal cells in each culture, cortical cells were seeded on 13-mm coverslips and stained for NeuN and DAPI. NeuN is a neuron-specific nuclear protein expressed at the start of neuronal terminal differentiation (Mullen et al. 1992), while DAPI binds double-stranded DNA and is hence employed as a general nuclear stain (Kapuscinski 1995). Neuronal cells are hence double-stained with DAPI and NeuN, while non-neuronal cells are stained only with DAPI. As described in

Section 2.17.2, NeuN-positive neurons tended to cluster toward the centre of the coverslip, becoming more infrequent with increasing radial distance. Five fields of view at 10x magnification were acquired to maximize the number of NeuN-positive cells present on the coverslip for analysis. These included the field of view at the centre of the cluster, together with fields of view immediately adjacent to the left, right, top and bottom of the centre field. The proportion of neuronal cells in culture was then calculated by obtaining of NeuN / DAPI nuclei counted.

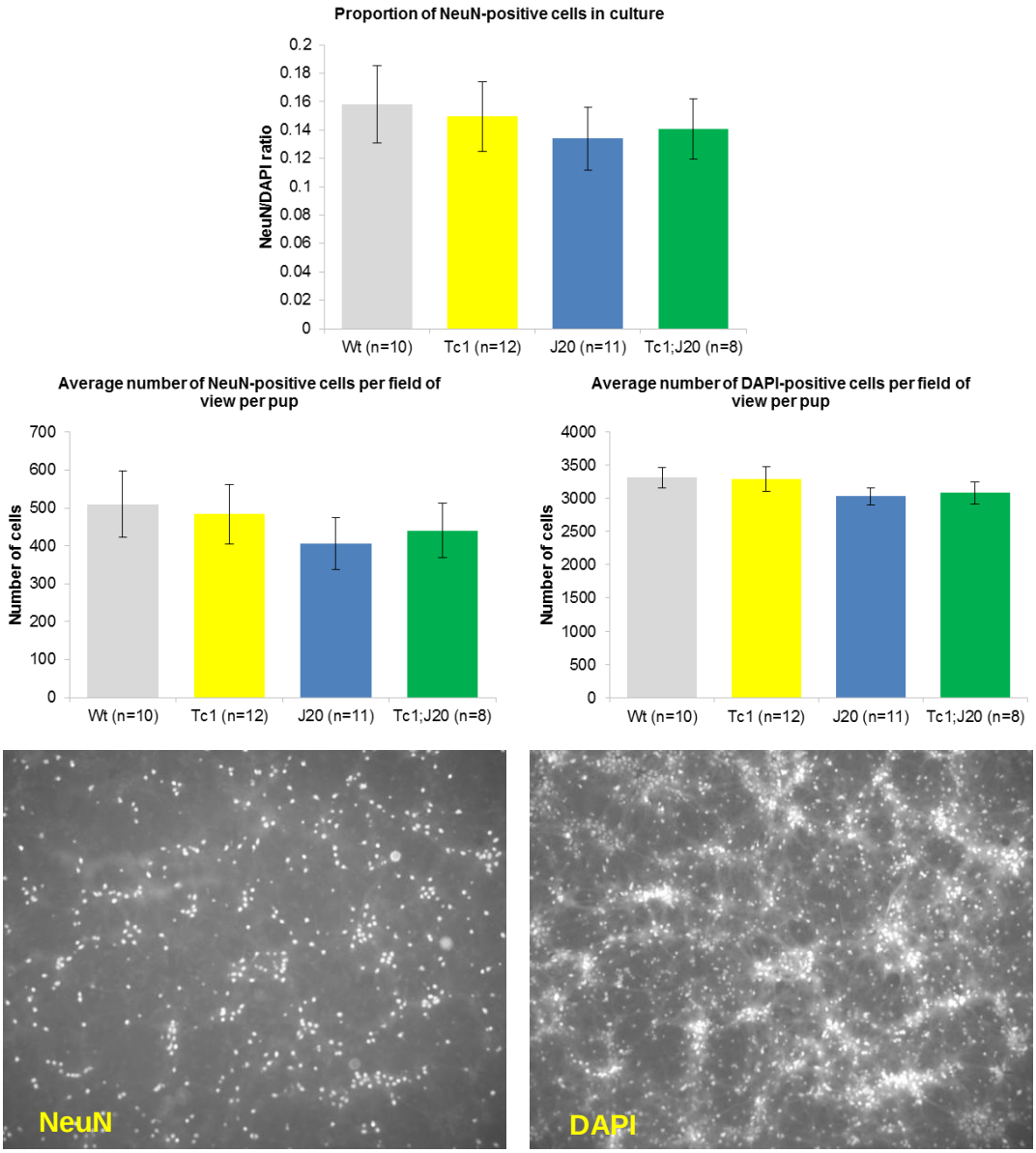

Figure 3.11 Influence of genotype on the proportion of neurons in culture.

Cell nuclei were labelled with NeuN, a neuron-specific marker, and DAPI, a nuclear marker for all cells. Five fields of view per coverslip were obtained for counting nuclei. No significant effect was observed of trisomy 21 or *APP* overexpression on the numbers of neurons (NeuN+), numbers of total cells (DAPI+), and the proportion of neuronal cells in culture (NeuN/DAPI ratio). Graph shows mean values (labelled) while error bars indicate SEM. Images are at 10x magnification.

There was no significant effect of trisomy 21 or *APP* overexpression on the average number of NeuN-positive cells per culture ((2-way ANOVA Tc1 status ($F(1,37) = 0.002$, $p = 0.963$); J20 status ($F(1,37) = 0.871$, $p = 0.357$); Tc1*J20 interaction ($F(1,37) = 0.145$, $p = 0.706$), or the proportion of neuronal cells in culture (NeuN/DAPI) ($F(1,37) = 0.001$, $p = 0.971$); J20 status ($F(1,37) = 0.440$, $p = 0.511$); Tc1*J20 interaction ($F(1,37) = 0.096$, $p = 0.758$). There was also no difference in the average number of DAPI-positive cells counted per field of view per pup ((ANOVA Tc1 status ($F(1,37) = 0.012$, $p = 0.914$); J20 status ($F(1,37) = 2.207$, $p = 0.146$); Tc1*J20 interaction ($F(1,37) = 0.051$, $p = 0.823$).

3.5.7. Hsa21 mosaicism in primary culture

To estimate the proportion of cells in culture that retained the Hsa21 chromosome, the genomic content of human *CLDN8* and mouse *Apob* in cell culture was quantified by qPCR relative to standard curve. *CLDN8* is encoded on Hsa21 and is trisomic in Tc1, while *Apob* is a mouse gene that is disomic in Tc1. Primers and probes to both genes were designed to be species-specific and hence would only detect human *CLDN8* and mouse *Apob* copy numbers. The proportion of trisomic cells was calculated based on the percentage of *CLDN8* to *Apob* expression – if all cells retained Hsa21, *CLDN8* present in one copy would be 50% of *Apob* levels present in two copies.

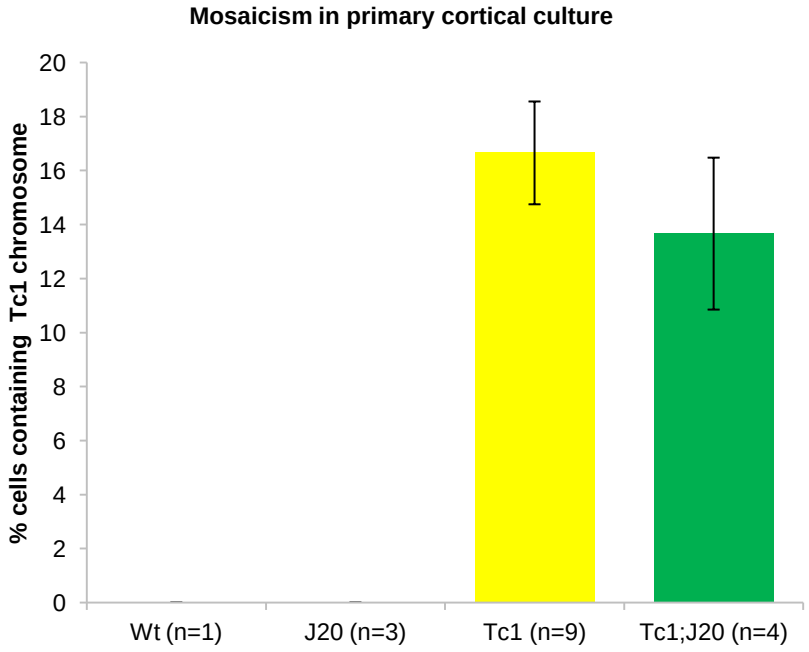

Figure 3.12 Proportion of primary cortical cells retaining the Hsa21 chromosome. This was determined by the relative genomic content of human *CLDN8* and mouse *Apob* present in the cell culture. There was no significant difference in mosaicism between Tc1 and Tc1;J20 cultures. Graph shows mean values while error bars indicate SEM.

As shown in Figure 3.12, on average Tc1 cultures had 16.7% trisomic cells with an SEM of 1.91%, while Tc1;J20 cultures had 13.7% trisomic cells on average, with an SEM of 2.81%. There was no significant effect of *APP* overexpression on mosaicism levels (independent samples t-test t(11) = 0.875, p = 0.400).

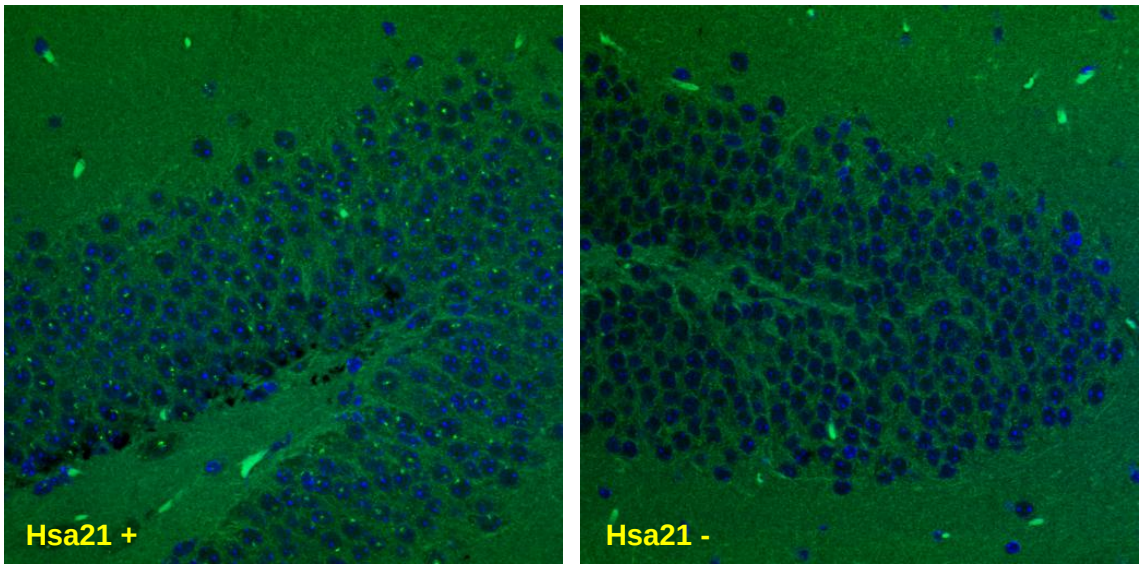

Sample	Genotype	Hippocampus; Dentate gyrus			Hippocampus; CA1		
		Hsa21 +	Hsa21 -	**% Hsa21+**	Hsa21 +	Hsa21 -	**% Hsa21+**
QN0021-09	Tc1	75	52	**59**	82	50	**61**
QN0017-09		38	31	**55**	50	57	**47**
QN0026-09		42	27	**61**	50	59	**46**
QN0018-09		69	30	**69**	56	53	**51**
			Mean	**61**		Mean	**51.25**
QN0020-09	Wt	0	133	**0**	0	85	**0**
QN0019-09		0	144	**0**	N/D	N/D	

Figure 3.13 Proportion of cells retaining the Hsa21 chromosome in adult Tc1 hippocampus.

Cells containing Hsa21 were identified by fluorescent *in situ* hybridization (FISH) in the dentate gyrus and CA1 regions of the hippocampus. Experiments were performed by Frances Wiseman.

Fluorescence *in situ* hybridization (FISH) was performed to detect Hsa21 in the hippocampal dentate gyrus and CA1 regions from four Tc1 and two Wt mice. The mean proportion of cells trisomic for Hsa21 was 61% (SEM 2.94%) in the dentate gyrus, and 51.25% (SEM 3.42%) in the CA1 region.

3.6. Discussion

3.6.1. Validity of primary cortical culture model in studying APP/Aβ phenotypes

Generating consistent, reproducible biochemical data from primary cortical cells was by far the greatest challenge in using the cell model above, due to wide variability in the APP/Aβ readouts obtained. This was firstly due to limited starting material because of the need to culture mice individually, and spread across a minimum of eight wells. Culture-to-culture variation in results therefore exerted strong effects, despite efforts to streamline the protocol and reduce the time taken per pup, and to select only cultures that appeared healthy at 14 DIV. It was necessary to adapt protocols routinely used for cortical homogenate to the limited amount of cellular material, such as by using a more sensitive protein quantification assay for primary cells to allow consistent protein loading in western blots.

Nonetheless, wide variation in results persisted, particularly in the measurement of Aβ production (Figure 3.7), in which three cultures did not produce any detectable human Aβ levels in any J20-positive wells; these entire cultures were excluded from analysis. However, hAPP was detectable by western blotting from these cells, and it remains unclear why no Aβ was secreted despite expression of the *APP* transgene in this minority of cases. Based on the remaining examined cultures, trisomy 21 does not alter the amount of human Aβ38, Aβ40 and Aβ42 secreted from neurons *in vitro,* and accumulated in media for 14 DIV (Figure 3.7). In comparison, *ex vivo* data from Tris-soluble fractions of 3-month old hippocampal tissues suggest that the expression of Aβ38 and Aβ40, but not Aβ42, is decreased by trisomy 21 (Figure 3.8). Tris-soluble fractions contain soluble forms of Aβ which have been used for the further study of Aβ oligomers (Holtta et al. 2013) and are distinct from Aβ found in plaque deposition (Shankar et al. 2009). Aβ production from primary cortical cells therefore does not reflect this population of Aβ species. As these results have been compared between cortical cells and hippocampal tissue, differences in result could also be attributed to tissue-based variation. The high variability from the cortical culture however suggests that any potential differences may have been lost in this variation.

The signal for human APP protein expression in cell lysates (Figure 3.1), as detected by antibody 6E10, was noticeably weaker than that obtained from cortical homogenates. This was indicated by relatively higher levels of background signal observed in Wt and Tc1 samples in the cell lysates. However, it was unexpected to

observe no difference in total APP expression (detected by antibody A8717) between all four genotypes in primary cells (Figure 3.3), compared to the 3-4 fold increase observed in cortical homogenates due to *APP* overexpression (Figure 3.4). Although there was insufficient material available for DNA extraction to verify transgene copy number levels in the cells, it is unlikely that transgene expression had decreased to such a negligible level. The detection of human Aβ indicates that the *APP* transgene is being expressed. Perhaps levels of APP were similar due to a relative increase in mouse APP expression from the high number of glial cells in culture, which do not express human *APP* as it transgene expression is driven by a neuron-specific promoter (Sasahara et al. 1991).

Using the same polyclonal A8717 antibody in APP to detect CTFs, the expression of CTFs similarly did not recapitulate *ex vivo* phenotypes in cell culture. While α-CTF and β-CTF levels were significantly increased by trisomy 21 in cortical homogenates (Figure 3.6), no difference was detected in the corresponding cortical lysates (Figure 3.5), which again displayed a wide variability in results. However, while there was no significant difference in APP levels between all four genotypes, CTFs were primarily detectable only in the *APP* overexpressing lysates. The increased CTF production *ex vivo* was not explained by changes in cortical BACE1 levels, which remained unaffected by trisomy (Figure 3.10). In primary cortical cells, BACE1 expression also remained at similar levels between the four genotypes (Figure 3.9), recapitulating these *ex vivo* observations. It remains unclear why there was a discrepancy between APP and CTF results produced using the same A8717 antibody. As a first step in unravelling this, and also to account for the high variability in Aβ and CTF results, we subsequently invested potential sources of variation discussed below

3.6.2. Investigating cell culture variability by assessing proportions of neuronal cells and levels of mosaicism

To account for the variability in APP/Aβ phenotypes and potentially provide normalization controls, the proportion of neuronal cells in culture and levels of Hsa21 mosaicism were investigated in cortical cultures. However, both neuron proportions and levels of mosaicism remained relatively consistent between the four genotypes, and hence were likely not accountable for the high variability in Aβ and CTF phenotypes. As anticipated, neurons accounted for a minority of the cells in culture, ranging from 13.4 – 15.8%. These values are also likely to be overestimates, as non-neuronal cells on the periphery of coverslips outside the five acquired fields of view were not included, while neurons were absent from these peripheral areas. While the

use of cytosine arabinofuranoside (AraC), an inhibitor of DNA synthesis, was considered to limit glial proliferation, we decided against its use due to its tendency to induce neuronal apoptosis (Ahlemeyer and Baumgart-Vogt 2005; Geller et al. 2001), with possibly an aggravated effect on metabolically stressed trisomic cells (Siegel and Amon 2012).

Retention of Hsa21 ranged from 6.67 – 23.95% as quantified by genomic levels of human *CLDN8* and mouse *Apob* measured by qPCR relative to a standard curve (Figure 3.12) While FISH offers a more sensitive and precise measure of mosaicism (Figure 3.13), its demand on time and labour made routine use for primary culture unpragmatic. However, based on combined data from our FISH results and qPCR data from O'Doherty et al. (2005) the mean percentage retention of Hsa21 in brain tissue was 58.63% (SEM 4%, n = 20). This was significantly higher than retention levels in primary culture (independent samples t-test $t(31) = 8.338$, $p < 0.0001$). Although quantification of mosaicism by qPCR does not reveal information about cell types, perhaps the consistently lower levels of mosaicism in culture may be due to slower proliferation rates of trisomic non-neuronal cells (Williams et al. 2008). This could be verified by FISH in primary cortical cultures.

3.6.3. Recommendations for future primary neuronal culture

The primary uncertainty engendered by the use of Tc1 cells lies in not knowing which cells are trisomic for Hsa21, precluding the possibility of performing single cell studies, such as in the characterization of neuronal trafficking or intracellular phenotypes. While efforts have been undertaken to develop markers for transchromosomic cells, these have proved difficult – for instance, the systematic design and generation of antibodies that preferentially bind human-specific isoforms of Hsa21 proteins failed to specifically label trisomic cells in histology (Wiseman et al. 2010). Other means of separating or distinguishing between trisomic and disomic cells during culture preparation remain to be explored, such as by using flow cytometry or possibly an exploitation of the neomycin resistance gene inserted into the Hsa21 chromosome. However, the potential biological effects of this antibiotic use on trisomic cells remains unknown.

We have also experienced that biochemical characterization of these cultures at population level also results in an unfeasibly high level of variation for studying APP/Aβ phenotypes, not explained by fluctuations in neuronal proportion or levels of mosaicism. However, in future work with non-mosaic DS models (Figure 1.3), steps can be taken to reduce the effect of glial proliferation which are not possible here. This could be in the form of neuronal cultures involving astroglial feeder layers (Kaech and

Banker 2006) – this involves preparing and expanding primary astroglial cultures of each genotype in advance, to be used to provide glial support to primary cortical neurons treated with AraC. For Tc1xJ20 cultures, mosaicism again hinders the ability to expand a stock supply of trisomic astrocytes. It will also be possible to study phenotypes on a single-cell level in these non-mosaic models.

Finally, there is a need to more thoroughly profile how APP/Aβ expression and processing may alter in the developmental course of primary neuronal cultures. For instance, a recent ontogenic characterization of synaptogenesis in primary cortical and hippocampal cultures revealed functional similarities and differences between the two culture types, including differences in the ratio of excitatory to inhibitory synapses (Harrill et al. 2015). The close but complex association of Aβ with synaptic activity, plasticity and loss (Spires-Jones and Hyman 2014; X. Cheng et al. 2014; Parihar and Brewer 2010; Schroeder and Koo 2005) suggests that a more comprehensive understanding of the development of this *in vitro* system will allow more precise use of this *in vitro* neuronal system.

Chapter 4. Investigating gliosis in trisomy 21 and APP/Aβ overexpression

4.1. Introduction

Neuroinflammation encompasses the reactive state of glial cells such as astrocytes and microglia, which mediate the innate immune response in the brain (Ben Haim et al. 2015; O'Callaghan et al. 2008). While the brain had once been perceived as an immunoprivileged organ protected by the blood-brain barrier, this perspective has fundamentally been altered by revelations that peripheral immune cells are capable of crossing the blood-brain barrier, that neurons and glial cells regulate immune responses, and even the recent discovery of lymphatic draining systems from the brain (Louveau et al. 2015; Carson et al. 2006). Indeed, neuroinflammation and innate immune activation have now been demonstrated as contributors to the pathogenesis of an array of neurodegenerative diseases (Ben Haim et al. 2015; Heneka et al. 2014). In parallel, DS has been characterised as a syndrome of chronic neuroinflammation (Wilcock and Griffin 2013) and oxidative stress (Butterfield et al. 2014), which triggers and interacts with pathways in neuroinflammation. Given the utility of the Tc1xJ20 model in dissecting differential effects of trisomy 21 and/or APP/Aβ overexpression, it will be of interest in understanding how features of neuroinflammation may differ between these two factors, and use this model to study how they may interact to modify features of AD-DS.

Microglia constitute about 10% of cells in the central nervous system (CNS), and are parenchymal tissue macrophages with ramified ('tree-like') branching processes. This characterises the morphology of their "resting" state, in which these highly motile processes constantly sample the surrounding microenvironment, allowing rapid responses to injury or disease by cell body migration, or by directing processes towards stimuli (Wake et al. 2009; Nimmerjahn et al. 2005). Indeed, two-photon microscopy has demonstrated that microglia are constantly on the move (Davalos et al. 2005; Nimmerjahn et al. 2005). Unlike other CNS macrophages found in the meninges, choroid plexus and perivascular space, microglia derive from a separate haematopoietic pool, the yolk sac (Alliot et al. 1999), before migrating to and developing in the neural tube (Ginhoux et al. 2010). In the CNS innate immune response they are therefore likely to play specialized roles different from bone marrow-

derived macrophages, possibly sustained by a local microglial progenitor pool (Ajami et al. 2007; Hickey et al. 1992).

Astrocytes are the most abundant non-neuronal cell type in the CNS, constituting up to 50% of all cells in the brain (Azevedo et al. 2009). They are also arguably the most diverse, able to perform a range of homeostatic tasks in the CNS (Parpura et al. 2012). Astrocytes occupy non-overlapping domains in the grey matter, partitioning neural tissue into astroglial-vascular units, thereby covering the majority of neurons and synaptic contacts, and connecting them to CNS vasculature (Nedergaard et al. 2003). This allows them to perform a variety of tasks, such as the clearance of metabolites from CNS parenchyma (Iliff and Nedergaard 2013), interstitial fluid homeostasis (Verkhratsky and Nedergaard 2014), modulation of synaptic transmission via neurotransmitters and trophic factors (Parpura et al. 2011; Malarkey and Parpura 2008) among other functions. In response to injury or disease, reactive astrogliosis occurs characterized by an upregulation of astrocytic structural proteins, including glial fibrillary acid protein (GFAP) and vimentin. This is accompanied by morphological changes such as hypertrophy of the cell soma and processes, and in tissue injury the formation of an astrocytic scar around lesions (Sofroniew 2009).

4.1.1. Neuroinflammation in AD

Multiple lines of evidence have implicated chronic, low levels of neuroinflammation as a risk factor for AD. Aging is the greatest risk factor for AD and is itself characterized by enhanced chronic inflammation with increasing age (Blasko et al. 2004). Lifestyle factors and health conditions predisposing to inflammation, such as a history of sepsis (Iwashyna et al. 2010; Holmes et al. 2009), reduced physical exercise (Scarmeas et al. 2009; Larson et al. 2006) and obesity (Misiak et al. 2012; Lee 2011) have been associated with increased AD risk, while non-steroidal anti-inflammatory drugs (NSAIDs) may contribute towards protection (Sastre and Gentleman 2010; Vlad et al. 2008; in t' Veld et al. 2001; Weggen et al. 2001). Correspondingly, elevated levels of pro-inflammatory mediators have been detected in the brain and CSF of patients with AD and are currently being assessed as biomarkers for disease progression (Kester et al. 2015; Brosseron et al. 2014; Yasuno et al. 2012).

Significantly in recent years, genome-wide association studies have identified AD risk loci which cluster in pathways including immune system inflammatory responses (Van Cauwenberghe et al. 2015). These include, for instance, the *HLA-DRB4-DRB1* region encoding major histocompatibility complex class II proteins (Lambert et al. 2013), and

CLU and *CR1,* which encode proteins interacting with the complement system (Lambert et al. 2009). Most prominently, risk variants associated with microglia have been identified in *TREM2* and *CD33* (Guerreiro et al. 2013; Jonsson et al. 2013; Hollingworth et al. 2011; Naj et al. 2011). *TREM2* was particularly exciting following subsequent network-based analysis of genotyping data and gene expression profiles from postmortem SAD brain tissue, specifying a node identifying innate immunity and microglia as the molecular system most strongly associated with SAD pathophysiology (Zhang et al. 2013). *CD33* is also a risk variant with a role in the immune response that is capable of modifying microglial function (Griciuc et al. 2013; Crocker et al. 2012). Further, it has been recently shown that *CD33* modulates *TREM2* expression (Chan et al. 2015). These genetic associations directly implicate the brain innate immune response as a mechanism underlying AD pathogenesis.

In parallel, the immunohistochemical analysis of microglia and astrocytes has also yielded clues into the behaviour of glial cells in response to AD pathology. Both astrocytes and microglia have been described clustering around amyloid plaques, accompanied by the elevated production of cytokines (Sastre et al. 2006; Ambrosini and Aloisi 2004), suggesting that Aβ presents an endogenous stimulus triggering these glial responses. Much debate however revolves around what the functional consequences of these glial responses are, and which of these represent the key neurotoxic events leading to neuronal loss and pathology in AD.

Microglia have been shown to associate closely with mature, dense-core plaques in AD, but not with the diffuse plaques of the non-demented aging brain (Heurtaux et al. 2010; Hashioka et al. 2008; von Bernhardi 2007; Itagaki et al. 1989). While it remains unclear what triggers this microglial activation in AD, Aβ application *in vivo* and *in vitro* have demonstrated the capability of Aβ in stimulating microglial responses (Njie et al. 2012; Reed-Geaghan et al. 2009; Alarcón et al. 2005). The ability of microglia to bind Aβ has also been established by the expression of numerous Aβ-binding receptors, together with the ability to uptake Aβ peptides by phagocytosis and other mechanisms (Solito and Sastre 2012). Microglial phagocytosis has been shown to reduce with aging (Zhao et al. 1996; Floden and Combs 2011; Hickman et al. 2008), accompanied by reductions in other functional properties in response to injury, including migration capacity and extension of ramified processes (Damani et al. 2011; Sheng et al. 1998). These observations suggest an increasingly dysfunctional microglial response with age leading to a proposed “glia dysregulation hypothesis” in AD (von Bernhardi et al. 2015). This is in line with the amyloid cascade hypothesis (Hardy and Selkoe 2002; Hardy and

Higgins 1992), where Aβ causes the abnormal activation of microglia, resulting in a cytotoxic immune response (Saud et al. 2005; Nguyen et al. 2002; Wyss-Coray and Mucke 2002). This response may be self-propagating given the possibility of neuroinflammation promoting further Aβ production and aggregation (Mosher and Wyss-Coray 2014).

However, this framework has been disputed. Although microglia are able to engulf Aβ, it has been argued that there is insufficient evidence demonstrating their ability to actually degrade the protein (Prokop et al. 2013). The ablation of microglia in *APP* transgenic mouse models did not alter plaque deposition and neuritic dystrophy (Grathwohl et al. 2009), suggesting microglial functions alone are insufficient to prevent Aβ pathology in mice. The use of *in vitro* models and acute stimulation of inflammation *in vivo* to extrapolate the deleterious effects of neuroinflammatory products has also been criticized for being unrepresentative of the low-level, chronic levels of neuroinflammation found in AD (Streit 2010). However, an alternative proposed hypothesis to microglial dysfunction in AD stems from an extension of morphological observations of microglial cells around Aβ plaques. In humans with SAD, microglia appear ramified around early diffuse plaques, but were described as dystrophic around late dense-core plaques, demonstrating signs of cytorrhexis (cytoplasmic fragmentation) (Streit et al. 2009; Sheng et al. 1997). Oxidised Aβ, found in 98% of dense-core plaques, was also found in dystrophic microglia (Head et al. 2001). Ultrastructural inspection of these microglia revealed lipofuscin deposits, cytoplasmic vacuolization and swollen endoplasmic reticula, consistent with features of cell senescence (Graeber and Streit 2010; Perlmutter et al. 1990; Itagaki et al. 1989). It has therefore been proposed based on these observations that Aβ microglial toxicity is mediated by 'frustrated phagocytosis', or an inability of microglial cells to clear Aβ, possibly leading to degeneration and loss of the neuronal support functions provided by microglia (Streit et al. 2014).

Therefore, while it remains a challenge to assign functional details to morphological plasticity, the close study of microglial morphology in the context of their microenvironment (for instance, their distances from plaques) could yield ideas about the health and functionality of these cells. Some important differences exist in this respect between humans and mouse models. In mice, microglial phenotypes have been classed based on morphological (Karperien et al. 2013; Jonas et al. 2012; Stence et al. 2001) and molecular (Selenica et al. 2013; Glanzer et al. 2007; Rock et al. 2005) criteria, as ramified, primed, reactive or amoeboid types of microglia. These

morphology types have also been described in humans (Torres-Platas et al. 2014; Sheng et al. 1997). However, dystrophic microglia found in humans are largely absent in mouse models, which may instead manifest in more subtle alterations such as reduced branching and finer processes (Baron et al. 2014). Such morphological differences may reflect intrinsic differences in microglia consequent of immunological evolutionary divergence (Seok et al. 2013; Mestas and Hughes 2004), or reduced degeneration in laboratory mice due to their sterile environment and shorter lifespan (Streit et al. 2014). Therefore, characterizing microglial pathological changes in mice requires the ability to identify more subtle alterations in morphology.

In astrocytes, many parallels can be drawn between neuroinflammation observed in these cells to those described above for microglia. Astrocyte reactivity and atrophy have been characterized in AD, often prior to the development of AD pathology. This has been repeatedly demonstrated in AD transgenic mouse models (Olabarria et al. 2010; Yeh et al. 2011; Verkhratsky et al. 2010), including in J20 mice (Beauquis et al. 2014; Beauquis et al. 2013). In post-mortem brain tissue from patients with AD, astroglial reactivity reflected by increased GFAP and S100β expression has also been described (Meda 2001; Griffin et al. 1998; Beach and McGeer 1988). No correlation has been observed between increased GFAP expression and Aβ load or dementia (Wharton et al. 2009). However, it has been established that astrocytes are capable of clearing Aβ through the expression of Aβ proteases (Pihlaja et al. 2011; Dorfman et al. 2010; Yin et al. 2006; Koistinaho et al. 2004), resulting in reduced amyloid load in AD transgenic models (Leissring et al. 2003; Marr et al. 2003). Astrocytes are furthermore the largest source of ApoE in the brain (Bu 2009) which remains the largest factor influencing SAD risk (Bertram and Tanzi 2008).

Morphologically, astrocyte reactivity is demonstrated by enlarged cell bodies, altered arborisation (Wilhelmsson et al. 2006), and polarization towards the site of injury, including towards Aβ plaques (Bardehle et al. 2013). This remains a mild form of "isomorphic" astrogliosis in AD, where astrocytes keep their territorial domains without formation of an astrocytic scar (Sofroniew 2009; Wilhelmsson et al. 2006). Unlike microglia, reactive astrocytes have also been found in plaque-free areas of the parenchyma, in addition to those surrounding Aβ plaques (Simpson et al. 2010). In addition, atrophic astrocytes have also been reported, similar to the age-dependent senescence proposed above in microglia (Streit et al. 2014). In the longitudinal characterization of the triple-transgenic AD mouse, atrophic astrocytes could be observed from a distance of 50 μm from plaques, in old mice at 18 months of age

(Olabarria et al. 2010). While the number of detectable GFAP-positive cells increases with age and AD, this is primarily due to upregulation of GFAP expression rather than proliferation, as astrocytes only account for less than 10% of proliferating cells both in AD patients and mouse models (Serrano-Pozo et al. 2013; Sirko et al. 2013; Kamphuis et al. 2012; Lepore et al. 2008). Unlike microglia, which remain relatively similar in size and morphology between humans and mice, human astrocytes are 2.6-fold larger, extend 10-fold more branches and are capable of propagating calcium waves 4-fold quicker than rodent astrocytes (Oberheim et al. 2009). Together with greater diversification in astrocyte subpopulation (Oberheim et al. 2006), human astrocytes exhibit an increased complexity that may allow greater functional competence in the human brain.

4.1.2. Neuroinflammation in DS

Alterations in neuroinflammation have been described in people with DS commencing from fetal stages, and lasting throughout life (Wilcock and Griffin 2013). Given the increased risk of AD following chronic low levels of neuroinflammation as described above, increasing attention is now being directed towards understanding whether neuroinflammatory responses in DS may become potential accelerators of AD neuropathogenesis. Several genes trisomic in DS have been linked to neuroinflammatory functions, of which most attention has been focused on *APP* and *S100B* (Griffin et al. 1989). *S100B* is an astrocyte-derived neurite extension factor (Kligman and Marshak 1985) which in healthy conditions contributes to the growth and maintenance of neurons (Barger et al. 1995). When highly expressed, as has been demonstrated both in DS and AD, *S100B* is associated with abnormal growth of dystrophic neuronal processes (Reeves et al. 1994; Marshak 1990), particularly in proximity to Aβ plaques (Mrak and Griffin 2001; Royston et al. 1999; Marshak et al. 1992). Products of both *APP* and *S100β* are capable of inducing the expression of cytokine IL-1 (Barger and Harmon 1997; Griffin et al. 1989), which has been associated with a series of pathological features relating to AD, including astrocytic and microglial activation (Li et al. 1998), tau hyperphosphorylation (Sheng et al. 2001; Sheng et al. 2000), increased acetylcholinesterase activity (Li et al. 2000) and decreased synaptosphysin expression (Li et al. 2003). In addition, IL-1 is able to induce the synthesis of both APP and S100β (Sheng et al. 1996), while S100β is itself also able to promote *APP* expression (Li et al. 1998). These events therefore potentially contribute to a self-propagating chronic neuroinflammatory state (Griffin and Mrak 2002).

Other gene candidates on Hsa21 have also been implicated in potential neuroinflammatory functions, albeit less strongly. Briefly, neural effects of *CXADR* could be explored, to determine if it displays a similar pro-inflammatory role as it does in the heart (Ito et al. 2000). The overexpression of both *TIAM1* (Cheon, Kim, Ovod, et al. 2003) and *SOD1* (Cenini et al. 2012) have been associated with increased oxidative stress via different mechanisms, triggering neuroinflammatory responses. Signalling pathways regulating cytokine production may also be altered following trisomy of components in these pathways, resulting in more proinflammatory signaling; these components include the IFN receptors *IFNAR1*, *IFNAR2* and *IFNGR2* (Kim et al. 1997), the serine-threonine kinase *RIPK4* which influences both TNFR1 and NFκB signaling (Dalal et al. 2012; Rountree et al. 2010; Meylan et al. 2002) and *PRMT2*, encoding an arginine methyltransferase that promotes neuroinflammation via JAK-STAT signalling pathways (Mowen et al. 2001).

In addition, DS is characterized by complex neurodevelopmental alterations in gliogenesis that likely contribute to the intellectual disability ubiquitous in DS. An evaluation of non-neuronal cell markers from 14 weeks of gestation to birth in DS individuals demonstrated region-specific alterations in the expression of different glial cell types, including defects in astrocyte production (Kanaumi et al. 2013). Interestingly, trisomy of *APP* in Ts65Dn mice was found to be responsible for increased astrogliogenesis and reduced neurogenesis, with effects exerted by two separate APP cleavage products (Trazzi et al. 2013). These lifelong alterations in glial development potentially culminate in a different neuroinflammatory milieu in DS, which could potentially influence AD pathogenesis. This was illuminated recently by a study of immunophenotypes in young and old patients with AD, together with young (without AD pathology) and old patients with DS (and AD pathology). Each of these groups was distinguishable by different immunophenotype patterns. Notably, old DS patients demonstrated an M2b phenotype which was never observed in patients with SAD (Wilcock et al. 2015). M2b is associated with the presence of immune complexes (Mosser and Edwards 2008; Edwards et al. 2006) and has been associated with increased clearance of amyloid deposits (Sudduth et al. 2013). This suggests that DS exhibits an altered neuroinflammatory profile from AD, both before and after the onset of AD pathology.

While few histopathological study of glial cells in DS have been performed, the investigators who identified and proposed the notion of senescent microglia have identified a mixture of healthy and dystrophic, cytorrhexic microglia in DS individuals in

their 40s, coincident with the appearance of tau pathology (Xue and Streit 2011). This was accompanied by a decrease in microglial numbers, albeit with wide variability between DS individuals. In a previous study (Streit et al. 2009), all microglia were senescent in two DS individuals over 50 years old with advanced AD pathology, suggesting that accelerated amyloidogenesis in DS may speed up microglial senescence as well. On the other hand, no morphological study of astrocytes or microglia has been performed in DS mouse models. Only one study has investigated numbers of microglia in Ts65Dn mice, demonstrating increased numbers of activated microglia in the hippocampus and basal forebrain at 18 months of age (Hunter et al. 2004).

This chapter therefore describes the development of a digital analysis protocol, using Definiens Developer, to systematically quantify morphological characteristics of microglia and astrocytes in Tc1xJ20 mice. We proceed to investigate how these parameters may be altered with age, trisomy 21 or APP/Aβ overexpression, and evaluate the validity of these results.

4.1.3. Aims

1. Quantify area and number of microglia and astrocytes present in hippocampal sections of 6 and 16-17 month old Tc1xJ20 mice
2. Measure the size of glial cell bodies, and the length and complexity of cellular processes in the same sections
3. Examine neuronal and astrocytic protein expression in cortical and hippocampal homogenate of 3-month old Tc1xJ20 mice

4.2. Results

In order to understand how glial phenotypes may be influenced by age, trisomy 21 and APP/Aβ overexpression, a digital protocol was developed to systematically identify discrete microglia and astrocytes, before quantifying the dimensions of cell bodies and cellular processes. As glial morphology is influenced by plaque deposition, we optimized the protocol using sections from 16-17 month old Tc1xJ20 mice, in which APP/Aβ overexpressing mice exhibit the heaviest Aβ plaque loads (Figure 1.13). These results were compared to 6-month old Tc1xJ20 mice, which exhibit early stages of plaque deposition (Mucke et al. 2000 and Figure 1.13). Table 4.1 below details the

sections that were used for analysis, including information about genotype, age and sex.

Table 4.1 Samples used for digital immunohistochemical analysis of microglia and astrocytes

Iba1				
Age	**Genotype**	**No. of mice**	**Male**	**Female**
6 months	Wt	5	0	5
	Tc1	4	0	4
	J20	3	0	3
	Tc1;J20	5	0	5
16-17 months	Wt	6	3	3
	Tc1	5	2	3
	J20	7	4	3
	Tc1;J20	7	4	3
GFAP				
Age	**Genotype**	**No. of mice**	**Male**	**Female**
6 months	Wt	8	3	5
	Tc1	6	1	5
	J20	8	5	3
	Tc1;J20	10	5	5
16-17 months	Wt	6	3	3
	Tc1	3	2	1
	J20	4	2	2
	Tc1;J20	5	4	1

4.2.1. Identification and characterization of microglia

As illustrated in Figures 4.1 and 4.6, the primary challenge in analyzing sections from 16-17-month old mice lay in separating individual glial cells with interwoven processes, and deciding which processes emerged from which respective cell bodies. This was performed using the observation that primary processes emanating from cell bodies were more darkly stained, before fading in staining intensity towards secondary branches and the terminal ends of each glial process. Therefore, our protocol identified primary processes using darker threshold levels of brown staining, before identifying potential ends of glial processes using lighter brown staining levels. It subsequently digitally “shrank” these light brown processes, to generate break points, before “growing” the process back to its original form for analysis. These break points were therefore used to determine which glial processes belonged to which cell bodies, hence offering a protocol that was more consistent and efficient than manual segmentation.

Regions were present where the dense mesh of glial cell bodies and processes was impossible to separate, and these were classified as ‘inseparable clusters’ of staining. These clusters were included in calculations for the overall area of immunostaining, but were excluded from our phenotyping of individual glial cells, since discrete cell bodies could not be identified within these clusters.

Figure 4.2 displays hippocampal sections from Wt, Tc1, J20 and Tc1;J20 mice, at 6 months and 16-17 months, to illustrate the morphological changes observed with genotype as elaborated in the results below. The top panel from each page of Figure 4.2 depicts Iba1 staining, and the bottom panel is colour coded for cell bodies (blue), processes (yellow) and inseparable clusters (black).

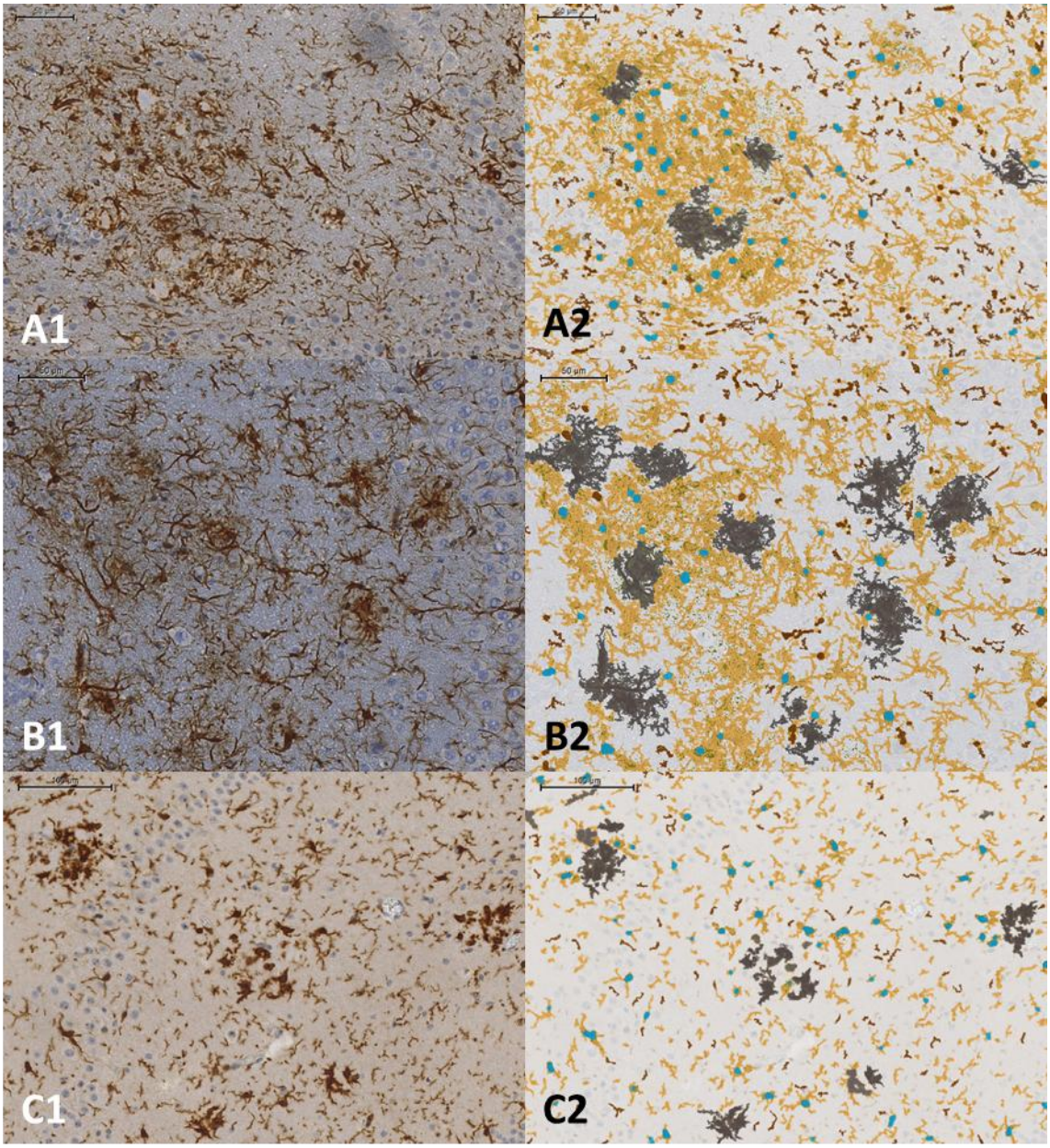

Figure 4.1 Identification and characterisation of microglial cells.

Images in each row are of the same field of view, with the left column displaying Iba1 staining and the right column colour coded for the analysis of the following features: blue areas indicate microglial cell bodies, yellow areas indicate microglial processes, and black areas represent 'inseparable clusters' where individual glial cells could not be distinguished. Figures A1 and A2 illustrate the specificity of detecting microglial cell bodies, even in regions of closely associated cells. Figures B1 and B2 illustrate 'inseparable clusters' resembling amyloid plaque deposition. Figures C1 and C2 illustrate examples of clustered microglia with touching cell bodies, which were unable to be segmented as individual cells, resulting in a proportion of false negatives classified as 'inseparable clusters', indicated by the colour black. Scale bars: A1-B2: 50 μM; C1-C2: 100 μM.

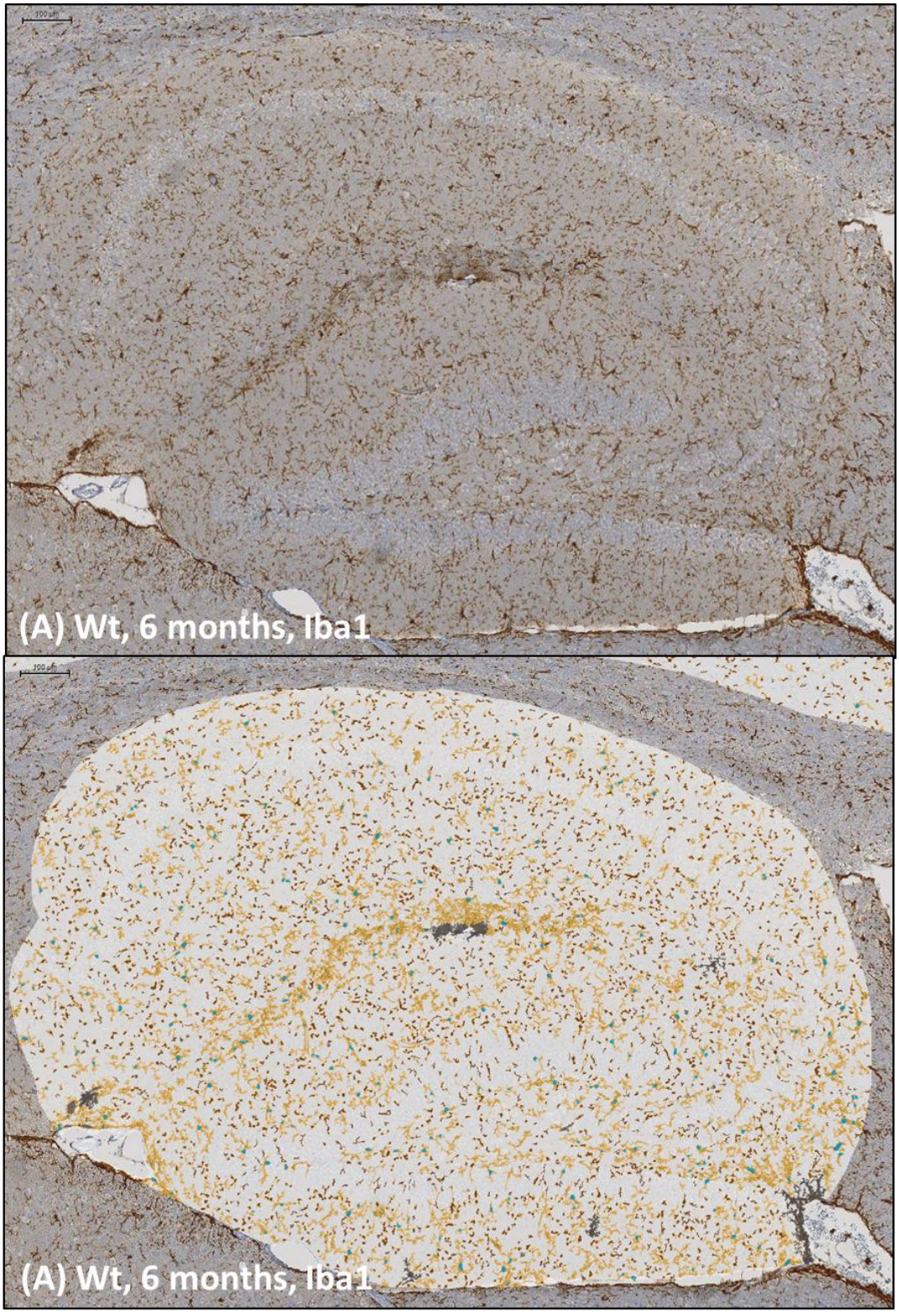

Figure 4.2. Increased microglial numbers and size with APP/Aβ overexpression in hippocampal sections from Tc1xJ20 mice

Figures 4.2A-D depict microglial cells identified in 6-month old Wt (4.2A), Tc1 (4.2B), J20 (4.2C) and Tc1;J20 (4.2D) sections, while Figures 4.2E-H show the respective genotypes at 16-17 months. The top panels illustrate Iba1 staining while the bottom panel is colour coded as follows: blue areas indicate microglial cell bodies, yellow areas indicate microglial processes, and black areas represent 'inseparable clusters' where individual glial cells could not be distinguished. Scale bars represent 100 μM.

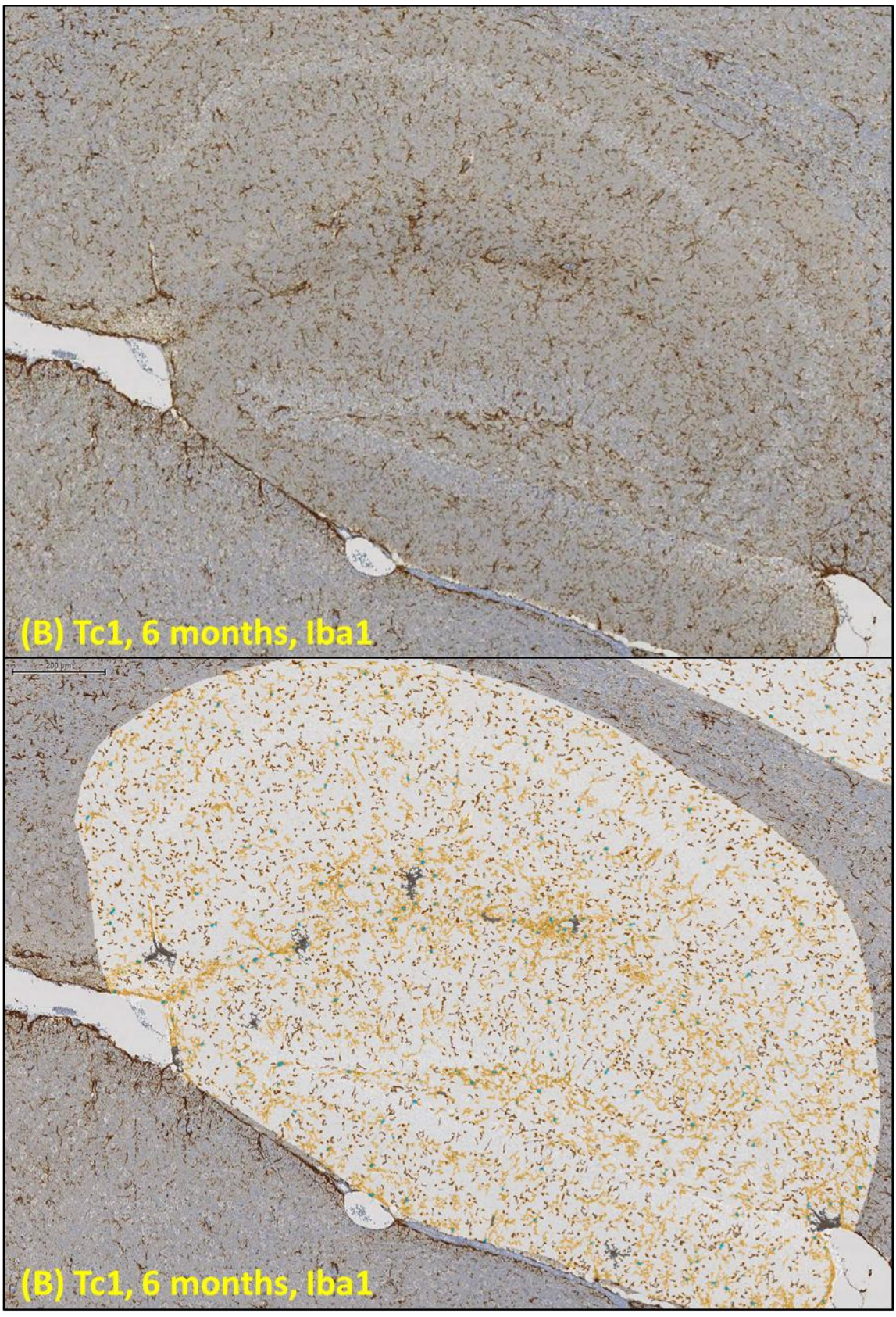
(B) Tc1, 6 months, Iba1
(B) Tc1, 6 months, Iba1

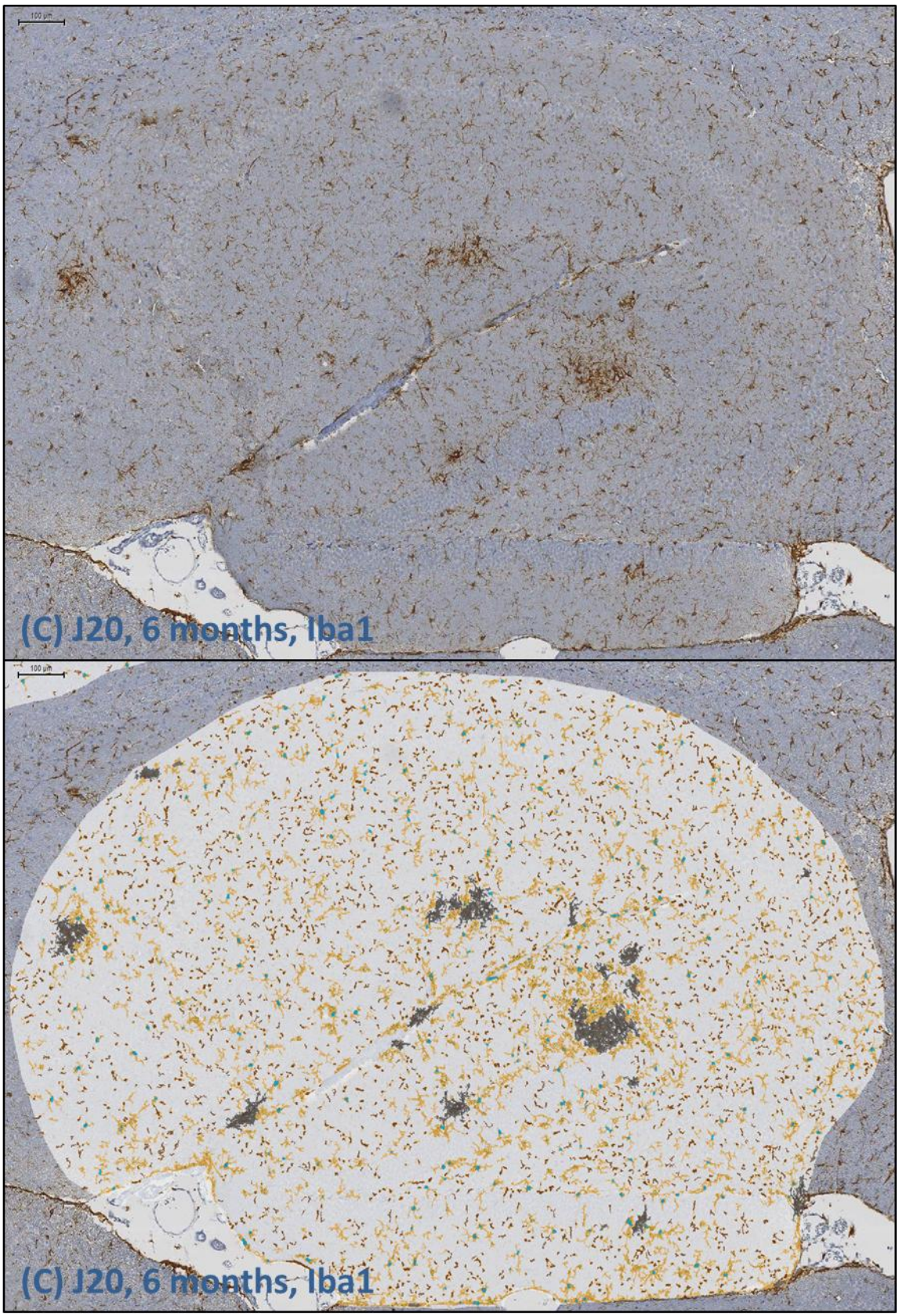
100 µm
(C) J20, 6 months, Iba1
100 µm
(C) J20, 6 months, Iba1

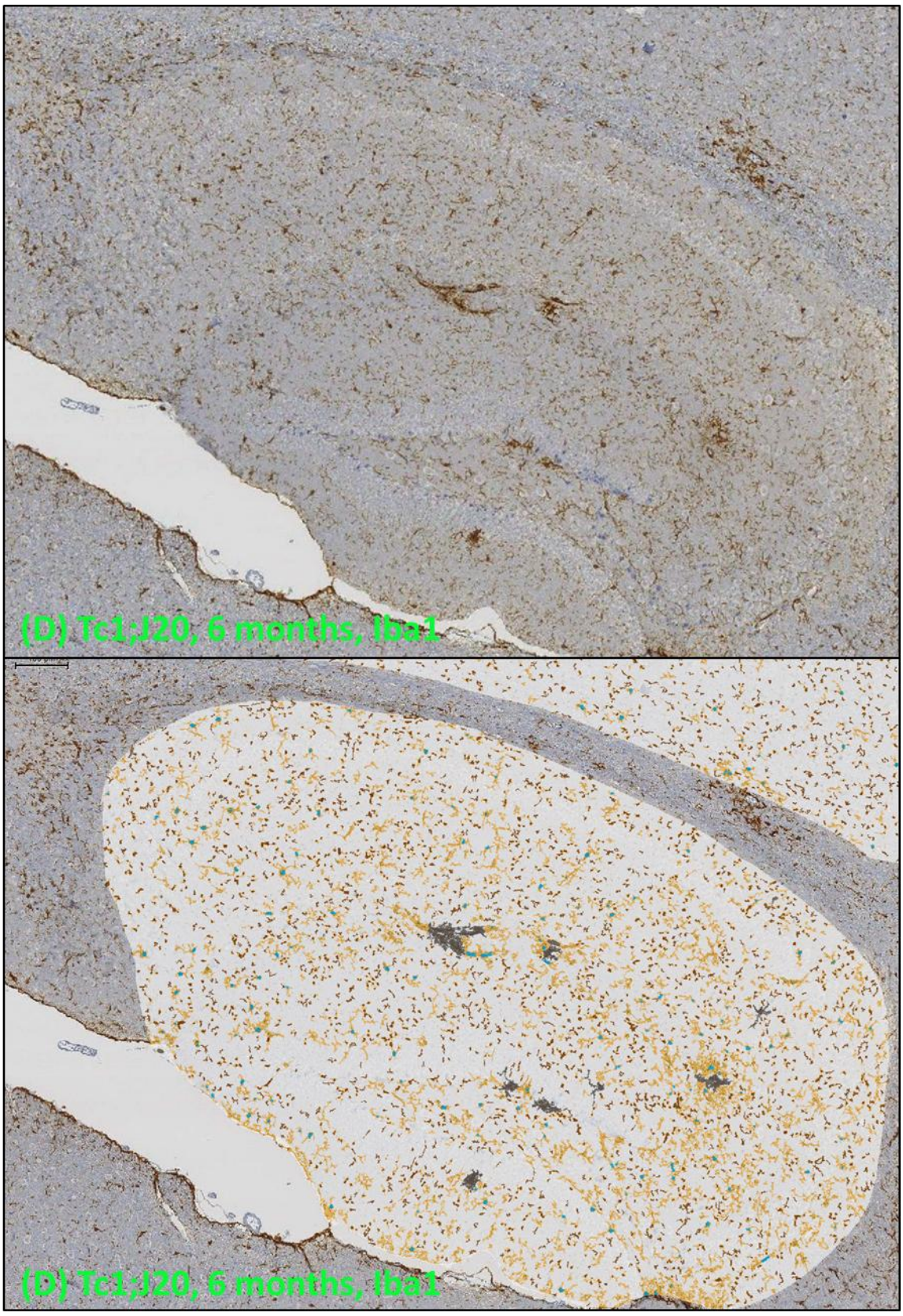
(D) Tc1;J20, 6 months, Iba1
(D) Tc1;J20, 6 months, Iba1

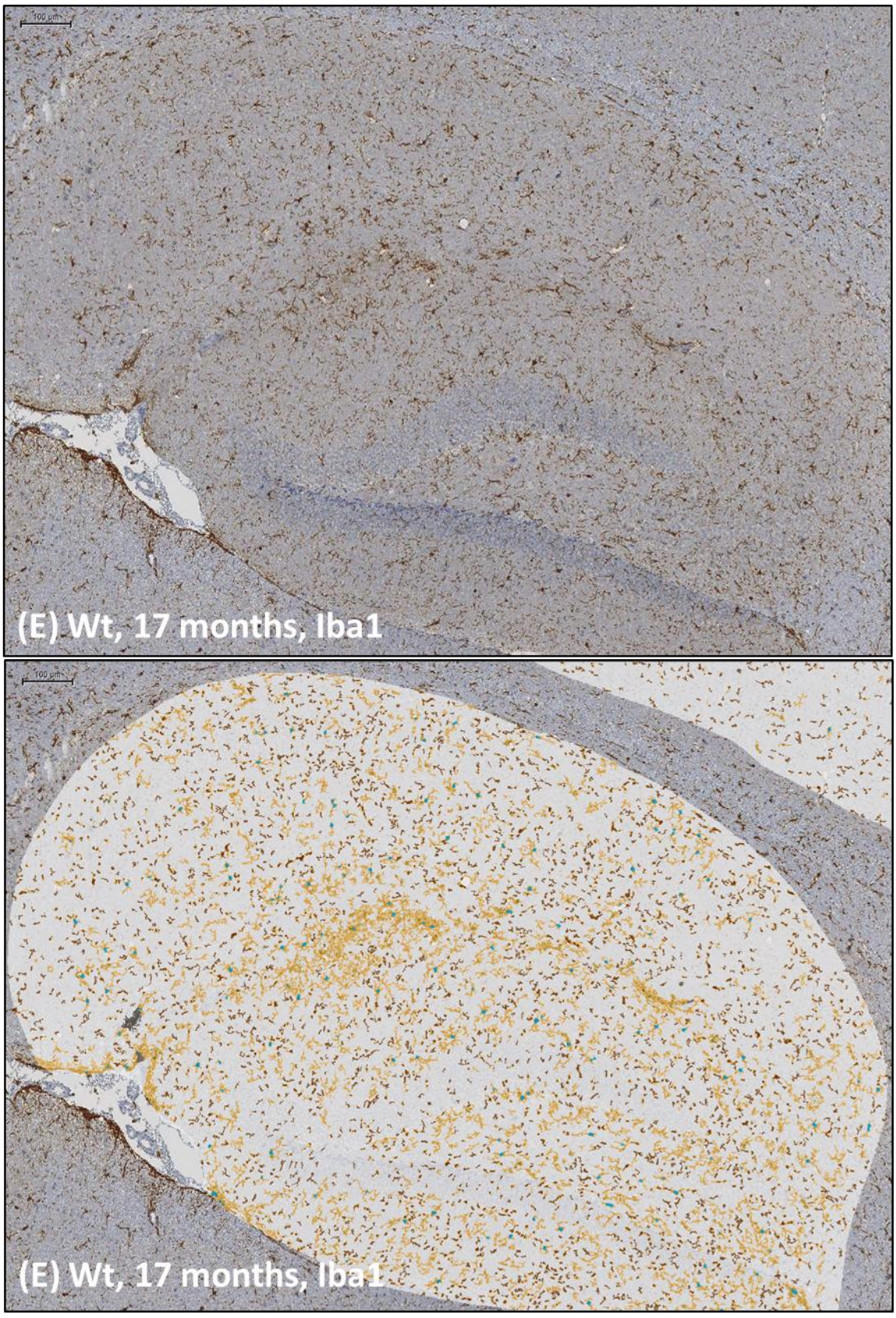
100 µm
(E) Wt, 17 months, Iba1
100 µm
(E) Wt, 17 months, Iba1

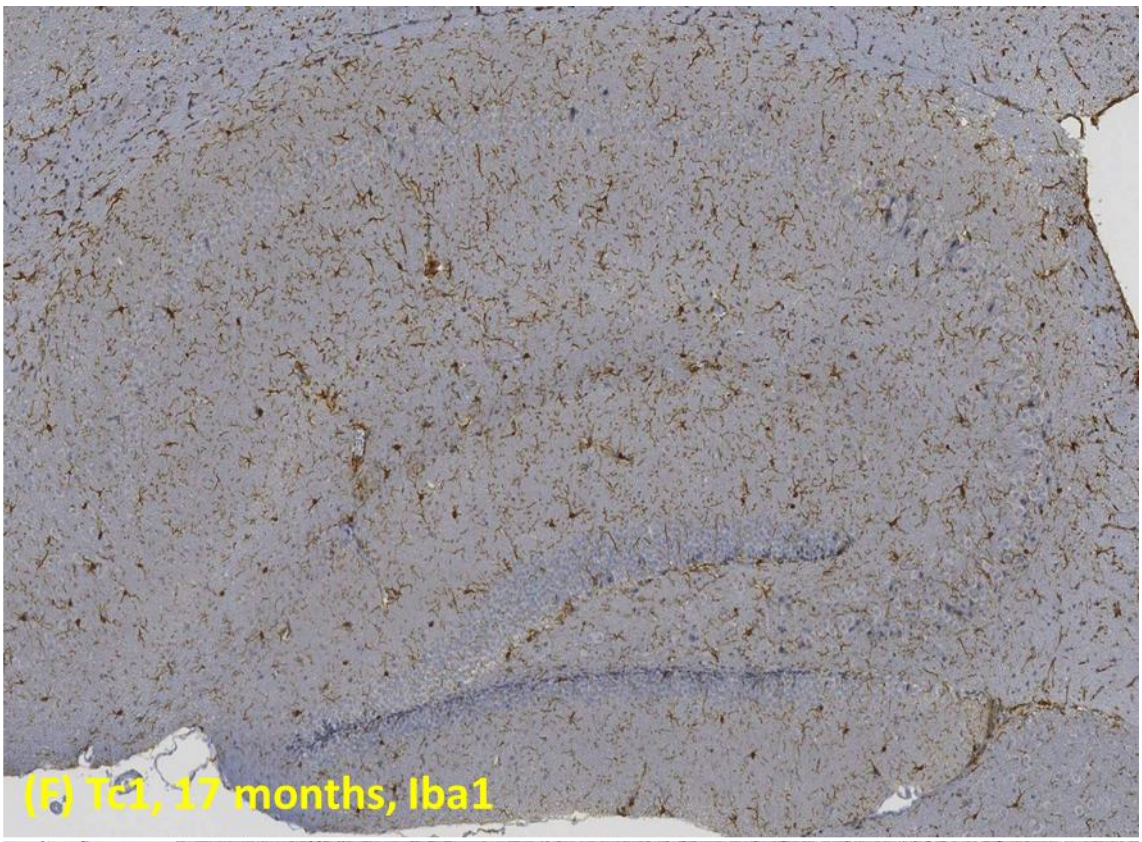
(F) Tc1, 17 months, Iba1

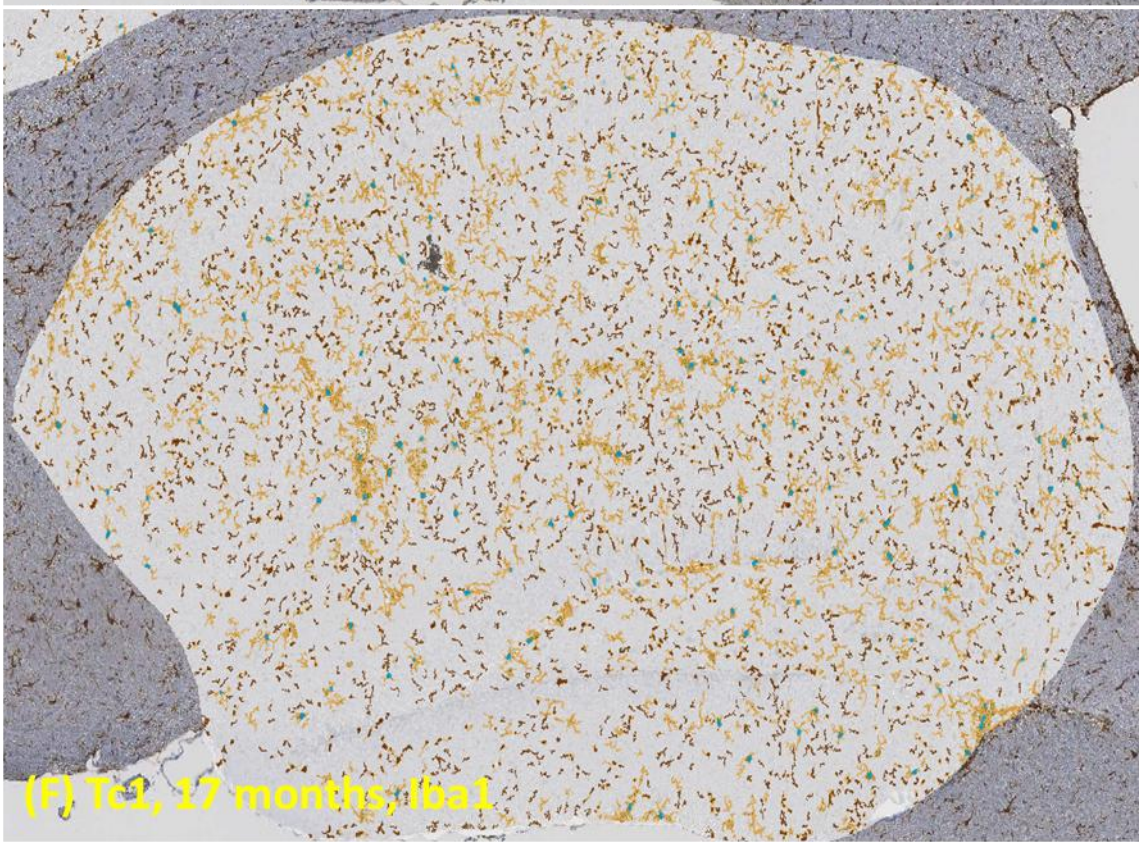
(F) Tc1, 17 months, Iba1

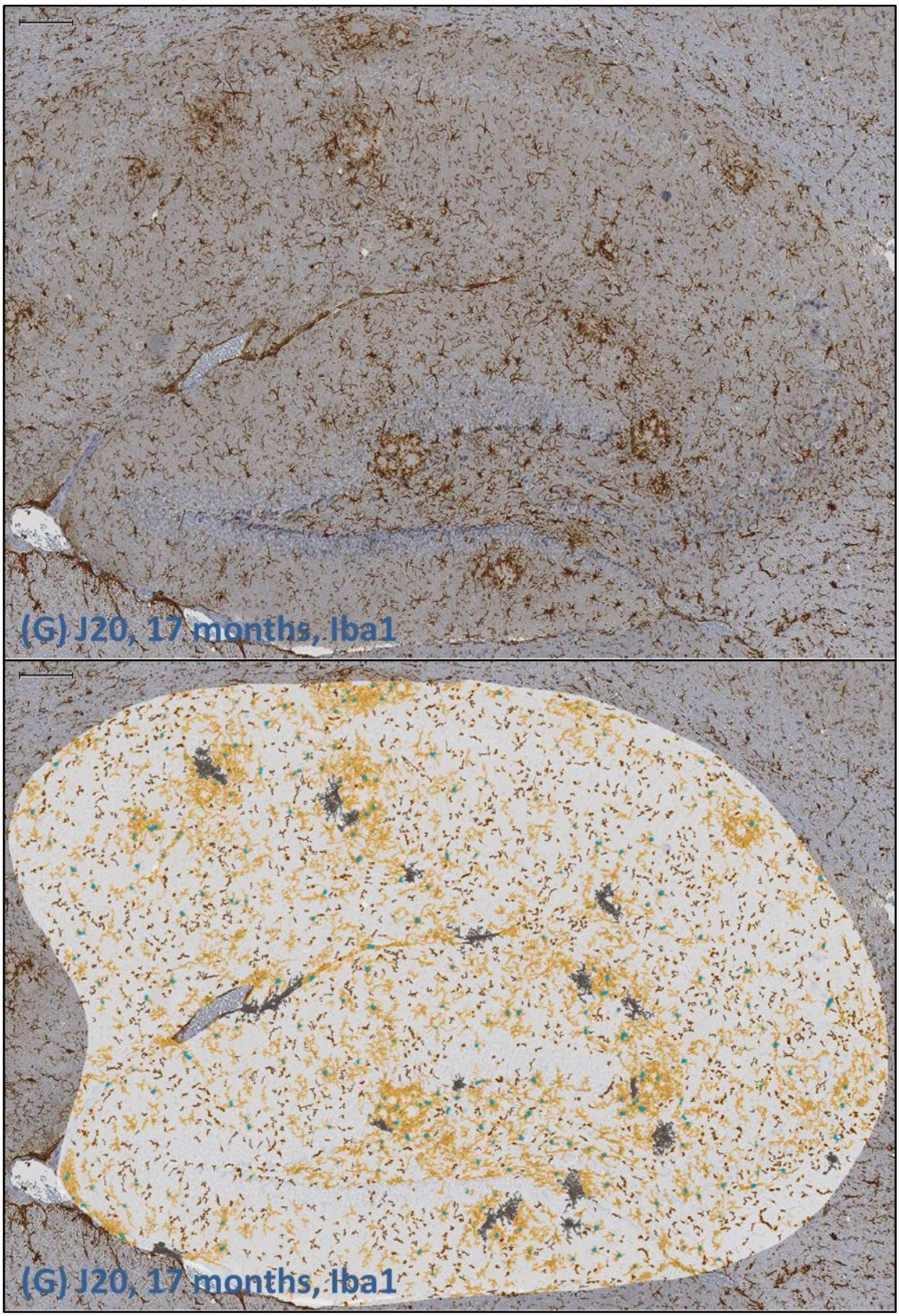
(G) J20, 17 months, Iba1
(G) J20, 17 months, Iba1

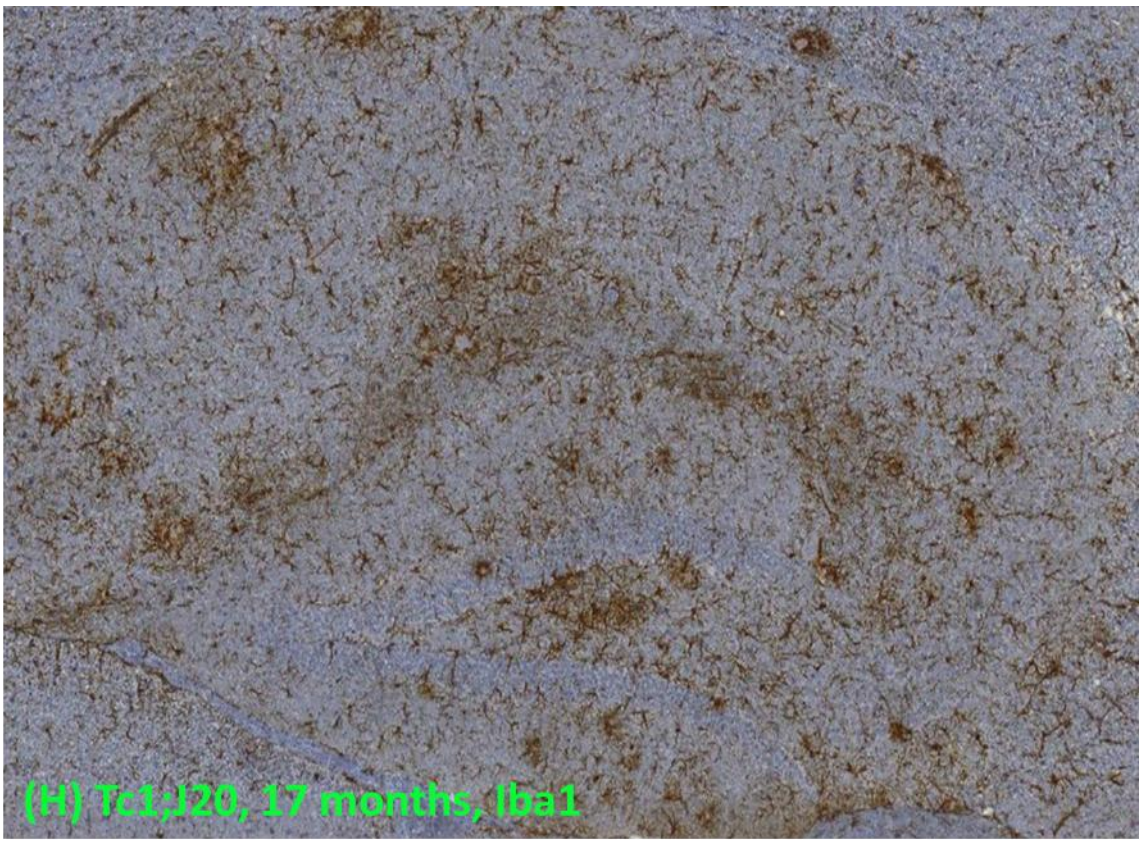
(H) Tc1;J20, 17 months, Iba1

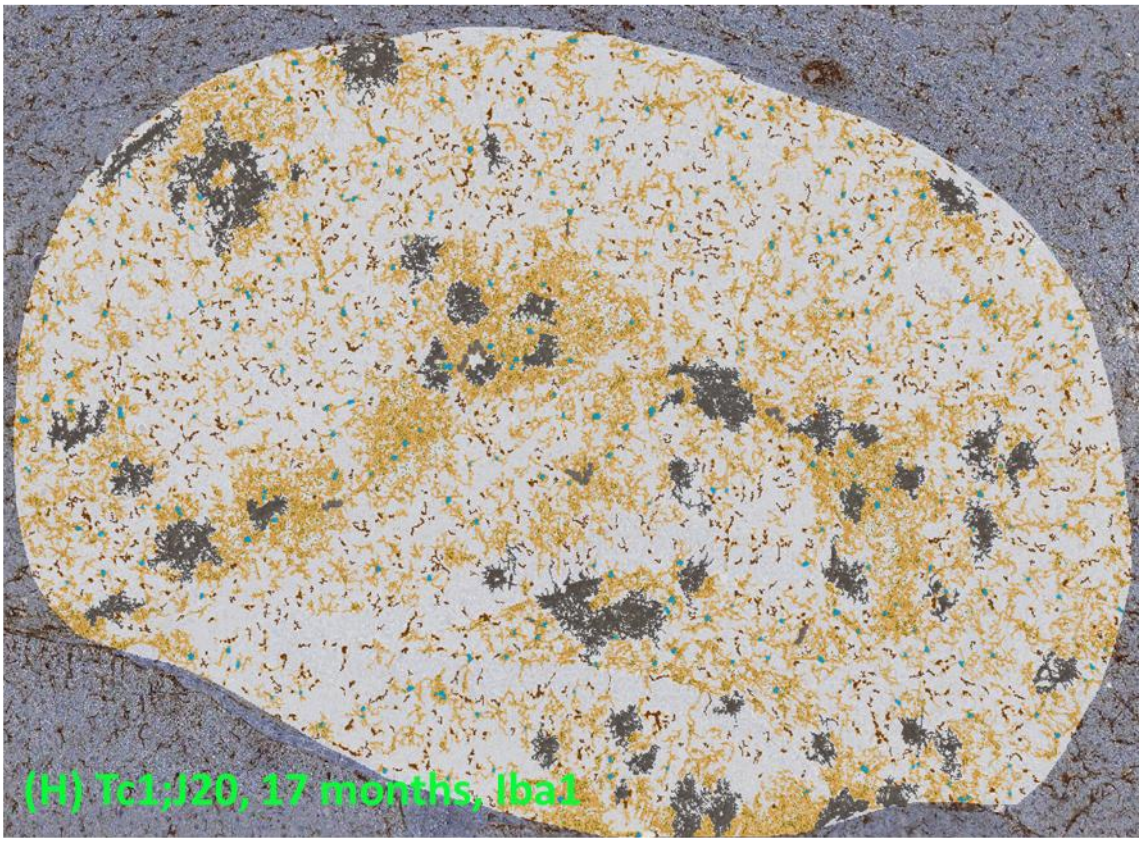
(H) Tc1;J20, 17 months, Iba1

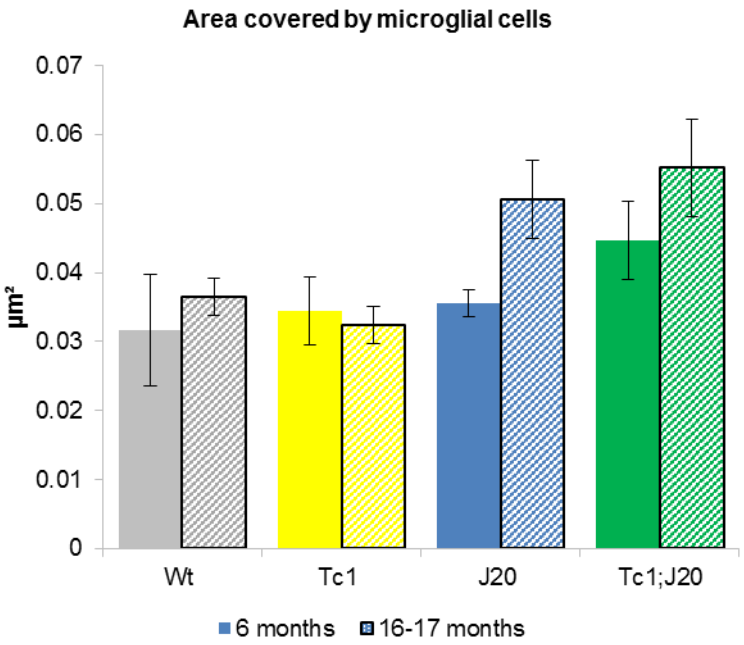

Figure 4.3 Total hippocampal surface area covered by microglia significantly increases with APP/Aβ overexpression.

Total area of Iba1 staining was calculated by summing the areas of cell bodies, cell processes and inseparable clusters. Total Iba1 area was expressed as a proportion of the total surface area of the hippocampus. APP/Aβ overexpression significantly increased total microglia area, but there was no significant influence of age or trisomy 21 on total microglia area. Graph shows mean values while error bars indicate SEM.

The area of Iba1 staining was quantified to determine if the surface area covered by microglia in the hippocampus was changed by age, trisomy 21 or APP/Aβ overexpression (Figure 4.3). Area of microglia surface area covered was normalized to the total area of the hippocampus, which had been manually identified and outlined prior to analysis. Areas included for analysis included all objects identified as cell bodies, cell processes, and the 'inseparable clusters' where discrete cell bodies could not be identified. Area of microglial staining was significantly increased with APP/Aβ overexpression (two-way ANOVA $F(1,34) = 8.955$, $p = 0.005$). There was no significant effect of trisomy 21 or age on microglial area.

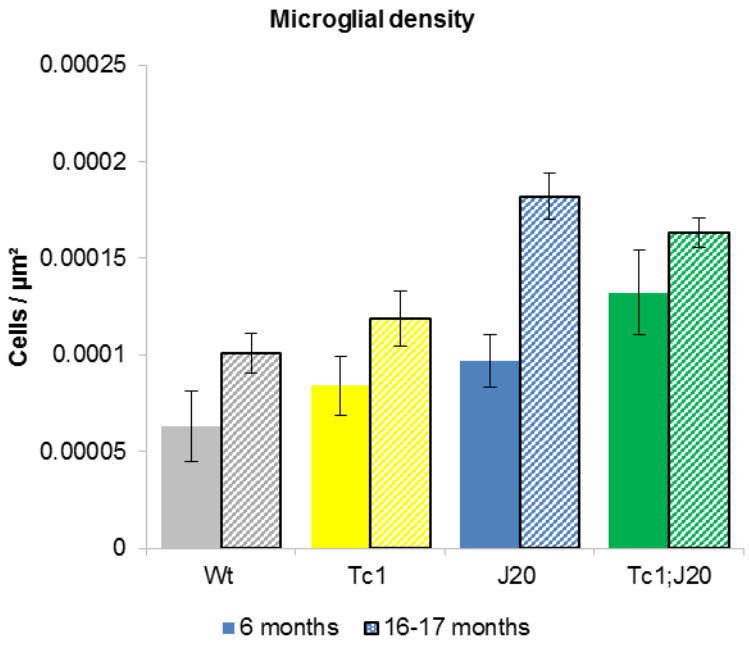

Figure 4.4 Hippocampal microglial density significantly increases with age and *APP* overexpression.

Density was calculated as the total number of cell bodies identified, expressed as a ratio to total hippocampal area. Both age and APP/Aβ overexpression increased microglia density but there was no significant effect of trisomy 21. Graph shows mean values while error bars indicate SEM.

To compare changes in the number of microglial cells in the hippocampus, the microglial density was calculated by dividing the total number of cell bodies by the total area of the hippocampus. Microglial density was significantly increased with APP/Aβ overexpression (two-way ANOVA $F(1,40) = 8.98$, $p = 0.005$). There was a significant interaction between age and *APP* overexpression suggesting that old age further increased the effect of APP/Aβ overexpression on microglial density (two-way ANOVA $F(1,40) = 3.245$, $p = 0.049$).

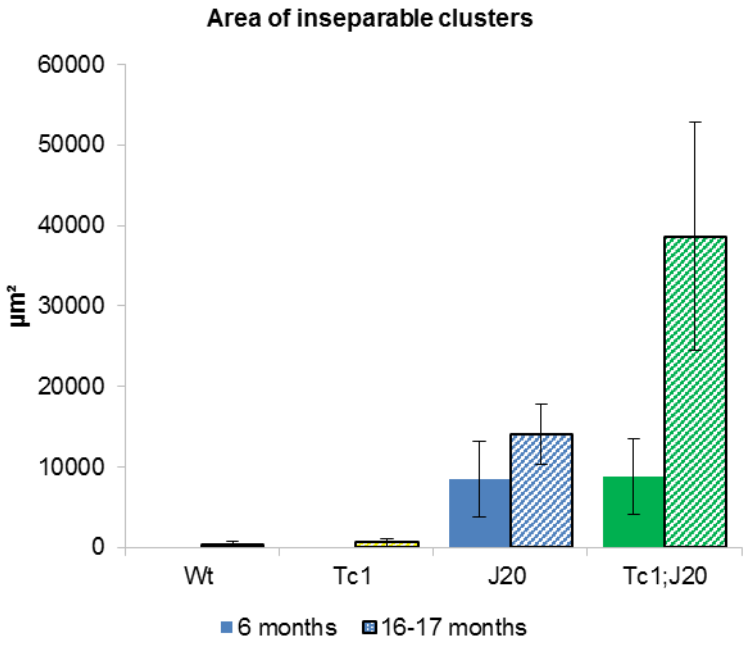

Figure 4.5 Area of microglial 'inseparable clusters' significantly increases with APP/Aβ overexpression.

The area of inseparable clusters, which were regions where discrete cell bodies could not be distinguished, was quantified. APP/Aβ overexpression significantly increased the area of inseparable clusters, while there was a trend towards increased area with age. There was no significant influence of trisomy 21 on inseparable clusters when studied across the four genotypes. Graph shows mean values while error bars indicate SEM.

'Inseparable clusters' were regions where our protocol could not distinguish discrete cell bodies, and were hence excluded from the characterization of individual cell phenotypes (Figure 4.1). The area of 'inseparable clusters' was significantly increased with APP/Aβ overexpression (two-way ANOVA $F(1,34) = 10.266$, $p = 0.003$). There was also a trend towards increased 'inseparable clusters' with age ($F(1,34) = 2.872$, $p = 0.099$), but there was no significant effect of trisomy 21 when studied across the four genotypes. When comparing the effect of trisomy 21 only on mice overexpressing APP/Aβ, there was a trend to increased area of inseparable clusters due to trisomy 21 (independent samples t-test $t(26) = -1.830$, $p = 0.079$) (Figure 4.5).

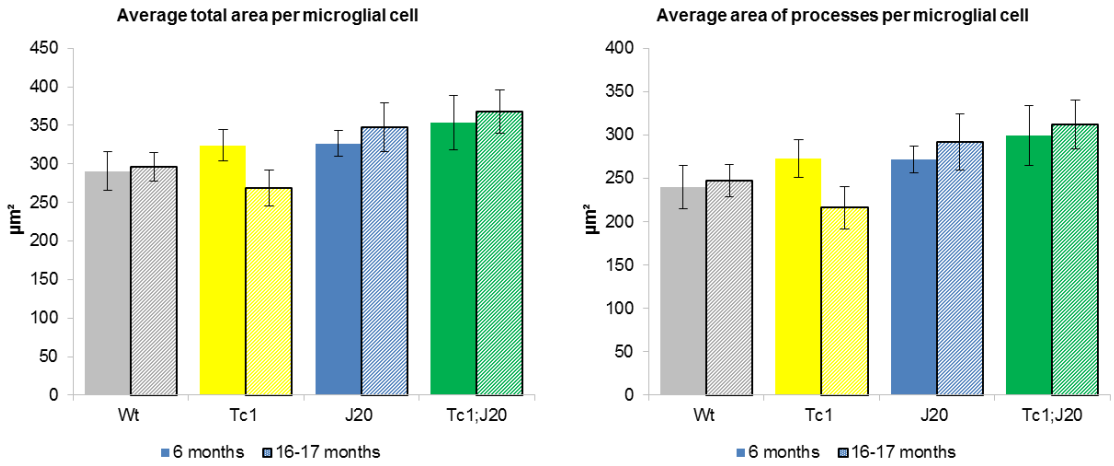

Figure 4.6 Average total area, and area of processes, per microglial cell increases with APP/Aβ overexpression.

The area per microglial cell was calculated by adding the area of cell body and area of cell processes in each microglial cell. APP/Aβ overexpression significantly increased the average area per microglial cell, as well as the average area of cell processes per microglial cell. There was no significant effect of trisomy 21 or age. Graph shows mean values while error bars indicate SEM.

The average total area of each microglial cell, which includes area for cell body and processes, was significantly increased with APP/Aβ overexpression (two-way ANOVA $F(1,34) = 5.796$, $p = 0.022$), with no significant effect of trisomy 21 or age. This pattern was closely reflected by the increase in the average area of processes per cell with APP/Aβ overexpression (two-way ANOVA $F(1,34) = 6.948$, $p = 0.013$), but with no significant influence of trisomy 21 or age (Figure 4.6).

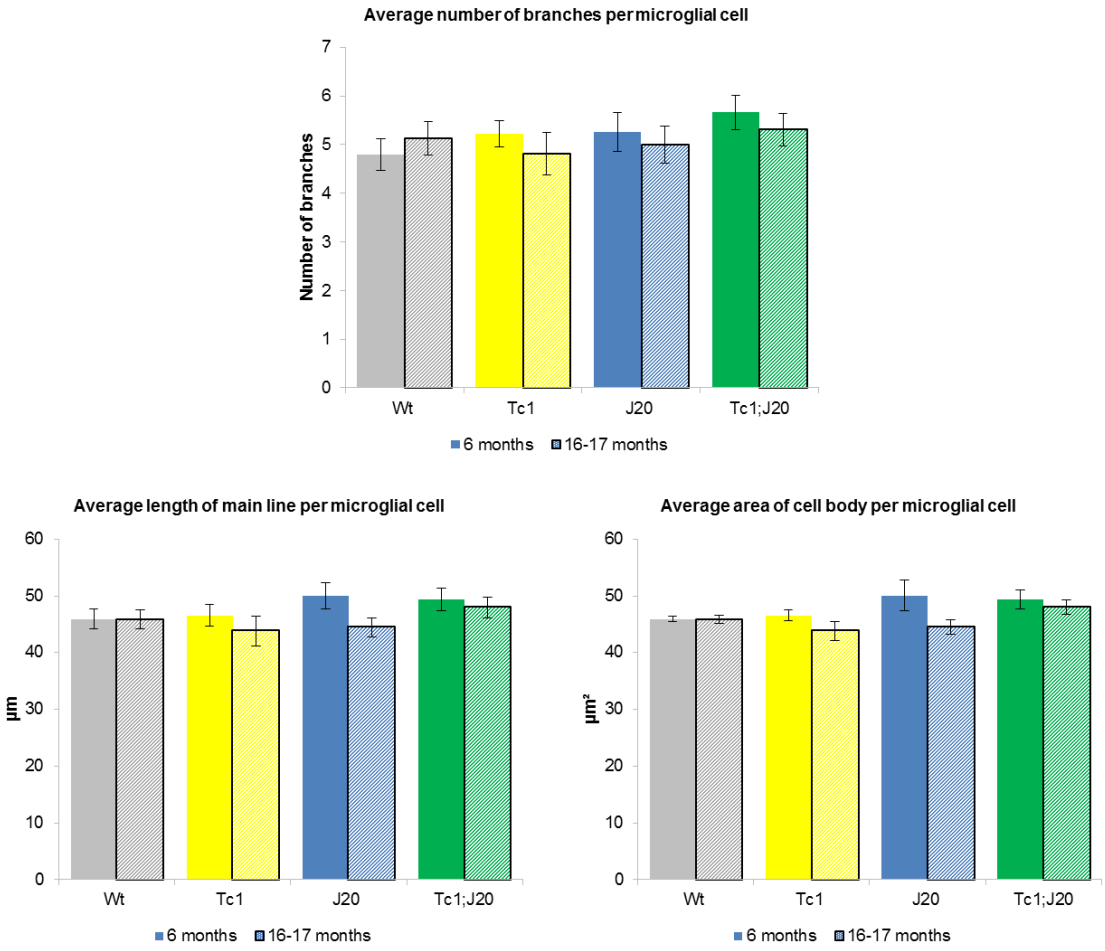

Figure 4.7 No significant differences in average number of branches, length of main line and area of cell body in microglial cells.

The main line measures the distance between the ends of the two longest processes per cell, while the number of branches per cell is determined from the main line. There was no significant effect of trisomy 21, APP/Aβ overexpression or age on the number of branches, length of main line and size of cell bodies per microglial cell. Graph shows mean values while error bars indicate SEM.

Although the average area of processes per microglial cell was significantly increased with APP/Aβ overexpression (Figure 4.6), this was not due to an increased number of branches, or of the general elongation of cells as measured by the main line, both of which were not influenced by age, trisomy 21 or APP/Aβ overexpression (Figure 4.7). The main line is the distance between the ends of the two longest processes. The increase in area per microglial cell was also not associated with an increase in average cell body size with age, trisomy 21 or APP/Aβ overexpression (Figure 4.7), therefore increased cell area with APP/Aβ overexpression (Figure 4.6) was accounted for primarily by an increase in the area of cell processes.

4.2.2. Identification and characterization of astrocytes

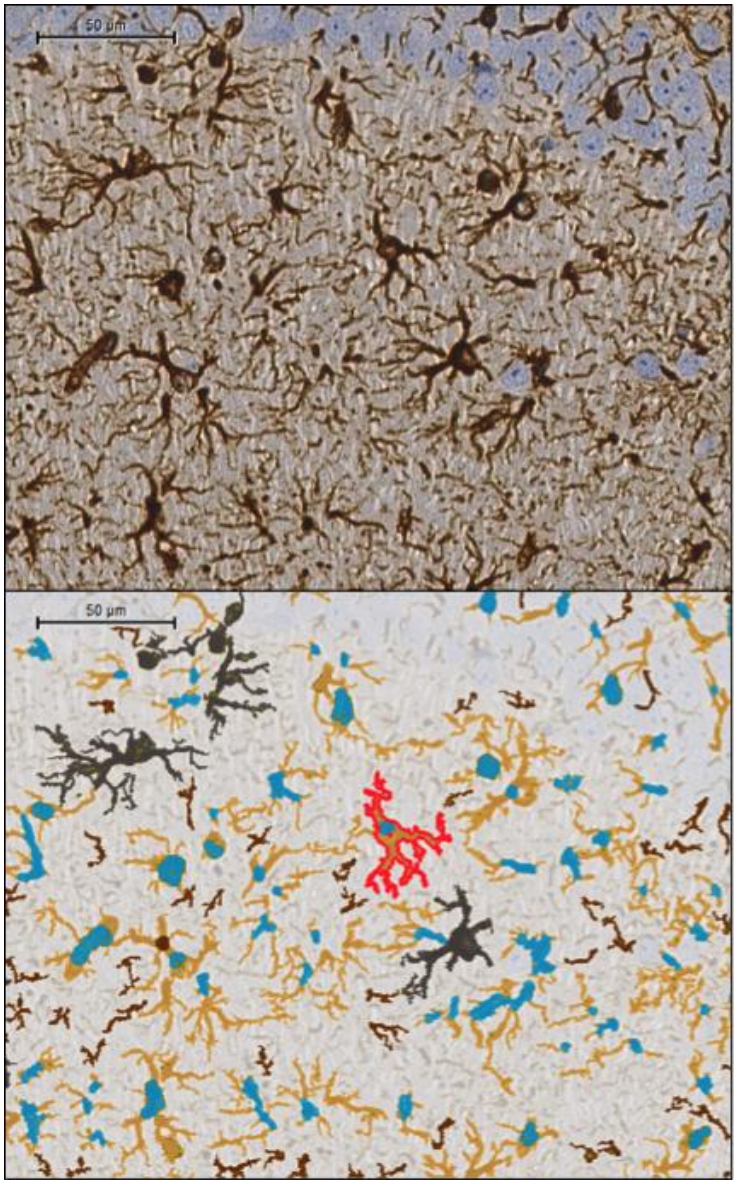

Figure 4.8 Identification and characterization of astrocytes (GFAP+).

The top picture displays astrocyte (GFAP) staining and the bottom picture is colour-coded for the analysis of the following features: blue areas indicate astrocytic cell bodies, yellow areas indicate astrocytic processes, and black areas represent 'inseparable clusters' where individual glial cells could not be distinguished. An example of an identified astrocyte is outlined in red. Scale bars represent 50 µM.

Figure 4.8 illustrates the identification of astrocytes in hippocampal sections stained with GFAP, and similarly colour coded to indicate cell bodies (blue), cell processes (yellow) and inseparable clusters (black). Figure 4.9 displays hippocampal sections from Wt, Tc1, J20 and Tc1;J20 mice at both 6 months (Figures 4.9A-D), and 16-17 months (Figures 4.9E-H) to illustrate the morphological changes observed primarily with age as elaborated in the results below.

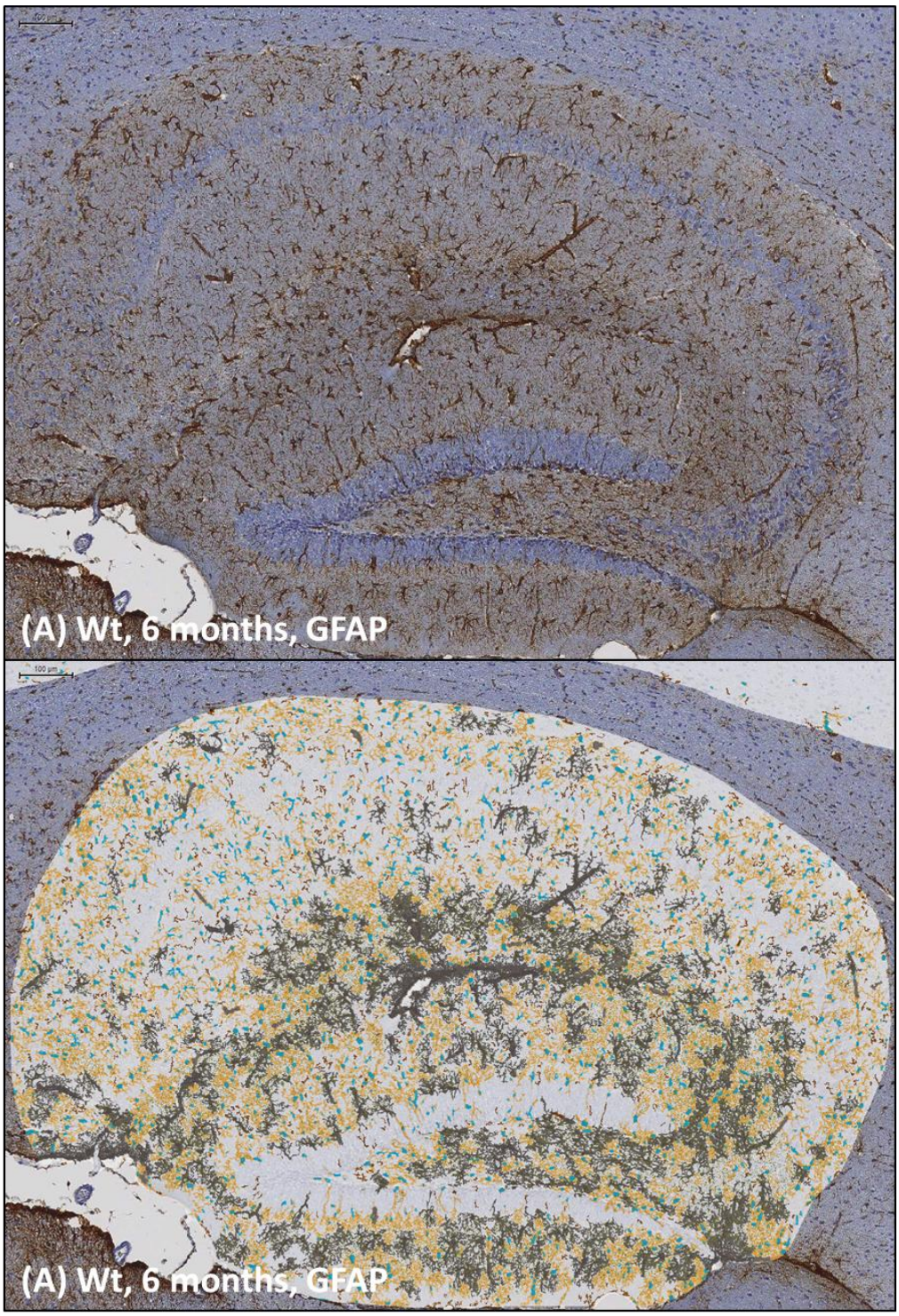

Figure 4.9 Area covered by astrocytes increases with age, but density of astrocytes reduces with age.

Figures 4.9A-D depict astrocytes identified in 6-month old Wt (A), Tc1 (B), J20 (C) and Tc1;J20 (D) sections, while Figures 4.9E-H show the respective genotypes at 16-17 months. The top panels illustrate GFAP staining while the bottom panel is colour coded as follows: blue areas indicate astrocyte cell bodies, yellow areas indicate processes, and black areas represent inseparable clusters. Regions of dark brown non-specific GFAP staining observable in the top panel appear to result in extensive regions of inseparable clusters (coloured black) shown in the bottom panels. These regions of inseparable clusters were particularly pronounced along the dentate gyrus. Scale bars represent 100 μM.


(B) Tc1, 6 months, GFAP

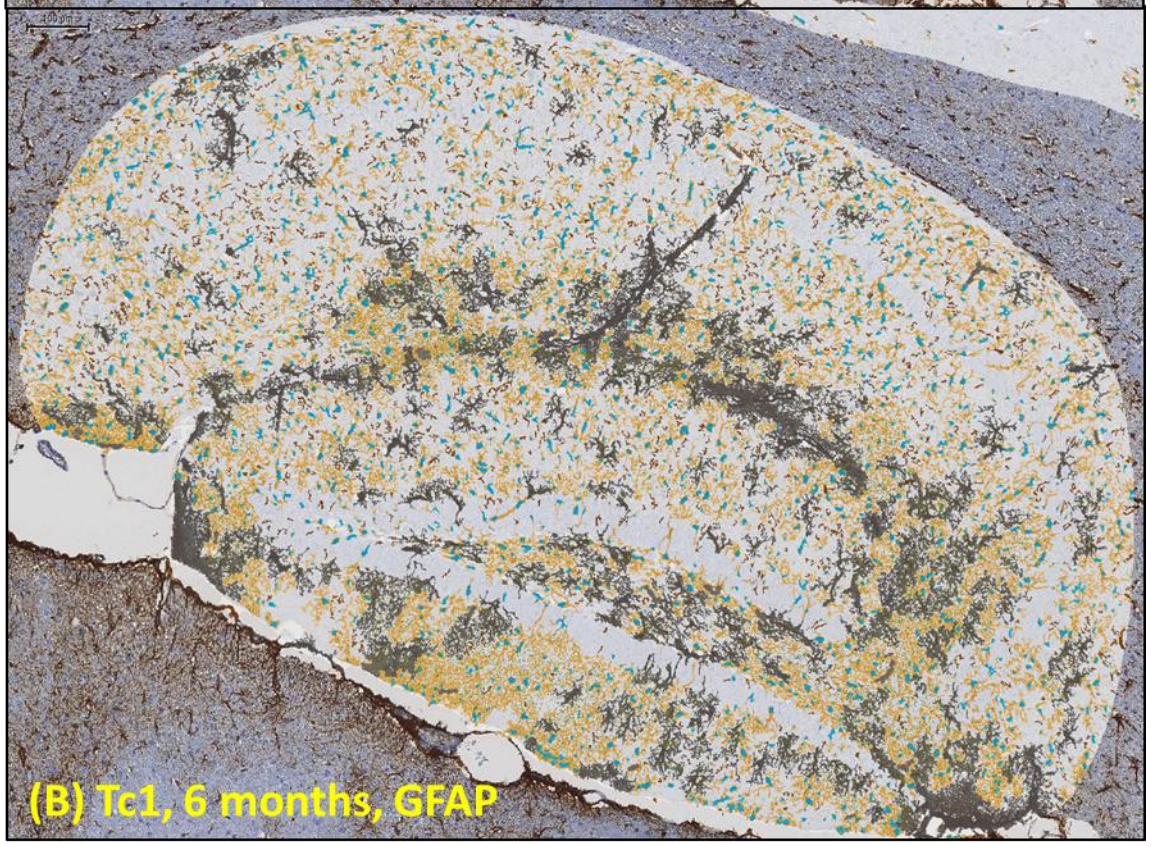
(B) Tc1, 6 months, GFAP

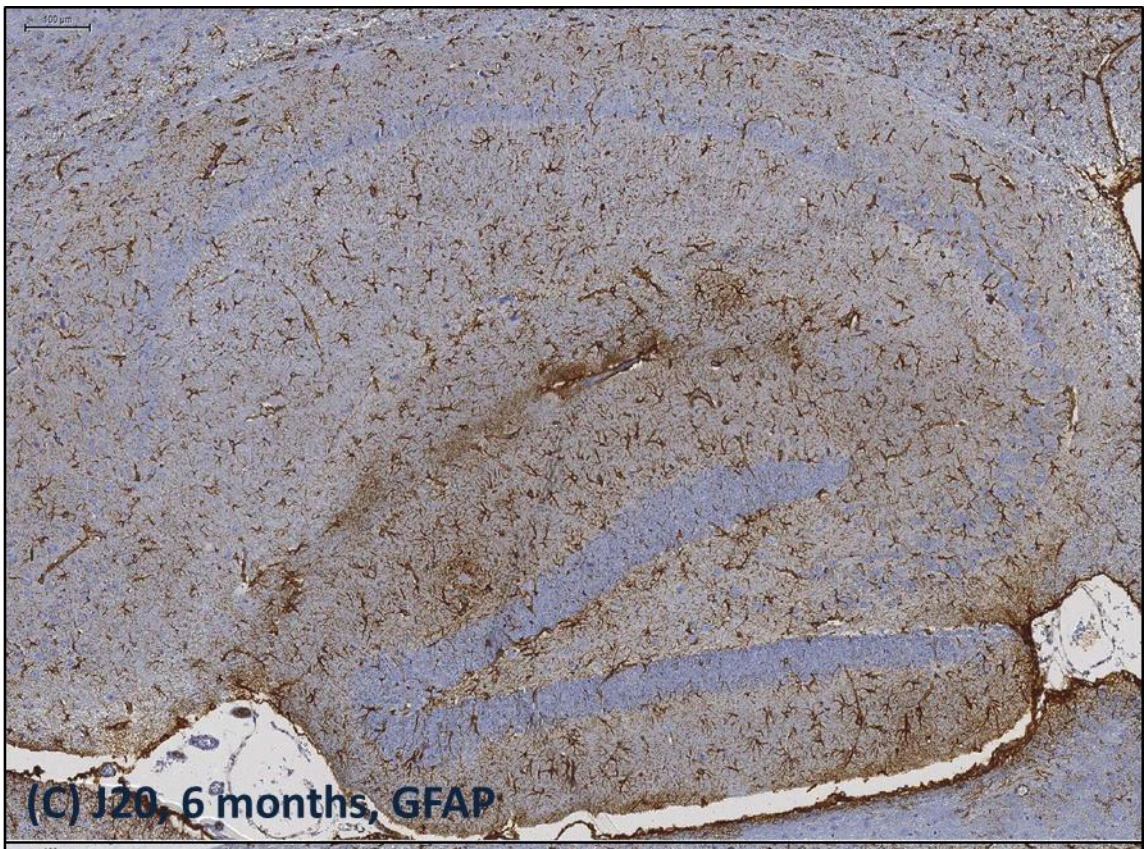
100 µm
(C) J20, 6 months, GFAP

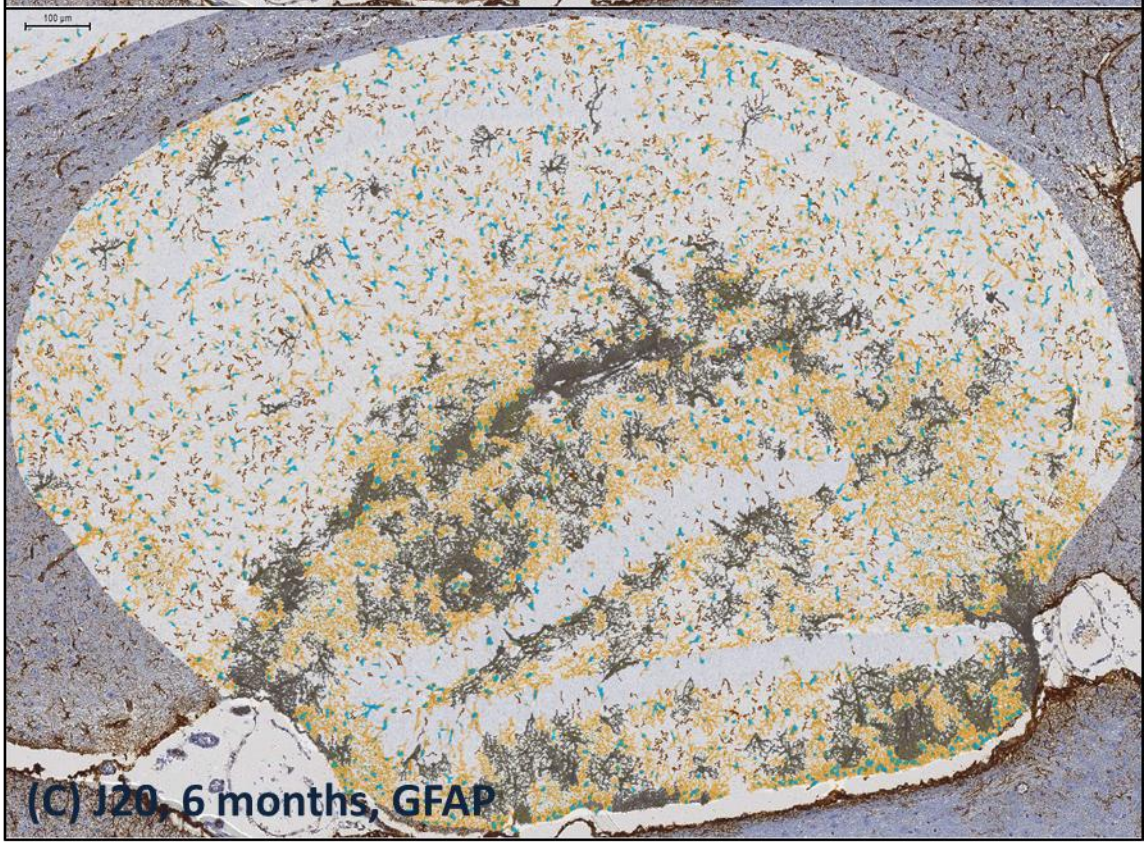
100 µm
(C) J20, 6 months, GFAP

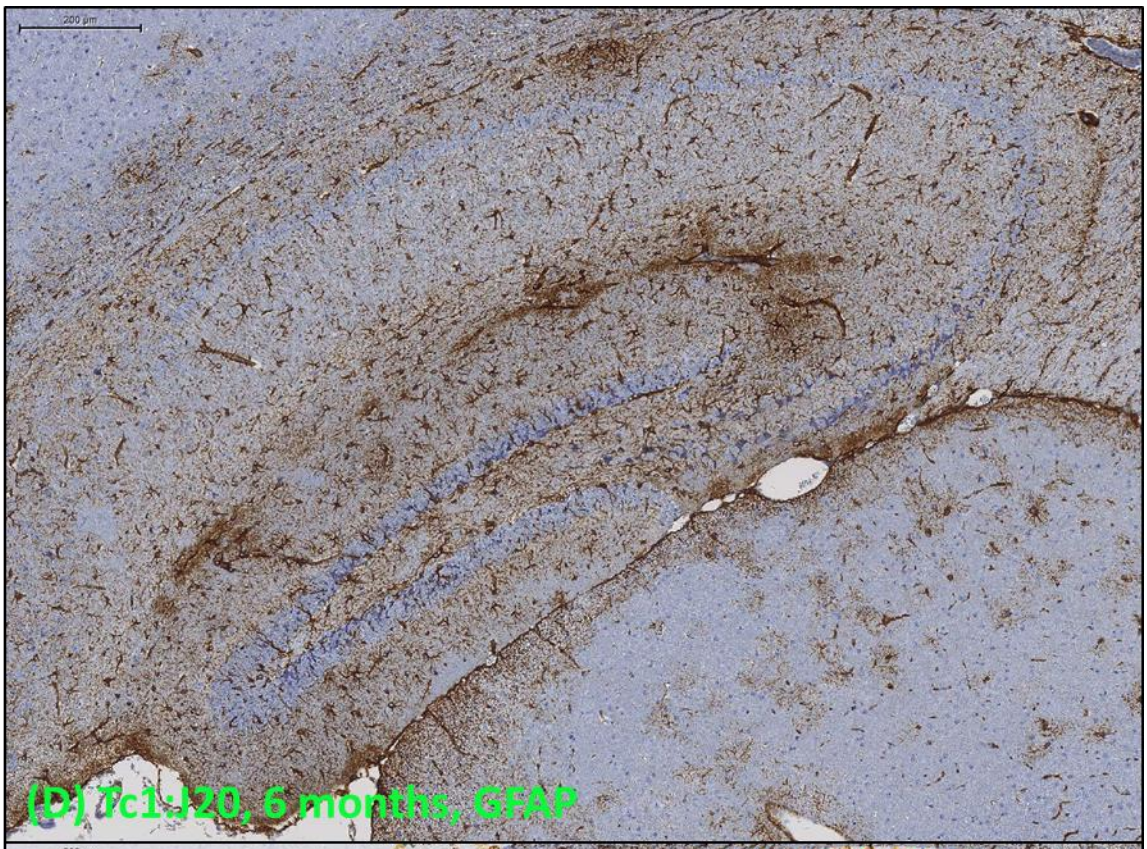
200 µm
(D) Tc1:J20, 6 months, GFAP

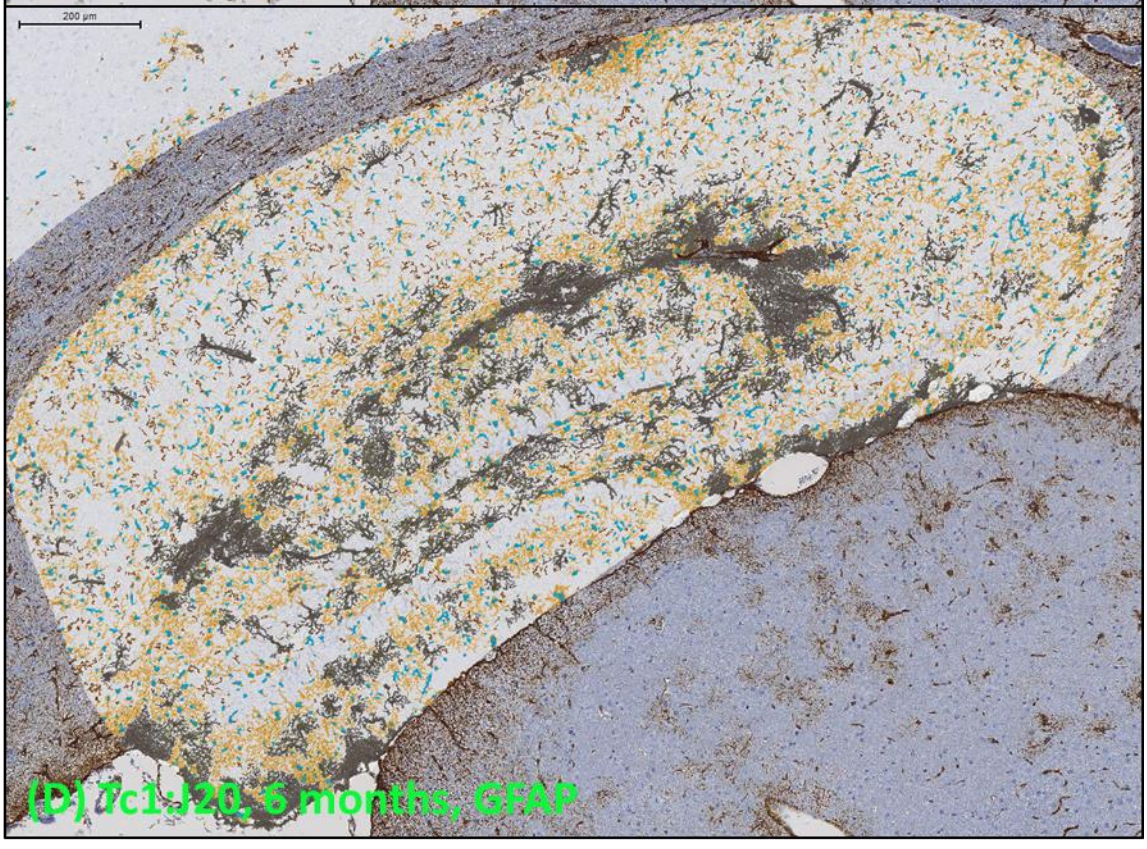
200 µm
(D) Tc1:J20, 6 months, GFAP

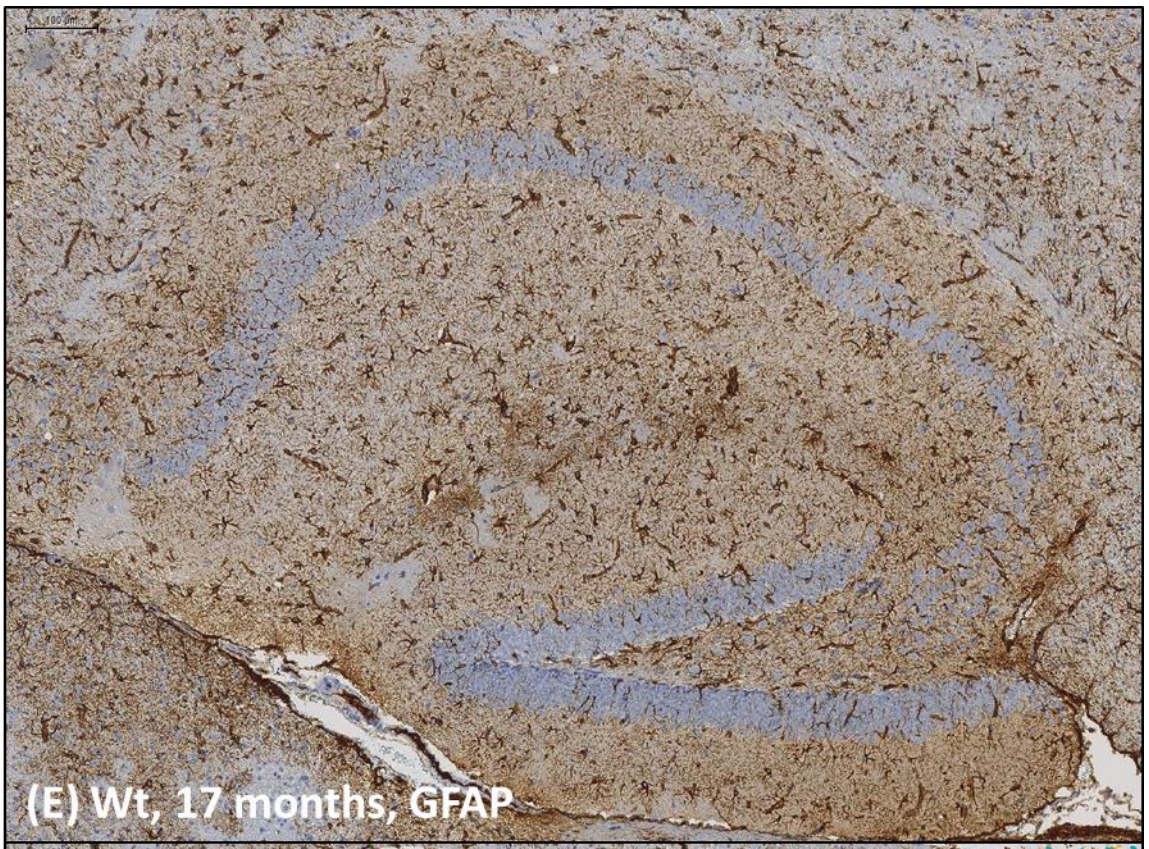
(E) Wt, 17 months, GFAP

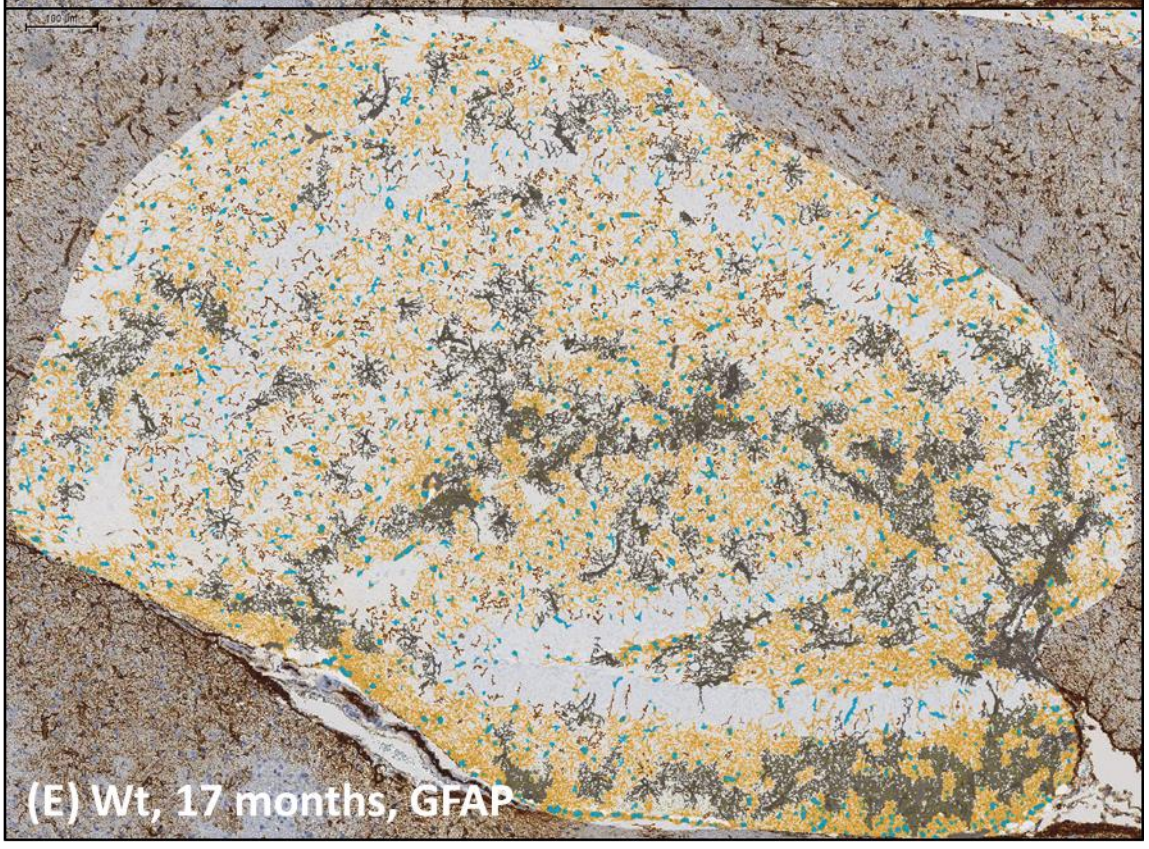
(E) Wt, 17 months, GFAP

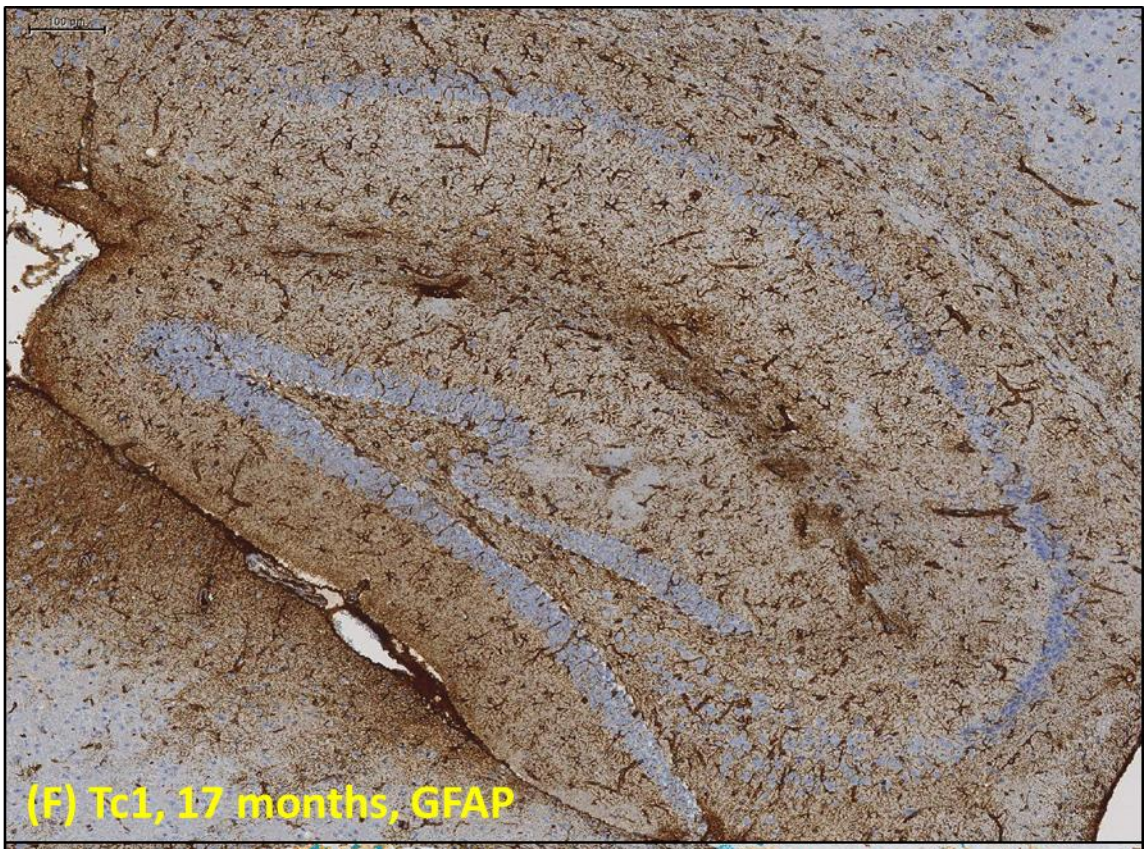
(F) Tc1, 17 months, GFAP

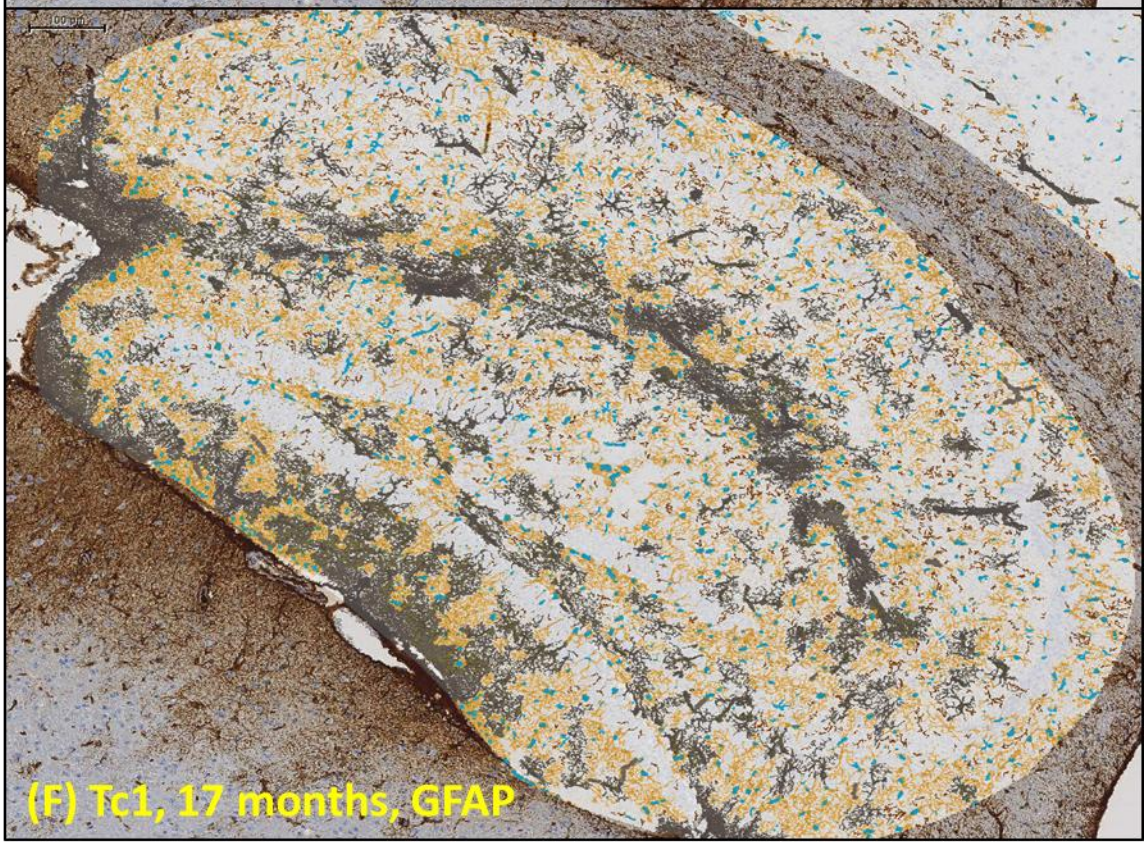
(F) Tc1, 17 months, GFAP

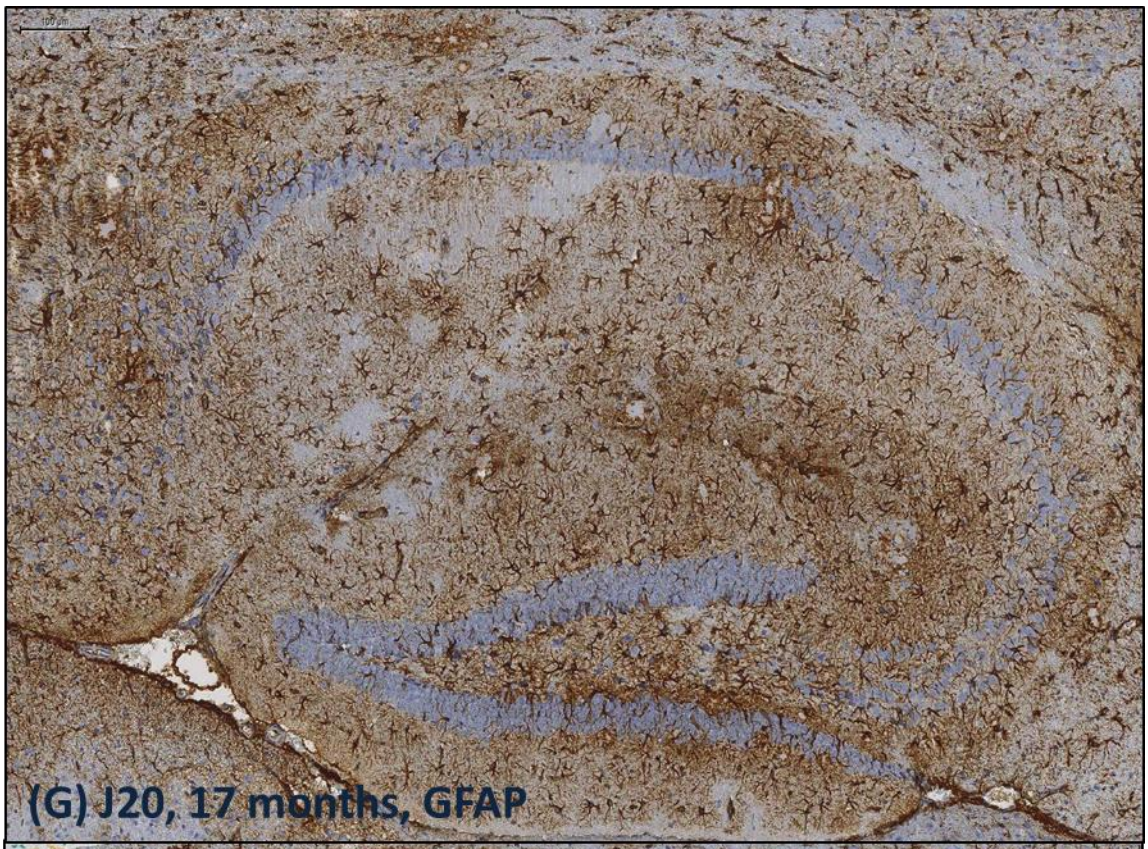
(G) J20, 17 months, GFAP

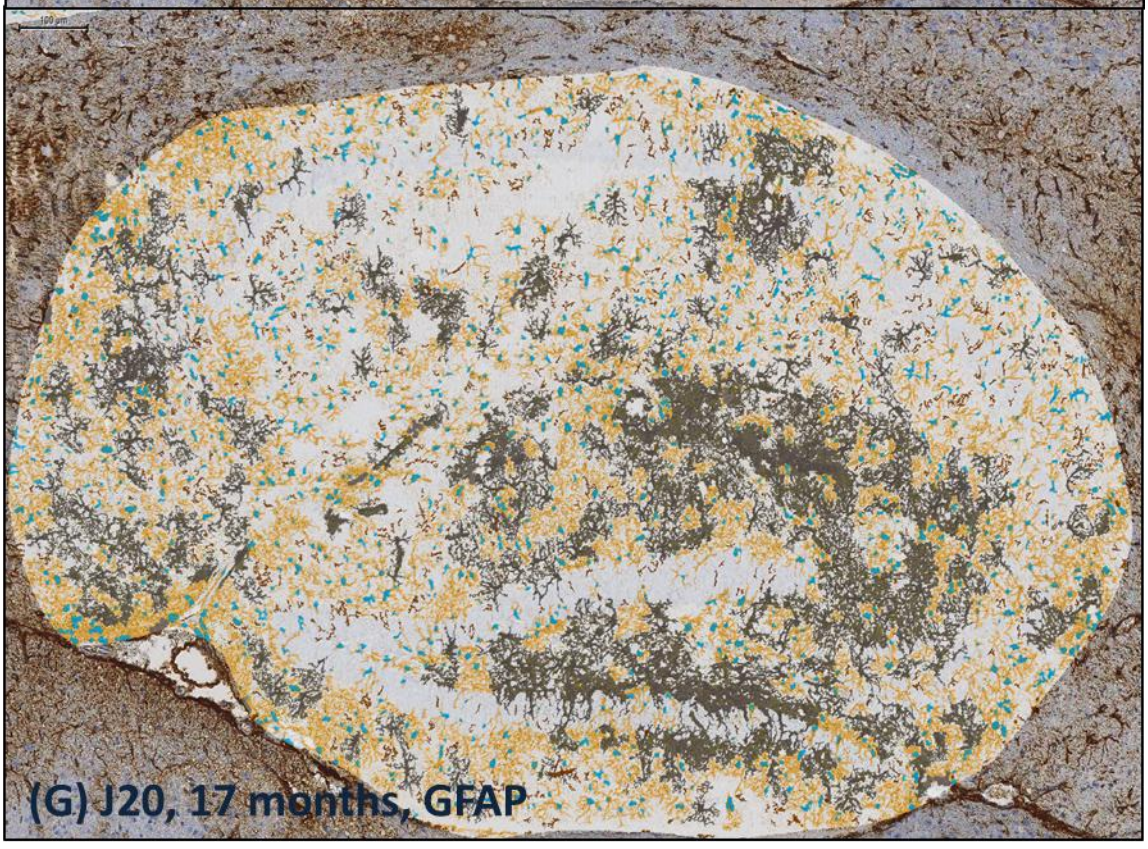
(G) J20, 17 months, GFAP

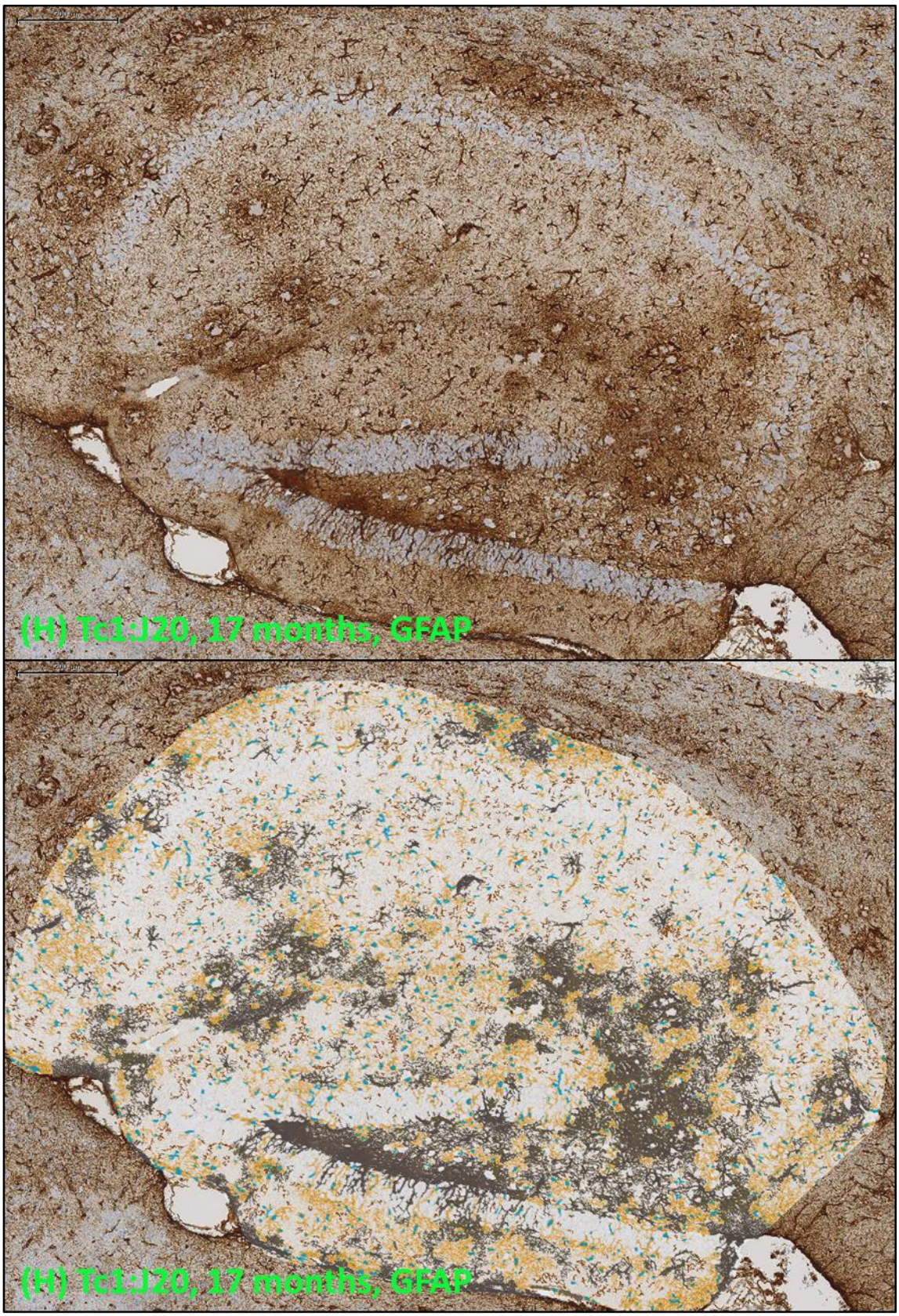
(H) Tc1:J20, 17 months, GFAP
(H) Tc1:J20, 17 months, GFAP

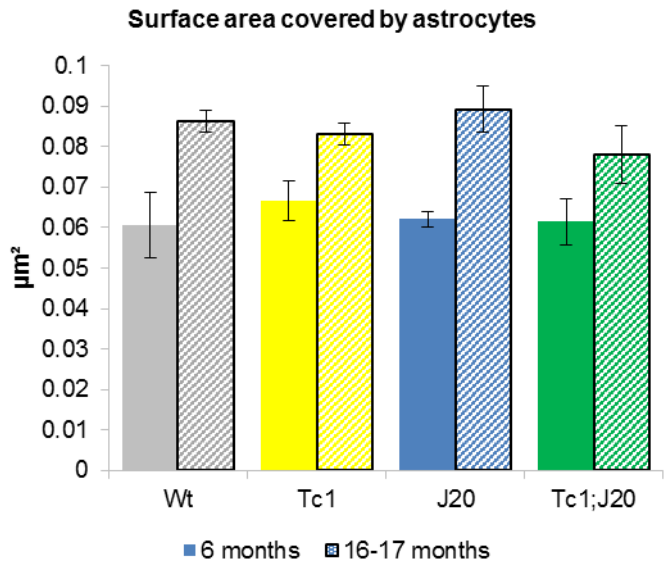

Figure 4.10 Total hippocampal surface area covered by astrocytes significantly increases with age.

Total area of astrocyte GFAP staining was calculated by summing the areas of cell bodies, cell processes and inseparable clusters. Total GFAP area was expressed as a proportion of the total surface area of the hippocampus. Age significantly increased total astrocyte area, but there was no significant influence of trisomy 21 or APP/Aβ overexpression on total astrocyte area. Graph shows mean values while error bars indicate SEM.

Similar to microglial area analysis, total astrocyte surface area was normalized to the area of the hippocampus, which had been manually identified and outlined prior to analysis. Areas included for analysis included all objects identified as cell bodies, cell processes, and inseparable clusters. Age significantly increased hippocampal surface area covered by astrocytes (2-way ANOVA $F(1, 42) = 6.711$ $p = 0.013$) but there was no significant effect of trisomy 21 or APP/Aβ overexpression (Figure 4.10).

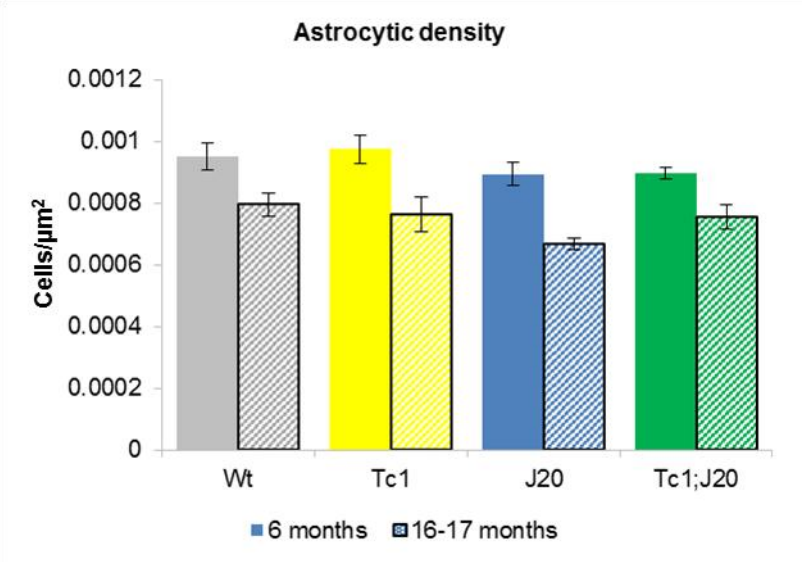

Figure 4.11 Astrocyte density in hippocampal sections significantly decreases with age and APP/Aβ overexpression.

Astrocyte density was calculated as the total number of cell bodies identified, expressed as a ratio to total hippocampal area. Both age and APP/Aβ overexpression significantly decreased astrocyte density but there was no significant effect of trisomy 21. Graph shows mean values while error bars indicate SEM.µ

To compare changes in the number of astrocytes in the hippocampus, astrocyte density was calculated by dividing the total number of cell bodies by the area of the hippocampus (Figure 4.11). Astrocyte density was significantly decreased with age (two-way ANOVA $F(1,42) = 40.172$, $p < 0.001$) and APP/Aβ overexpression ($F(1,42) = 5.414$, $p = 0.025$). There was no significant influence of trisomy 21.

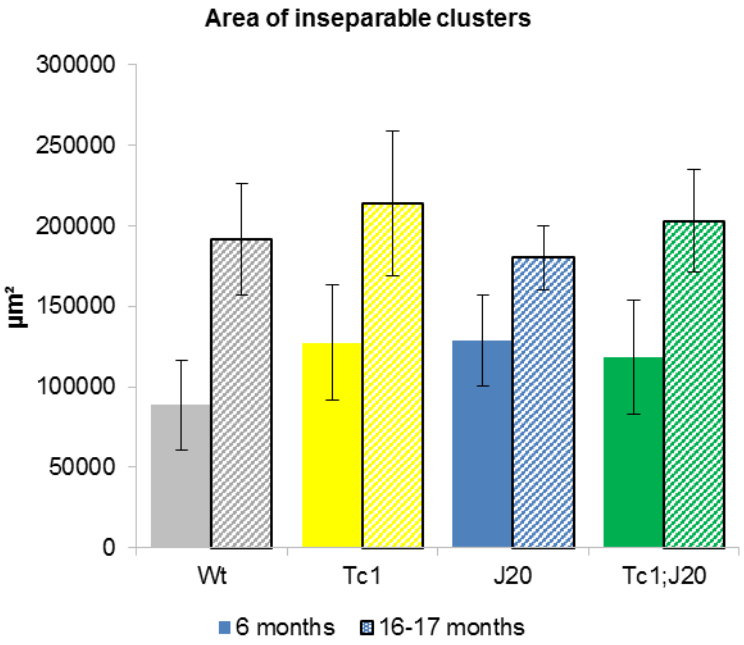

Figure 4.12 Area of astrocytic 'inseparable clusters' significantly increases with age. The area of inseparable clusters, which were regions where discrete cell bodies could not be distinguished, was quantified. Age significantly increased the area of inseparable clusters but there was no significant influence of trisomy 21 or APP/Aβ overexpression on inseparable clusters. Graph shows mean values while error bars indicate SEM.

The area of inseparable clusters was significantly increased with age (two-way ANOVA $F(1,42) = 9.666$, $p = 0.003$). These clusters include the regions coloured black in Figure 4.9**,** which appear to correspond with dark brown non-specific GFAP staining. There was no significant influence of trisomy 21 or APP/Aβ overexpression.

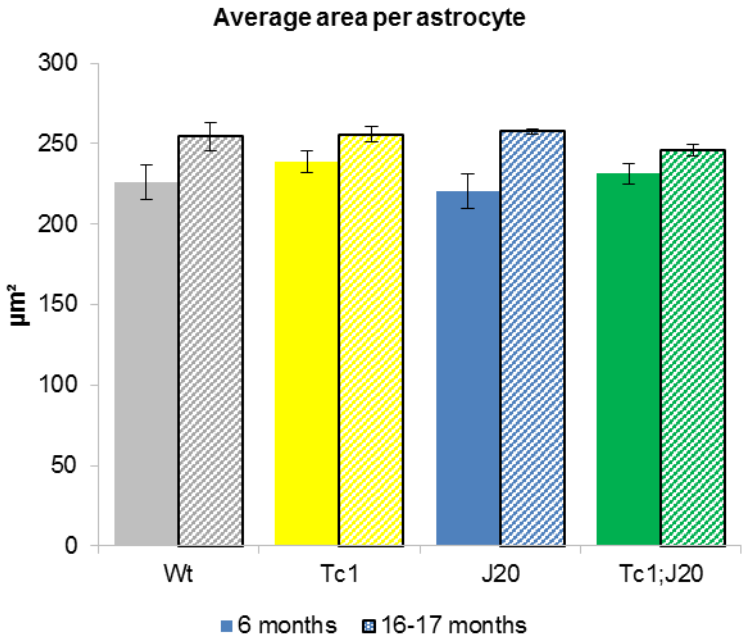

Figure 4.13 Average area per astrocyte increases with age.

The area per astrocyte was calculated by adding the area of cell body and area of cell processes in each cell. Age significantly increased the total area per astrocyte, but there was no significant effect of trisomy 21 or APP/Aβ overexpression. Graph shows mean values while error bars indicate SEM.

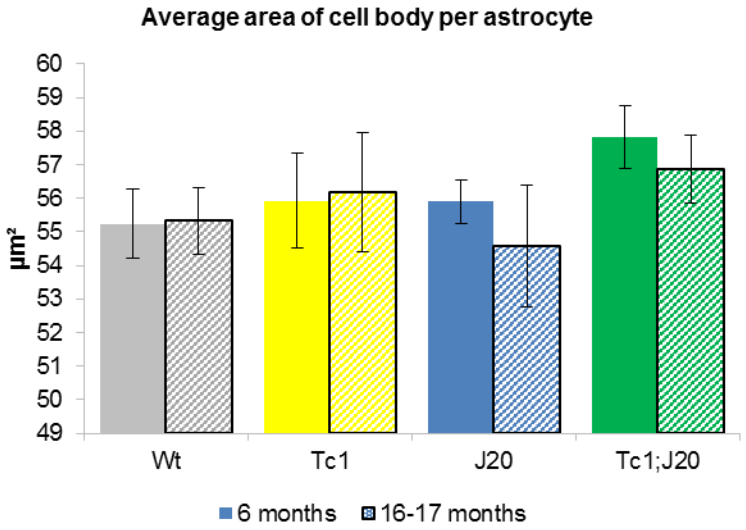

Figure 4.14 Average astrocyte cell body area is not altered by age, trisomy 21 or APP/Aβ overexpression.

Graph shows mean values while error bars indicate SEM.

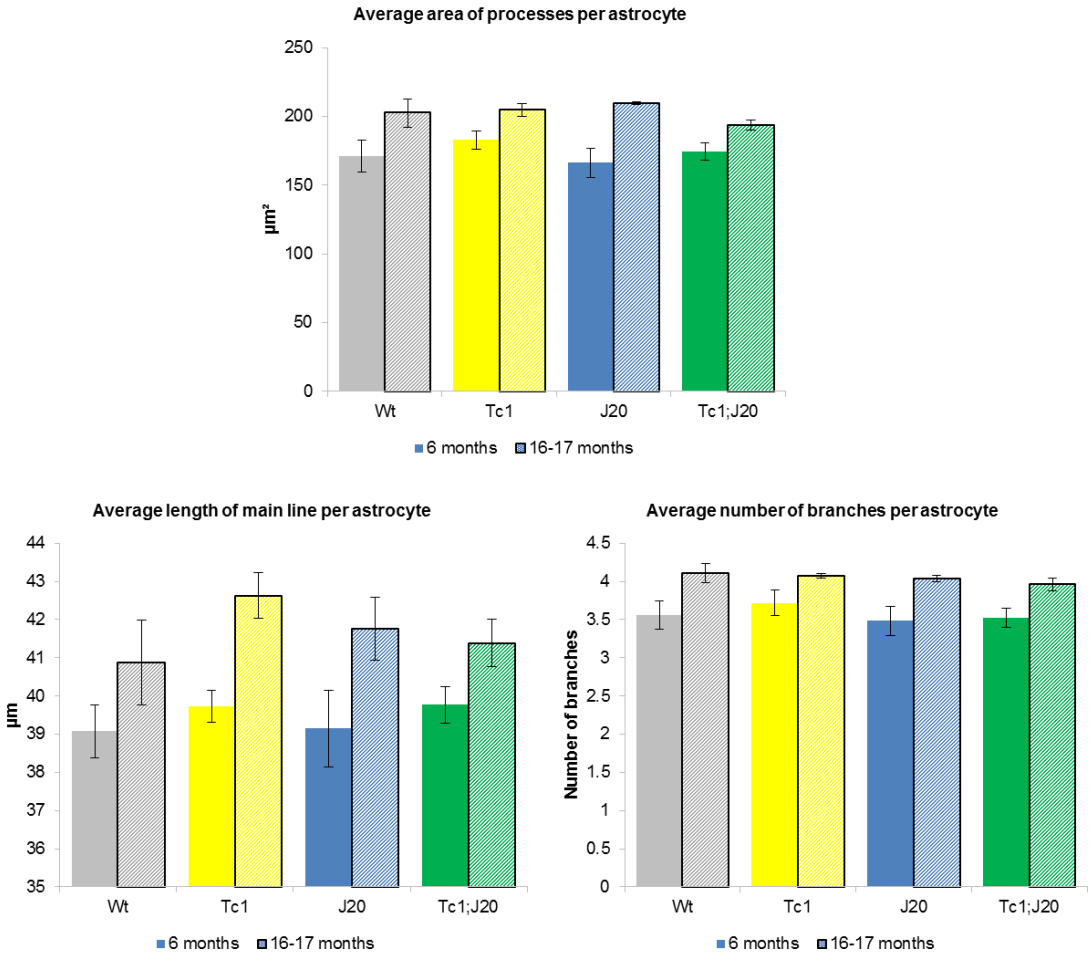

Figure 4.15 Average area of astrocyte processes increases with age, together with increased length of the main line and number of branches per astrocyte.

The main line measures the distance between the ends of the two longest processes per cell, while the number of branches per cell is determined from the main line. Age significantly increased the average area of processes per cell. This was contributed to by increased length of the main line and increased branching from the main line. There was no effect of trisomy 21 or APP/Aβ overexpression on the above measurements. Graph shows mean values while error bars indicate SEM.

The average total area per astrocyte was significantly increased with age (two-way ANOVA $F(1,42) = 13.357$, $p = 0.001$), but not significantly changed by trisomy 21 or APP/Aβ overexpression (Figure 4.15). This was not due to alterations in cell body size, which was not altered by age, trisomy 21 or APP/Aβ overexpression (Figure 4.14). However, the average area of processes per astrocyte was increased with age ($F(1,42) = 16.746$, $p < 0.001$), both due to elongation of the main line with age ($F(1,42) = 13.937$, $p = 0.001$) and an increased number of branches ($F(1,42) = 14.957$, $p < 0.001$) (Figure 4.15). Trisomy 21 and APP/Aβ overexpression both did not influence any of these parameters.

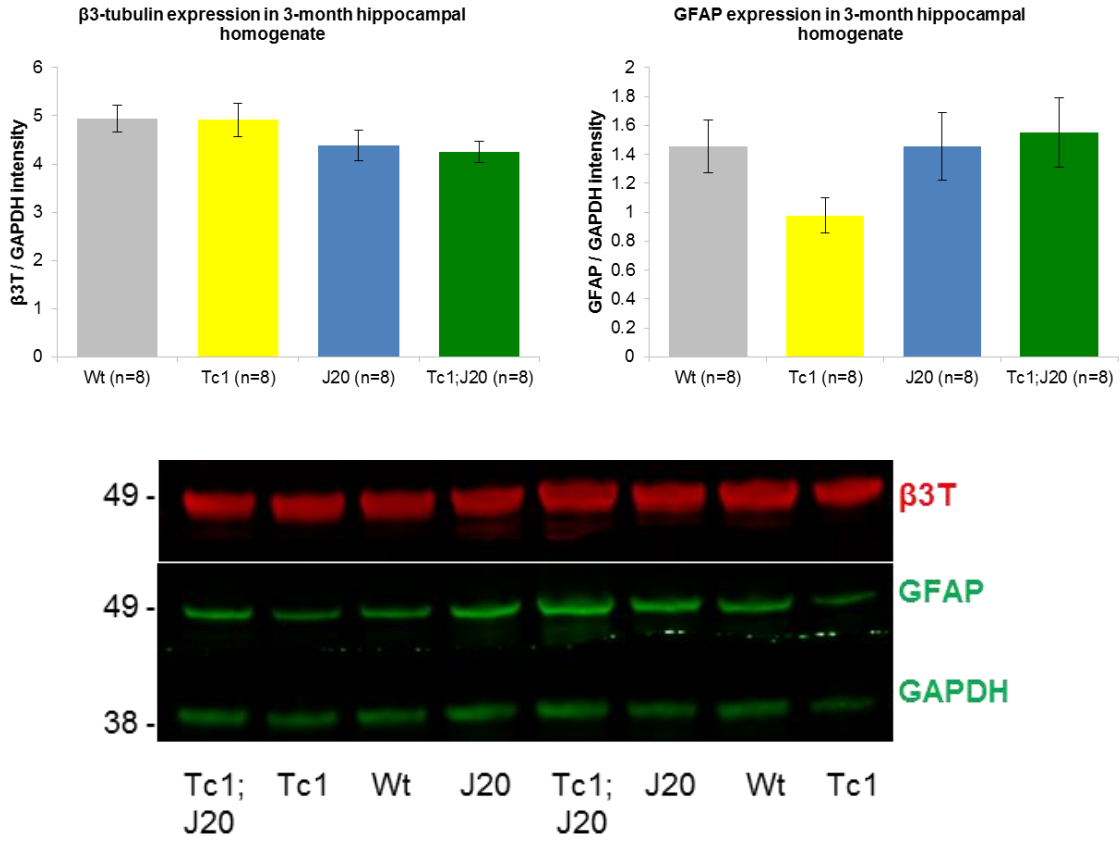

Figure 4.16 β3T and GFAP protein expression in hippocampal homogenate from 3-month old mice

β3T (55 kDa) and GFAP (50 kDa) are of similar molecular weights and resolve at overlapping positions following gel electrophoresis. Simultaneous detection was performed using secondary antibodies conjugated with infrared dyes emitting different wavelengths, generating the red β3T band and green GFAP band as illustrated. APP/Aβ overexpression significantly decreased β3T protein expression levels. Graph shows mean values while error bars indicate SEM.

To investigate effects of trisomy 21 and APP/Aβ overexpression on astrocyte and neuron levels in 3-month old mice prior to plaque deposition, protein expression of GFAP and β3-tubulin (β3T) respectively were quantified by western blots. β3T is the major constituent of neuronal microtubules (Tischfield et al. 2010). In 3-month old hippocampal homogenate, APP/Aβ overexpression significantly reduced β3T expression (2-way ANOVA $F(1,28) = 2.995$ $p = 0.046$), with no significant difference in trisomy 21. GFAP protein expression remained unchanged by trisomy 21 and APP/Aβ overexpression (Figure 4.16).

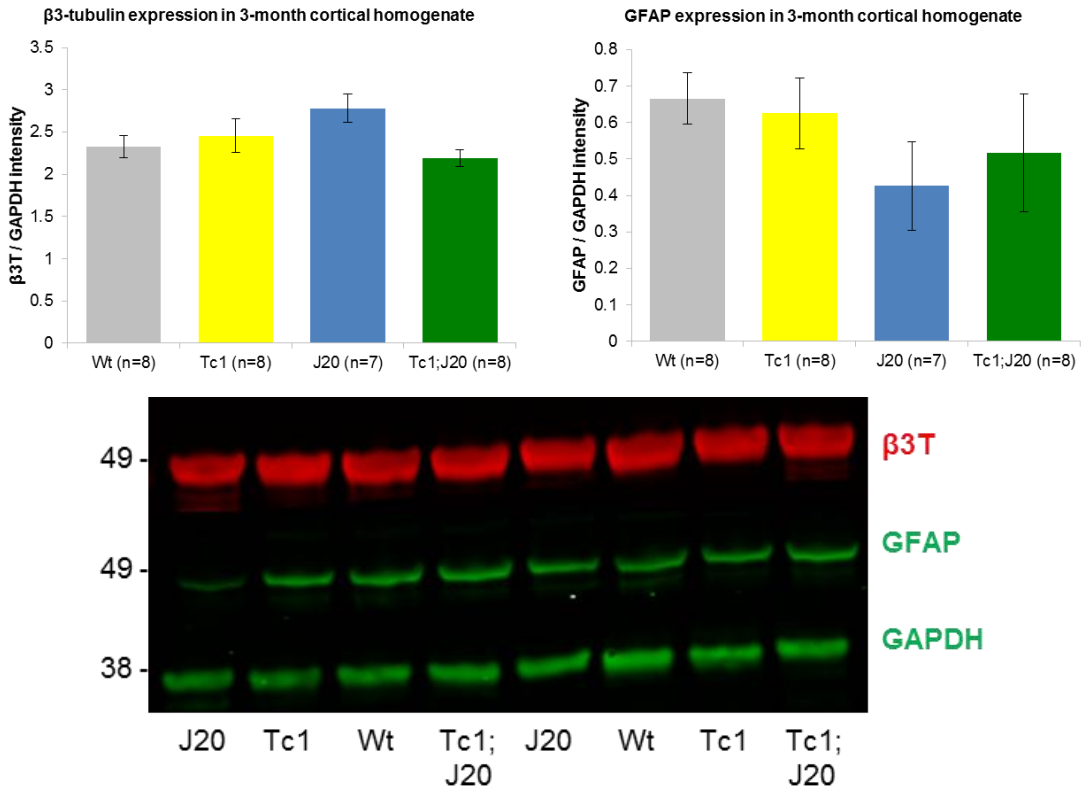

Figure 4.17 β3T and GFAP protein expression in hippocampal homogenate from 3-month old mice

β3T (55 kDa) and GFAP (50 kDa) are of similar molecular weights and resolve at overlapping positions following gel electrophoresis. Simultaneous detection was performed using secondary antibodies conjugated with infrared dyes emitting different wavelengths, generating the red β3T band and green GFAP band as illustrated. There was no significant effect of trisomy 21 or APP/Aβ overexpression on levels of both β3T and GFAP. Graph shows mean values while error bars indicate SEM.

In 3-month old cortical homogenate, there was no significant effect of trisomy 21 or APP/Aβ overexpression on β3T or GFAP protein expression, when analysed by 2-way ANOVA (Figure 4.17).

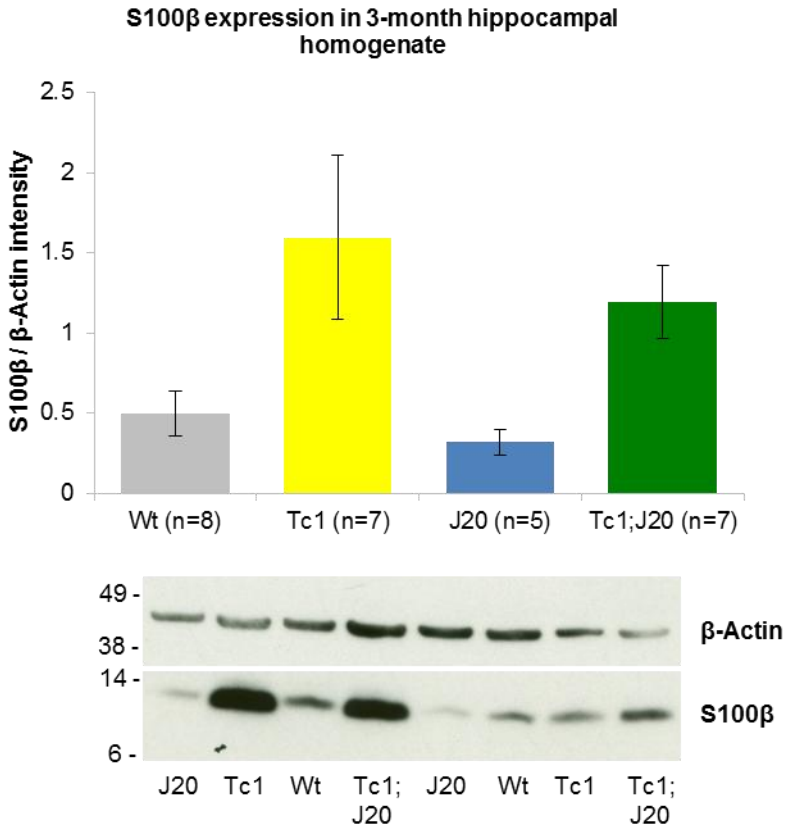

Figure 4.18 Trisomy 21 increases hippocampal S100β protein expression in 3-month old mice

S100B is duplicated and hence is expressed in four copies in Tc1 and Tc1;J20 mice. Trisomy 21 significantly increases S100β protein expression but there was no effect of APP/Aβ overexpression on S100β expression. Graph shows mean values while error bars indicate SEM.

S100β is an alternative astrocytic marker to GFAP and is encoded on Hsa21. In Tc1 mice, *S100B* is duplicated and hence expressed in four copies (Gribble et al. 2013). In hippocampal homogenate from 3-month old Tc1xJ20 mice, trisomy 21 significantly increased S100β protein expression (2-way ANOVA ($F(1,23) = 10.126$, $p = 0.004$). There was no significant effect of APP/Aβ overexpression on S100β protein expression (Figure 4.18).

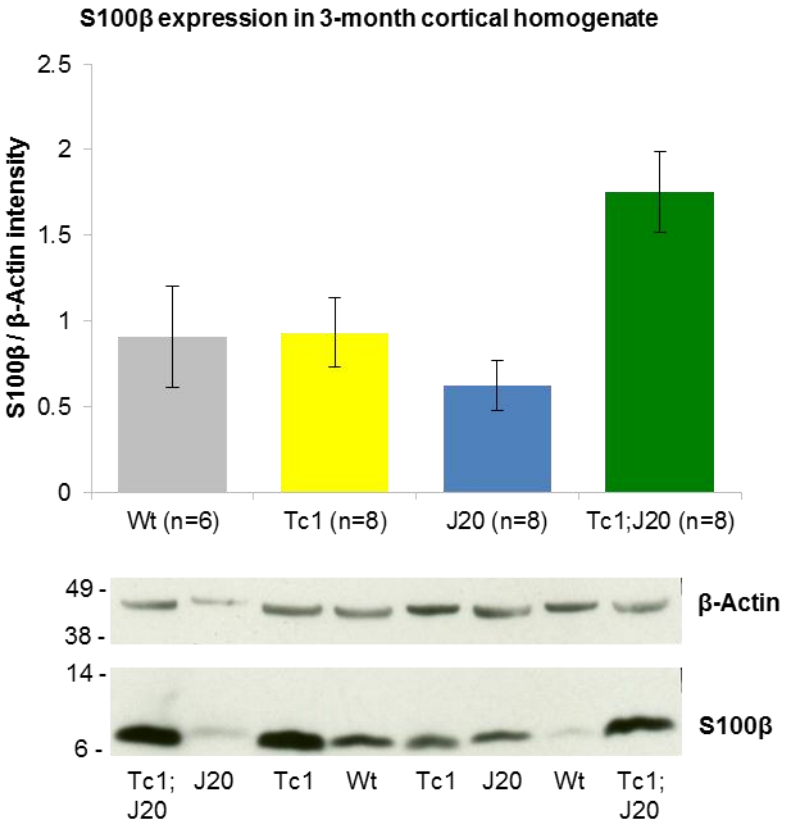

Figure 4.19 Trisomy 21 increases cortical S100β protein expression in 3-month old mice, which is further increased with APP/Aβ overexpression

S100B is duplicated and hence is expressed in four copies in Tc1 and Tc1;J20 mice. There was no significant difference in S100β expression between Wt and Tc1. However, trisomy 21 interacted with APP/Aβ overexpression to increase S100β expression levels in Tc1;J20 mice. Graph shows mean values while error bars indicate SEM.

In cortical homogenate from 3-month old Tc1xJ20 mice, trisomy 21 increased S100β protein expression when studied across all four Tc1xJ20 genotypes (2-way ANOVA $F(1,26) = 7.023$, $p = 0.014$). APP/Aβ overexpression interacted with trisomy 21 to further increase S100β in Tc1;J20 mice (trisomy 21*APP/Aβ overexpression interaction $F(1,26) = 6.477$, $p = 0.017$)). However, there was no significant difference in S100β expression when compared between Wt and Tc1 (independent samples t-test $t(9) = -1.302$, $p = 0.225$) (Figure 4.19).

4.3. Discussion

A digital protocol was developed using Definiens Developer to identify glial cells in immunohistochemical sections, before quantifying measurements of their cell body size and area of cellular processes. While this has been successfully performed for microglia identified by Iba1, studying GFAP-positive astrocytes has proved more problematic due to variations in background staining intensity.

4.3.1. Successful identification of discrete microglial cells

As microglial cells proliferate in response to inflammatory stimuli (Moraga et al. 2015; Mosher and Wyss-Coray 2014), and much attention has focused on the morphology of individual cells as an indicator of reactivity, it was important to ensure that the protocol identified cell bodies with few false positives to ensure morphological features of individual cells were accurately represented. As illustrated in Figure 4.1A, this was successfully performed even in regions of higher densities of microglial cells. However, false negatives have been observed where microglial cells have been excluded for being too closely associated (Figure 4.1C); where present, these cells accounted for less than 2% of the total cell count automatically identified. Although we have not performed the congophilic or Aβ-directed immunohistochemistry required to illustrated plaque deposition, clusters were found in microglial groups surrounding spherical gaps resembling amyloid plaques (Figure 4.1B). This was supported by the observation that the increase in area of microglial inseparable clusters approximately doubled in Tc1;J20 compared to J20 mice, at 16-17 months, resembling the increase in area of plaque deposition observed at this age. Therefore, since regions of clustered microglia tend to be excluded from analysis, our protocol appears best suited to characterizing morphological phenotypes of cells located away from Aβ plaques involving microglial clusters. As elaborated below, this is likely to exclude microglia with an amoeboid morphology.

4.3.2. Increased microglial reactivity in APP/Aβ overexpression

APP/Aβ overexpression was the primary influence on microglial phenotypes across the hippocampus, manifesting in an increase in both the number (Figure 4.4) and size of microglial cells (Figure 4.5). The increase in size was due to an increase in the area of processes (Figure 4.5), without no difference in the degree of branching and length of main line (Figure 4.6). This suggests that in general the increased area could be due to an increased number and/or thickness of microglial processes with *APP*

overexpression, rather than further arborisation and extension of processes. Further work therefore needs to verify whether the diameter and number of processes has indeed increased. However, as the cell body and cell processes have been defined as separate objects in our analysis, we have been unable to quantify the number of processes emerging directly from cell bodies due to an inability to encode this in Definiens Developer. We will therefore need to troubleshoot this with technical advisors from Definiens.

As our protocol has been successful in quantifying the dimensions of cell bodies and processes in discrete microglial cells, the next step would to attribute these features to the different morphological classes representing microglial activation states. For instance, in a study on J20 mice at 3, 9, and 15 months of age, an increase in "microglial activation score" was observed to be influenced by APP/Aβ overexpression and age in hippocampal subregions (Pomilio et al. 2015), as also observed in this study. This score was based on the nominal scoring of morphology from ramified to amoeboid phenotypes (Figure 4.20**,** Pomilio et al. 2015). Amoeboid microglia have been shown to be the morphological subtype most closely associated with Aβ plaques (Baron et al. 2014). As it is likely that amoeboid cells would be excluded together with 'inseparable clusters' in our analysis, the increase in the number and/or thickness of processes in our results may point towards a general shift in microglial morphology to the "reactive" form as shown in Figure 4.20.

In collaboration with a neuropathologist, parameters could be created which in combination could be used to distinguish between morphological classes, particularly those with intermediate levels of branching. In microglia, these parameters could include a combination of the width and length of the main line to represent the thickness of ramifications, the "shape index" to represent the tortuosity of branches, and other parameters to refine the allocation of morphological classes. To include amoeboid reactive microglial cells currently excluded from analysis, a more stringent cell body selection could be applied around a fixed radius from areas identified as putative plaques. For instance, one could use a 25 μM radius from a plaque, within which microglia numbers have been shown to decrease with age, linked to an increase in plaque-associated dystrophic neurites due to reduced microglial protection from Aβ42 toxicity (Condello et al. 2015).

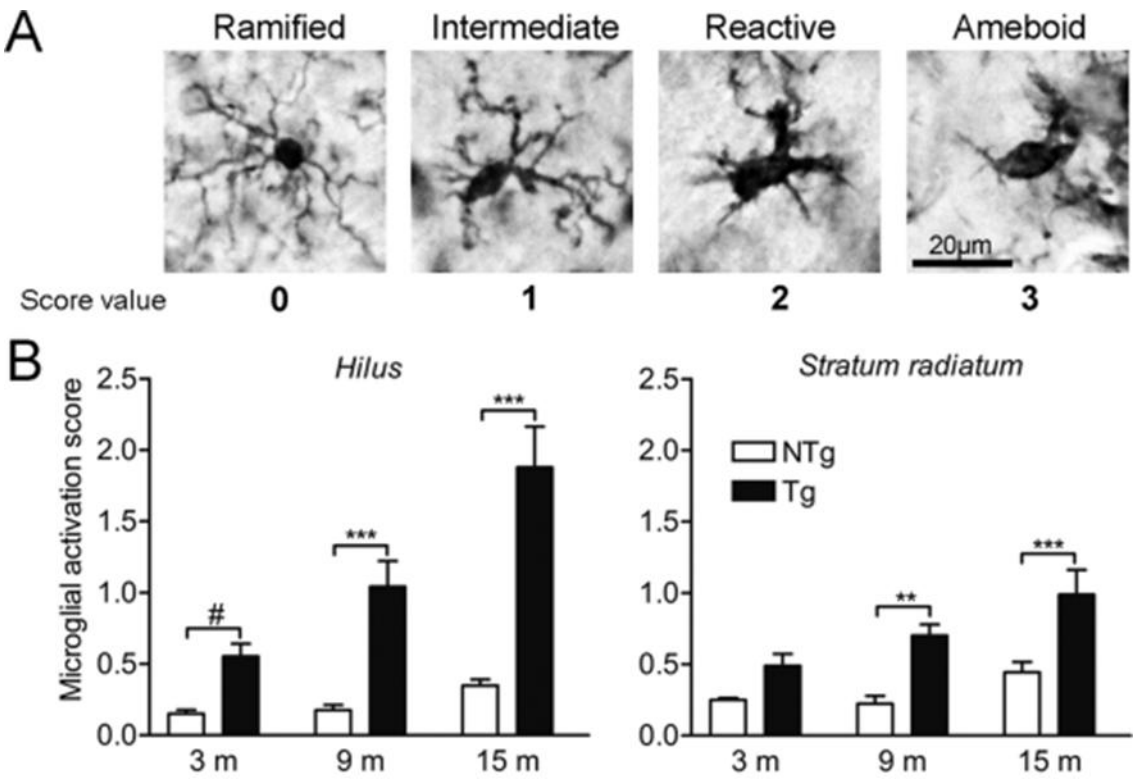

Figure 4.20. **Increased microglial activation with APP/Aβ overexpression and age, based on the nominal scoring of morphology class.**

Figure adapted from Fig. 3 from Pomilio et al., 2015. "Tg" indicates J20 mice while "NTg" indicates Wt mice. (A) illustrates examples of each morphological class together with a nominal score. (B) plots activation scores calculated by the proportion of each morphological class multipled by its nominal score.

Improving this protocol as above would therefore potentially allow the consistent analysis of more subtle changes in microglial morphology, removing potential bias in sampling and individual variations in judgment with manual classification. This could also be applied for more refined segmentation of regions of interest, such as by subdividing analysis in different hippocampal subregions, or analyzing morphologies based on distances from amyloid plaques. This will potentially allow such an automatic analysis protocol to tease out smaller changes in morphology that are difficult to be judged by eye, such as the thinning of microglial processes associated with senescence.

4.3.3. Artefacts in astrocyte characterization due to variations in background staining intensity

While we were capable of identifying discrete astrocytes (Figure 4.8), characterization of astrogliosis was more challenging due to uneven GFAP brown staining across the hippocampus. This resulted either in patches of false negatives, where darker regions

were included as “inseparable clusters” of cells, or false positives, where lighter brown staining adjacent to darker brown inseparable clusters was classified as processes (Figure 4.9). These regions featured primarily in the dentate gyrus, which was generally stained a darker brown than the rest of the hippocampus (Figure 4.9). Interestingly, this pattern of darker staining around the dentate gyrus appears to extend to Aβ plaque immunohistochemistry, as demonstrated by Figure 5D of a study by Mucke and colleagues (Figure 4.21), and our own J20-positive sections stained for amyloid plaques. Although it remains unclear why there would be increased Aβ plaque deposition around these areas, the artefacts in astrocyte staining created by darker brown regions cannot only be related to Aβ plaque deposition, as these artefacts were also observed in WT and Tc1 mice, which do not develop plaques. Therefore, the darker brown staining is likely to be non-specific, and learning how to more specifically identify astrocytes in these regions may be relevant to identifying individual plaques in Aβ immunohistochemistry.

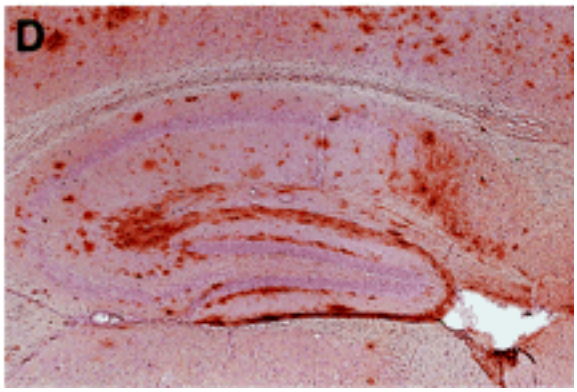

Figure 4.21 Aβ plaque deposition in 10-month old J20 hippocampal section, showing intense staining around the dentate gyrus.

Adapted from Mucke et al. 2000.

Consequently, while we demonstrated an age-dependent increase in hippocampal astrocyte coverage with age, due to an increase in the area of processes (Figure 4.15), two results suggest a problem with our analysis. Firstly, there was a general increase with age but no effect of APP/Aβ overexpression on the area of ‘inseparable clusters’ (Figure 4.12). As discussed above, Wt and Tc1 mice do not exhibit plaque deposition, hence these clusters do not reflect astrogliosis in response to Aβ accumulation. Furthermore, astrocytes do not form astrocytic scars in AD or with aging (Sofroniew 2009). Therefore, these clusters are likely to be an artefact due to the regions of darker brown background staining (Figure 4.9). Secondly, astrocytic density decreased

significantly with age and APP/Aβ overexpression, which goes against observations that astrocyte numbers remain unchanged in both AD patients and mouse models with age and Aβ accumulation (Serrano-Pozo et al. 2013; Kamphuis et al. 2012). The decrease in astrocyte density with age could therefore be due to the increase in inseparable clusters with age, which would have resulted in an increased number of astrocytes excluded from analysis, due to the inability to separate them. Future work therefore needs to address how to identify astrocytes amidst varying levels of background intensity. One potential approach could be to segment the dentate gyrus as a separate region for analysis, and apply a higher threshold for background staining in this region.

While the digital immunohistochemical analysis of astrocyte phenotypes remains unresolved, study of astrocytic and neuronal protein expression has yielded some insight. As sections from 3-month old Tc1xJ20 brains were not prepared for digital analysis, GFAP and S100β protein expression were examined in hippocampal and cortical homogenates as a measure for levels of astrogliosis (Figures 4.16-19). At 3 months, no amyloid plaques are yet observed in APP/Aβ-overexpressing mice (Wright et al. 2013), hence phenotypes presented at this age may reflect early stages of pathogenesis prior to Aβ deposition. No significant difference in GFAP expression was observed across all genotypes in both hippocampal and cortical tissue (Figures 4.16-4.17). However, this stands in contrast to the increase in GFAP-positive astrocytes counted in the hippocampal CA1 and CA3 regions of 12-week old J20 mice (Wright et al. 2013), possibly reflecting a lack of sensitivity in western blots and semi-quantitative densitometric analysis (Taylor et al. 2013).

S100β protein expression was also quantified as a second astrocytic marker (Gerlach et al. 2006). Unlike *GFAP*, *S100B* is encoded on Hsa21 and has been previously shown to increase S100β protein expression in both hippocampus and cortex of Tc1 mice (Ahmed et al. 2013), which express four copies of this gene due to a duplication in the Hsa21 chromosome (Gribble et al. 2013). While we demonstrated an increase in S100β in the hippocampus in both Tc1 and Tc1;J20 (Figure 4.19), S100β was not significantly increased in Tc1 cortex compared to Wt (Figure 4.18). This resulted in a 2-fold increase in Tc1;J20 cortical S100β levels compared to Tc1 (Figure 4.18). Further work needs to be done to confirm levels of S100β expression in Tc1 cortical tissue, before exploring the idea that APP/Aβ overexpression may exacerbate astrogliosis indicated by S100β in the cortex.

S100β labels a subtype of mature astrocytes that associate with blood vessels, and express NG2 (Wang and Bordey 2008). S100 proteins have been shown to be differentially expressed in the development of human hippocampus and temporal cortex (Chan et al. 2003), and S100β expression in the cortex alters temporally from fetal development to old age (Tiu et al. 2000). In rodent cortex, about 40% of astrocytes stained positively for S100β were negative for GFAP, while 80% were positive for both GFAP and S100β in the hippocampus (Bushong et al. 2002; Ogata and Kosaka 2002). Therefore, it is possible that differences in the proportion of astrocytic cell types expressing S100β in cortical and hippocampal tissues may result in a differential response to APP/Aβ overexpression, should there indeed be an interaction effect between trisomy 21 and APP/Aβ overexpression in cortical but not hippocampal tissue (Figures 4.18-19). This however remains speculative and will require an immunohistochemical study of S100β/GFAP double-stained glial cells in cortical tissues to confirm, and the digital protocol we developed above could potentially be applied to such a study.

The upregulation of S100β in trisomy 21 is relevant to the study of synergistic effects of inflammation between *S100B* and *APP*, particularly in association with IL-1 (Barger and Harmon 1997; Griffin et al. 1989). It will therefore be interesting to investigate if the increased S100β expression in Tc1;J20 may manifest itself in astrocytic morphological changes reflected by S100β, and cytokine profiles associated with inflammation, in cortical tissue. While we did segment cortical tissue as a region of interest, this was eventually not included in the final analysis as Iba1-positive and GFAP-positive cells were both relatively sparsely distributed in the cortex, compared to hippocampal tissue which was fully covered by both types of cells. Therefore only hippocampal analysis was performed due to a greater confidence in capturing a more generalizable glial phenotype, which we could use for assessing the validity of our results.

To gain insight into whether the expression of neuronal markers was altered at 3 months, we quantified the expression of β3-tubulin (β3T), the major constituent of neuronal microtubules (Tischfield et al. 2010). This revealed a subtle, but significant, reduction in β3T expression in mice with APP/Aβ overexpression, which was unexpected given the lack of neuronal loss observed at this age in all hippocampal regions studied (Wright et al. 2013). Immunoblotting could be repeated with a different marker of neuronal microtubules to verify this result, such as using MAP2, a neuronal dendritic marker (Soltani et al. 2005).

4.3.4. Trisomy 21 does not significantly alter any glial phenotype when studied across the hippocampus

None of the morphological measurements in microglia and astrocytes were significantly altered by trisomy 21. While this suggests that trisomy 21 has no effect on glial reactivity, this may also be because morphological alterations in trisomy 21 are too subtle to be revealed by the broad analysis of phenotypes across the hippocampus. In humans, immunophenotype classes have been recently shown to distinguish between old and young individuals with DS, AD or both (AD-DS) (Wilcock et al. 2015). As immunophenotypes have been associated with changes in morphology (Jensen et al. 1997) there is value in further developing this protocol for a more targeted, sensitive approach at phenotyping microglial morphology. Despite the lifelong chronic conditions of oxidative stress and neuroinflammation in DS (Perluigi and Butterfield 2012), the lack of an observable effect of trisomy 21 may suggest that these effects manifest more subtly compared to the transgenic overexpression of *APP* which aggressively promotes amyloidosis.

4.3.5. Conclusion

In summary, we have developed a digital protocol capable of systematically separating cells with closely-associated processes, identifying individual cell bodies and hence describing single cells in immunohistochemical analysis. This has been particularly successful for microglial cells, where quantification of the area, length and branching of processes has suggested a general shift to a reactive morphology with APP/Aβ overexpression in the hippocampus; future work needs to confirm this with a blinded manual classification of morphology in these sections. On the other hand, improvements need to be made to account for variability in brown staining for GFAP, before greater confidence can be placed in the characterization of morphological traits in single astrocytes. Once this is optimized there is potential in using this protocol for the systematic, finer dissection of glial phenotypes in smaller subregions, or with reference to other objects such as distances from plaques. This may potentially bring out subtler phenotypes influenced by trisomy 21, which may currently be obscured by broad hippocampal-wide characterization.

Chapter 5. Investigating effects of trisomy 21 and APP/Aβ overexpression on mRNA expression profiles

5.1. Introduction

The Tc1xJ20 cross allows us the unique opportunity to investigate how the presence of Trisomy 21 modifies pathological features relating to APP/Aβ overexpression observed in the J20 mouse, such as the exacerbation of amyloidosis, reduced survival rates and deficits in learning and memory. In Chapters 3 and 4, we had examined this using hypothesis-driven approaches: in Chapter 3, developing an *in vitro* model was undertaken with the wider aim of evaluating the importance of candidate genes on Hsa21, which when trisomic may influence APP/Aβ phenotypes relating to cell biology; in Chapter 4, we investigated if changes in glial morphology and protein expression were concomitant pathological features modified by the presence of Tc1 and/or J20 genotypes. In contrast, this chapter describes a transcriptomic approach which does not assume *a priori* hypotheses, but instead seeks to generate new avenues for research by comparing the mRNA transcription levels between each Tc1xJ20 genotype, to observe how the presence of Trisomy 21 or mutant *APP* overexpression may influence gene expression patterns, and hence identify new areas to be explored.

In the transcriptomic characterisation of AD and DS so far, the bulk of studies have employed hybridization-based approaches, involving the targeted binding of probes to fluorescently labeled cDNA, on commercial or custom-made microarrays. These results have, however been largely discordant, potentially reflecting limitations such as high background signal due to cross-hybridisation artefacts (Okoniewski and Miller 2006), a limited dynamic range of detection, and the ambiguous mapping of short reads (Sutherland et al. 2011). In addition, microarrays rely on existing knowledge of the genome, and offer limited or no information on splice isoforms and non-coding RNA sequences (Wang et al. 2009). These are significant limitations, as altered gene expression and alternative splicing have been observed both as part of normal aging and in the development of AD (Stilling et al. 2014; Twine et al. 2011). However, their requirement for relatively small quantities of RNA starting material has facilitated studies of more specific brain regions and cell types, for instance through the use of laser capture microdissection (Kim et al. 2015).

We have, however, employed RNA-seq to study the transcriptome of the Tc1xJ20 cross, in collaboration with Dr. Manuela Zanda and Dr. Vincent Plagnol of the UCL Genetics Institute. RNA-seq employs next-generation sequencing technologies to allow a more cost-effective, higher-resolution sequencing method than traditional Sanger sequencing. In addition, it produces a measurement of transcript levels that can be more precise and detailed than other methods such as microarrays, including information on transcriptional structure, splicing patterns and post-transcriptional modifications (Wang et al. 2009). In brief, RNA-seq involves the reverse transcription of a population of total RNA to form a cDNA library with adapters to one or both ends of each fragment. This cDNA, with or without amplification, is sequenced to obtain reads (short DNA fragments) that are either aligned to reference transcripts, or assembled *de novo.* This library of reads can subsequently be annotated, quantified to determine transcription levels or further analyzed to provide information on splicing isoforms or transcriptional structures.

In this study, RNA-seq was performed on total hippocampal RNA obtained from 3-month old Tc1xJ20 cross progeny, using 3 mice per genotype. At 3 months of age, no plaque deposition is yet observable in J20 and Tc1;J20 mice (Mucke et al. 2000, and Chapter 1), hence any transcriptional differences reflect early changes in gene expression patterns prior to amyloid deposition. The RNA-seq data obtained was subsequently compared between three pairs of genotypes to identify genes that are differentially expressed: 1) to investigate the effect of trisomy 21 alone on mRNA expression, Tc1 data was compared with Wt ("Tc1/Wt"); 2) to discern the effects of *APP* transgene expression on mRNA expression, J20 was compared to Wt ("J20/Wt"); 3) to study how trisomy 21 modifies gene expression in the context of *APP* overexpression, Tc1;J20 data was compared to J20 ("Tc1;J20/J20"). We are currently unable to determine any interaction effects between trisomy 21 and mutant *APP* overexpression, as analysis across all four genotypes has yet to be performed to study effects of Tc1 genotype status and J20 genotype status across Tc1xJ20. However, insights into how transcription regulation can be affected by genotype based on pair-wise comparison can offer clues into how each genotype may result in phenotypic differences.

After identifying a list of genes that is significantly differentially expressed between these genotype pairs, one would like to understand how these may exert potential effects on biological function. To this end, we used the internet browser-based Database for Annotation, Visualisation, and Integrated Discovery (DAVID v6.7,

National Institute of Allergy and Infectious Diseases/National Institutes of Health, USA) to describe how differentially expressed genes (DEGs) could be classified into functionally-enriched clusters (Huang et al. 2009). We performed functional annotation clustering on genes that were significantly differentially expressed between each of the genotype pairs – Tc1/Wt, J20/Wt and Tc1;J20/J20 – to discover functions associated with groups of DEGs.

Finally, we were interested in determining whether the differences in candidate gene expression between genotypes observed in hippocampal RNA-seq was also generalizable to cortical gene expression, since both tissues have been studied in tandem for APP/Aβ-related pathology (see Chapters 1 and 3). To this end, we identified candidate genes from hippocampal RNA-seq data based on their potential relevance to AD pathogenesis, as elaborated for each gene in the Results section, together with confirmation of their expression in mouse cortex and hippocampus using the Allen Mouse Brain Atlas (Lein et al. 2007). Expression levels for candidate genes were quantified in 3-month old Tc1xJ20 cortical tissue using reverse transcription qPCR (qRT-PCR). These results were subsequently compared to hippocampal gene expression results obtained from RNA-seq. qRT-PCRs have been routinely used to verify RNA-seq results for single genes as the two platforms have been shown to demonstrate a strong level of concordance (C. Wang et al. 2014; Su et al. 2014). While it would have been ideal, in addition, to validate the RNA-seq gene expression data using Tc1xJ20 hippocampal tissue for qRT-PCR, this tissue was unavailable due to high demand for its use in other studies by the group into disease mechanisms. Therefore the value in this study will be in evaluating the concordance of candidate gene RNA expression patterns across hippocampal and cortical tissues.

5.1.1. Aims

1. Identify genes differentially expressed between Tc1 and Wt and compare to gene expression between Tc1;J20 and J20
2. Group differentially expressed genes between Tc1/Wt, Tc1;J20/J20 and J20/Wt into functional clusters using DAVID
3. Compare hippocampal gene expression from RNA-seq with cortical gene expression by qRT-PCR

5.2. Results

5.2.1. Differentially expressed genes identified between Tc1/Wt, Tc1;J20/J20 and J20/Wt

Supplementary Tables 1 to 3 detail genes that were significantly downregulated or upregulated in Tc1 compared to Wt (Tc1/Wt), J20/Wt and Tc1;J20/J20. Following sequencing, for each gene a mean read count was obtained; these were used to calculate the ratio of expression levels between the pairs of genotypes under comparison. An adjusted p-value was calculated to take into account multiple testing by applying a false discovery rate (FDR) correction; genes listed in Supplementary Tables 1-3 are significant following FDR correction and hence have an adjusted p-value < 0.05. These genes were subsequently used for functional annotation clustering in DAVID (Section 5.3.2) to identify functions associated with these DEGs.

Table 5.1 below lists DEGs that were significantly different between Tc1/Wt, and compares these results with the corresponding values from the comparison between Tc1;J20/J20. This therefore identifies gene transcription that is significantly changed by trisomy 21, and further illustrates whether this change in gene transcription is similarly influenced by trisomy 21 in APP/Aβ overexpression. Out of the 65 genes compared between Tc1/Wt that were significantly different, 5 genes remained significantly altered by trisomy 21 in Tc1;J20/J20.

Table 5.1 Effect of trisomy 21 on differential gene expression in Tc1/Wt and Tc1;J20/J20.

Genes listed here are differentially expressed significantly in Tc1 compared to Wt (Tc1/Wt), apart form *Arc* which is differentially expressed significantly in Tc1;J20/J20 but not Tc1/Wt. Genes are listed in order of increasing relative expression between Tc1/Wt. In the corresponding results for Tc1;J20/J20, most genes were no longer significantly differentially expressed; genes that remained significantly different, with adjusted p-values of <0.05 in Tc1;J20/J20, are indicated by a green adjusted p-value.

Ensembl ID (Release 81, July 2015)	Gene	Adj. p-value Wt / Tc1	Mean read count Wt	Mean read count Tc1	Adj. p-value J20 / Tc1;J20	Mean read count J20	Mean read count Tc1;J20	Relative Expression Tc1 / Wt	Relative Expression Tc1;J20 / J20	Chromosome (Mmu)
ENSMUSG00000021250	Fos	0.00001	520	119	0.002	531	119	0.23	0.22	12
ENSMUSG00000000303	Cdh1	0.004	61	15	0.9998	70	52	0.24	0.74	8
ENSMUSG00000004885	Crabp2	0.01	90	29	0.9998	101	79	0.32	0.78	3
ENSMUSG00000069372	Ctxn3	0.03	76	24	0.9998	82	70	0.32	0.86	18
ENSMUSG00000024650	Slc22a6	0	282	91	0.9998	386	303	0.32	0.78	19
ENSMUSG00000040310	Alx4	0.04	66	22	0.9998	93	86	0.33	0.93	2
ENSMUSG00000037868	Egr2	0.04	74	26	0.8992	79	21	0.35	0.26	10
ENSMUSG00000024190	Dusp1	0.0001	644	276	0.0004	793	400	0.43	0.50	17
ENSMUSG00000005087	Cd44	0.01	176	82	0.9998	277	271	0.46	0.98	2
ENSMUSG00000020423	Btg2	0.0000001	646	316	0.01	699	357	0.49	0.51	1
ENSMUSG00000028364	Tnc	0.02	383	192	0.9998	513	459	0.5	0.89	4
ENSMUSG00000038418	Egr1	0.02	2828	1523	0.9796	2940	1695	0.54	0.58	18
ENSMUSG00000053279	Aldh1a1	0.01	1830	998	0.00000004	1975	1081	0.55	0.55	19
ENSMUSG00000020241	Col6a2	0.01	947	521	0.9998	1352	1431	0.55	1.06	10
ENSMUSG00000030270	Cpne9	0	744	417	0.9998	1154	985	0.56	0.85	6
ENSMUSG00000092035	Peg10	0	529	294	0.9998	964	750	0.56	0.78	6
ENSMUSG00000022602	Arc	0.35	2923	1683	0.008	3543	1406	0.58	0.40	15
ENSMUSG00000040701	Ap1g2	0.02	566	341	0.9998	559	529	0.6	0.95	14
ENSMUSG00000052837	Junb	0.07	1148	685	0.0127	1318	816	0.6	0.62	8
ENSMUSG00000040495	Chrm4	0.01	536	328	0.2967	674	521	0.61	0.77	2
ENSMUSG00000021453	Gadd45g	0.04	555	345	0.9998	666	600	0.62	0.90	13
ENSMUSG00000000142	Axin2	0.01	977	620	0.9752	1101	946	0.63	0.86	11
ENSMUSG00000000184	Ccnd2	0.01	2479	1562	0.5118	2679	2189	0.63	0.82	6
ENSMUSG00000005774	Rfx5	0.01	849	536	0.2207	947	776	0.63	0.82	3
ENSMUSG00000044037	Als2cl	0.01	702	452	0.9998	846	736	0.64	0.87	9
ENSMUSG00000071341	Egr4	0.03	547	352	0.9998	514	328	0.64	0.64	6
ENSMUSG00000074575	Kcng1	0.03	709	464	0.9998	928	859	0.65	0.93	2
ENSMUSG00000018476	Kdm6b	0	1963	1272	0.9998	2370	2306	0.65	0.97	11
ENSMUSG00000018537	Pcgf2	0	1299	850	0.9998	1529	1524	0.65	1.00	11
ENSMUSG00000034771	Tle2	0	1762	1170	0.9998	1851	1791	0.66	0.97	10
ENSMUSG00000035835	BC005764	0.002	1585	1068	0.9998	2019	1708	0.67	0.85	10
ENSMUSG00000020893	Per1	0.003	3568	2537	0.9998	4194	3560	0.71	0.85	11
ENSMUSG00000002871	Tpra1	0.02	1295	914	0.9998	1389	1474	0.71	1.06	6
ENSMUSG00000047945	Marcksl1	0.03	1929	1384	0.9998	1927	1631	0.72	0.85	4
ENSMUSG00000025145	Lrrc45	0.02	3114	2296	0.9998	3668	3485	0.74	0.95	11
ENSMUSG00000028137	Celf3	0.01	7911	5939	0.9998	9542	8632	0.75	0.90	3
ENSMUSG00000028249	Sdcbp	0.02	7756	8406	0.9998	9594	11117	1.08	1.16	4
ENSMUSG00000049313	Sorl1	0.03	12721	13747	0.9998	16304	18964	1.08	1.16	9
ENSMUSG00000029657	Hsph1	0.01	10168	11095	0.9998	14692	15256	1.09	1.04	5
ENSMUSG00000031618	Nr3c2	0.02	3843	4179	0.9998	4818	5934	1.09	1.23	8
ENSMUSG00000023913	Pla2g7	0.01	5826	6375	0.9998	7582	7194	1.09	0.95	17
ENSMUSG00000045733	Sprn	0.03	4712	5142	No result	No result	No result	1.09	No result	7
ENSMUSG00000024873	Cnih2	0.03	10206	11268	0.9998	12629	13622	1.1	1.08	19
ENSMUSG00000022761	Lztr1	0.02	7928	8685	0.9998	10807	11881	1.1	1.10	16
ENSMUSG00000030729	Pgm2l1	0.01	10617	11708	0.9998	16381	16058	1.1	0.98	7
ENSMUSG00000037111	Setd7	0.02	5429	5989	0.9998	7147	7917	1.1	1.11	3
ENSMUSG00000035547	Capn5	0.03	2430	2698	0.9998	2955	3416	1.11	1.16	7
ENSMUSG00000026787	Gad2	0.01	4936	5468	0.9998	7772	9582	1.11	1.23	2
ENSMUSG00000052087	Rgs14	0.01	4518	5041	0.9998	6524	7739	1.12	1.19	13
ENSMUSG00000050711	Scg2	0.01	3623	4057	0.9998	5260	5547	1.12	1.05	1
ENSMUSG00000058897	Col25a1	0.02	2964	3352	0.9998	3550	4303	1.13	1.21	3
ENSMUSG00000050321	Neto1	0	3754	4242	0.9998	5259	5588	1.13	1.06	18
ENSMUSG00000030209	Grin2b	0	3449	3941	0.9998	5044	4812	1.14	0.95	6
ENSMUSG00000005360	Slc1a3	0	15408	17632	0.9998	17942	19061	1.14	1.06	15
ENSMUSG00000018322	Tomm34	0	3015	3439	0.9998	3756	4263	1.14	1.14	2
ENSMUSG00000030226	Lmo3	0	2306	2678	0.9998	2917	3010	1.16	1.03	6
ENSMUSG00000028648	Ndufs5	0.01	1505	1746	0.9998	2078	2486	1.16	1.20	4
ENSMUSG00000063297	Luzp2	0	4318	5060	0.9998	5296	5642	1.17	1.07	7
ENSMUSG00000039470	Zdhhc2	0.04	1567	1853	0.9998	905	943	1.18	1.04	8
ENSMUSG00000021613	Hapln1	0.02	755	905	0.9998	1123	1408	1.2	1.25	13

ENSMUSG00000030772	Dkk3	0	9916	11978	0.9998	13110	14018	1.21	1.07	7
ENSMUSG00000055540	Epha6	0.02	2687	3325	0.9998	4265	4222	1.24	0.99	16
ENSMUSG00000059325	Hopx	0	1500	1864	0.9312	1982	2403	1.24	1.21	5
ENSMUSG00000059991	Nptx2	0.02	594	738	0.9998	1201	1055	1.24	0.88	5
ENSMUSG00000020635	Fkbp1b	0.01	803	1008	0.9998	1258	1354	1.25	1.08	12
ENSMUSG00000048070	Pirt	0.01	36	85	0.9998	61	84	2.37	1.37	11

5.2.2. Identifying functional clusters from differentially expressed genes

Having generated lists of DEGs in comparing transcriptional profiles between Tc1/Wt, J20/Wt and Tc1;J20/J20 (Supplementary Tables 1-3), I sought to understand if there were any functional relationships between these genes, by performing functional annotation clustering using DAVID. This tool grouped DEGs (Supplementary Tables 1-3) that featured associated functions in common, as annotated in the DAVID Knowledgebase which integrates more than 40 publicly-available functional annotation sources (B. T. Sherman et al. 2007). Clustering was performed at the lowest stringency classification to identify as many potential functions as possible, given the stringent selection of DEGs based on FDR-adjusted p-values. Table 5.2 summarizes the functional clusters associated with differential expression between Tc1;J20/J20, Tc1/Wt and J20/Wt. The enrichment scores (in brackets) reflect the geometric mean of all enrichment p-values for each annotation term, per gene member, in the group – these indicate the relative importance of gene groups, and are not absolute p-values. To emphasise this relative nature, a minus log transformation was applied on the p-values, therefore an enrichment score greater than 1.3 reflects significant p-values less than 0.05 (Huang et al. 2009; Hosack et al. 2003). Table 5.2 was interpreted from the full DAVID output in Supplementary Tables 4-6, which expands on every annotation term and its associated DEGs, used to calculate the enrichment score for the overall cluster.

Table 5.2 Functional clusters associated with the differentially expressed genes identified between each pair of genotypes.

The enrichment score (in brackets) reflects the geometric mean of all enrichment p-values for annotation terms within the cluster, and offers a relative significance value for the cluster. Enrichment scores >1.3 correspond to significant p-values <0.05, and are indicated by an asterisk.

Annotation Cluster	Tc1;J20 vs J20 (14 out of 28 genes clustered)	Tc1 vs Wt (19 out of 64 genes clustered)	J20 vs Wt (14 out of 24 genes clustered)
1	Cytoplasmic vesicles and plasma membrane (1.52*)	Extracellular regions (1.89*)	Signalling peptides (3.30*)
2	Embryonic development (0.94)	Transcription regulation (1.44*)	Glycosylation and transmembrane proteins (2.95*)
3	Cytoplasmic vesicles and ion binding (0.82)	Cytoplasmic vesicles (1.33*)	Cellular homeostasis, neurotransmission, gliogenesis (2.63*)
4	Ion transport, glycosylation and membrane (0.65)	Carbohydrate binding (1.19)	Extracellular matrix and cell adhesion (2.01*)
5	Signalling peptides (0.46)	Regulation of synaptic transmission, cognition (1.18)	Ion transport (1.20)
6	Organelle lumen (0.39)	Embryonic development (1.18)	Cell membrane (0.91)
7	Transcription regulation (0.15)	Cellular ion/chemical homeostasis (1.10)	Cell/membrane/insoluble fraction (0.80)
8		Gland development, extracellular matrix, cell adhesion (1.04)	Transmembrane region (0.67)
9		Fibronectin proteins (0.94)	Ion binding (0.44)
10		Protein glycosylation (0.90)	Nucleotide binding (0.13)
11		Transcription regulation (0.88)	
12		Immune cell activation (0.83)	
13		Plasma membrane (0.76)	
14		Wnt signalling (0.77)	
15		Inflammatory/wound/defence response (0.74)	
16		Epithelial development (0.71)	
17		Cell junction, synapse (0.66)	
18		Zinc-finger DNA binding (0.51)	
19		Nucleoplasm and organelle lumen (0.45)	
20		Ion transport (0.38)	

Transcriptional differences relating to cytoplasmic vesicles is the only significantly-associated annotation cluster in Tc1;J20/J20, and is also significant in Tc1/Wt; this indicates that the presence of trisomy 21 is sufficient to alter the gene expression associated with cytoplasmic vesicles even in the context of APP/Aβ overexpression. However, altered gene expression relating to transcriptional regulation and extracellular regions is only significant in Tc1/Wt and lost in the presence of APP/Aβ overexpression. The annotation clusters associated with J20/Wt strongly influence gene expression relating to cell signaling and membrane-related functions, such as cell adhesion and transmembrane protein modifications.

5.2.3. Investigating the concordance of candidate gene expression between hippocampal and cortical samples

Finally, we were interested in determining whether the differences in candidate gene expression levels between genotypes observed using hippocampal RNA-seq was also generalizable to cortical gene expression, since both tissues have been studied in parallel for APP/Aβ-related pathology (see Chapters 1 and 4). To this end, we identified candidate genes from hippocampal RNA-seq data based on their potential relevance to AD pathogenesis, as elaborated for each gene below, as well as confirmation of their expression in mouse cortex and hippocampus using the Allen Mouse Brain Atlas (Lein et al. 2007). Expression levels for candidate genes were quantified in 3-month old Tc1xJ20 cortical tissue using reverse transcription qPCR (qRT-PCR).

5.2.3.3. *App*

App was the only gene validated by qRT-PCR in both hippocampal and cortical tissues, to complement the group's studies on APP/Aβ performed in both tissues so far.

Hippocampal RNA expression that was analyzed by RNA-seq demonstrated no significant difference in *App* mean read counts, in Tc1 compared to wildtype (adjusted p = 0.9784) and in Tc1;J20 compared to J20 (adjusted p = 0.9998). In hippocampal RNA quantified by qRT-PCR, there was no significant effect of Tc1 or J20 status, or the interaction between Tc1 and J20 status, on *App* expression (2-way ANOVA Tc1 status $F(1, 28) = 0.065$, $p = 0.800$; J20 status $F(1, 28) = 1.464$, $p = 0.236$; Tc1*J20 interaction $F(1, 28) = 0.000$, $p = 1.000$). In cortical RNA, there was also no significant effect of Tc1 or J20 status, or the interaction between Tc1 and J20 status, on *App* expression (Tc1 status $F(1,40) = 0.055$, $p = 0.815$; J20 status $F(1, 40) = 0.177$, $p = 0.676$; Tc1*J20 interaction $F(1, 40) = 1.031$, $p = 0.316$). While *App* expression was shown to be not significantly different across genotypes in both tissue types, the directions of change in hippocampal qRT-PCR analysis more closely resembled hippocampal RNA-seq results, in a non-significant ~1.3-fold increase in *App* expression in J20-positive mice compared to J20-negative mice. This was compared to the wider variability observed in cortical tissue resulting in no clear trend.

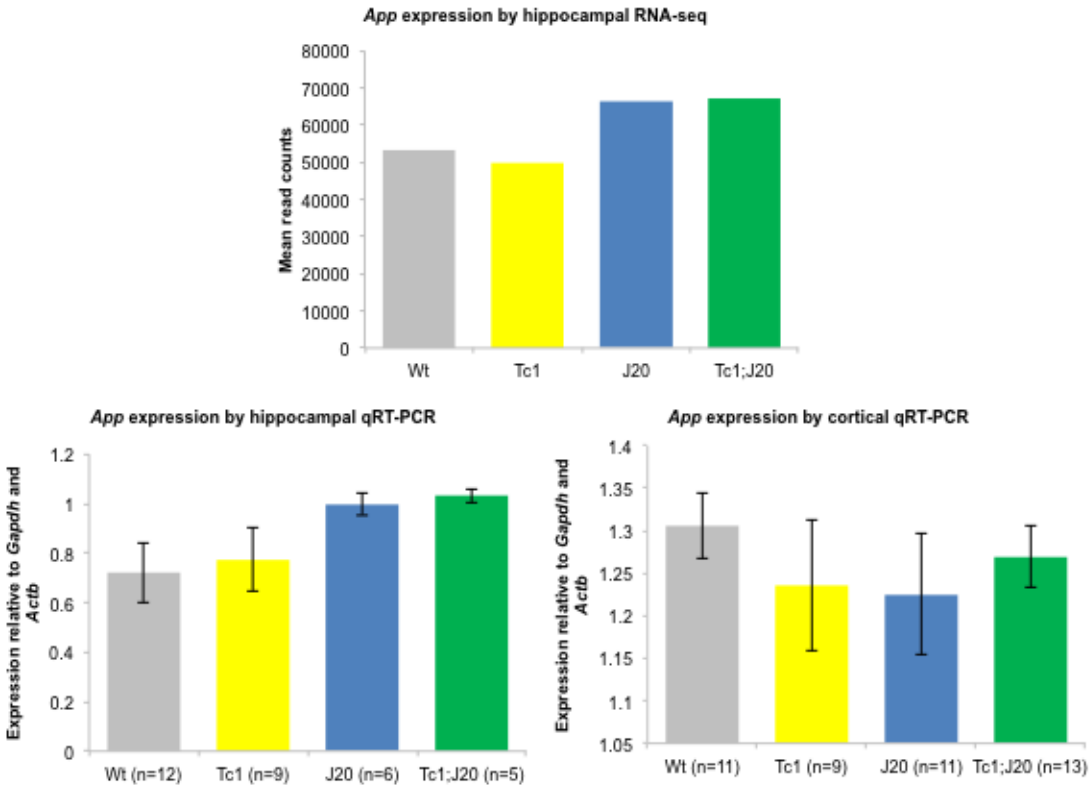

Figure 5.1 Comparison of *App* hippocampal RNA-seq results with hippocampal and cortical *App* RNA expression quantified by qRT-PCR.

Hippocampal RNA-seq data shows no significant difference in *App* reads in trisomic compared to non-trisomic mice. This was validated in both hippocampal and cortical RNA quantified by qRT-PCR. Graph shows mean values (labelled) while error bars indicate SEM.

Apart from *App*, All other RNA expression levels quantified by qRT-PCR were only performed on cortical tissue from 3-month old Tc1xJ20 mice. These candidate genes were selected based on their potential relevance to AD pathogenesis, which will be briefly introduced for each gene prior to the results comparing hippocampal RNA-seq with cortical qRT-PCR expression results.

5.2.3.4. Immediate-Early Genes (IEGs): *Arc*, *Dusp1*, *Egr1*, *Fos*

Immediate-Early Genes (IEGs) comprise of a group of rapid response genes that do not require protein synthesis for their expression (Saha and Dudek 2013). Many IEGs encode transcription factors that activate a downstream activity-dependent transcriptional programme, in response to a wide variety of cell stimuli (Leslie and Nedivi 2011). In neurons, IEGs were of particular interest because of the proposed importance of immediate gene induction as an integral step in the consolidation of long-

term potentiation, to explain how synaptic changes may exert long-term effects on memory (Cortés-Mendoza et al. 2013; Dragunow 1996). Many neuronal IEG transcripts such as *Arc* can be detected within 2 min of a stimulus (Guzowski et al. 1999), and this reliable temporal expression is now commonly used to track neuronal activity in response to specific stimuli (Cruz et al. 2013).

In AD, synaptic activity is one of the most important factors regulating Aβ levels, for instance by influencing APP internalisation and cleavage (X. Cheng et al. 2014). Arc, in particular, has been closely associated with APP/Aβ levels through a variety of synaptic receptors. Under basal conditions, *Arc* is transcribed at low levels (Rao et al. 2006). It is, however, tightly regulated by neuronal activity (Korb and Finkbeiner 2011), as observed by its dramatic upregulation through receptor activity including BDNF tyrosine kinase receptors (Ying et al. 2002), metabotropic glutamate receptors (Waung et al. 2008), muscarinic acetylcholine receptors (Teber et al. 2004) and NMDA receptors (Steward and Worley 2001). Increased Aβ levels in mouse and cell models have been shown to impair Arc expression (Wang et al. 2006; Palop et al. 2005), while conversely Arc is required for activity-dependent increases in APP trafficking and Aβ production (Wu et al. 2011). The downregulation of IEGs by APP also extends to genes including *Egr1* and *Fos* (Hendrickx et al. 2014), while *Egr1* and *Fos* downregulation have also been observed in AD mouse models (Hendrickx et al. 2014; Christensen et al. 2013; Dickey et al. 2004; Dickey et al. 2003) and in patients at Braak stages of AD with cognitive impairment (Bossers et al. 2010). While *Arc*, *Egr1* and *Fos* are "promiscuous" and induced by a wide range of stimuli, *Dusp1* has been identified as an IEG induced by depolarisation, but not growth factors or neurotrophins, possibly playing a more restricted role in regulating specific downstream functional responses in neurons following depolarisation (Machado et al. 2008).

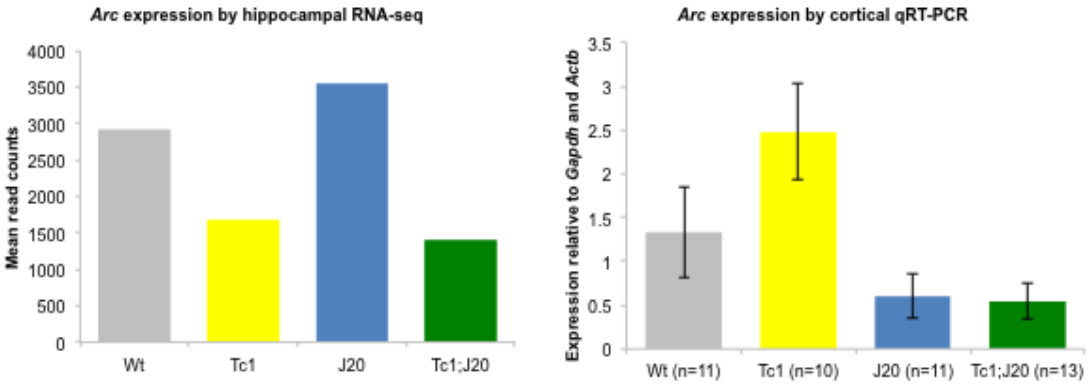

Figure 5.2 Comparison of *Arc* hippocampal RNA-seq results with cortical *Arc* RNA expression by qRT-PCR

Hippocampal RNA-seq data suggests that trisomy 21 reduces the expression of *Arc* reads compared to non-trisomic mice. In cortical RNA, however, there was no significant effect of trisomy 21 on *Arc* expression. Instead, *Arc* expression is significantly downregulated by APP/Aβ overexpression. Graph shows mean values while error bars indicate SEM**.**

Hippocampal RNA expression that was analyzed by RNA-seq demonstrated a non-significant decrease in *Arc* mean read count in Tc1 compared to Wt (adjusted p = 0.353), but a significant decrease in Tc1;J20 compared to J20 (adjusted p = 0.008). In cortical RNA, there was a significant effect of APP/Aβ overexpression on *Arc* expression (2-way ANOVA APP/Aβ overexpression $F(1,41) = 11.543$, $p = 0.002$). However, there was no significant effect of trisomy 21, or the interaction between trisomy 21 and APP/Aβ overexpression, on *Arc* expression (2-way ANOVA trisomy 21 $F(1,41) = 1.917$, $p = 0.174$; interaction $F(1,41) = 2.361$, $p = 0.132$).

Hippocampal RNA expression that was analyzed by RNA-seq demonstrated a significant decrease in *Dusp1* mean read count in Tc1 compared to wildtype (adjusted $p < 0.001$), but a non-significant decrease in Tc1;J20 compared to J20 (adjusted p = 0.9998). In cortical RNA, there was no significant effect of trisomy 21 or APP/Aβ overexpression on *Dusp1* expression, and no significant interaction effect (2-way ANOVA trisomy 21 $F(1,39) = 0.413$, $p = 0.524$; APP/Aβ overexpression $F(1,39) = 0.881$, $p = 0.354$; interaction $F(1,39) = 0.478$, $p = 0.494$). Therefore hippocampal RNA-seq data suggests an effect of trisomy 21 in reduced *Dusp1* expression compared to non-trisomic mice. However, there was no clear effect of genotype on *Dusp1* expression in cortical qRT-PCR as *Dusp1* expression levels remained similar across all four genotypes.

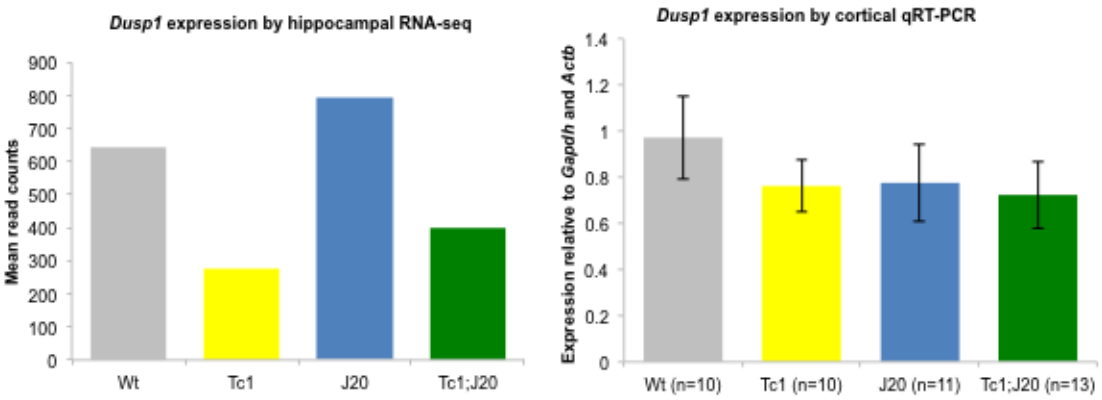

Figure 5.3 Comparison of *Dusp1* hippocampal RNA-seq results with cortical *Dusp1* RNA expression by qRT-PCR.

Hippocampal RNA-seq data suggests that trisomy 21 reduces the expression of *Dusp1* reads compared to non-trisomic mice. In cortical RNA, however, there is no significant effect of trisomy 21 or APP/Aβ overexpression on *Dusp1* expression, with similar *Dusp1* expression levels across all four genotypes. Graph shows mean values while error bars indicate SEM.

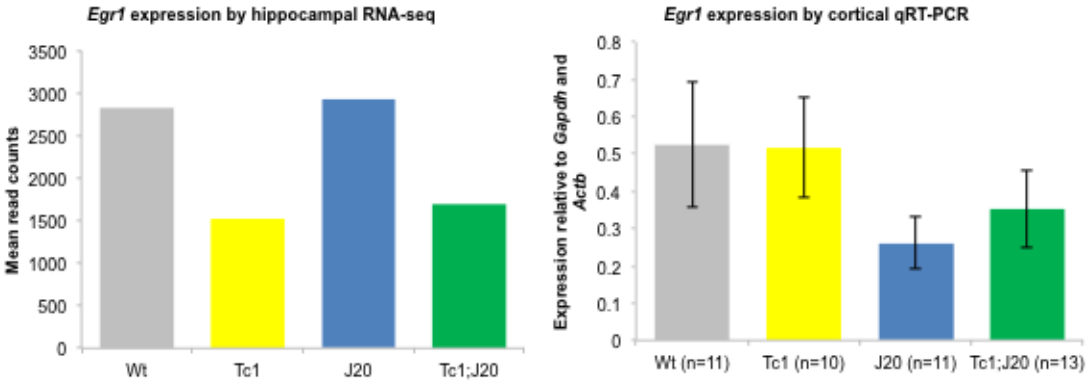

Figure 5.4 Comparison of *Egr1* hippocampal RNA-seq results with cortical *Egr1* RNA expression by qRT-PCR.

Hippocampal RNA-seq data suggests that trisomy 21 reduces the expression of *Egr1* reads compared to non-trisomic mice. In cortical RNA, however, there was a non-significant trend for decreased *Egr1* expression in APP/Aβ overexpression, and no significant effect of trisomy 21 on *Egr1* expression. Graph shows mean values while error bars indicate SEM.

Hippocampal RNA expression that was analyzed by RNA-seq demonstrated a significant decrease in *Egr1* mean read count in Tc1 compared to wildtype (adjusted p = 0.023), but a non-significant decrease in Tc1;J20 compared to J20 (adjusted p = 0.9796). In cortical RNA, there was a non-significant trend towards decreased *Egr1* expression in APP/Aβ overexpression (2-way ANOVA F(1,39) = 2.994, p = 0.091), while there was no significant effect of trisomy 21, or interaction between trisomy 21 and APP/Aβ overexpression on *Egr1* expression (trisomy 21 F(1,41) = 0.112, p = 0.740; interaction F(1,39) = 0.160, p = 0.692). Therefore *Egr1* expression appears to be downregulated by trisomy 21 in the hippocampus, but is downregulated by presence APP/Aβ overexpression in the cortex.

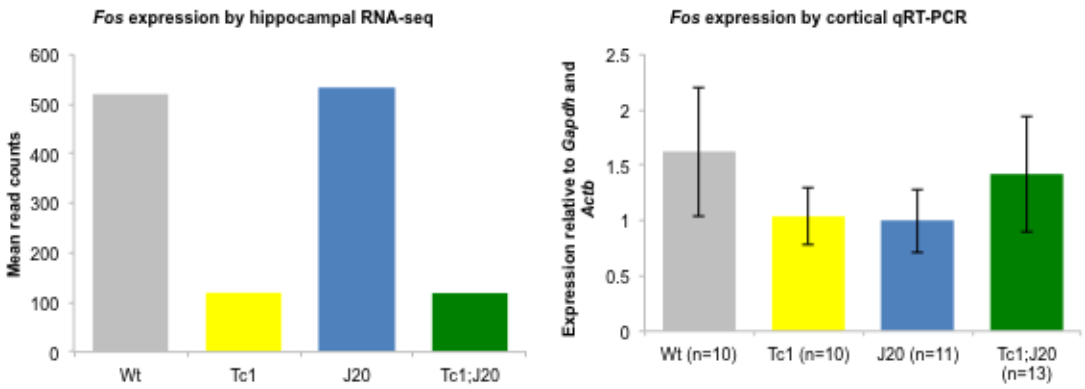

Figure 5.5 Comparison of *Fos* hippocampal RNA-seq results with cortical *Fos* RNA expression by qRT-PCR.

Hippocampal RNA-seq data suggests that trisomy 21 reduces *Fos* expression compared to non-trisomic mice. In cortical RNA, however, there was no significant effect of trisomy 21 or APP/Aβ overexpression on *Fos* expression, with no clear trend, and wide variability of expression levels. Graph shows mean values while error bars indicate SEM.

Hippocampal RNA expression that was analyzed by RNA-seq demonstrated a significant decrease in *Fos* mean read count in Tc1 compared to wildtype (adjusted p < 0.001), but a non-significant decrease in Tc1;J20 compared to J20 (adjusted p = 0.9998). In cortical RNA, there was no significant effect of trisomy 21 or APP/Aβ overexpression on *Fos* expression, and no significant interaction between (2-way ANOVA trisomy 21 F(1,39) = 0.040, p = 0.843; APP/Aβ overexpression F(1,39) = 0.059, p = 0.810; interaction F(1,39) = 1.151, p = 0.290). Therefore hippocampal RNA-seq data suggests an effect of trisomy 21 in reduced *Fos* expression compared to non-trisomic mice. However, there was no clear effect of genotype on *Fos* expression in cortical qRT-PCR, with wide variability of expression levels measured.

5.2.3.5. *Per1*

Period1 (Per1) is a clock gene encoding a transcriptional repressor that contributes to the regulation of circadian rhythm. In both DS and sporadic AD, sleep disturbances have been observed. In DS, sleep fragmentation is a consistent feature (Fernandez and Edgin 2013; Churchill et al. 2012; Diomedi et al. 1999; Levanon et al. 1999), while memory decline in AD could result from an impairment of sleep-dependent memory consolidation, due to disturbances in circadian rhythm (Weldemichael and Grossberg 2010; Rauchs et al. 2008). In patients with preclinical and clinical AD, the rhythmic expression of *PER1* is lost in the suprachiasmatic nucleus, the 'master clock' of the brain (Wu et al. 2006). In addition, *PER1* expression in AD also displays altered synchronization with other circadian oscillators in the cingulate cortex and the bed nucleus of the stria terminalis, regions involved in decision making and motivation (Cermakian et al. 2011). This may be partly due to inhibition by the overexpression of the TGF-β cytokine in neurons in AD (Gast et al. 2012).

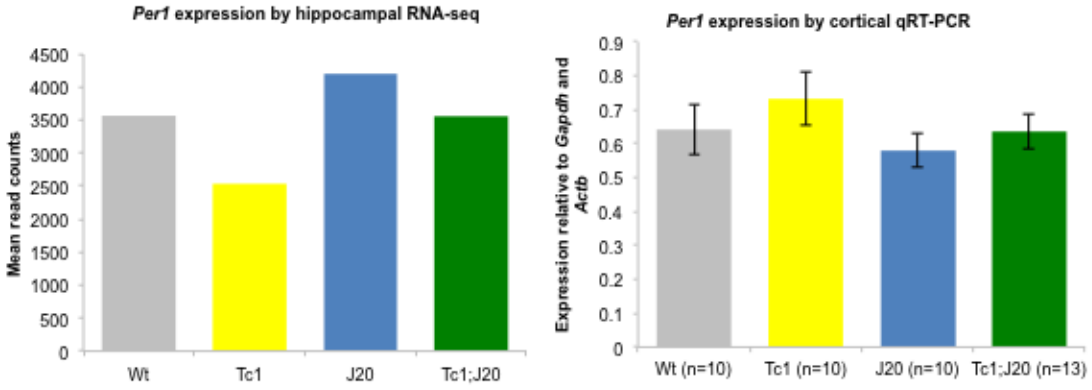

Figure 5.6 Comparison of *Per1* hippocampal RNA-seq results with cortical *Per1* RNA expression by qRT-PCR.

Hippocampal RNA-seq data suggests that trisomy 21 reduces the expression of *Per1* expresion compared to non-trisomic mice. However in cortical qRT-PCR there was no significant effect of trisomy 21 or APP/Aβ overexpression on *Per1* expression in cortical RNA. Graph shows mean values while error bars indicate SEM.

Hippocampal RNA expression that was analyzed by RNA-seq demonstrated a significant decrease in *Per1* mean read count in Tc1 compared to wildtype (adjusted p = 0.003), but a non-significant decrease in Tc1;J20 compared to J20 (adjusted p = 0.9998). In cortical RNA, there was no significant effect of trisomy 21 or APP/Aβ overexpression on *Per1* expression, and no significant interaction (2-way ANOVA trisomy 21 $F(1,39) = 1.337$, $p = 0.255$; APP/Aβ overexpression $F(1,39) = 1.558$, $p =$

0.219; interaction F(1,39) = 0.072, p = 0.790). An additional analysis of the effects of sex was performed in the cortical qRT-PCR results. There was no significant effect of sex on *Per1* expression (ANOVA Sex F(1,41) = 0.141, p = 0.710). In summary hippocampal RNA-seq data suggests an effect of trisomy 21 in reduced *Per1* expression compared to non-trisomic mice. However, there was no clear effect of genotype on *Egr1* expression in cortical qRT-PCR as expression levels remained similar across all four genotypes.

5.2.3.6. *Chrm4*

Chrm4 is a muscarinic cholinergic receptor (type M4) which has largely been studied in the context of schizophrenia (Seo et al. 2014; Scarr et al. 2013; Rietschel et al. 2012). In AD, it has been suggested that the M4 receptor type may be selectively compromised in the dentate gyrus and CA4 hippocampal regions (Mulugeta et al. 2003).

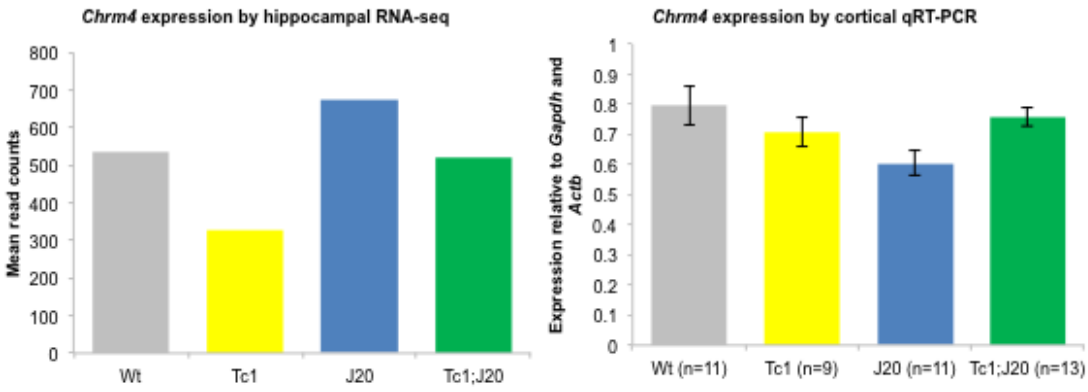

Figure 5.7 Comparison of *Chrm4* hippocampal RNA-seq results with cortical *Chrm4* RNA expression by qRT-PCR.

RNA-seq data suggests that trisomy 21 reduces the expression of *Chrm4* reads compared to non-trisomic mice. However, there was no significant effect of trisomy 21 or APP/Aβ overexpression on *Chrm4* expression in cortical RNA, with no clear trend observable across the genotypes. Graph shows mean values while error bars indicate SEM.

Hippocampal RNA expression that was analyzed by RNA-seq demonstrated a significant decrease in *Chrm4* mean read count in Tc1 compared to wildtype (adjusted p = 0.009), but a non-significant decrease in Tc1;J20 compared to J20 (adjusted p = 0.297). In cortical RNA, there was no significant effect of trisomy 21 or APP/Aβ overexpression on *Chrm4* expression, though there was significant interaction between

trisomy 21 and APP/Aβ overexpression (2-way ANOVA trisomy 21 F(1,40) = 0.452, p = 0.505; APP/Aβ overexpression F(1,40) = 2.284, p = 0.139; interaction F(1,40) = 6.687, p = 0.013). Therefore, hippocampal RNA-seq suggests a downregulation of *Chrm4* due to the presence of trisomy 21. On the contrary, there was no clear effect of genotype on *Chrm4* expression in cortical qRT-PCR.

5.2.3.7. *Snx27*

Sorting nexins (SNX) belong to a large family of proteins containing a conserved PX domain, many of which have been shown to regulate protein sorting in the endosomal network (Cullen and Korswagen 2011). The PX (phagocytic oxidase homologous region) domain of SNX27 colocalises with EEA1 in early endosomes and transferrin receptors in recycling endosomes (Cai 2011), but also contains an additional PDZ domain (Dlg homologous region) not found in other PX domain proteins (Rincón et al. 2007). In DS, SNX27 deficiency was first shown to contribute to synaptic and cognitive deficits, linked to the dysregulation of glutamate receptor trafficking (Loo et al. 2014; Wang et al. 2013). This was due to downregulated transcription of *SNX27* by its transcription factor, C/EBPβ, which is in turn regulated by Hsa21-encoded miRNA, miR-155 (Wang et al. 2013). More recently, SNX27 deficiency was shown to increase Aβ production, by modulating γ-secretase activity via its PDZ domain (X. Wang et al. 2014).

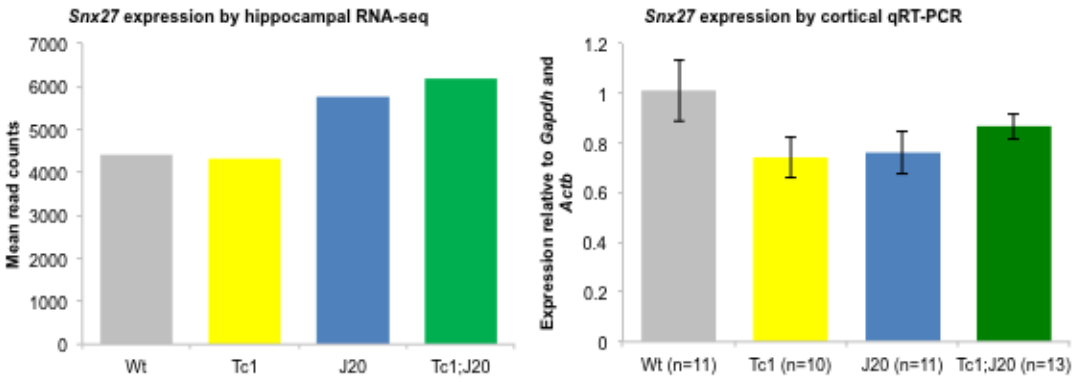

Figure 5.8 Comparison of *Snx27* hippocampal RNA-seq results with cortical *Snx27* RNA expression by qRT-PCR.

RNA-seq data suggested a non-significant increase in *Snx27* reads in APP/Aβ overexpression. However in cortical qRT-PCR, there was no significant effect of trisomy 21 or APP/Aβ overexpression on *Snx27* expression. Graph shows mean values while error bars indicate SEM.

Hippocampal RNA expression that was analyzed by RNA-seq demonstrated a non-significant increase in *Snx27* average read count in J20-positive genotypes compared to J20-negative genotypes (Tc1;J20*J20 adjusted p = 0.9998, Tc1*Wt adjusted p = 0.8705). This was not replicated in cortical RNA quantified by qRT-PCR. In cortical RNA, there was no significant effect of trisomy 21 or APP/Aβ overexpression on *Snx27* expression, though there was significant interaction between trisomy 21 and APP/Aβ overexpression (2-way ANOVA trisomy 21 F(1,41) = 0.928, p = 0.341; APP/Aβ overexpression F(1,41) = 0.043, p = 0.468; interaction F(1,41) = 4.919, p = 0.032). Therefore, hippocampal RNA-seq suggests a subtle upregulation of *Snx27* in APP/Aβ overexpression, though this was non-significant. On the contrary, there was no clear effect of genotype on *Snx27* expression in cortical qRT-PCR.

5.3. Discussion

5.3.1. Functional clustering identifies effect of trisomy on hippocampal transcription relating to cytoplasmic vesicles

Functional clustering analysis was performed using DAVID (Huang et al. 2009) to identify potential functional differences that may arise from differential gene expression. This identified clustering associated with cytoplasmic vesicles as the most significant feature in comparisons between both pairs of trisomic and euploid genotypes (Tc1;J20/J20 and Tc1/Wt), suggesting that trisomy 21 significantly alters vesicular transcriptional regulation. This is particularly exciting in light of previous work by the group showing that the increased amyloid deposition observed in Tc1;J20 compared to J20 is potentially mediated by altered APP trafficking, which occurs through a network including endocytic and recycling vesicles (Haass et al. 2012, and Chapter 1). DEGs implicated in cytoplasmic vesicular function between Tc1;J20/J20 include *ARC, CAPN11, DSP, KCNC4, SCGN, SLC17A8, TRF*; those implicated in Tc1/Wt include *ALS2CL*, *AP1G2*, *GAD2, GRIN2B,* and *SDCBP*. These illustrate a few potential functional alterations that may be further investigated and verified. For instance, potential glutamatergic and GABAergic signalling alterations are reflected by differences in expression in *SLC17A8*, a vesicular glutamate transporter, the NMDA glutamate receptor *GRIN2B*, and *GAD2* which is involved in GABA synthesis. *ALS2CL* serves as a guanine nucleotide exchange factor for an early endosome-associated GTPase, Rab5, while *AP1G2* may be relevant to clathrin coat formation in late endosomes or multivesicular bodies.

Cytoplasmic vesicle abnormalities have been frequently associated with AD. Significantly, multiple steps of the APP processing, secretion and recycling pathway through the endosomal system have been suggested to be dysfunctional in AD. For instance, dysfunctional retromer function has been suggested to impair BACE1 and APP recycling, leading to prolonged APP exposure to BACE1 and hence increased downstream Aβ production (Trousdale and Kim 2015; Das et al. 2013). Exosomes have also been suggested to modulate Aβ aggregation, given that they contain components for Aβ synthesis and degradation, possibly by influencing the equilibrium between soluble and insoluble Aβ species (Toro et al. 2015; Joshi et al. 2015; Simons and Raposo 2009). Numerous lysosomal pathological changes and upregulated autophagy have also been observed in AD neurons (Orr and Oddo 2013). The further dysregulation of transcription relating to cytoplasmic vesicles by trisomy 21 may therefore potentially interact with these phenotypes in AD-DS and compound dysfunction. Trisomy of Hsa21 genes has previously been linked with potential roles in vesicular disorders, which may be connected with the transcriptional differences identified above. Trisomy of *App* (Salehi et al. 2006) and *Synj1* (Cossec et al. 2012) have been linked to the enlargement of early endosomes, while the concomitant upregulation of all three fly homologues for *Itsn1, Rcan1/Dscr1* and *Synj1* was required for impaired vesicle recycling (Chang and Min 2009). Duplications of *DOPEY2* (Barbosa et al. 2010), which encodes a protein involved in endosome-Golgi trafficking, have been associated with SAD (Swaminathan, Huentelman, et al. 2012; Swaminathan, Shen, et al. 2012), though this association remains to be replicated (Chapman et al. 2013). The genetic deletion of *CSTB*, which expresses a lysosomal cathepsin inhibitor, decreases Aβ deposition and cognitive deficits (Yang et al. 2011). However, four of the above genes (*APP, SYNJ1, RCAN1, ITSN1*) are not functionally trisomic in the Tc1 model (Gribble et al. 2013), hence trisomy of these genes does not account for the differential transcription associated with cytoplasmic vesicles, in Trisomy 21.

It will therefore be of great interest to discover if there are any differentiating vesicular phenotypes between the genotypes in Tc1xJ20. However, further work needs to be undertaken to verify that the above transcriptional changes also manifest at a functional level, as RNA expression only partially predicts protein expression. In eukaryotes, generally ~40% of variation in protein concentration can be explained by mRNA levels; the remaining 60% would likely be due to a combination of post-transcriptional

regulation and unexplained variation (Payne 2015; de Sousa Abreu et al. 2009; Maier et al. 2009). In addition, mRNAs are produced at a much slower rate than proteins in mammalian cells, but are much more unstable, with an average half life of hours rather than days (Schwanhäusser et al. 2011; Sharova et al. 2009). However, these average half-life values are highly variable between proteins, depending on their structure and hence likely function – for instance, mammalian metabolic proteins tend to be very stable while proteins involved in transcription regulation tend to be quickly degrade (Schwanhäusser et al. 2011). However, aside from translation and protein degradation rates, it appears that the strongest remaining influence on protein levels is mRNA abundance, and not biological or experimental noise (Vogel and Marcotte 2012). Therefore, transcriptomics and proteomics need to be studied together to understand the complex regulation processes underlying how differential gene expression may influence functional effects of different genotypes.

5.3.2. Effects of genotype on gene expression differ in cortical and hippocampal tissue

5.3.2.1. *App*

While *App* expression was shown to be not significantly changed by trisomy 21 or APP/Aβ overexpression in both hippocampal and cortical tissue, the directions of change in hippocampal qRT-PCR analysis more closely resembled hippocampal RNA-seq results, compared to the wider variability observed in cortical tissue resulting in no clear trend. This suggests subtle tissue-specific differences between hippocampal and cortical *App* expression. However, the lack of a significant effect of the J20 transgene on *App* expression indicates that *APP* overexpression does not significantly modify endogenous *App* expression, avoiding this confounding effect on mRNA expression. On the other hand, the lack of a significant effect of trisomy at 3 months is in line with studies undertaken in Ts65Dn mice, which are functionally trisomic for *App*, where *App* expression levels in hemibrain samples remained similar to disomic mice at 5 months (Choi et al. 2009). However, Ts65Dn *App* expression increased to trisomic levels at 12 months, suggesting an age-dependent dysregulation of *App* expression (Choi et al. 2009), in line with age-dependent increases in APP protein (Choi et al. 2009; Contestabile et al. 2006; Seo and Isacson 2005) and the enlarged early endosome phenotype shown to require *App* trisomy (Salehi et al. 2006).

While Tc1 mice are not functionally trisomic for *App*, it may still be of interest to examine *App* expression at older ages, as an age-dependent upregulation of *App* expression is also observed in a mouse model of accelerated senescence (Cho et al. 1995), while people with DS exhibit signs of premature aging (Horvath et al. 2015; Zigman 2013). This may be especially interesting should any alterations in cytoplasmic vesicular or endosomal phenotypes be found.

5.3.2.2. Immediate-Early Genes

A striking feature of the hippocampal RNA-seq results indicating that at least eight DEGs were highly-expressed IEGs (*Arc, Btg2, Dusp1, Egr1, Egr2, Egr4, Fos, Junb*), which were downregulated in both trisomic genotypes compared to their respective disomic controls (Table 5.1). In contrast, this was not replicated in cortical qRT-PCR analysis, which demonstrated either no effect of genotype on IEG expression (*Dusp1* and *Fos*), or decreased expression due to presence of the J20 transgene rather than Trisomy 21 (*Arc* and *Egr1*). Another feature of cortical IEG expression was a wide variability of results obtained, particularly for *Arc*. These stark differences may be due to differences in IEG patterns of expression between these tissues. Hippocampal and cortical networks have been proposed to be organised as complementary systems in processes underlying memory formation (McClelland and Goddard 1996), which exerts effects on patterns of IEG activation in each tissue. This has been demonstrated in differential IEG expression in response to different forms of stimuli, including sleep and various forms of learning (Xie et al. 2014; Hartzell et al. 2013; Ribeiro et al. 2007). In addition, complex cell-type- and stimulus-specific IEG expression patterns may contribute to the variability of IEG expression, as exemplified by *Arc*, which was expressed only in certain non-GABAergic rat neurons following exploration of a novel environment, but expressed in GABAergic neurons following an electroconvulsive seizure (Vazdarjanova et al. 2006). As we will discuss below, considerable differences between cortical and hippocampal tissue exist which need to be taken into account while considering differential gene expression. It will therefore be useful to re-validate RNA-seq data with qRT-PCR of Tc1xJ20 hippocampal RNA to confirm the patterns of differential expression. Further work also needs to be undertaken in quantifying IEG protein and RNA expression using the same biological samples to determine with more certainty the effect of trisomy on IEG expression.

While IEGs have not been directly studied in people with Down syndrome, increased protein levels of Arc, cFos and phospho-cFos have been detected in Tc1 hippocampal tissues in a proteomic study, but no increases in Egr1 were detected (Ahmed et al. 2013). Interestingly, in the same proteomics study (Ahmed et al. 2013), no differences in IEG protein expression were observed in Ts65Dn mice compared to wildtype. On the other hand, reduced IEG baseline RNA expression, or activation following memory stimulation, have been reported in Ts65Dn, supporting an effect of trisomy in altering IEG expression patterns (Braudeau et al. 2011). These results therefore highlight the value of quantifying protein and RNA expression levels using the same samples, from the same brain tissue type, to mitigate the high variability in IEG expression and better understand how trisomy 21 or *APP* overexpression influences IEG-related phenotypes.

5.3.2.3. *Per1*

Our RNA-seq data suggests that trisomy significantly downregulates *Per1* expression in the hippocampus, which was not replicated in qRT-PCR analysis of cortical RNA. Circadian *Per1* expression has been demonstrated in both tissues in the mouse (Rath et al. 2013; Jilg et al. 2010). However, rhythmic gene expression can vary between subregions in each of these tissues (Harbour et al. 2013; Feillet et al. 2008), and may be further influenced by sex differences. For instance, females demonstrated rhythmic clock gene expression in hippocampal CA1 and CA3 regions, which was not significantly observed in male CA1 and CA3 (Chun et al. 2015). In our cortical qRT-PCR data, however, there was no significant effect of sex on *Per1* expression. Tc1 mice exhibit fragmented sleep patterns comparable to people with DS (Heise et al. 2015), although *PER1* has not been studied in people with DS. Further work could therefore focus on Per1 expression in Tc1xJ20 hippocampus relating to circadian rhythm to describe if this downregulation also manifests in temporal alterations.

5.3.2.4. *Chrm4*

Similar to other significantly altered genes in the hippocampal RNA-seq data, *Chrm4* appears to be significantly downregulated by trisomy 21. However, unlike *Per1* and the IEGs, which fluctuate relatively quickly in response to stimuli or time of day, *Chrm4* expression appears relatively stable and invariant cross a wide range of tissues, including cortex and hippocampus, according to an aggregated gene annotation resource, BioGPS (Wu et al. 2013; Lattin et al. 2008). Nonetheless, cortical qRT-PCR demonstrated no significant difference in *Chrm4* expression across the genotypes.

5.3.2.5. *Snx27*

Snx27 expression was investigated in light of its localization to endosomes and influence on Aβ production, which is relevant to the exacerbation of amyloidosis by trisomy 21 in Tc1;J20 mice. In both hippocampal RNA-seq and cortical qRT-PCR there was no significant influence of trisomy 21 or APP/Aβ overexpression on *Snx27* expression, suggesting that altered transcriptional regulation of *Snx27* is not a factor contributing to the exacerbation of amyloidosis. To confirm this, future work needs to be carried out investigating changes in Snx27 protein expression levels.

5.3.3. Discordance between hippocampal and cortical RNA expression

None of the significant results obtained from hippocampal RNA-seq, indicating a downregulation of candidate genes in trisomy, was successfully replicated in cortical qRT-PCR, including *Chrm4* which is expressed at similar levels across both tissue types. While cross-platform differences could be a source of variability, qRT-PCRs have been routinely used to verify RNA-seq results for single genes and have demonstrated a strong concordance with RNA-seq and microarray data (C. Wang et al. 2014; Su et al. 2014). Care was also taken to ensure that qPCR probe designed included all transcript variants produced which would be captured in the RNA-seq results. All Taqman expression assays purchased for qRT-PCR were verified to cover all transcript variants as described in RefSeq (Pruitt et al. 2014). All genes verified by qRT-PCR also demonstrated strong expression levels in RNA-seq, with a minimum average read count of 118.67 (observed in *Fos* expression in Tc1). Discordance in results between qRT-PCR and RNA-seq would therefore unlikely be due to probe bias or issues of low sensitivity. The use of housekeeping genes *Actb* and *Gapdh* was also suitable due to their highly non-significant fold changes in expression between the genotypes, further normalized to their geometric mean for increased reliability (Vandesompele et al. 2002).

Aside from these technical differences, the discordance between hippocampal and cortical results could be due to complex differences between cortical and hippocampal gene regulation and function, which is also beginning to be comprehensively illustrated using RNA-seq techniques. A recent study performed large-scale single-cell RNA-seq on mouse somatosensory cortex (S1) and hippocampal CA1 regions, both of which are included in our dissections for cortical and hippocampal tissue (Zeisel et al. 2015). Although both S1 and CA1 contained interneurons of almost every subclass, showing a

close transcriptional relationship in terms of interneurons, pyramidal neurons from the S1 and CA1 region were molecularly distinct subclasses. In addition, the S1 reflected a general increase in gene expression across non-neuronal molecular subtypes compared to the CA1. Perhaps this results in a transcriptional landscape in S1 that is more heterogeneous than that for CA1, which may by extension possibly dilute effects of Tc1xJ20 genotype on gene expression. Thus this may partially account for the high variability in cortical qRT-PCR, which is further increased by any potential differences in proportions of mosaic cells.

The closer study of brain region-specific transcriptomes in SAD has also demonstrated how gene regulation may vary between tissue types, and yield insights into pathogenesis. RNA-seq using human temporal pole tissue has been successfully performed to identify not only gene expression, but splicing and methylation differences, in sequences surrounding loci associated with late-onset AD (Humphries et al. 2015). In a separate study on frontal and temporal lobes, aberrant splicing and differential promoter use was discovered in tissue from AD patients compared to control, altering the expression of genes including *APOE*, the most established risk factor for late-onset AD (Twine et al. 2011). These studies also highlight the added value of RNA-seq in identifying differences in epigenetic regulation as potential mechanisms underlying AD pathogenesis. In addition, an RNA-seq study of parietal cortex in AD has pointed out lipid metabolism as a functional difference in this region, with a transcriptome profile distinct from other regions such as the frontal and temporal lobes (Mills et al. 2013). In DS, however, RNA-seq has only been published in a study using human trisomic endothelial progenitor cells (Costa et al. 2011), and none in brain tissue. Our results above have suggested that strong effects of trisomy 21 in the downregulation of hippocampal genes may be a phenotype specific to this region, hence further validation with hippocampal qRT-PCR, as well as cortical RNA-seq, could be considered to illustrate how trisomy 21 and APP/Aβ overexpression may differentially influence hippocampal and cortical gene expression.

5.3.4. Future work

This RNA-seq project has yielded a library illustrating a snapshot of all RNA transcripts expressed in the hippocampus of 3-month old Tc1xJ20 mice. As mentioned in the introduction to this chapter, further statistical analysis needs to be undertaken to examine any interaction effects between trisomy 21 and APP/Aβ overexpression on

gene expression levels, to understand how trisomy 21 may augment or buffer against effects exerted by APP/Aβ overexpression.

Analysis of changes in splicing patterns and proportions of gene isoforms expressed in this dataset will also be intriguing, as presence of the extra Hsa21 chromosome has been shown to alter gene regulation in multiple ways. Hsa21 encodes microRNAs (Gribble et al. 2013) and genes involved in post-translational histone modification (Dekker et al. 2014), which regulate gene expression via different mechanisms. Histone methylation correlates strongly with genome-wide domains of dysregulated gene expression in DS, which are conserved between humans and the orthologous regions in Ts65Dn (Letourneau et al. 2014); in Tc1, the rearrangement of the chromosome may hence exert an effect on this form of epigenetic regulation. Studying Tc1xJ20 mice would allow comparisons of how splice patterns altered by *APP* overexpression are modified by trisomy 21, further offering avenues for further investigation into functional effects. It may also be useful to check if trisomy 21 influences the splicing of the *APP* transgene itself, since the J20 transgene was designed to express all three *APP* splice isoforms (Mucke et al. 2000).

Finally, the above analyses performed using RNA-seq could be replicated for Tc1xJ20 mice at older time points, to trace changes in the transcriptome prior to plaque deposition (3 months), at the start of plaque deposition (6 months for instance), and at late stages of disease (12-16 months). This will contribute to identifying age-dependent transcriptional changes which may be more relevant to AD, since age remains its highest risk factor (Bush and Beail 2004). It may also identify transcriptional markers of accelerated aging in DS, which has been characterized as a syndrome of accelerated aging both in clinical (Zigman 2013; Lott 2012) and epigenetic terms (Horvath et al. 2015).

Chapter 6. Discussion

The work in this thesis has explored using different approaches – *in vitro*, *ex vivo* and *in silico* – to study how trisomy 21 and APP/Aβ overexpression may interact to influence AD phenotypes, using a novel mouse model of AD-DS. Previous work by the group had shown that trisomy 21 from Tc1 mice was sufficient to exacerbate mortality, cognitive deficits and Aβ deposition, associated with APP/Aβ overexpression in J20 mice. As the Tc1 mouse is not functionally trisomic for *APP*, this demonstrated that trisomy of Hsa21 genes, apart from *APP*, modulates Aβ accumulation and its associated deficits. As attention in the group focused on characterising mechanisms underlying the exacerbation of Aβ accumulation by trisomy 21, this project sought to complement their efforts by 1) developing methods to characterise phenotypes *in vitro* from candidate genes on Hsa21, and 2) exploring other functional consequences relating to exacerbated Aβ accumulation by trisomy 21, specifically changes in glial morphology and hippocampal RNA expression.

6.1. *In vitro* modelling of APP/Aβ phenotypes influenced by trisomy 21

Chapter 3 described the development of a primary cortical cell model, with the aim of evaluating the role of candidate genes on Hsa21 that may influence Aβ accumulation. As we were interested in how trisomy 21 may modulate amyloidosis at early stages of pathogenesis, we compared APP and Aβ phenotypes in this cell model to results obtained from 3-month old progeny of Tc1xJ20 crosses, where J20 and Tc1;J20 mice demonstrate cognitive deficits (Figure 1.9Figure 1.10) but not plaque deposition (Wright et al. 2013). Unfortunately, primary cortical cells did not replicate the effects of trisomy 21 in increasing total APP and CTF production, or reducing soluble Aβ38 and Aβ40, which were observed using cortical and hippocampal tissue from 3-month old mice. This was due in part to wide variability in the APP/Aβ results obtained from primary cells.

As mosaicism precluded the ability to characterise single cell phenotypes in our model, due to uncertainty over whether specific cells in a Tc1-positive culture had retained the Hsa21 chromosome, APP/Aβ phenotypes in Tc1xJ20 primary culture could only be studied across all cells in an entire culture population. This posed a significant limitation to the characterization of neuronal mechanisms that could be altered by trisomy 21. Furthermore, neurons accounted for less than 20% of cells in each culture, further complicating the interpretation of phenotypes relating to APP/Aβ overexpression by a

transgene driven by a neuron-specific promoter. Therefore, the techniques learned during the development of this primary culture protocol should be taken forward for use in non-mosaic DS mouse models, which would allow the characterization of single neurons in culture. Using these models would also allow the exploration of culture methods that would reduce glial proliferation, such as by co-culturing neurons with astrocyte feeder layers previously prepared.

To overcome the problems mosaicism causes, cancer biology is a field of study that could be followed for developments in investigating and managing this phenotype. Neoplasia is associated with genetic instability and the presence of somatic mosaicism in tumours, which most commonly manifests as aneuploidy (Davidsson 2014). In trying to understand whether aneuploidy is a driver or a result of uncontrolled cancer growth, studies are underway investigating the epigenetic effects of aneuploidy in cancer, and methods to distinguish and characterise the heterogenous mixture of cell genomes present in tumours (Baslan et al. 2015; Davidsson 2014). While it currently is not possible to sort live mosaic cells viably for separate study, these developments may in future enhance the use of Tc1 mice by studying differential effects on the presence and absence of trisomy 21 on cells in the same animal. Managing issues of mosaicism will also be a challenge in the use of the emerging genome editing tool CRISPR/Cas9, which often results in mosaicism following microinjection of *Cas9* into zygotes during a period of active replication (Ablain et al. 2015; Singh et al. 2014). The benefits of separating trisomic and non-trisomic cells from within the same organism was demonstrated in the generation of isogenic induced pluripotent stem cell lines from fibroblasts of an adult with mosaic DS (Murray et al. 2015). Therefore, while the characterization of neuronal phenotypes in primary cultures should now be taken forward to non-mosaic models, the *in vitro* study of how trisomy 21 in Tc1 influences neuronal phenotypes can be revisited following developments in sorting mosaic cells.

6.2. Investigate cytoplasmic vesicular phenotypes

Our RNA-seq data comparing differentially expressed genes between Tc1xJ20 progeny genotype pairs has suggested that trisomy 21 alters the transcriptional regulation of genes associated with cytoplasmic vesicles in the hippocampus of 3-month old Tc1 compared to Wt, and Tc1;J20 compared to J20. This is in line with emerging immunohistochemical evidence from the group suggesting that altered APP processing observed in progeny of Tc1xJ20 may be an outcome of altered APP trafficking through the endo-lysosomal system while it is proteolytically cleaved.

As discussed in Chapter 5, Tc1 mice are not functionally trisomic for Hsa21 genes, such as *APP, SYNJ1, RCAN1* and *ITSN1,* which have been previously implicated in endosomal alterations when overexpressed(Gribble et al. 2013; Cossec et al. 2012; Chang and Min 2009; Salehi et al. 2006). Therefore, any endosomal alteration in Tc1;J20 compared to J20, and Tc1 compared to Wt, may be due to previously unassessed candidate genes. To functionally characterize vesicular trafficking, methods for the live cell imaging of APP transport in primary neurons have been well-established (Buggia-Prévot et al. 2014; Steuble et al. 2012; Bhalla et al. 2012; Tampellini and Gouras 2011). However, this involves the characterisation of individual neurons, which renders the use of Tc1 cultures problematic due to mosaicism. Therefore, to assess the influence of potential candidate genes in phenotypes of individual neurons using the Tc1xJ20 cross, we may need to overexpress candidate Hsa21 genes in Wt and J20 neurons, with the caveat that overexpression levels may not reflect expression levels in trisomy 21.

6.3. Emerging focus on neuroinflammation in trisomy 21 in AD-DS

In Chapter 4, we began development of a digital protocol to analyse immunohistochemical sections, identify glial cell bodies and processes, and quantify morphological dimensions that may yield insight into how glial reactivity alters with genotype and age. This was sensitive in identifying microglial cells, but required further improvements for astrocytes, to correct false results generated by variable background staining. While broad analysis of glial morphological measurements across the hippocampus suggested that APP/Aβ overexpression and age are stronger factors in influencing phenotypic changes than any potential effects of trisomy 21, this is in line with the observation that DS presents with chronic, low-level neuroinflammation and oxidative stress throughout life (Wilcock and Griffin 2013; Perluigi and Butterfield 2012), which may accelerate AD pathogenesis but not manifest as striking phenotypes. For instance, while this result is preliminary, the increase in S100β protein expression by APP/Aβ overexpression in hippocampal homogenate at 3 months suggested an interaction effect between astrogliosis and APP/Aβ production. Our analysis protocol could therefore be adapted for astrocytes identified with S100β to understand how the upregulation of S100β expression manifests morphologically. To contribute to teasing out functional differences based on morphology, future work could focus on assigning combinations of morphological parameters to classify glial cells into morphological subtypes currently used to ascribe glial reactive states.

There is also much further scope for functionally characterizing glial cells in DS mouse models – only three studies have investigated functional characteristics of primary astrocytes in Ts65Dn (Ballestín et al. 2014; Sahir et al. 2006; Bambrick et al. 2003), while no studies of primary microglia have been undertaken. Indeed, work using human astrocytes has offered interesting insights. For example, primary astrocytes from DS fetal cortical tissue displayed morphologically fragmented mitochondria, and functionally appeared to be dampened as a protective response against damage caused by the excessive generation of reactive oxygen species (Helguera et al. 2013). However, DS fetal cortical astrocytes also appeared to be more protective than euploid astrocytes against hydrogen peroxide-induced oxidative damage, indicating a greater antioxidant capacity (Sebastià et al. 2004). These studies could be taken further using primary astrocyte cultures from DS mouse models trisomic for different Hsa21 orthologous regions, to allow us to understand which genes may influence whether chronic neuroinflammation in DS results in protective or damaging responses.

6.4. Discordant phenotypes between cortex and hippocampus

Despite the high levels of PDGF-β-driven expression of *APP* from the J20 transgene array in cortical and hippocampal neurons, and correspondingly exacerbated plaque deposition in both tissues, our RNA-seq and glial immunohistochemistry results have demonstrated that results in one tissue cannot simply be generalized to the other. This is reflected in the poor recapitulation of hippocampal RNA-seq differential gene expression in cortical tissue, as well as differences in the observable density of astrocytes and microglia stained with GFAP and Iba1. This may reflect a much greater heterogeneity in cortical compared to hippocampal composition (Zeisel et al. 2015). By extension, the use of cortical tissue for primary neuronal culture may therefore have contributed to the variability in results, and future studies should employ hippocampal tissues instead.

6.5. The value of DS mouse models in future AD-DS research

Individuals with DS develop the most common genetic form of AD, largely due to the expression of three *APP* copies (Ness et al. 2012), but the variation in presentation of AD-DS, despite universal early AD neuropathology, indicates that other genetic and environmental factors modulate AD-DS pathogenesis. This has spurred rapidly increasing momentum in the AD-DS field, including multicentre longitudinal studies across a battery of AD-DS biomarkers in people with DS (Rafii et al. 2015; Dekker et al.

2015; Schupf et al. 2015), and the development of induced pluripotent stem cells for DS (Chang et al. 2015; Murray et al. 2015; Shi et al. 2012), which provide for the first time a trisomic *in vitro* model that recapitulates AD pathology.

However, the greatest strength of DS mouse models remains the ability to generate hypotheses by mapping phenotypes to critical genomic regions. This includes potentially dosage-sensitive non-coding regions, such as the 29 microRNAs encoded on Hsa21 (MirBase release 21, Griffiths-Jones 2004), which are increasingly studied in AD pathogenesis due to their regulation of molecular pathways associated with AD (Veerappan et al. 2013). Despite its drawbacks relating to mosaicism and chromosomal structural rearrangements (Gribble et al. 2013), the Tc1 mouse remains the only DS mouse model carrying a human chromosome, which may model uniquely human aspects of gene expression, including the diversity of RNA expression (Lin et al. 2014) and regulatory behaviour in transcription factor binding (Y. Cheng et al. 2014). The Tc1xJ20 cross has also been the first model to demonstrate that trisomy 21 apart from *APP* exacerbates AD pathology, and future work could employ the series of segmentally trisomic DS mouse models to narrow down regions on Hsa21 that similarly exacerbate, or protect against, this effect. Much of this project has focused on developing methods to complement the *in vivo* characterization of neuronal APP/Aβ phenotypes in Tc1xJ20, and it is hoped that they can be built on and applied to future work employing crosses between DS and AD mouse models.

Ultimately, this research must relate back from mouse to human tissues and integrate with the study of human induced pluripotent stem cells and histopathological and other samples. However, the mouse gives us a uniquely tractable system for finding phenotypes and dissecting the underlying molecular pathways. This study is one of the first to work with mice to model AD-DS and has been informative for future routes to analysing this disorder – which has relevance for both the Down syndrome population and the euploid population at risk for Alzheimer's disease.

Supplementary Tables

Supplementary Table 1 Differential gene expression identified between 3-month Tc1;J20 and J20 mice following RNA-seq of hippocampal tissue

Genes downregulated in Tc1;J20 compared to J20						
Ensembl ID	**Gene name**	**Adjusted p-value**	**J20 avg read counts**	**Tc1;J20 avg read counts**	**Ratio Tc1;J20 / J20**	**Chromosome (Mmu)**
ENSMUSG00000021250	Fos	0.002	531.33	118.67	0.22	12
ENSMUSG00000022602	Arc	0.008	3542.67	1405.67	0.40	15
ENSMUSG00000024190	Dusp1	0.000	792.67	399.67	0.50	17
ENSMUSG00000020423	Btg2	0.010	699.33	357.33	0.51	1
ENSMUSG00000063953	Amd2	0.030	162.33	88.00	0.54	10
ENSMUSG00000053279	Aldh1a1	0.000	1975.00	1080.67	0.55	19
ENSMUSG00000028195	Cyr61	0.020	212.33	117.00	0.55	3
ENSMUSG00000052837	Junb	0.013	1318.33	816.00	0.62	8
ENSMUSG00000035355	Kcnh4	0.041	289.67	191.33	0.66	11
ENSMUSG00000046962	Zfp295	0.023	795.67	594.67	0.75	16
ENSMUSG00000074923	Pak6	0.000	3215.00	2458.67	0.76	2
ENSMUSG00000042104	Uggt2	0.001	3824.33	2948.67	0.77	14
ENSMUSG00000027895	Kcnc4	0.015	2641.33	2040.00	0.77	3
ENSMUSG00000064125	BC068157	0.017	1717.00	1350.00	0.79	8
ENSMUSG00000028698	Pik3r3	0.020	2104.67	1677.00	0.80	4
ENSMUSG00000037362	Nov	0.004	7640.67	6130.67	0.80	15
ENSMUSG00000032503	Arpp21	0.048	10678.33	8723.33	0.82	9
Genes upregulated in Tc1;J20 compared to J20						
Ensembl ID	**Gene name**	**Adjusted p-value**	**J20 avg read counts**	**Tc1;J20 avg read counts**	**Ratio Tc1;J20 / J20**	**Chromosome (Mmu)**
ENSMUSG00000029772	Ahcyl2	0.017	10660.67	13593.67	1.28	6
ENSMUSG00000034674	Tdg	0.031	1185.33	1589.33	1.34	10
ENSMUSG00000032554	Trf	0.000	9384.33	12909.67	1.38	9
ENSMUSG00000019935	Slc17a8	0.003	318.67	506.67	1.59	10
ENSMUSG00000018339	Gpx3	0.007	226.67	379.00	1.67	11
ENSMUSG00000054889	Dsp	0.014	1027.00	1753.67	1.71	13
ENSMUSG00000072774	Zfp951	0.001	45.33	118.67	2.62	5
ENSMUSG00000050063	Klk6	0.000	43.00	124.33	2.89	7
ENSMUSG00000021337	Scgn	0.004	28.00	86.67	3.10	13
ENSMUSG00000058626	Capn11	0.019	11.33	53.00	4.68	17
ENSMUSG00000056436	Cyct	0.020	0.00	10.67	NA	2

Supplementary Table 2 Differential gene expression identified between 3-month Tc1 and Wt mice following RNA-seq of hippocampal tissue

Genes downregulated in Tc1 compared to Wt						
Ensembl ID	**Gene name**	**Adjusted p-value**	**Wt avg read counts**	**Tc1 avg read counts**	**Ratio Tc1 / Wt**	**Chromosome (Mmu)**
ENSMUSG00000021250	Fos	0.00001	520.00	119.33	0.23	12
ENSMUSG00000000303	Cdh1	0.004	61.33	14.67	0.24	8
ENSMUSG00000069372	Ctxn3	0.03	76.00	24.33	0.32	18
ENSMUSG00000004885	Crabp2	0.01	90.33	29.00	0.32	3
ENSMUSG00000024650	Slc22a6	0.00	282.33	91.00	0.32	19
ENSMUSG00000040310	Alx4	0.04	66.33	22.00	0.33	2
ENSMUSG00000037868	Egr2	0.04	74.00	26.00	0.35	10
ENSMUSG00000024190	Dusp1	0.00	643.67	276.33	0.43	17
ENSMUSG00000005087	Cd44	0.01	175.67	81.67	0.46	2
ENSMUSG00000020423	Btg2	0.00	645.67	315.67	0.49	1
ENSMUSG00000028364	Tnc	0.02	383.00	192.33	0.50	4
ENSMUSG00000038418	Egr1	0.02	2827.67	1523.33	0.54	18
ENSMUSG00000053279	Aldh1a1	0.01	1830.33	997.67	0.55	19
ENSMUSG00000020241	Col6a2	0.01	946.67	521.00	0.55	10
ENSMUSG00000092035	Peg10	0.00	529.00	294.33	0.56	6
ENSMUSG00000030270	Cpne9	0.00	744.33	417.33	0.56	6
ENSMUSG00000040701	Ap1g2	0.02	565.67	340.67	0.60	14
ENSMUSG00000040495	Chrm4	0.01	536.00	327.67	0.61	2
ENSMUSG00000021453	Gadd45g	0.04	555.00	344.67	0.62	13
ENSMUSG00000000184	Ccnd2	0.01	2479.00	1561.67	0.63	6
ENSMUSG00000005774	Rfx5	0.01	848.67	536.00	0.63	3
ENSMUSG00000000142	Axin2	0.01	976.67	619.67	0.63	11
ENSMUSG00000071341	Egr4	0.03	547.33	351.67	0.64	6
ENSMUSG00000044037	Als2cl	0.01	701.67	452.33	0.64	9
ENSMUSG00000018476	Kdm6b	0.00	1962.67	1271.67	0.65	11
ENSMUSG00000074575	Kcng1	0.03	709.33	464.00	0.65	2
ENSMUSG00000018537	Pcgf2	0.00	1299.00	850.33	0.65	11
ENSMUSG00000034771	Tle2	0.00	1762.00	1169.67	0.66	10
ENSMUSG00000035835	BC005764	0.00	1584.67	1068.33	0.67	10
ENSMUSG00000002871	Tpra1	0.02	1295.33	913.67	0.71	6
ENSMUSG00000020893	Per1	0.00	3568.00	2537.33	0.71	11
ENSMUSG00000047945	Marcksl1	0.03	1928.67	1384.00	0.72	4
ENSMUSG00000025145	Lrrc45	0.02	3114.00	2295.67	0.74	11
ENSMUSG00000028137	Celf3	0.01	7910.67	5938.67	0.75	3
Genes upregulated in Tc1 compared to Wt						
Ensembl ID	**Gene name**	**Adjusted p-value**	**Wt avg read counts**	**Tc1 avg read counts**	**Ratio Tc1 / Wt**	**Chromosome (Mmu)**
ENSMUSG00000049313	Sorl1	0.03	12720.67	13747.33	1.08	9
ENSMUSG00000028249	Sdcbp	0.02	7756.00	8406.00	1.08	4
ENSMUSG00000031618	Nr3c2	0.02	3842.67	4179.33	1.09	8

ENSMUSG00000029657	Hsph1	0.01	10168.33	11094.67	1.09	5
ENSMUSG00000045733	Sprn	0.03	4712.33	5141.67	1.09	7
ENSMUSG00000023913	Pla2g7	0.01	5825.67	6375.00	1.09	17
ENSMUSG00000022761	Lztr1	0.02	7928.33	8684.67	1.10	16
ENSMUSG00000030729	Pgm2l1	0.01	10616.67	11708.33	1.10	7
ENSMUSG00000037111	Setd7	0.02	5428.67	5989.00	1.10	3
ENSMUSG00000024873	Cnih2	0.03	10206.33	11268.33	1.10	19
ENSMUSG00000026787	Gad2	0.01	4936.33	5467.67	1.11	2
ENSMUSG00000035547	Capn5	0.03	2430.00	2698.00	1.11	7
ENSMUSG00000052087	Rgs14	0.01	4518.33	5041.33	1.12	13
ENSMUSG00000050711	Scg2	0.01	3622.67	4056.67	1.12	1
ENSMUSG00000050321	Neto1	0.00	3754.00	4242.33	1.13	18
ENSMUSG00000058897	Col25a1	0.02	2964.33	3352.33	1.13	3
ENSMUSG00000018322	Tomm34	0.00	3015.33	3438.67	1.14	2
ENSMUSG00000030209	Grin2b	0.00	3448.67	3940.67	1.14	6
ENSMUSG00000005360	Slc1a3	0.00	15408.33	17631.67	1.14	15
ENSMUSG00000028648	Ndufs5	0.01	1504.67	1746.00	1.16	4
ENSMUSG00000030226	Lmo3	0.00	2306.00	2677.67	1.16	6
ENSMUSG00000063297	Luzp2	0.00	4317.67	5060.00	1.17	7
ENSMUSG00000039470	Zdhhc2	0.04	1567.00	1852.67	1.18	8
ENSMUSG00000021613	Hapln1	0.02	755.33	904.67	1.20	13
ENSMUSG00000030772	Dkk3	0.00	9916.33	11977.67	1.21	7
ENSMUSG00000055540	Epha6	0.02	2687.00	3325.33	1.24	16
ENSMUSG00000059991	Nptx2	0.02	594.33	738.00	1.24	5
ENSMUSG00000059325	Hopx	0.00	1499.67	1864.33	1.24	5
ENSMUSG00000020635	Fkbp1b	0.01	803.33	1007.67	1.25	12
ENSMUSG00000048070	Pirt	0.01	36.00	85.33	2.37	11

Supplementary Table 3 Differential gene expression identified between 3-month J20 and Wt mice following RNA-seq of hippocampal tissue

Genes downregulated in J20 compared to Wt						
Ensembl ID	**Gene name**	**Adjusted p-value**	**Wt avg read counts**	**J20 avg read counts**	**Ratio J20 / Wt**	**Chromosome (Mmu)**
ENSMUSG00000028971	Cort	0.0002	142.67	66.33	0.46495327	4
ENSMUSG00000028011	Tdo2	0.01	294.00	139.67	0.47505669	3
ENSMUSG00000054889	Dsp	0.0002	1963.33	1027.00	0.52308998	13
ENSMUSG00000036915	Kirrel2	0.01	340.00	232.33	0.68333333	7
ENSMUSG00000041828	Abca8a	0.002	935.00	697.33	0.74581105	11
ENSMUSG00000049892	Rasd1	0.00002	692.67	524.00	0.75649663	11
ENSMUSG00000030592	Ryr1	0.001	2674.67	2333.67	0.87250748	7
ENSMUSG00000033327	Tnxb	0.002	1297.00	1159.00	0.89360062	17
ENSMUSG00000013523	Bcas1	0.00002	4017.33	3593.00	0.89437438	2
ENSMUSG00000040998	Npnt	0.01	920.00	829.33	0.90144928	3

ENSMUSG00000035456	Prdm8	0.01	1893.00	1730.00	0.91389329	5
ENSMUSG00000025348	Itga7	0.01	1478.33	1394.33	0.94317926	10
ENSMUSG00000032554	Trf	0.01	9554.00	9384.33	0.9822413	9
Genes upregulated in J20 compared to Wt						
Ensembl ID	**Gene name**	**Adjusted p-value**	**Wt avg read counts**	**J20 avg read counts**	**Ratio J20 / Wt**	**Chromosome (Mmu)**
ENSMUSG00000040136	Abcc8	0.03	2406.67	2433.00	1.01094183	7
ENSMUSG00000049281	Scn3b	0.04	7120.67	7422.00	1.04231814	9
ENSMUSG00000037362	Nov	0.0005	4369.67	7640.67	1.74856968	15
ENSMUSG00000035431	Sstr1	0.01	671.33	1239.67	1.84657398	12
ENSMUSG00000019929	Dcn	0.000001	2918.67	5509.00	1.88750571	10
ENSMUSG00000025572	Tmc6	0.0003	375.33	956.33	2.54795737	11
ENSMUSG00000021478	Drd1a	0.03	139.67	388.00	2.77804296	13
ENSMUSG00000001119	Col6a1	0.04	3512.67	9934.33	2.82814576	10

Supplementary Table 4 Functional Annotation Clustering by DAVID for significantly differentially expressed genes between Tc1;J20 and J20 (14 out of 28 genes not included in clustering)

Annotation Cluster 1	Enrichment Score: 1.5205695350095656											
Category	Term	Count	%	PValue	Genes	List Total	Pop Hits	Pop Total	Fold Enrichment	Bonferroni	Benjamini	FDR
GOTERM_CC_FAT	GO:0031410~cytoplasmic vesicle	5	18.52	0.00	SLC17A8, SCGN, ARC, CAPN11, TRF	16	508	12504	7.69	0.19	0.19	2.70
GOTERM_CC_FAT	GO:0031982~vesicle	5	18.52	0.00	SLC17A8, SCGN, ARC, CAPN11, TRF	16	519	12504	7.53	0.20	0.11	2.91
SP_PIR_KEYWORDS	cytoplasmic vesicle	4	14.81	0.00	SLC17A8, SCGN, ARC, CAPN11	24	232	17854	12.83	0.28	0.28	3.47
GOTERM_CC_FAT	GO:0016023~cytoplasmic membrane-bounded vesicle	4	14.81	0.01	SLC17A8, ARC, CAPN11, TRF	16	414	12504	7.55	0.63	0.28	12.22
GOTERM_CC_FAT	GO:0031988~membrane-bounded vesicle	4	14.81	0.01	SLC17A8, ARC, CAPN11, TRF	16	420	12504	7.44	0.64	0.23	12.68
GOTERM_CC_FAT	GO:0030054~cell junction	3	11.11	0.11	SLC17A8, ARC, DSP	16	470	12504	4.99	1.00	0.78	70.07
GOTERM_CC_FAT	GO:0044459~plasma membrane part	5	18.52	0.12	SLC17A8, SCGN, ARC, KCNC4, DSP	16	1633	12504	2.39	1.00	0.77	74.87
GOTERM_CC_FAT	GO:0005886~plasma membrane	5	18.52	0.47	SLC17A8, SCGN, ARC, KCNC4, DSP	16	2906	12504	1.34	1.00	0.99	99.89
SP_PIR_KEYWORDS	membrane	5	18.52	0.95	SLC17A8, SCGN, ARC, KCNC4, KCNH4	24	5507	17854	0.68	1.00	1.00	100.00
Annotation Cluster 2	Enrichment Score: 0.9395554594932174											
Category	Term	Count	%	PValue	Genes	List Total	Pop Hits	Pop Total	Fold Enrichment	Bonferroni	Benjamini	FDR
GOTERM_BP_FAT	GO:0001701~in utero embryonic development	3	11.11	0.07	JUNB, CYR61, AMD2	23	267	13588	6.64	1.00	0.95	60.41
GOTERM_BP_FAT	GO:0043009~chordate embryonic development	3	11.11	0.15	JUNB, CYR61, AMD2	23	421	13588	4.21	1.00	0.99	87.50
GOTERM_BP_FAT	GO:0009792~embryonic development ending in birth or egg hatching	3	11.11	0.15	JUNB, CYR61, AMD2	23	425	13588	4.17	1.00	0.98	87.92
Annotation Cluster 3	Enrichment Score: 0.823826763165674											
Category	Term	Count	%	PValue	Genes	List Total	Pop Hits	Pop Total	Fold Enrichment	Bonferroni	Benjamini	FDR
GOTERM_CC_FAT	GO:0031410~cytoplasmic vesicle	5	18.52	0.00	SLC17A8, SCGN, ARC, CAPN11, TRF	16	508	12504	7.69	0.19	0.19	2.70
GOTERM_CC_	GO:0031982~vesicle	5	18.	0.00	SLC17A8, SCGN, ARC, CAPN11, TRF	16	519	12504	7.53	0.20	0.11	2.91

FAT			52									
GOTERM_MF_FAT	GO:0046872~metal ion binding	7	25.93	0.65	SLC17A8, SCGN, KCNC4, CAPN11, CYCT, ZFP295, TRF	23	3850	13288	1.05	1.00	1.00	100.00
GOTERM_MF_FAT	GO:0043169~cation binding	7	25.93	0.66	SLC17A8, SCGN, KCNC4, CAPN11, CYCT, ZFP295, TRF	23	3885	13288	1.04	1.00	1.00	100.00
GOTERM_MF_FAT	GO:0043167~ion binding	7	25.93	0.67	SLC17A8, SCGN, KCNC4, CAPN11, CYCT, ZFP295, TRF	23	3934	13288	1.03	1.00	1.00	100.00
SP_PIR_KEYWORDS	metal-binding	3	11.11	0.88	CYCT, ZFP295, TRF	24	2682	17854	0.83	1.00	1.00	100.00
GOTERM_MF_FAT	GO:0046914~transition metal ion binding	3	11.11	0.95	CYCT, ZFP295, TRF	23	2608	13288	0.66	1.00	1.00	100.00
Annotation Cluster 4	Enrichment Score: 0.6491479259755761											
Category	Term	Count	%	PValue	Genes	List Total	Pop Hits	Pop Total	Fold Enrichment	Bonferroni	Benjamini	FDR
SP_PIR_KEYWORDS	ion transport	4	14.81	0.03	SLC17A8, KCNC4, KCNH4, TRF	24	543	17854	5.48	0.96	0.80	30.02
GOTERM_BP_FAT	GO:0030001~metal ion transport	4	14.81	0.03	SLC17A8, KCNC4, KCNH4, TRF	23	442	13588	5.35	1.00	0.99	35.64
GOTERM_BP_FAT	GO:0006812~cation transport	4	14.81	0.05	SLC17A8, KCNC4, KCNH4, TRF	23	515	13588	4.59	1.00	0.96	47.90
GOTERM_MF_FAT	GO:0046873~metal ion transmembrane transporter activity	3	11.11	0.08	KCNC4, KCNH4, TRF	23	290	13288	5.98	1.00	1.00	62.14
GOTERM_BP_FAT	GO:0015672~monovalent inorganic cation transport	3	11.11	0.09	SLC17A8, KCNC4, KCNH4	23	303	13588	5.85	1.00	0.96	68.76
GOTERM_BP_FAT	GO:0006811~ion transport	4	14.81	0.11	SLC17A8, KCNC4, KCNH4, TRF	23	712	13588	3.32	1.00	0.97	76.55
SP_PIR_KEYWORDS	transport	5	18.52	0.14	SLC17A8, KCNC4, CYCT, KCNH4, TRF	24	1571	17854	2.37	1.00	0.95	81.01
UP_SEQ_FEATURE	glycosylation site:N-linked (GlcNAc...)	4	14.81	0.84	NOV, SLC17A8, KCNC4, TRF	21	3444	16021	0.89	1.00	1.00	100.00
SP_PIR_KEYWORDS	glycoprotein	4	14.81	0.87	NOV, SLC17A8, KCNC4, TRF	24	3600	17854	0.83	1.00	1.00	100.00
SP_PIR_KEYWORDS	membrane	5	18.52	0.95	SLC17A8, SCGN, ARC, KCNC4, KCNH4	24	5507	17854	0.68	1.00	1.00	100.00
SP_PIR_KEYWORDS	transmembrane	3	11.11	1.00	SLC17A8, KCNC4, KCNH4	24	5237	17854	0.43	1.00	1.00	100.00
GOTERM_CC_FAT	GO:0016021~integral to membrane	3	11.11	1.00	SLC17A8, KCNC4, KCNH4	16	5709	12504	0.41	1.00	1.00	100.00
GOTERM_CC_FAT	GO:0031224~intrinsic to membrane	3	11.11	1.00	SLC17A8, KCNC4, KCNH4	16	5914	12504	0.40	1.00	1.00	100.00
Annotation	Enrichment Score: 0.46193983998995747											

Cluster 5												
Category	Term	Count	%	PValue	Genes	List Total	Pop Hits	Pop Total	Fold Enrichment	Bonferroni	Benjamini	FDR
GOTERM_CC_FAT	GO:0005576~extracellular region	6	22.22	0.04	NOV, KLK6, SCGN, GPX3, TRF, CYR61	16	1680	12504	2.79	0.96	0.49	35.84
SP_PIR_KEYWORDS	Secreted	5	18.52	0.11	NOV, SCGN, GPX3, TRF, CYR61	24	1420	17854	2.62	1.00	0.98	71.00
UP_SEQ_FEATURE	signal peptide	4	14.81	0.74	NOV, GPX3, TRF, CYR61	21	2963	16021	1.03	1.00	1.00	100.00
SP_PIR_KEYWORDS	signal	4	14.81	0.76	NOV, GPX3, TRF, CYR61	24	2970	17854	1.00	1.00	1.00	100.00
UP_SEQ_FEATURE	disulfide bond	3	11.11	0.82	NOV, TRF, CYR61	21	2379	16021	0.96	1.00	1.00	100.00
SP_PIR_KEYWORDS	disulfide bond	3	11.11	0.85	NOV, TRF, CYR61	24	2469	17854	0.90	1.00	1.00	100.00
Annotation Cluster 6	Enrichment Score: 0.39114241255156623											
Category	Term	Count	%	PValue	Genes	List Total	Pop Hits	Pop Total	Fold Enrichment	Bonferroni	Benjamini	FDR
GOTERM_CC_FAT	GO:0070013~intracellular organelle lumen	3	11.11	0.40	FOS, CYCT, TDG	16	1133	12504	2.07	1.00	0.99	99.56
GOTERM_CC_FAT	GO:0043233~organelle lumen	3	11.11	0.40	FOS, CYCT, TDG	16	1136	12504	2.06	1.00	0.99	99.57
GOTERM_CC_FAT	GO:0031974~membrane-enclosed lumen	3	11.11	0.42	FOS, CYCT, TDG	16	1174	12504	2.00	1.00	0.99	99.68
Annotation Cluster 7	Enrichment Score: 0.147153733319145											
Category	Term	Count	%	PValue	Genes	List Total	Pop Hits	Pop Total	Fold Enrichment	Bonferroni	Benjamini	FDR
GOTERM_BP_FAT	GO:0006355~regulation of transcription, DNA-dependent	3	11.11	0.70	FOS, JUNB, KCNH4	23	1465	13588	1.21	1.00	1.00	100.00
GOTERM_BP_FAT	GO:0051252~regulation of RNA metabolic process	3	11.11	0.71	FOS, JUNB, KCNH4	23	1488	13588	1.19	1.00	1.00	100.00
GOTERM_BP_FAT	GO:0045449~regulation of transcription	4	14.81	0.72	FOS, BTG2, JUNB, KCNH4	23	2227	13588	1.06	1.00	1.00	100.00

Supplementary Table 5 Functional Annotation Clustering by DAVID for differentially expressed genes between Tc1 and Wt (45 out of 64 genes not included in analysis)

Annotation Cluster 1	Enrichment Score: 1.8905528090556378											
Category	Term	Count	%	PValue	Genes	List Total	Pop Hits	Pop Total	Fold Enrichment	Bonferroni	Benjamini	FDR
GOTERM_CC_FAT	GO:0044421~extracellular region part	9	14.29	0.00	HAPLN1, DKK3, SLC1A3, TNC, SORL1, COL6A2, PLA2G7, COL25A1, SCG2	38	774	12504	3.83	0.18	0.18	1.85
GOTERM_CC_FAT	GO:0005576~extracellular region	11	17.46	0.02	HAPLN1, DKK3, SLC1A3, NPTX2, TNC, SORL1, COL6A2, PLA2G7, COL25A1, LUZP2, SCG2	38	1680	12504	2.15	0.93	0.49	21.78
GOTERM_CC_FAT	GO:0005615~extracellular space	5	7.94	0.06	DKK3, SORL1, PLA2G7, COL25A1, SCG2	38	511	12504	3.22	1.00	0.52	52.83
Annotation Cluster 2	Enrichment Score: 1.4350518575032696											
Category	Term	Count	%	PValue	Genes	List Total	Pop Hits	Pop Total	Fold Enrichment	Bonferroni	Benjamini	FDR
GOTERM_BP_FAT	GO:0000122~negative regulation of transcription from RNA polymerase II promoter	6	9.52	0.00	EGR1, PCGF2, RFX5, HOPX, PER1, KDM6B	51	231	13588	6.92	0.63	0.63	2.28
GOTERM_BP_FAT	GO:0006357~regulation of transcription from RNA polymerase II promoter	9	14.29	0.00	EGR1, FOS, PCGF2, EGR2, RFX5, HOPX, PER1, ALX4, KDM6B	51	616	13588	3.89	0.67	0.42	2.50
GOTERM_BP_FAT	GO:0045892~negative regulation of transcription, DNA-dependent	6	9.52	0.01	EGR1, PCGF2, RFX5, HOPX, PER1, KDM6B	51	308	13588	5.19	0.97	0.69	7.67
GOTERM_BP_FAT	GO:0051253~negative regulation of RNA metabolic process	6	9.52	0.01	EGR1, PCGF2, RFX5, HOPX, PER1, KDM6B	51	310	13588	5.16	0.97	0.59	7.87
GOTERM_BP_FAT	GO:0016481~negative regulation of transcription	6	9.52	0.01	EGR1, PCGF2, RFX5, HOPX, PER1, KDM6B	51	372	13588	4.30	1.00	0.61	15.93
SP_PIR_KEYWORDS	DNA binding	5	7.94	0.01	EGR1, FOS, PCGF2, EGR2, ALX4	62	258	17854	5.58	0.85	0.85	13.21
SP_PIR_KEYWORDS	transcription regulation	12	19.05	0.01	EGR1, PCGF2, EGR2, BTG2, LMO3, EGR4, NR3C2, HOPX, PER1, SETD7, TLE2, ALX4	62	1546	17854	2.24	0.90	0.69	16.33
GOTERM_BP_FAT	GO:0045934~negative regulation of nucleobase, nucleoside, nucleotide and nucleic acid metabolic process	6	9.52	0.01	EGR1, PCGF2, RFX5, HOPX, PER1, KDM6B	51	397	13588	4.03	1.00	0.66	20.16
GOTERM_BP_FAT	GO:0051172~negative regulation of nitrogen compound metabolic process	6	9.52	0.02	EGR1, PCGF2, RFX5, HOPX, PER1, KDM6B	51	401	13588	3.99	1.00	0.64	20.89
GOTERM_BP_FAT	GO:0010629~negative regulation of gene expression	6	9.52	0.02	EGR1, PCGF2, RFX5, HOPX, PER1, KDM6B	51	410	13588	3.90	1.00	0.64	22.57

GOTERM_BP_FAT	GO:0010558~negative regulation of macromolecule biosynthetic process	6	9.52	0.02	EGR1, PCGF2, RFX5, HOPX, PER1, KDM6B	51	418	13588	3.82	1.00	0.63	24.11
GOTERM_BP_FAT	GO:0031327~negative regulation of cellular biosynthetic process	6	9.52	0.02	EGR1, PCGF2, RFX5, HOPX, PER1, KDM6B	51	430	13588	3.72	1.00	0.55	26.52
GOTERM_BP_FAT	GO:0009890~negative regulation of biosynthetic process	6	9.52	0.02	EGR1, PCGF2, RFX5, HOPX, PER1, KDM6B	51	434	13588	3.68	1.00	0.54	27.35
GOTERM_BP_FAT	GO:0045449~regulation of transcription	15	23.81	0.03	EGR1, EGR2, LMO3, EGR4, RFX5, NR3C2, TLE2, FOS, PCGF2, BTG2, HOPX, SETD7, PER1, ALX4, KDM6B	51	2227	13588	1.79	1.00	0.60	33.28
SP_PIR_KEYWORDS	Transcription	12	19.05	0.04	EGR1, PCGF2, EGR2, BTG2, LMO3, EGR4, NR3C2, HOPX, PER1, SETD7, TLE2, ALX4	62	1769	17854	1.95	1.00	0.69	35.50
GOTERM_BP_FAT	GO:0010605~negative regulation of macromolecule metabolic process	6	9.52	0.04	EGR1, PCGF2, RFX5, HOPX, PER1, KDM6B	51	506	13588	3.16	1.00	0.71	43.58
GOTERM_BP_FAT	GO:0006355~regulation of transcription, DNA-dependent	11	17.46	0.04	EGR1, FOS, PCGF2, EGR2, RFX5, NR3C2, HOPX, PER1, SETD7, ALX4, KDM6B	51	1465	13588	2.00	1.00	0.68	44.23
GOTERM_BP_FAT	GO:0051252~regulation of RNA metabolic process	11	17.46	0.04	EGR1, FOS, PCGF2, EGR2, RFX5, NR3C2, HOPX, PER1, SETD7, ALX4, KDM6B	51	1488	13588	1.97	1.00	0.69	47.33
GOTERM_BP_FAT	GO:0016570~histone modification	3	4.76	0.05	PCGF2, HOPX, KDM6B	51	92	13588	8.69	1.00	0.68	49.73
GOTERM_BP_FAT	GO:0016569~covalent chromatin modification	3	4.76	0.05	PCGF2, HOPX, KDM6B	51	96	13588	8.33	1.00	0.70	52.47
GOTERM_BP_FAT	GO:0006350~transcription	12	19.05	0.05	EGR1, PCGF2, EGR2, BTG2, LMO3, EGR4, NR3C2, HOPX, PER1, SETD7, TLE2, ALX4	51	1772	13588	1.80	1.00	0.68	56.46
GOTERM_MF_FAT	GO:0003677~DNA binding	11	17.46	0.05	EGR1, FOS, PCGF2, PEG10, EGR2, RFX5, EGR4, NR3C2, HOPX, ALX4, KDM6B	44	1781	13288	1.87	1.00	0.99	49.58
GOTERM_BP_FAT	GO:0016568~chromatin modification	4	6.35	0.06	PCGF2, HOPX, SETD7, KDM6B	51	236	13588	4.52	1.00	0.67	57.59
GOTERM_MF_FAT	GO:0003700~transcription factor activity	6	9.52	0.10	EGR1, FOS, EGR2, NR3C2, HOPX, ALX4	44	776	13288	2.34	1.00	0.98	73.90
GOTERM_MF_FAT	GO:0043565~sequence-specific DNA binding	5	7.94	0.10	FOS, NR3C2, HOPX, ALX4, KDM6B	44	556	13288	2.72	1.00	0.96	73.97
GOTERM_BP_FAT	GO:0006325~chromatin organization	4	6.35	0.11	PCGF2, HOPX, SETD7, KDM6B	51	315	13588	3.38	1.00	0.80	82.24
GOTERM_BP_FAT	GO:0051276~chromosome organization	4	6.35	0.19	PCGF2, HOPX, SETD7, KDM6B	51	404	13588	2.64	1.00	0.90	95.33
SP_PIR_KEYWORDS	dna-binding	8	12.70	0.20	EGR1, FOS, PCGF2, PEG10, EGR2, EGR4, NR3C2, ALX4	62	1404	17854	1.64	1.00	0.95	93.36
SP_PIR_KEY	nucleus	16	25.	0.31	EGR1, EGR2, EGR4, CRABP2,	62	3808	17854	1.21	1.00	0.96	98.9

WORDS			40		NR3C2, TLE2, FOS, HSPH1, PCGF2, PEG10, HOPX, CELF3, SETD7, PER1, ALX4, KDM6B							1
GOTERM_MF_FAT	GO:0030528~transcription regulator activity	6	9.52	0.35	EGR1, FOS, EGR2, NR3C2, HOPX, ALX4	44	1206	13288	1.50	1.00	1.00	99.50
SP_PIR_KEYWORDS	zinc	8	12.70	0.47	EGR1, ZDHHC2, PCGF2, PEG10, EGR2, LMO3, EGR4, NR3C2	62	1886	17854	1.22	1.00	0.98	99.95
GOTERM_MF_FAT	GO:0008270~zinc ion binding	8	12.70	0.53	EGR1, ZDHHC2, PCGF2, PEG10, EGR2, LMO3, EGR4, NR3C2	44	2105	13288	1.15	1.00	1.00	99.99
Annotation Cluster 3	Enrichment Score: 1.332915614511585											
Category	Term	Count	%	PValue	Genes	List Total	Pop Hits	Pop Total	Fold Enrichment	Bonferroni	Benjamini	FDR
GOTERM_CC_FAT	GO:0016023~cytoplasmic membrane-bounded vesicle	5	7.94	0.03	GAD2, AP1G2, GRIN2B, SDCBP, ALS2CL	38	414	12504	3.97	0.99	0.50	32.22
GOTERM_CC_FAT	GO:0031988~membrane-bounded vesicle	5	7.94	0.03	GAD2, AP1G2, GRIN2B, SDCBP, ALS2CL	38	420	12504	3.92	0.99	0.47	33.45
GOTERM_CC_FAT	GO:0031410~cytoplasmic vesicle	5	7.94	0.06	GAD2, AP1G2, GRIN2B, SDCBP, ALS2CL	38	508	12504	3.24	1.00	0.59	52.20
GOTERM_CC_FAT	GO:0031982~vesicle	5	7.94	0.07	GAD2, AP1G2, GRIN2B, SDCBP, ALS2CL	38	519	12504	3.17	1.00	0.51	54.52
Annotation Cluster 4	Enrichment Score: 1.1865626775990343											
Category	Term	Count	%	PValue	Genes	List Total	Pop Hits	Pop Total	Fold Enrichment	Bonferroni	Benjamini	FDR
GOTERM_MF_FAT	GO:0005539~glycosaminoglycan binding	3	4.76	0.05	HAPLN1, CD44, COL25A1	44	114	13288	7.95	1.00	1.00	48.31
GOTERM_MF_FAT	GO:0001871~pattern binding	3	4.76	0.06	HAPLN1, CD44, COL25A1	44	128	13288	7.08	1.00	0.98	55.72
GOTERM_MF_FAT	GO:0030247~polysaccharide binding	3	4.76	0.06	HAPLN1, CD44, COL25A1	44	128	13288	7.08	1.00	0.98	55.72
GOTERM_MF_FAT	GO:0030246~carbohydrate binding	4	6.35	0.08	HAPLN1, CD44, NPTX2, COL25A1	44	317	13288	3.81	1.00	0.98	65.20
Annotation Cluster 5	Enrichment Score: 1.181688072473878											
Category	Term	Count	%	PValue	Genes	List Total	Pop Hits	Pop Total	Fold Enrichment	Bonferroni	Benjamini	FDR
GOTERM_BP_FAT	GO:0044057~regulation of system process	5	7.94	0.01	EGR2, SLC1A3, GRIN2B, HOPX, FKBP1B	51	201	13588	6.63	0.98	0.56	8.99
GOTERM_BP_FAT	GO:0010033~response to organic substance	7	11.11	0.01	EGR1, FOS, EGR2, SLC1A3, GRIN2B, SLC22A6, FKBP1B	51	505	13588	3.69	1.00	0.61	14.15
GOTERM_BP_	GO:0007611~learning or memory	3	4.7	0.04	EGR1, EGR2, GRIN2B	51	89	13588	8.98	1.00	0.68	47.6

FAT			6									4
GOTERM_BP_FAT	GO:0050804~regulation of synaptic transmission	3	4.76	0.05	EGR2, SLC1A3, GRIN2B	51	100	13588	7.99	1.00	0.69	55.14
GOTERM_BP_FAT	GO:0051969~regulation of transmission of nerve impulse	3	4.76	0.06	EGR2, SLC1A3, GRIN2B	51	107	13588	7.47	1.00	0.68	59.62
GOTERM_BP_FAT	GO:0007610~behavior	5	7.94	0.06	EGR1, EGR2, SLC1A3, GRIN2B, SCG2	51	405	13588	3.29	1.00	0.68	61.06
GOTERM_BP_FAT	GO:0031644~regulation of neurological system process	3	4.76	0.06	EGR2, SLC1A3, GRIN2B	51	113	13588	7.07	1.00	0.69	63.25
GOTERM_BP_FAT	GO:0050877~neurological system process	6	9.52	0.76	EGR1, GAD2, EGR2, SLC1A3, GRIN2B, FKBP1B	51	1681	13588	0.95	1.00	1.00	100.00
GOTERM_BP_FAT	GO:0050890~cognition	4	6.35	0.92	EGR1, EGR2, SLC1A3, GRIN2B	51	1480	13588	0.72	1.00	1.00	100.00
Annotation Cluster 6	Enrichment Score: 1.1759506676333606											
Category	Term	Count	%	PValue	Genes	List Total	Pop Hits	Pop Total	Fold Enrichment	Bonferroni	Benjamini	FDR
GOTERM_BP_FAT	GO:0003002~regionalization	5	7.94	0.01	PCGF2, EGR2, BTG2, ALX4, AXIN2	51	214	13588	6.23	0.99	0.57	11.06
GOTERM_BP_FAT	GO:0009952~anterior/posterior pattern formation	4	6.35	0.02	PCGF2, BTG2, ALX4, AXIN2	51	153	13588	6.97	1.00	0.61	24.50
GOTERM_BP_FAT	GO:0043009~chordate embryonic development	6	9.52	0.02	PCGF2, GRIN2B, HOPX, CDH1, ALX4, AXIN2	51	421	13588	3.80	1.00	0.59	24.71
GOTERM_BP_FAT	GO:0009792~embryonic development ending in birth or egg hatching	6	9.52	0.02	PCGF2, GRIN2B, HOPX, CDH1, ALX4, AXIN2	51	425	13588	3.76	1.00	0.57	25.51
GOTERM_BP_FAT	GO:0007389~pattern specification process	5	7.94	0.02	PCGF2, EGR2, BTG2, ALX4, AXIN2	51	284	13588	4.69	1.00	0.56	26.34
GOTERM_BP_FAT	GO:0042981~regulation of apoptosis	6	9.52	0.05	ALDH1A1, PCGF2, BTG2, CDH1, ALX4, SCG2	51	553	13588	2.89	1.00	0.70	54.73
GOTERM_BP_FAT	GO:0043067~regulation of programmed cell death	6	9.52	0.05	ALDH1A1, PCGF2, BTG2, CDH1, ALX4, SCG2	51	560	13588	2.85	1.00	0.69	56.37
GOTERM_BP_FAT	GO:0010941~regulation of cell death	6	9.52	0.06	ALDH1A1, PCGF2, BTG2, CDH1, ALX4, SCG2	51	563	13588	2.84	1.00	0.67	57.06
GOTERM_BP_FAT	GO:0001701~in utero embryonic development	4	6.35	0.07	PCGF2, GRIN2B, HOPX, CDH1	51	267	13588	3.99	1.00	0.72	68.73
GOTERM_BP_FAT	GO:0048562~embryonic organ morphogenesis	3	4.76	0.12	ALDH1A1, PCGF2, ALX4	51	161	13588	4.96	1.00	0.82	84.75
GOTERM_BP_FAT	GO:0048598~embryonic morphogenesis	4	6.35	0.15	ALDH1A1, PCGF2, CRABP2, ALX4	51	359	13588	2.97	1.00	0.86	90.40
GOTERM_BP_FAT	GO:0043066~negative regulation of apoptosis	3	4.76	0.22	PCGF2, BTG2, SCG2	51	239	13588	3.34	1.00	0.92	97.53
GOTERM_BP_FAT	GO:0048568~embryonic organ development	3	4.76	0.22	ALDH1A1, PCGF2, ALX4	51	241	13588	3.32	1.00	0.92	97.65

GOTERM_BP_FAT	GO:0043069~negative regulation of programmed cell death	3	4.76	0.23	PCGF2, BTG2, SCG2	51	244	13588	3.28	1.00	0.92	97.83
GOTERM_BP_FAT	GO:0060548~negative regulation of cell death	3	4.76	0.23	PCGF2, BTG2, SCG2	51	245	13588	3.26	1.00	0.92	97.89
GOTERM_BP_FAT	GO:0001501~skeletal system development	3	4.76	0.28	PCGF2, ALX4, AXIN2	51	285	13588	2.80	1.00	0.94	99.29
Annotation Cluster 7	Enrichment Score: 1.0998921485509967											
Category	Term	Count	%	PValue	Genes	List Total	Pop Hits	Pop Total	Fold Enrichment	Bonferroni	Benjamini	FDR
GOTERM_BP_FAT	GO:0044057~regulation of system process	5	7.94	0.01	EGR2, SLC1A3, GRIN2B, HOPX, FKBP1B	51	201	13588	6.63	0.98	0.56	8.99
GOTERM_BP_FAT	GO:0010033~response to organic substance	7	11.11	0.01	EGR1, FOS, EGR2, SLC1A3, GRIN2B, SLC22A6, FKBP1B	51	505	13588	3.69	1.00	0.61	14.15
GOTERM_BP_FAT	GO:0019226~transmission of nerve impulse	4	6.35	0.05	GAD2, EGR2, GRIN2B, FKBP1B	51	226	13588	4.72	1.00	0.70	53.70
GOTERM_BP_FAT	GO:0006873~cellular ion homeostasis	4	6.35	0.07	EGR2, GRIN2B, NR3C2, FKBP1B	51	261	13588	4.08	1.00	0.71	66.71
GOTERM_BP_FAT	GO:0055082~cellular chemical homeostasis	4	6.35	0.08	EGR2, GRIN2B, NR3C2, FKBP1B	51	268	13588	3.98	1.00	0.71	69.06
GOTERM_BP_FAT	GO:0007267~cell-cell signaling	4	6.35	0.09	GAD2, GRIN2B, TNC, FKBP1B	51	290	13588	3.67	1.00	0.75	75.82
GOTERM_BP_FAT	GO:0050801~ion homeostasis	4	6.35	0.09	EGR2, GRIN2B, NR3C2, FKBP1B	51	293	13588	3.64	1.00	0.75	76.66
GOTERM_BP_FAT	GO:0019725~cellular homeostasis	4	6.35	0.13	EGR2, GRIN2B, NR3C2, FKBP1B	51	343	13588	3.11	1.00	0.85	87.87
GOTERM_BP_FAT	GO:0048878~chemical homeostasis	4	6.35	0.15	EGR2, GRIN2B, NR3C2, FKBP1B	51	365	13588	2.92	1.00	0.86	91.24
GOTERM_BP_FAT	GO:0042592~homeostatic process	4	6.35	0.36	EGR2, GRIN2B, NR3C2, FKBP1B	51	584	13588	1.82	1.00	0.97	99.88
GOTERM_BP_FAT	GO:0050877~neurological system process	6	9.52	0.76	EGR1, GAD2, EGR2, SLC1A3, GRIN2B, FKBP1B	51	1681	13588	0.95	1.00	1.00	100.00
Annotation Cluster 8	Enrichment Score: 1.0368572127696145											
Category	Term	Count	%	PValue	Genes	List Total	Pop Hits	Pop Total	Fold Enrichment	Bonferroni	Benjamini	FDR
GOTERM_BP_FAT	GO:0022612~gland morphogenesis	3	4.76	0.04	CD44, TNC, CDH1	51	84	13588	9.52	1.00	0.70	44.09
KEGG_PATHWAY	mmu04512:ECM-receptor interaction	3	4.76	0.04	CD44, TNC, COL6A2	23	83	5738	9.02	0.84	0.84	31.62
GOTERM_CC_FAT	GO:0005578~proteinaceous extracellular matrix	4	6.35	0.06	HAPLN1, SLC1A3, TNC, COL6A2	38	297	12504	4.43	1.00	0.60	49.25

GOTERM_CC_FAT	GO:0031012~extracellular matrix	4	6.35	0.06	HAPLN1, SLC1A3, TNC, COL6A2	38	309	12504	4.26	1.00	0.55	52.69
SP_PIR_KEYWORDS	cell adhesion	4	6.35	0.14	CD44, TNC, COL6A2, CDH1	62	380	17854	3.03	1.00	0.95	83.89
GOTERM_BP_FAT	GO:0007155~cell adhesion	5	7.94	0.15	HAPLN1, CD44, TNC, COL6A2, CDH1	51	561	13588	2.37	1.00	0.86	91.25
GOTERM_BP_FAT	GO:0022610~biological adhesion	5	7.94	0.15	HAPLN1, CD44, TNC, COL6A2, CDH1	51	562	13588	2.37	1.00	0.86	91.36
GOTERM_BP_FAT	GO:0048732~gland development	3	4.76	0.16	CD44, TNC, CDH1	51	197	13588	4.06	1.00	0.87	93.05
SP_PIR_KEYWORDS	extracellular matrix	3	4.76	0.16	HAPLN1, TNC, COL6A2	62	213	17854	4.06	1.00	0.94	88.60
Annotation Cluster 9	Enrichment Score: 0.94433856637788											
Category	Term	Count	%	PValue	Genes	List Total	Pop Hits	Pop Total	Fold Enrichment	Bonferroni	Benjamini	FDR
UP_SEQ_FEATURE	domain:Fibronectin type-III 2	3	4.76	0.08	EPHA6, TNC, SORL1	62	120	16021	6.46	1.00	1.00	65.53
UP_SEQ_FEATURE	domain:Fibronectin type-III 1	3	4.76	0.08	EPHA6, TNC, SORL1	62	121	16021	6.41	1.00	1.00	66.07
INTERPRO	IPR008957:Fibronectin, type III-like fold	3	4.76	0.13	EPHA6, TNC, SORL1	60	187	17763	4.75	1.00	1.00	81.10
INTERPRO	IPR003961:Fibronectin, type III	3	4.76	0.13	EPHA6, TNC, SORL1	60	191	17763	4.65	1.00	1.00	82.24
SMART	SM00060:FN3	3	4.76	0.19	EPHA6, TNC, SORL1	39	191	9131	3.68	1.00	1.00	86.36
Annotation Cluster 10	Enrichment Score: 0.9047956237291621											
Category	Term	Count	%	PValue	Genes	List Total	Pop Hits	Pop Total	Fold Enrichment	Bonferroni	Benjamini	FDR
GOTERM_CC_FAT	GO:0005576~extracellular region	11	17.46	0.02	HAPLN1, DKK3, SLC1A3, NPTX2, TNC, SORL1, COL6A2, PLA2G7, COL25A1, LUZP2, SCG2	38	1680	12504	2.15	0.93	0.49	21.78
SP_PIR_KEYWORDS	glycoprotein	20	31.75	0.03	HAPLN1, SPRN, TPRA1, TNC, SORL1, COL25A1, CDH1, LUZP2, NETO1, DKK3, EPHA6, CHRM4, SLC1A3, GRIN2B, CD44, BC005764, NPTX2, COL6A2, PLA2G7, SLC22A6	62	3600	17854	1.60	0.99	0.68	29.09
UP_SEQ_FEATURE	glycosylation site:N-linked (GlcNAc...)	19	30.16	0.09	HAPLN1, SPRN, TPRA1, TNC, SORL1, CDH1, LUZP2, NETO1, DKK3, EPHA6, CHRM4, SLC1A3, GRIN2B, CD44, BC005764, NPTX2, COL6A2, PLA2G7, SLC22A6	62	3444	16021	1.43	1.00	1.00	71.10

SP_PIR_KEYWORDS	signal	14	22.22	0.20	SPRN, TNC, SORL1, CDH1, LUZP2, NETO1, DKK3, EPHA6, GRIN2B, CD44, NPTX2, COL6A2, PLA2G7, SCG2	62	2970	17854	1.36	1.00	0.94	93.71
SP_PIR_KEYWORDS	Secreted	8	12.70	0.21	HAPLN1, DKK3, NPTX2, TNC, COL6A2, PLA2G7, LUZP2, SCG2	62	1420	17854	1.62	1.00	0.93	94.10
UP_SEQ_FEATURE	signal peptide	14	22.22	0.33	SPRN, TNC, SORL1, CDH1, LUZP2, NETO1, DKK3, EPHA6, GRIN2B, CD44, NPTX2, COL6A2, PLA2G7, SCG2	62	2963	16021	1.22	1.00	1.00	99.56
SP_PIR_KEYWORDS	disulfide bond	9	14.29	0.62	HAPLN1, DKK3, CHRM4, CD44, TNC, SORL1, COL6A2, CDH1, NETO1	62	2469	17854	1.05	1.00	1.00	100.00
Annotation Cluster 11	Enrichment Score: 0.8768030592615519											
Category	Term	Count	%	PValue	Genes	List Total	Pop Hits	Pop Total	Fold Enrichment	Bonferroni	Benjamini	FDR
GOTERM_BP_FAT	GO:0006357~regulation of transcription from RNA polymerase II promoter	9	14.29	0.00	EGR1, FOS, PCGF2, EGR2, RFX5, HOPX, PER1, ALX4, KDM6B	51	616	13588	3.89	0.67	0.42	2.50
GOTERM_BP_FAT	GO:0010033~response to organic substance	7	11.11	0.01	EGR1, FOS, EGR2, SLC1A3, GRIN2B, SLC22A6, FKBP1B	51	505	13588	3.69	1.00	0.61	14.15
SP_PIR_KEYWORDS	DNA binding	5	7.94	0.01	EGR1, FOS, PCGF2, EGR2, ALX4	62	258	17854	5.58	0.85	0.85	13.21
GOTERM_MF_FAT	GO:0003700~transcription factor activity	6	9.52	0.10	EGR1, FOS, EGR2, NR3C2, HOPX, ALX4	44	776	13288	2.34	1.00	0.98	73.90
GOTERM_BP_FAT	GO:0045944~positive regulation of transcription from RNA polymerase II promoter	4	6.35	0.14	EGR1, FOS, EGR2, ALX4	51	358	13588	2.98	1.00	0.86	90.26
GOTERM_BP_FAT	GO:0045893~positive regulation of transcription, DNA-dependent	4	6.35	0.20	EGR1, FOS, EGR2, ALX4	51	416	13588	2.56	1.00	0.91	96.20
GOTERM_BP_FAT	GO:0051254~positive regulation of RNA metabolic process	4	6.35	0.20	EGR1, FOS, EGR2, ALX4	51	419	13588	2.54	1.00	0.91	96.40
SP_PIR_KEYWORDS	dna-binding	8	12.70	0.20	EGR1, FOS, PCGF2, PEG10, EGR2, EGR4, NR3C2, ALX4	62	1404	17854	1.64	1.00	0.95	93.36
SP_PIR_KEYWORDS	activator	4	6.35	0.23	EGR1, EGR2, SETD7, ALX4	62	484	17854	2.38	1.00	0.92	95.67
GOTERM_BP_FAT	GO:0045941~positive regulation of transcription	4	6.35	0.25	EGR1, FOS, EGR2, ALX4	51	475	13588	2.24	1.00	0.93	98.74
GOTERM_BP_FAT	GO:0010628~positive regulation of gene expression	4	6.35	0.27	EGR1, FOS, EGR2, ALX4	51	488	13588	2.18	1.00	0.93	99.03
GOTERM_BP_FAT	GO:0045935~positive regulation of nucleobase, nucleoside, nucleotide and nucleic acid metabolic process	4	6.35	0.29	EGR1, FOS, EGR2, ALX4	51	510	13588	2.09	1.00	0.94	99.39
GOTERM_BP_	GO:0051173~positive regulation of nitrogen	4	6.3	0.31	EGR1, FOS, EGR2, ALX4	51	526	13588	2.03	1.00	0.95	99.5

FAT	compound metabolic process		5									7
GOTERM_BP_FAT	GO:0010557~positive regulation of macromolecule biosynthetic process	4	6.35	0.31	EGR1, FOS, EGR2, ALX4	51	530	13588	2.01	1.00	0.95	99.60
GOTERM_BP_FAT	GO:0031328~positive regulation of cellular biosynthetic process	4	6.35	0.33	EGR1, FOS, EGR2, ALX4	51	552	13588	1.93	1.00	0.96	99.76
GOTERM_BP_FAT	GO:0009891~positive regulation of biosynthetic process	4	6.35	0.34	EGR1, FOS, EGR2, ALX4	51	557	13588	1.91	1.00	0.96	99.78
GOTERM_MF_FAT	GO:0030528~transcription regulator activity	6	9.52	0.35	EGR1, FOS, EGR2, NR3C2, HOPX, ALX4	44	1206	13288	1.50	1.00	1.00	99.50
GOTERM_BP_FAT	GO:0010604~positive regulation of macromolecule metabolic process	4	6.35	0.41	EGR1, FOS, EGR2, ALX4	51	633	13588	1.68	1.00	0.98	99.97
Annotation Cluster 12	Enrichment Score: 0.8327248658019032											
Category	Term	Count	%	PValue	Genes	List Total	Pop Hits	Pop Total	Fold Enrichment	Bonferroni	Benjamini	FDR
GOTERM_BP_FAT	GO:0042110~T cell activation	3	4.76	0.07	EGR1, GADD45G, FKBP1B	51	116	13588	6.89	1.00	0.70	65.00
GOTERM_BP_FAT	GO:0046649~lymphocyte activation	3	4.76	0.16	EGR1, GADD45G, FKBP1B	51	191	13588	4.18	1.00	0.86	92.03
GOTERM_BP_FAT	GO:0045321~leukocyte activation	3	4.76	0.19	EGR1, GADD45G, FKBP1B	51	219	13588	3.65	1.00	0.90	95.90
GOTERM_BP_FAT	GO:0001775~cell activation	3	4.76	0.23	EGR1, GADD45G, FKBP1B	51	246	13588	3.25	1.00	0.91	97.94
Annotation Cluster 13	Enrichment Score: 0.7857744371440335											
Category	Term	Count	%	PValue	Genes	List Total	Pop Hits	Pop Total	Fold Enrichment	Bonferroni	Benjamini	FDR
GOTERM_CC_FAT	GO:0044459~plasma membrane part	11	17.46	0.02	GAD2, EPHA6, CHRM4, GRIN2B, CD44, SDCBP, CDH1, COL25A1, SLC22A6, KCNG1, TOMM34	38	1633	12504	2.22	0.89	0.67	18.45
GOTERM_CC_FAT	GO:0005887~integral to plasma membrane	6	9.52	0.02	EPHA6, GRIN2B, SDCBP, COL25A1, SLC22A6, KCNG1	38	531	12504	3.72	0.91	0.55	20.11
GOTERM_CC_FAT	GO:0031226~intrinsic to plasma membrane	6	9.52	0.02	EPHA6, GRIN2B, SDCBP, COL25A1, SLC22A6, KCNG1	38	552	12504	3.58	0.94	0.43	22.99
SP_PIR_KEYWORDS	glycoprotein	20	31.75	0.03	HAPLN1, SPRN, TPRA1, TNC, SORL1, COL25A1, CDH1, LUZP2, NETO1, DKK3, EPHA6, CHRM4, SLC1A3, GRIN2B, CD44, BC005764, NPTX2, COL6A2, PLA2G7, SLC22A6	62	3600	17854	1.60	0.99	0.68	29.09
GOTERM_CC_FAT	GO:0005886~plasma membrane	14	22.22	0.07	SPRN, COL25A1, CDH1, GAD2, EPHA6, CHRM4, SLC1A3, GRIN2B, CD44, COL6A2, SDCBP, SLC22A6, KCNG1, TOMM34	38	2906	12504	1.59	1.00	0.50	56.06

SP_PIR_KEYWORDS	membrane	25	39.68	0.10	AP1G2, TPRA1, SORL1, NR3C2, CTXN3, CDH1, NETO1, GAD2, NDUFS5, SLC1A3, CD44, GRIN2B, BC005764, COL6A2, SLC22A6, KCNG1, TOMM34, ZDHHC2, SPRN, COL25A1, RGS14, CHRM4, EPHA6, CNIH2, SDCBP	62	5507	17854	1.31	1.00	0.90	71.31
UP_SEQ_FEATURE	topological domain:Extracellular	10	15.87	0.45	EPHA6, CHRM4, SLC1A3, GRIN2B, CD44, SORL1, CDH1, COL25A1, SLC22A6, NETO1	62	2174	16021	1.19	1.00	1.00	99.97
GOTERM_CC_FAT	GO:0031224~intrinsic to membrane	19	30.16	0.50	ZDHHC2, SPRN, TPRA1, SORL1, CTXN3, COL25A1, CDH1, NETO1, GAD2, EPHA6, CHRM4, SLC1A3, GRIN2B, CNIH2, CD44, BC005764, SDCBP, SLC22A6, KCNG1	38	5914	12504	1.06	1.00	0.99	99.97
UP_SEQ_FEATURE	transmembrane region	16	25.40	0.63	ZDHHC2, TPRA1, SORL1, CTXN3, COL25A1, CDH1, NETO1, EPHA6, CHRM4, SLC1A3, GRIN2B, CNIH2, CD44, BC005764, SLC22A6, KCNG1	62	4113	16021	1.01	1.00	1.00	100.00
UP_SEQ_FEATURE	topological domain:Cytoplasmic	11	17.46	0.63	EPHA6, CHRM4, SLC1A3, GRIN2B, CD44, SORL1, CDH1, COL25A1, SLC22A6, KCNG1, NETO1	62	2780	16021	1.02	1.00	1.00	100.00
GOTERM_CC_FAT	GO:0016021~integral to membrane	17	26.98	0.68	ZDHHC2, TPRA1, SORL1, CTXN3, COL25A1, CDH1, NETO1, EPHA6, CHRM4, SLC1A3, GRIN2B, CNIH2, CD44, BC005764, SDCBP, SLC22A6, KCNG1	38	5709	12504	0.98	1.00	1.00	100.00
SP_PIR_KEYWORDS	transmembrane	16	25.40	0.83	ZDHHC2, TPRA1, SORL1, CTXN3, COL25A1, CDH1, NETO1, EPHA6, CHRM4, SLC1A3, GRIN2B, CNIH2, CD44, BC005764, SLC22A6, KCNG1	62	5237	17854	0.88	1.00	1.00	100.00
SP_PIR_KEYWORDS	receptor	7	11.11	0.86	EPHA6, CHRM4, GRIN2B, CD44, SORL1, NR3C2, NETO1	62	2465	17854	0.82	1.00	1.00	100.00
Annotation Cluster 14	Enrichment Score: 0.7694797971693238											
Category	Term	Count	%	PValue	Genes	List Total	Pop Hits	Pop Total	Fold Enrichment	Bonferroni	Benjamini	FDR
SP_PIR_KEYWORDS	wnt signaling pathway	3	4.76	0.06	DKK3, TLE2, AXIN2	62	118	17854	7.32	1.00	0.81	53.55
GOTERM_BP_FAT	GO:0016055~Wnt receptor signaling pathway	3	4.76	0.08	DKK3, TLE2, AXIN2	51	130	13588	6.15	1.00	0.73	72.42
GOTERM_BP_FAT	GO:0007166~cell surface receptor linked signal transduction	6	9.52	0.97	DKK3, EPHA6, CHRM4, TLE2, AXIN2, RGS14	51	2495	13588	0.64	1.00	1.00	100.00

Annotation Cluster 15	Enrichment Score: 0.7366499193910733											
Category	Term	Count	%	PValue	Genes	List Total	Pop Hits	Pop Total	Fold Enrichment	Bonferroni	Benjamini	FDR
GOTERM_BP_FAT	GO:0009611~response to wounding	4	6.35	0.14	SLC1A3, CD44, PLA2G7, KDM6B	51	347	13588	3.07	1.00	0.85	88.55
GOTERM_BP_FAT	GO:0006954~inflammatory response	3	4.76	0.20	CD44, PLA2G7, KDM6B	51	225	13588	3.55	1.00	0.90	96.47
GOTERM_BP_FAT	GO:0006952~defense response	4	6.35	0.23	GRIN2B, CD44, PLA2G7, KDM6B	51	448	13588	2.38	1.00	0.92	97.88
Annotation Cluster 16	Enrichment Score: 0.7056449766195889											
Category	Term	Count	%	PValue	Genes	List Total	Pop Hits	Pop Total	Fold Enrichment	Bonferroni	Benjamini	FDR
GOTERM_BP_FAT	GO:0002009~morphogenesis of an epithelium	3	4.76	0.13	ALDH1A1, CD44, TNC	51	173	13588	4.62	1.00	0.85	88.13
GOTERM_BP_FAT	GO:0048729~tissue morphogenesis	3	4.76	0.22	ALDH1A1, CD44, TNC	51	238	13588	3.36	1.00	0.92	97.46
GOTERM_BP_FAT	GO:0060429~epithelium development	3	4.76	0.26	ALDH1A1, CD44, TNC	51	271	13588	2.95	1.00	0.93	98.95
Annotation Cluster 17	Enrichment Score: 0.6750834475977373											
Category	Term	Count	%	PValue	Genes	List Total	Pop Hits	Pop Total	Fold Enrichment	Bonferroni	Benjamini	FDR
GOTERM_CC_FAT	GO:0044456~synapse part	3	4.76	0.13	GAD2, CHRM4, GRIN2B	38	212	12504	4.66	1.00	0.71	79.94
SP_PIR_KEYWORDS	cell junction	4	6.35	0.15	GAD2, CHRM4, GRIN2B, CDH1	62	392	17854	2.94	1.00	0.94	85.92
GOTERM_CC_FAT	GO:0030054~cell junction	4	6.35	0.16	GAD2, CHRM4, GRIN2B, CDH1	38	470	12504	2.80	1.00	0.77	86.90
SP_PIR_KEYWORDS	synapse	3	4.76	0.16	GAD2, CHRM4, GRIN2B	62	213	17854	4.06	1.00	0.94	88.60
GOTERM_CC_FAT	GO:0045202~synapse	3	4.76	0.24	GAD2, CHRM4, GRIN2B	38	319	12504	3.09	1.00	0.87	96.02
SP_PIR_KEYWORDS	cell membrane	6	9.52	0.71	SPRN, GAD2, CHRM4, GRIN2B, CDH1, SLC22A6	62	1713	17854	1.01	1.00	1.00	100.00
Annotation Cluster 18	Enrichment Score: 0.5080706079496419											
Category	Term	Count	%	PValue	Genes	List Total	Pop Hits	Pop Total	Fold Enrichment	Bonferroni	Benjamini	FDR
SP_PIR_KEYWORDS	zinc finger	3	4.76	0.02	EGR1, PCGF2, EGR2	62	66	17854	13.09	0.97	0.68	22.98

GOTERM_MF_FAT	GO:0003677~DNA binding	11	17.46	0.05	EGR1, FOS, PCGF2, PEG10, EGR2, RFX5, EGR4, NR3C2, HOPX, ALX4, KDM6B	44	1781	13288	1.87	1.00	0.99	49.58
SP_PIR_KEYWORDS	dna-binding	8	12.70	0.20	EGR1, FOS, PCGF2, PEG10, EGR2, EGR4, NR3C2, ALX4	62	1404	17854	1.64	1.00	0.95	93.36
SP_PIR_KEYWORDS	zinc-finger	7	11.11	0.23	EGR1, ZDHHC2, PCGF2, PEG10, EGR2, EGR4, NR3C2	62	1204	17854	1.67	1.00	0.94	95.55
UP_SEQ_FEATURE	zinc finger region:C2H2-type 3	3	4.76	0.25	EGR1, EGR2, EGR4	62	252	16021	3.08	1.00	1.00	97.84
UP_SEQ_FEATURE	zinc finger region:C2H2-type 1	3	4.76	0.25	EGR1, EGR2, EGR4	62	254	16021	3.05	1.00	1.00	97.94
UP_SEQ_FEATURE	zinc finger region:C2H2-type 2	3	4.76	0.26	EGR1, EGR2, EGR4	62	259	16021	2.99	1.00	1.00	98.19
GOTERM_MF_FAT	GO:0046872~metal ion binding	15	23.81	0.36	ZDHHC2, EGR1, EGR2, LMO3, EGR4, NR3C2, CDH1, PGM2L1, PEG10, PCGF2, GRIN2B, NPTX2, KDM6B, KCNG1, SCG2	44	3850	13288	1.18	1.00	1.00	99.54
GOTERM_MF_FAT	GO:0043169~cation binding	15	23.81	0.37	ZDHHC2, EGR1, EGR2, LMO3, EGR4, NR3C2, CDH1, PGM2L1, PEG10, PCGF2, GRIN2B, NPTX2, KDM6B, KCNG1, SCG2	44	3885	13288	1.17	1.00	1.00	99.65
GOTERM_MF_FAT	GO:0043167~ion binding	15	23.81	0.39	ZDHHC2, EGR1, EGR2, LMO3, EGR4, NR3C2, CDH1, PGM2L1, PEG10, PCGF2, GRIN2B, NPTX2, KDM6B, KCNG1, SCG2	44	3934	13288	1.15	1.00	1.00	99.77
SP_PIR_KEYWORDS	zinc	8	12.70	0.47	EGR1, ZDHHC2, PCGF2, PEG10, EGR2, LMO3, EGR4, NR3C2	62	1886	17854	1.22	1.00	0.98	99.95
INTERPRO	IPR013087:Zinc finger, C2H2-type/integrase, DNA-binding	3	4.76	0.51	EGR1, EGR2, EGR4	60	514	17763	1.73	1.00	1.00	99.98
GOTERM_MF_FAT	GO:0008270~zinc ion binding	8	12.70	0.53	EGR1, ZDHHC2, PCGF2, PEG10, EGR2, LMO3, EGR4, NR3C2	44	2105	13288	1.15	1.00	1.00	99.99
SP_PIR_KEYWORDS	metal-binding	10	15.87	0.58	EGR1, ZDHHC2, PCGF2, PEG10, EGR2, LMO3, EGR4, NPTX2, NR3C2, KDM6B	62	2682	17854	1.07	1.00	0.99	100.00
GOTERM_MF_FAT	GO:0046914~transition metal ion binding	9	14.29	0.63	EGR1, ZDHHC2, PCGF2, PEG10, EGR2, LMO3, EGR4, NR3C2, KDM6B	44	2608	13288	1.04	1.00	1.00	100.00
INTERPRO	IPR015880:Zinc finger, C2H2-like	3	4.76	0.66	EGR1, EGR2, EGR4	60	676	17763	1.31	1.00	1.00	100.00
INTERPRO	IPR007087:Zinc finger, C2H2-type	3	4.76	0.67	EGR1, EGR2, EGR4	60	681	17763	1.30	1.00	1.00	100.00
SMART	SM00355:ZnF_C2H2	3	4.76	0.78	EGR1, EGR2, EGR4	39	676	9131	1.04	1.00	1.00	100.00
Annotation	Enrichment Score: 0.4449828443325495											

Cluster 19												
Category	Term	Count	%	PValue	Genes	List Total	Pop Hits	Pop Total	Fold Enrichment	Bonferroni	Benjamini	FDR
SP_PIR_KEYWORDS	DNA binding	5	7.94	0.01	EGR1, FOS, PCGF2, EGR2, ALX4	62	258	17854	5.58	0.85	0.85	13.21
SP_PIR_KEYWORDS	dna-binding	8	12.70	0.20	EGR1, FOS, PCGF2, PEG10, EGR2, EGR4, NR3C2, ALX4	62	1404	17854	1.64	1.00	0.95	93.36
GOTERM_CC_FAT	GO:0044451~nucleoplasm part	3	4.76	0.45	FOS, PCGF2, ALX4	38	513	12504	1.92	1.00	0.98	99.90
GOTERM_CC_FAT	GO:0005654~nucleoplasm	3	4.76	0.53	FOS, PCGF2, ALX4	38	599	12504	1.65	1.00	0.99	99.99
GOTERM_CC_FAT	GO:0031981~nuclear lumen	3	4.76	0.75	FOS, PCGF2, ALX4	38	883	12504	1.12	1.00	1.00	100.00
GOTERM_CC_FAT	GO:0070013~intracellular organelle lumen	3	4.76	0.86	FOS, PCGF2, ALX4	38	1133	12504	0.87	1.00	1.00	100.00
GOTERM_CC_FAT	GO:0043233~organelle lumen	3	4.76	0.86	FOS, PCGF2, ALX4	38	1136	12504	0.87	1.00	1.00	100.00
GOTERM_CC_FAT	GO:0031974~membrane-enclosed lumen	3	4.76	0.87	FOS, PCGF2, ALX4	38	1174	12504	0.84	1.00	1.00	100.00
Annotation Cluster 20	Enrichment Score: 0.3771934009216371											
Category	Term	Count	%	PValue	Genes	List Total	Pop Hits	Pop Total	Fold Enrichment	Bonferroni	Benjamini	FDR
GOTERM_BP_FAT	GO:0006811~ion transport	5	7.94	0.27	SLC1A3, GRIN2B, SLC22A6, FKBP1B, KCNG1	51	712	13588	1.87	1.00	0.93	99.01
GOTERM_BP_FAT	GO:0030001~metal ion transport	3	4.76	0.49	GRIN2B, FKBP1B, KCNG1	51	442	13588	1.81	1.00	0.99	100.00
GOTERM_BP_FAT	GO:0006812~cation transport	3	4.76	0.57	GRIN2B, FKBP1B, KCNG1	51	515	13588	1.55	1.00	1.00	100.00

Supplementary Table 6 Functional Annotation Clustering by DAVID for differentially expressed genes between J20 and Wt (10 out of 24 genes not included in analysis)

Enrichment Score: 3.297362616814331											
Term	Count	%	PValue	Genes	List Total	Pop Hits	Pop Total	Fold Enrichment	Bonferroni	Benjamini	FDR
disulfide bond	12	50.00	0.000003	NOV, NTF3, SSTR1, SCN3B, NPNT, ITGA7, UNC5D, DCN, CORT, KIRREL2, DRD1A, TRF	21	2379	16021	3.85	0.00	0.00	0.04
disulfide bond	12	50.00	0.0001	NOV, NTF3, SSTR1, SCN3B, NPNT, ITGA7, UNC5D, DCN, CORT, KIRREL2, DRD1A, TRF	23	2469	17854	3.77	0.00	0.00	0.06
signal peptide	12	50.00	0.0003	NOV, TNXB, NTF3, SCN3B, NPNT, ITGA7, COL6A1, UNC5D, DCN, CORT, KIRREL2, TRF	21	2963	16021	3.09	0.03	0.01	0.31
signal	12	50.00	0.0003	NOV, TNXB, NTF3, SCN3B, NPNT, ITGA7, COL6A1, UNC5D, DCN, CORT, KIRREL2, TRF	23	2970	17854	3.14	0.02	0.01	0.32
Secreted	7	29.17	0.01	NOV, NTF3, NPNT, COL6A1, DCN, CORT, TRF	23	1420	17854	3.83	0.36	0.09	6.22
GO:0005576~extracellular region	8	33.33	0.02	NOV, TNXB, NTF3, NPNT, COL6A1, DCN, CORT, TRF	22	1680	12504	2.71	0.60	0.17	15.00
Enrichment Score: 2.9474436079315622											
Term	Count	%	PValue	Genes	List Total	Pop Hits	Pop Total	Fold Enrichment	Bonferroni	Benjamini	FDR
disulfide bond	12	50.00	0.00	NOV, NTF3, SSTR1, SCN3B, NPNT, ITGA7, UNC5D, DCN, CORT, KIRREL2, DRD1A, TRF	21	2379	16021	3.85	0.00	0.00	0.04
disulfide bond	12	50.00	0.00	NOV, NTF3, SSTR1, SCN3B, NPNT, ITGA7, UNC5D, DCN, CORT, KIRREL2, DRD1A, TRF	23	2469	17854	3.77	0.00	0.00	0.06
glycosylation site:N-linked (GlcNAc...)	13	54.17	0.00	NOV, TMC6, NTF3, SSTR1, SCN3B, ABCA8A, ITGA7, COL6A1, UNC5D, DCN, KIRREL2, DRD1A, TRF	21	3444	16021	2.88	0.02	0.01	0.24
glycoprotein	13	54.17	0.00	NOV, TMC6, NTF3, SSTR1, SCN3B, ABCA8A, ITGA7, COL6A1, UNC5D, DCN, KIRREL2, DRD1A, TRF	23	3600	17854	2.80	0.03	0.01	0.39
transmembrane region	9	37.50	0.12	TMC6, GM98, SSTR1, SCN3B, ABCA8A, ITGA7, UNC5D, KIRREL2, DRD1A	21	4113	16021	1.67	1.00	0.97	75.39
topological domain:Cytoplasmic	7	29.17	0.12	TMC6, SSTR1, SCN3B, ITGA7, UNC5D, KIRREL2, DRD1A	21	2780	16021	1.92	1.00	0.95	76.36
Enrichment Score: 2.6262605397920833											
Term	Count	%	PValue	Genes	List Total	Pop Hits	Pop Total	Fold Enrichment	Bonferroni	Benjamini	FDR
GO:0044057~regulation of system process	5	20.83	0.00	GM98, NTF3, RYR1, DRD1A, TRF	18	201	13588	18.78	0.04	0.04	0.13
GO:0006873~cellular ion homeostasis	5	20.	0.00	GM98, NTF3, RYR1, DRD1A, TRF	18	261	1358	14.46	0.10	0.05	0.36

		83					8				
GO:0055082~cellular chemical homeostasis	5	20.83	0.00	GM98, NTF3, RYR1, DRD1A, TRF	18	268	13588	14.08	0.11	0.04	0.40
GO:0051969~regulation of transmission of nerve impulse	4	16.67	0.00	GM98, NTF3, DRD1A, TRF	18	107	13588	28.22	0.11	0.03	0.41
GO:0031644~regulation of neurological system process	4	16.67	0.00	GM98, NTF3, DRD1A, TRF	18	113	13588	26.72	0.13	0.03	0.49
GO:0031646~positive regulation of neurological system process	3	12.50	0.00	GM98, DRD1A, TRF	18	24	13588	94.36	0.15	0.03	0.56
GO:0050801~ion homeostasis	5	20.83	0.00	GM98, NTF3, RYR1, DRD1A, TRF	18	293	13588	12.88	0.15	0.02	0.56
GO:0019725~cellular homeostasis	5	20.83	0.00	GM98, NTF3, RYR1, DRD1A, TRF	18	343	13588	11.00	0.25	0.04	1.01
GO:0048878~chemical homeostasis	5	20.83	0.00	GM98, NTF3, RYR1, DRD1A, TRF	18	365	13588	10.34	0.31	0.04	1.28
GO:0019228~regulation of action potential in neuron	3	12.50	0.00	GM98, NTF3, DRD1A	18	45	13588	50.33	0.43	0.05	1.95
GO:0010001~glial cell differentiation	3	12.50	0.00	GM98, NTF3, DRD1A	18	48	13588	47.18	0.47	0.06	2.21
GO:0042063~gliogenesis	3	12.50	0.00	GM98, NTF3, DRD1A	18	52	13588	43.55	0.53	0.06	2.59
GO:0001508~regulation of action potential	3	12.50	0.00	GM98, NTF3, DRD1A	18	54	13588	41.94	0.55	0.06	2.79
GO:0032844~regulation of homeostatic process	3	12.50	0.00	GM98, RYR1, TRF	18	60	13588	37.74	0.63	0.07	3.42
GO:0042592~homeostatic process	5	20.83	0.01	GM98, NTF3, RYR1, DRD1A, TRF	18	584	13588	6.46	0.87	0.13	6.92
GO:0042391~regulation of membrane potential	3	12.50	0.01	GM98, NTF3, DRD1A	18	119	13588	19.03	0.98	0.21	12.43
GO:0051960~regulation of nervous system development	3	12.50	0.01	GM98, NTF3, TRF	18	148	13588	15.30	1.00	0.29	18.28
GO:0051240~positive regulation of multicellular organismal process	3	12.50	0.02	GM98, DRD1A, TRF	18	163	13588	13.89	1.00	0.30	21.55
GO:0019226~transmission of nerve impulse	3	12.50	0.03	GM98, NTF3, DRD1A	18	226	13588	10.02	1.00	0.43	36.22
GO:0005783~endoplasmic reticulum	4	16.67	0.16	TMC6, NTF3, RYR1, DRD1A	22	838	12504	2.71	1.00	0.71	82.73
GO:0050877~neurological system process	3	12.50	0.64	GM98, NTF3, DRD1A	18	1681	13588	1.35	1.00	1.00	100.00
Enrichment Score: 2.011038625171804											
Term	Count	%	PValue	Genes	List Total	Pop Hits	Pop Total	Fold Enrichment	Bonferroni	Benjamini	FDR

mmu04512:ECM-receptor interaction	4	16.67	0.00	TNXB, NPNT, ITGA7, COL6A1	14	83	5738	19.75	0.01	0.01	0.54
GO:0005578~proteinaceous extracellular matrix	5	20.83	0.00	TNXB, NPNT, COL6A1, DCN, TRF	22	297	12504	9.57	0.07	0.07	1.33
GO:0031012~extracellular matrix	5	20.83	0.00	TNXB, NPNT, COL6A1, DCN, TRF	22	309	12504	9.20	0.08	0.04	1.54
extracellular matrix	4	16.67	0.00	TNXB, NPNT, COL6A1, DCN	23	213	17854	14.58	0.15	0.04	2.25
Secreted	7	29.17	0.01	NOV, NTF3, NPNT, COL6A1, DCN, CORT, TRF	23	1420	17854	3.83	0.36	0.09	6.22
GO:0044420~extracellular matrix part	3	12.50	0.01	TNXB, NPNT, TRF	22	92	12504	18.53	0.44	0.18	9.69
GO:0005576~extracellular region	8	33.33	0.02	NOV, TNXB, NTF3, NPNT, COL6A1, DCN, CORT, TRF	22	1680	12504	2.71	0.60	0.17	15.00
GO:0007155~cell adhesion	4	16.67	0.03	TNXB, NPNT, ITGA7, COL6A1	18	561	13588	5.38	1.00	0.45	35.41
GO:0022610~biological adhesion	4	16.67	0.03	TNXB, NPNT, ITGA7, COL6A1	18	562	13588	5.37	1.00	0.43	35.54
GO:0044421~extracellular region part	5	20.83	0.04	TNXB, NPNT, COL6A1, DCN, TRF	22	774	12504	3.67	0.88	0.30	31.46
mmu04510:Focal adhesion	3	12.50	0.07	TNXB, ITGA7, COL6A1	14	198	5738	6.21	0.72	0.47	41.78
cell adhesion	3	12.50	0.08	NPNT, ITGA7, COL6A1	23	380	17854	6.13	1.00	0.57	57.50
Enrichment Score: 1.1988372775752527											
Term	Count	%	PValue	Genes	List Total	Pop Hits	Pop Total	Fold Enrichment	Bonferroni	Benjamini	FDR
GO:0030001~metal ion transport	4	16.67	0.02	SCN3B, RYR1, ABCC8, TRF	18	442	13588	6.83	1.00	0.31	20.74
GO:0006812~cation transport	4	16.67	0.02	SCN3B, RYR1, ABCC8, TRF	18	515	13588	5.86	1.00	0.39	29.47
GO:0006811~ion transport	4	16.67	0.06	SCN3B, RYR1, ABCC8, TRF	18	712	13588	4.24	1.00	0.61	55.36
GO:0046873~metal ion transmembrane transporter activity	3	12.50	0.06	SCN3B, RYR1, TRF	20	290	13288	6.87	1.00	0.96	51.51
ion transport	3	12.50	0.14	SCN3B, RYR1, TRF	23	543	17854	4.29	1.00	0.71	80.00
transport	4	16.67	0.30	SCN3B, ABCA8A, RYR1, TRF	23	1571	17854	1.98	1.00	0.83	97.73
Enrichment Score: 0.9065794834487225											
Term	Co	%	PVal	Genes	List	Pop	Pop	Fold	Bonfer	Benja	FD

	unt		ue		Total	Hits	Total	Enrichment	roni	mini	R
GO:0000267~cell fraction	4	16.67	0.08	SSTR1, RYR1, RASD1, DRD1A	22	596	12504	3.81	0.99	0.47	54.05
cell membrane	5	20.83	0.15	SSTR1, ABCA8A, KIRREL2, RASD1, DRD1A	23	1713	17854	2.27	1.00	0.70	82.54
lipoprotein	3	12.50	0.16	SSTR1, RASD1, DRD1A	23	589	17854	3.95	1.00	0.69	84.32
Enrichment Score: 0.8003627619833209											
Term	Count	%	PValue	Genes	List Total	Pop Hits	Pop Total	Fold Enrichment	Bonferroni	Benjamini	FDR
GO:0000267~cell fraction	4	16.67	0.08	SSTR1, RYR1, RASD1, DRD1A	22	596	12504	3.81	0.99	0.47	54.05
receptor	6	25.00	0.18	SSTR1, ITGA7, RYR1, UNC5D, DRD1A, ABCC8	23	2465	17854	1.89	1.00	0.66	87.00
GO:0005624~membrane fraction	3	12.50	0.21	SSTR1, RYR1, DRD1A	22	510	12504	3.34	1.00	0.77	90.30
GO:0005626~insoluble fraction	3	12.50	0.22	SSTR1, RYR1, DRD1A	22	528	12504	3.23	1.00	0.75	91.58
Enrichment Score: 0.6711992262673527											
Term	Count	%	PValue	Genes	List Total	Pop Hits	Pop Total	Fold Enrichment	Bonferroni	Benjamini	FDR
Immunoglobulin domain	3	12.50	0.10	SCN3B, UNC5D, KIRREL2	23	443	17854	5.26	1.00	0.62	67.55
transmembrane region	9	37.50	0.12	TMC6, GM98, SSTR1, SCN3B, ABCA8A, ITGA7, UNC5D, KIRREL2, DRD1A	21	4113	16021	1.67	1.00	0.97	75.39
topological domain:Cytoplasmic	7	29.17	0.12	TMC6, SSTR1, SCN3B, ITGA7, UNC5D, KIRREL2, DRD1A	21	2780	16021	1.92	1.00	0.95	76.36
topological domain:Extracellular	6	25.00	0.12	SSTR1, SCN3B, ITGA7, UNC5D, KIRREL2, DRD1A	21	2174	16021	2.11	1.00	0.93	78.12
transmembrane	10	41.67	0.17	TMC6, GM98, SSTR1, SCN3B, ABCA8A, ITGA7, RYR1, UNC5D, KIRREL2, DRD1A	23	5237	17854	1.48	1.00	0.67	85.23
IPR007110:Immunoglobulin-like	3	12.50	0.17	SCN3B, UNC5D, KIRREL2	23	604	17763	3.84	1.00	1.00	87.06
receptor	6	25.00	0.18	SSTR1, ITGA7, RYR1, UNC5D, DRD1A, ABCC8	23	2465	17854	1.89	1.00	0.66	87.00
IPR013783:Immunoglobulin-like fold	3	12.50	0.19	SCN3B, UNC5D, KIRREL2	23	644	17763	3.60	1.00	1.00	89.80
membrane	10	41.67	0.21	TMC6, GM98, SSTR1, SCN3B, ABCA8A, ITGA7, UNC5D, KIRREL2, RASD1, DRD1A	23	5507	17854	1.41	1.00	0.70	91.53

GO:0016021~integral to membrane	11	45.83	0.51	TMC6, GM98, SSTR1, SCN3B, ABCA8A, ITGA7, RYR1, UNC5D, KIRREL2, DRD1A, ABCC8	22	5709	12504	1.10	1.00	0.97	99.92
GO:0031224~intrinsic to membrane	11	45.83	0.57	TMC6, GM98, SSTR1, SCN3B, ABCA8A, ITGA7, RYR1, UNC5D, KIRREL2, DRD1A, ABCC8	22	5914	12504	1.06	1.00	0.97	99.98
GO:0007166~cell surface receptor linked signal transduction	3	12.50	0.85	SSTR1, ITGA7, DRD1A	18	2495	13588	0.91	1.00	1.00	100.00
Enrichment Score: 0.44011598056537116											
Term	Count	%	PValue	Genes	List Total	Pop Hits	Pop Total	Fold Enrichment	Bonferroni	Benjamini	FDR
GO:0046873~metal ion transmembrane transporter activity	3	12.50	0.06	SCN3B, RYR1, TRF	20	290	13288	6.87	1.00	0.96	51.51
ion transport	3	12.50	0.14	SCN3B, RYR1, TRF	23	543	17854	4.29	1.00	0.71	80.00
GO:0005509~calcium ion binding	3	12.50	0.34	NPNT, ITGA7, RYR1	20	840	13288	2.37	1.00	1.00	98.97
GO:0046872~metal ion binding	7	29.17	0.49	PRDM8, TDO2, SCN3B, NPNT, ITGA7, RYR1, TRF	20	3850	13288	1.21	1.00	1.00	99.94
GO:0043169~cation binding	7	29.17	0.50	PRDM8, TDO2, SCN3B, NPNT, ITGA7, RYR1, TRF	20	3885	13288	1.20	1.00	1.00	99.95
GO:0043167~ion binding	7	29.17	0.51	PRDM8, TDO2, SCN3B, NPNT, ITGA7, RYR1, TRF	20	3934	13288	1.18	1.00	1.00	99.96
metal-binding	3	12.50	0.86	PRDM8, TDO2, TRF	23	2682	17854	0.87	1.00	1.00	100.00
GO:0046914~transition metal ion binding	3	12.50	0.91	PRDM8, TDO2, TRF	20	2608	13288	0.76	1.00	1.00	100.00
Enrichment Score: 0.13068431417330523											
Term	Count	%	PValue	Genes	List Total	Pop Hits	Pop Total	Fold Enrichment	Bonferroni	Benjamini	FDR
nucleotide-binding	3	12.50	0.61	ABCA8A, RASD1, ABCC8	23	1631	17854	1.43	1.00	0.99	99.99
GO:0032553~ribonucleotide binding	3	12.50	0.75	ABCA8A, RASD1, ABCC8	20	1796	13288	1.11	1.00	1.00	100.00
GO:0032555~purine ribonucleotide binding	3	12.50	0.75	ABCA8A, RASD1, ABCC8	20	1796	13288	1.11	1.00	1.00	100.00
GO:0017076~purine nucleotide binding	3	12.50	0.77	ABCA8A, RASD1, ABCC8	20	1871	13288	1.07	1.00	1.00	100.00
GO:0000166~nucleotide binding	3	12.50	0.84	ABCA8A, RASD1, ABCC8	20	2183	13288	0.91	1.00	1.00	100.00

References

Ablain, J., Durand, E.M., Yang, S., et al., 2015. A CRISPR/Cas9 Vector System for Tissue-Specific Gene Disruption in Zebrafish. *Dev. Cell*, 32, 756–764.

Abner, E.L., Schmitt, F.A., Nelson, P.T., et al., 2015. The Statistical Modeling of Aging and Risk of Transition Project: Data Collection and Harmonization Across 11 Longitudinal Cohort Studies of Aging, Cognition, and Dementia. *Obs. Stud.*, 1, 56–73.

Adams, D. and Oliver, C., 2010. The relationship between acquired impairments of executive function and behaviour change in adults with Down syndrome. *J. Intellect. Disabil. Res.*, 54, 393–405.

Ahlemeyer, B. and Baumgart-Vogt, E., 2005. Optimized protocols for the simultaneous preparation of primary neuronal cultures of the neocortex, hippocampus and cerebellum from individual newborn (P0.5) C57Bl/6J mice. *J. Neurosci. Methods*, 149, 110–20.

Ahmed, M.M., Dhanasekaran, A.R., Tong, S., et al., 2013. Protein profiles in Tc1 mice implicate novel pathway perturbations in the Down syndrome brain. *Hum. Mol. Genet.*, 22, 1709–24.

Ajami, B., Bennett, J.L., Krieger, C., et al., 2007. Local self-renewal can sustain CNS microglia maintenance and function throughout adult life. *Nat. Neurosci.*, 10, 1538–43.

Alarcón, R., Fuenzalida, C., Santibáñez, M., et al., 2005. Expression of scavenger receptors in glial cells. Comparing the adhesion of astrocytes and microglia from neonatal rats to surface-bound beta-amyloid. *J. Biol. Chem.*, 280, 30406–15.

Alford, K.A., Slender, A., Vanes, L., et al., 2010. Perturbed hematopoiesis in the Tc1 mouse model of Down syndrome. *Blood*, 115, 2928–37.

Alliot, F., Godin, I. and Pessac, B., 1999. Microglia derive from progenitors, originating from the yolk sac, and which proliferate in the brain. *Dev. Brain Res.*, 117, 145–152.

Ambrosini, E. and Aloisi, F., 2004. Chemokines and Glial Cells: A Complex Network in the Central Nervous System. *Neurochem. Res.*, 29, 1017–1038.

Annaert, W. and De Strooper, B., 2000. Neuronal models to study amyloid precursor protein expression and processing in vitro. *Biochim. Biophys. Acta - Mol. Basis Dis.*, 1502, 53–62.

Antonarakis, S.E., 1991. Parental origin of the extra chromosome in trisomy 21 as indicated by analysis of DNA polymorphisms. Down Syndrome Collaborative Group. *NEJM*, 324, 872–6.

Argellati, F., Massone, S., d'Abramo, C., et al., 2006. Evidence against the overexpression of APP in Down syndrome. *IUBMB Life*, 58, 103–6.

Azevedo, F.A.C., Carvalho, L.R.B., Grinberg, L.T., et al., 2009. Equal numbers of neuronal and nonneuronal cells make the human brain an isometrically scaled-up primate brain. *J. Comp. Neurol.*, 513, 532–41.

Balducci, C. and Forloni, G., 2011. APP transgenic mice: their use and limitations. *NeuroMol. Med.*, 13, 117–37.

Ball, S.L., Holland, A.J., Hon, J., et al., 2006. Personality and behaviour changes mark the early stages of Alzheimer's disease in adults with Down's syndrome: findings from a prospective population-based study. *Int. J. Geriatr. Psychiatry*, 21, 661–73.

Ball, S.L., Holland, A.J., Treppner, P., et al., 2008. Executive dysfunction and its association with personality and behaviour changes in the development of Alzheimer's disease in adults with Down syndrome and mild to moderate learning disabilities. *Br. J. Clin. Psychol.*, 47, 1–29.

Ballard, C., Gauthier, S., Corbett, A., et al., 2011. Alzheimer's disease. *Lancet*, 377, 1019–31.

Ballestín, R., Blasco-Ibáñez, J.M., Crespo, C., et al., 2014. Astrocytes of the murine model for Down Syndrome Ts65Dn display reduced intracellular ionic zinc. *Neurochem. Int.*, 75, 48–53.

Bambrick, L.L., Yarowsky, P.J. and Krueger, B.K., 2003. Altered astrocyte calcium homeostasis and proliferation in theTs65Dn mouse, a model of Down syndrome. *J. Neurosci. Res.*, 73, 89–94.

Banker, G.A. and Cowan, W.M., 1979. Further observations on hippocampal neurons in dispersed cell culture. *J. Comp. Neurol.*, 187, 469–93.

Banker, G.A. and Cowan, W.M., 1977. Rat hippocampal neurons in dispersed cell culture. *Brain Res.*, 126, 397–425.

Barbosa, S., Pratte, D., Schwarz, H., et al., 2010. Oligomeric Dop1p is part of the endosomal Neo1p-Ysl2p-Arl1p membrane remodeling complex. *Traffic*, 11, 1092–106.

Bardehle, S., Krüger, M., Buggenthin, F., et al., 2013. Live imaging of astrocyte responses to acute injury reveals selective juxtavascular proliferation. *Nat. Neurosci.*, 16, 580–6.

Barger, S.W., Van Eldik, L.J. and Mattson, M.P., 1995. S100 beta protects hippocampal neurons from damage induced by glucose deprivation. *Brain Res.*, 677, 167–70.

Barger, S.W. and Harmon, A.D., 1997. Microglial activation by Alzheimer amyloid precursor protein and modulation by apolipoprotein E. *Nature*, 388, 878–81.

Baron, R., Babcock, A.A., Nemirovsky, A., et al., 2014. Accelerated microglial pathology is associated with Aβ plaques in mouse models of Alzheimer's disease. *Aging Cell*, 13, 584–95.

Baslan, T., Kendall, J., Ward, B., et al., 2015. Optimizing sparse sequencing of single cells for highly multiplex copy number profiling. *Genome Res.*, 25, 714–24.

Beach, T.G. and McGeer, E.G., 1988. Lamina-specific arrangement of astrocytic gliosis and senile plaques in Alzheimer's disease visual cortex. *Brain Res.*, 463, 357–361.

Beaudoin, G.M.J., Lee, S.-H., Singh, D., et al., 2012. Culturing pyramidal neurons from the early postnatal mouse hippocampus and cortex. *Nat. Protoc.*, 7, 1741–54.

Beauquis, J., Pavía, P., Pomilio, C., et al., 2013. Environmental enrichment prevents astroglial pathological changes in the hippocampus of APP transgenic mice, model of Alzheimer's disease. *Exp. Neurol.*, 239, 28–37.

Beauquis, J., Vinuesa, A., Pomilio, C., et al., 2014. Neuronal and glial alterations, increased anxiety, and cognitive impairment before hippocampal amyloid deposition in PDAPP mice, model of Alzheimer's disease. *Hippocampus*, 24, 257–269.

Von Bernhardi, R., 2007. Glial cell dysregulation: a new perspective on Alzheimer disease. *Neurotox. Res.*, 12, 215–32.

Von Bernhardi, R., Eugenín-von Bernhardi, L. and Eugenín, J., 2015. Microglial cell dysregulation in brain aging and neurodegeneration. *Front. Aging Neurosci.*, 7, 124.

Bertram, L. and Tanzi, R.E., 2008. Thirty years of Alzheimer's disease genetics: the implications of systematic meta-analyses. *Nat. Rev. Neurosci.*, 9, 768–78.

Bhalla, A., Vetanovetz, C.P., Morel, E., et al., 2012. The location and trafficking routes of the neuronal retromer and its role in amyloid precursor protein transport. *Neurobiol. Dis.*, 47, 126–134.

Biffi, E., Regalia, G., Menegon, A., et al., 2013. The influence of neuronal density and maturation on network activity of hippocampal cell cultures: A methodological study. *PLoS One*, 8, e83899.

Bittles, A.H. and Glasson, E.J., 2004. Clinical, social, and ethical implications of changing life expectancy in Down syndrome. *Dev. Med. Child Neurol.*, 46, 282–6.

Blasko, I., Stampfer-Kountchev, M., Robatscher, P., et al., 2004. How chronic inflammation can affect the brain and support the development of Alzheimer's disease in old age: the role of microglia and astrocytes. *Aging Cell*, 3, 169–76.

Blennow, K., de Leon, M.J. and Zetterberg, H., 2006. Alzheimer's disease. *Lancet*, 368, 387–403.

Bomben, V., Holth, J., Reed, J., et al., 2014. Bexarotene reduces network excitability in models of Alzheimer's disease and epilepsy. *Neurobiol. Aging*, 35, 2091–5.

Bossers, K., Wirz, K.T.S., Meerhoff, G.F., et al., 2010. Concerted changes in transcripts in the prefrontal cortex precede neuropathology in Alzheimer's disease. *Brain*, 133, 3699–723.

Braak, H. and Braak, E., 1991. Neuropathological stageing of Alzheimer-related changes. *Acta Neuropathol.*, 82, 239–259.

Braidy, N., Muñoz, P., Palacios, A.G., et al., 2012. Recent rodent models for Alzheimer's disease: clinical implications and basic research. *J. Neural Transm.*, 119, 173–95.

Braudeau, J., Dauphinot, L., Duchon, A., et al., 2011. Chronic Treatment with a Promnesiant GABA-A α5-Selective Inverse Agonist Increases Immediate Early Genes Expression during Memory Processing in Mice and Rectifies Their Expression Levels in a Down Syndrome Mouse Model. *Adv. Pharmacol. Sci.*, 2011, 153218.

Brault, V., Duchon, A., Romestaing, C., et al., 2015. Opposite Phenotypes of Muscle Strength and Locomotor Function in Mouse Models of Partial Trisomy and Monosomy 21 for the Proximal Hspa13-App Region. *PLoS Genet.*, 11, e1005062.

Brault, V., Pereira, P., Duchon, A., et al., 2006. Modeling chromosomes in mouse to explore the function of genes, genomic disorders, and chromosomal organization. *PLoS Genet.*, 2, e86.

Brosseron, F., Krauthausen, M., Kummer, M., et al., 2014. Body fluid cytokine levels in mild cognitive impairment and Alzheimer's disease: a comparative overview. *Mol. Neurobiol.*, 50, 534–44.

Bu, G., 2009. Apolipoprotein E and its receptors in Alzheimer's disease: pathways, pathogenesis and therapy. *Nat. Rev. Neurosci.*, 10, 333–44.

Buggia-Prévot, V., Fernandez, C.G., Riordan, S., et al., 2014. Axonal BACE1 dynamics and targeting in hippocampal neurons: a role for Rab11 GTPase. *Mol. Neurodegener.*, 9, 1.

Burns, A. and Iliffe, S., 2009. Alzheimer's disease. *BMJ*, 338, b158.

Bush, A. and Beail, N., 2004. Risk factors for dementia in people with down syndrome: issues in assessment and diagnosis. *Am. J. Ment. Retard.*, 109, 83–97.

Bushong, E.A., Martone, M.E., Jones, Y.Z., et al., 2002. Protoplasmic astrocytes in CA1 stratum radiatum occupy separate anatomical domains. *J. Neurosci.*, 22, 183–92.

Butterfield, D.A., Di Domenico, F., Swomley, A.M., et al., 2014. Redox proteomics analysis to decipher the neurobiology of Alzheimer-like neurodegeneration: overlaps in Down's syndrome and Alzheimer's disease brain. *Biochem. J.*, 463, 177–89.

Cai, X.D., Golde, T.E. and Younkin, S.G., 1993. Release of excess amyloid beta protein from a mutant amyloid beta protein precursor. *Science*, 259, 514–6.

Carlson, G.A., Borchelt, D.R., Dake, A., et al., 1997. Genetic modification of the phenotypes produced by amyloid precursor protein overexpression in transgenic mice. *Hum. Mol. Genet.*, 6, 1951–1959.

Carson, M.J., Doose, J.M., Melchior, B., et al., 2006. CNS immune privilege: hiding in plain sight. *Immunol. Rev.*, 213, 48–65.

Castellani, R.J. and Perry, G., 2014. The complexities of the pathology-pathogenesis relationship in Alzheimer disease. *Biochem. Pharmacol.*, 88, 671–6.

Cataldo, A.M., Peterhoff, C.M., Troncoso, J.C., et al., 2000. Endocytic pathway abnormalities precede amyloid beta deposition in sporadic Alzheimer's disease and Down syndrome: differential effects of APOE genotype and presenilin mutations. *Am J Pathol*, 157, 277–286.

Van Cauwenberghe, C., Van Broeckhoven, C. and Sleegers, K., 2015. The genetic landscape of Alzheimer disease: clinical implications and perspectives. *Genet. Med.*

Cenini, G., Dowling, A.L.S., Beckett, T.L., et al., 2012. Association between frontal cortex oxidative damage and beta-amyloid as a function of age in Down syndrome. *Biochim. Biophys. Acta - Mol. Basis Dis.*, 1822, 130–138.

Cermakian, N., Lamont, E.W., Boudreau, P., et al., 2011. Circadian clock gene expression in brain regions of Alzheimer 's disease patients and control subjects. *J. Biol. Rhythms*, 26, 160–70.

Chan, G., White, C.C., Winn, P.A., et al., 2015. CD33 modulates TREM2: convergence of Alzheimer loci. *Nat. Neurosci.*, In press.

Chan, W.Y., Xia, C.-L., Dong, D.-C., et al., 2003. Differential expression of S100 proteins in the developing human hippocampus and temporal cortex. *Microsc. Res. Tech.*, 60, 600–13.

Chang, C.-Y., Chen, S.-M., Lu, H.-E., et al., 2015. N-butylidenephthalide Attenuates Alzheimer's Disease-Like Cytopathy in Down Syndrome Induced Pluripotent Stem Cell-Derived Neurons. *Sci. Rep.*, 5, 8744.

Chang, K.T. and Min, K.-T.T., 2009. Upregulation of three Drosophila homologs of human chromosome 21 genes alters synaptic function: implications for Down syndrome. *Proc. Natl. Acad. Sci. U. S. A.*, 106, 17117–17122.

Chapman, J., Rees, E., Harold, D., et al., 2013. A genome-wide study shows a limited contribution of rare copy number variants to Alzheimer's disease risk. *Hum. Mol. Genet.*, 22, 816–24.

Cheng, X., Wu, J., Geng, M., et al., 2014. Role of synaptic activity in the regulation of amyloid beta levels in Alzheimer's disease. *Neurobiol. Aging*, 35, 1217–32.

Cheng, Y., Ma, Z., Kim, B.-H., et al., 2014. Principles of regulatory information conservation between mouse and human. *Nature*, 515, 371–375.

Cheon, M.S., Bajo, M., Kim, S.H., et al., 2003. Protein levels of genes encoded on chromosome 21 in fetal Down syndrome brain: challenging the gene dosage effect hypothesis (Part II). *Amino Acids*, 24, 119–25.

Cheon, M.S., Dierssen, M., Kim, S.H., et al., 2008. Protein expression of BACE1, BACE2 and APP in Down syndrome brains. *Amino Acids*, 35, 339–43.

Cheon, M.S., Kim, S.H., Ovod, V., et al., 2003. Protein levels of genes encoded on chromosome 21 in fetal Down syndrome brain: challenging the gene dosage effect hypothesis (Part III). *Amino Acids*, 24, 127–134.

Cheon, M.S., Kim, S.H., Yaspo, M.-L., et al., 2003. Protein levels of genes encoded on chromosome 21 in fetal Down syndrome brain: challenging the gene dosage effect hypothesis (Part I). *Amino Acids*, 24, 111–7.

Cheon, M.S., Shim, K.S., Kim, S.H., et al., 2003. Protein levels of genes encoded on chromosome 21 in fetal Down syndrome brain: Challenging the gene dosage effect hypothesis (Part IV). *Amino Acids*, 25, 41–7.

De Chiara, G., Marcocci, M.E., Civitelli, L., et al., 2010. APP Processing Induced by Herpes Simplex Virus Type 1 (HSV-1) Yields Several APP Fragments in Human and Rat Neuronal Cells J. A. Blaho, ed. *PLoS One*, 5, e13989.

Cho, H.S., Kim, S.S., Choi, W., et al., 1995. Age-related changes of mRNA expression of amyloid precursor protein in the brain of senescence-accelerated mouse. *Comp. Biochem. Physiol. B. Biochem. Mol. Biol.*, 112, 399–404.

Choi, J.H.K., Berger, J.D., Mazzella, M.J., et al., 2009. Age-dependent dysregulation of brain amyloid precursor protein in the Ts65Dn Down syndrome mouse model. *J. Neurochem.*, 110, 1818–27.

Choong, X.Y., Tosh, J.L., Pulford, L.J., et al., 2015. Dissecting Alzheimer disease in Down syndrome using mouse models. *Front. Behav. Neurosci.*, In press.

Christensen, D.Z., Thomsen, M.S. and Mikkelsen, J.D., 2013. Reduced basal and novelty-induced levels of activity-regulated cytoskeleton associated protein (Arc) and c-Fos mRNA in the cerebral cortex and hippocampus of APPswe/PS1ΔE9 transgenic mice. *Neurochem. Int.*, 63, 54–60.

Chun, L.E., Woodruff, E.R., Morton, S., et al., 2015. Variations in Phase and Amplitude of Rhythmic Clock Gene Expression across Prefrontal Cortex, Hippocampus, Amygdala, and

Hypothalamic Paraventricular and Suprachiasmatic Nuclei of Male and Female Rats. *J. Biol. Rhythms*, 30, 417–36.

Churchill, S.S., Kieckhefer, G.M., Landis, C. a., et al., 2012. Sleep measurement and monitoring in children with Down syndrome: A review of the literature, 1960-2010. *Sleep Med. Rev.*, 16, 477–488.

Cissé, M., Halabisky, B., Harris, J., et al., 2011. Reversing EphB2 depletion rescues cognitive functions in Alzheimer model. *Nature*, 469, 47–52.

Cissé, M., Sanchez, P.E., Kim, D.H., et al., 2011. Ablation of cellular prion protein does not ameliorate abnormal neural network activity or cognitive dysfunction in the J20 line of human amyloid precursor protein transgenic mice. *J. Neurosci.*, 31, 10427–31.

Citron, M., Oltersdorf, T., Haass, C., et al., 1992. Mutation of the beta-amyloid precursor protein in familial Alzheimer's disease increases beta-protein production. *Nature*, 360, 672–4.

Cohen, E., Ivenshitz, M., Amor-Baroukh, V., et al., 2008. Determinants of spontaneous activity in networks of cultured hippocampus. *Brain Res.*, 1235, 21–30.

Condello, C., Yuan, P., Schain, A., et al., 2015. Microglia constitute a barrier that prevents neurotoxic protofibrillar Aβ42 hotspots around plaques. *Nat. Commun.*, 6, 6176.

Contestabile, A., Fila, T., Bartesaghi, R., et al., 2006. Choline acetyltransferase activity at different ages in brain of Ts65Dn mice, an animal model for Down's syndrome and related neurodegenerative diseases. *J. Neurochem.*, 97, 515–26.

Conti, E., Galimberti, G., Piazza, F., et al., 2010. Increased soluble APPalpha, Abeta 1-42, and anti-Abeta 1-42 antibodies in plasma from down syndrome patients. *Alzheimer Dis. Assoc. Disord.*, 24, 96–100.

Coppus, A., Evenhuis, H., Verberne, G.-J., et al., 2006. Dementia and mortality in persons with Down's syndrome. *J. Intellect. Disabil. Res.*, 50, 768–77.

Coppus, A.M.W., Schuur, M., Vergeer, J., et al., 2012. Plasma β amyloid and the risk of Alzheimer's disease in Down syndrome. *Neurobiol. Aging*, 33, 1988–94.

Corder, E.H., Saunders, A.M., Strittmatter, W.J., et al., 1993. Gene dose of apolipoprotein E type 4 allele and the risk of Alzheimer's disease in late onset families. *Science*, 261, 921–923.

Cortés-Mendoza, J., Díaz de León-Guerrero, S., Pedraza-Alva, G., et al., 2013. Shaping synaptic plasticity: the role of activity-mediated epigenetic regulation on gene transcription. *Int. J. Dev. Neurosci.*, 31, 359–69.

Cossec, J.C., Lavaur, J., Berman, D.E., et al., 2012. Trisomy for synaptojanin1 in down syndrome is functionally linked to the enlargement of early endosomes. *Hum. Mol. Genet.*, 21, 3156–3172.

Costa, V., Angelini, C., D'Apice, L., et al., 2011. Massive-scale rna-seq analysis of non ribosomal transcriptome in human trisomy 21. *PLoS One*, 6, e18493.

Crocker, P.R., McMillan, S.J. and Richards, H.E., 2012. CD33-related siglecs as potential modulators of inflammatory responses. *Ann. N. Y. Acad. Sci.*, 1253, 102–111.

Cruz, F.C., Koya, E., Guez-Barber, D.H., et al., 2013. New technologies for examining the role of neuronal ensembles in drug addiction and fear. *Nat. Rev. Neurosci.*, 14, 743–54.

Cullen, D.K., Gilroy, M.E., Irons, H.R., et al., 2010. Synapse-to-neuron ratio is inversely related to neuronal density in mature neuronal cultures. *Brain Res.*, 1359, 44–55.

Cullen, P.J. and Korswagen, H.C., 2011. Sorting nexins provide diversity for retromer-dependent trafficking events. *Nat. Cell Biol.*, 14, 29–37.

Dalal, N. V, Pranski, E.L., Tansey, M.G., et al., 2012. RNF11 modulates microglia activation through NF-κB signalling cascade. *Neurosci. Lett.*, 528, 174–9.

Damani, M.R., Zhao, L., Fontainhas, A.M., et al., 2011. Age-related alterations in the dynamic behavior of microglia. *Aging Cell*, 10, 263–76.

Das, U., Scott, D.A., Ganguly, A., et al., 2013. Activity-induced convergence of APP and BACE-1 in acidic microdomains via an endocytosis-dependent pathway. *Neuron*, 79, 447–60.

Davalos, D., Grutzendler, J., Yang, G., et al., 2005. ATP mediates rapid microglial response to local brain injury in vivo. *Nat. Neurosci.*, 8, 752–8.

Davidsson, J., 2014. The epigenetic landscape of aneuploidy: constitutional mosaicism leading the way? *Epigenomics*, 6, 45–58.

Davisson, M.T., Schmidt, C., Reeves, R.H., et al., 1993. Segmental trisomy as a mouse model for Down syndrome. *Prog. Clin. Biol. Res.*, 384, 117–33.

Deacon, R.M.J. and Rawlins, J.N.P., 2006. T-maze alternation in the rodent. *Nat. Protoc.*, 1, 7–12.

Dekker, A.D., Coppus, A.M.W., Vermeiren, Y., et al., 2015. Serum MHPG strongly predicts conversion to Alzheimer's disease in behaviorally characterized subjects with Down syndrome. *J. Alzheimer's Dis.*, 43, 871–91.

Dekker, A.D., De Deyn, P.P. and Rots, M.G., 2014. Epigenetics: the neglected key to minimize learning and memory deficits in Down syndrome. *Neurosci. Biobehav. Rev.*, 45, 72–84.

Del-Aguila, J.L., Koboldt, D.C., Black, K., et al., 2015. Alzheimer's disease: rare variants with large effect sizes. *Curr. Opin. Genet. Dev.*, 33, 49–55.

Dickey, C.A., Gordon, M.N., Mason, J.E., et al., 2004. Amyloid suppresses induction of genes critical for memory consolidation in APP + PS1 transgenic mice. *J. Neurochem.*, 88, 434–42.

Dickey, C.A., Loring, J.F., Montgomery, J., et al., 2003. Selectively reduced expression of synaptic plasticity-related genes in amyloid precursor protein + presenilin-1 transgenic mice. *J. Neurosci.*, 23, 5219–26.

Dierssen, M., Herault, Y. and Estivill, X., 2009. Aneuploidy: from a physiological mechanism of variance to Down syndrome. *Physiol. Rev.*, 89, 887–920.

Diomedi, M., Curatolo, P., Scalise, A., et al., 1999. Sleep abnormalities in mentally retarded autistic subjects: Down's syndrome with mental retardation and normal subjects. *Brain Dev.*, 21, 548–53.

Donahue, J.E., Khurana, J.S. and Adelman, L.S., 1998. Intracerebral hemorrhage in two patients with Down's syndrome and cerebral amyloid angiopathy. *Acta Neuropathol.*, 95, 213–6.

Dorfman, V.B., Pasquini, L., Riudavets, M., et al., 2010. Differential cerebral deposition of IDE and NEP in sporadic and familial Alzheimer's disease. *Neurobiol. Aging*, 31, 1743–57.

Dragunow, M., 1996. A role for immediate-early transcription factors in learning and memory. *Behav. Genet.*, 26, 293–9.

Duchon, A., Raveau, M., Chevalier, C., et al., 2011. Identification of the translocation breakpoints in the Ts65Dn and Ts1Cje mouse lines: relevance for modeling Down syndrome. *Mamm. Genome*, 22, 674–84.

Dunlevy, L., Bennett, M., Slender, A., et al., 2010. Down's syndrome-like cardiac developmental defects in embryos of the transchromosomic Tc1 mouse. *Cardiovasc. Res.*, 88, 287–295.

Dyrks, T., Weidemann, A., Multhaup, G., et al., 1988. Identification, transmembrane orientation and biogenesis of the amyloid A4 precursor of Alzheimer's disease. *EMBO J.*, 7, 949–57.

Edwards, J.P., Zhang, X., Frauwirth, K.A., et al., 2006. Biochemical and functional characterization of three activated macrophage populations. *J. Leukoc. Biol.*, 80, 1298–307.

Egensperger, R., Weggen, S., Ida, N., et al., 1999. Reverse relationship between beta-amyloid precursor protein and beta-amyloid peptide plaques in Down's syndrome versus sporadic/familial Alzheimer's disease. *Acta Neuropathol.*, 97, 113–8.

Elder, G. a., Gama Sosa, M. a. and De Gasperi, R., 2010. Transgenic mouse models of Alzheimer's disease. *Mt. Sinai J. Med.*, 77, 69–81.

Evenhuis, H.M., 1990. The natural history of dementia in Down's syndrome. *Arch. Neurol.*, 47, 263–7.

Feillet, C.A., Mendoza, J., Albrecht, U., et al., 2008. Forebrain oscillators ticking with different clock hands. *Mol. Cell. Neurosci.*, 37, 209–21.

Fernandez, F. and Edgin, J.O., 2013. Poor Sleep as a Precursor to Cognitive Decline in Down Syndrome : A Hypothesis. *J. Alzheimer's Dis. Park.*, 3, 124.

Floden, A.M. and Combs, C.K., 2011. Microglia demonstrate age-dependent interaction with amyloid-β fibrils. *J. Alzheimer's Dis.*, 25, 279–93.

Flores-Ramírez, F., Palacios-Guerrero, C., García-Delgado, C., et al., 2015. Cytogenetic Profile in 1,921 Cases of Trisomy 21 Syndrome in Mexican Patients. *Arch. Med. Res.*, 46, 484–489.

Freeman, S.B., Bean, L.H., Allen, E.G., et al., 2008. Ethnicity, sex, and the incidence of congenital heart defects: a report from the National Down Syndrome Project. *Genet. Med.*, 10, 173–80.

Galante, M., Jani, H., Vanes, L., et al., 2009. Impairments in motor coordination without major changes in cerebellar plasticity in the Tc1 mouse model of Down syndrome. *Hum. Mol. Genet.*, 18, 1449–1463.

Games, D., Adams, D., Alessandrini, R., et al., 1995. Alzheimer-type neuropathology in transgenic mice overexpressing V717F beta-amyloid precursor protein. *Nature*, 373, 523–7.

Gast, H., Gordic, S., Petrzilka, S., et al., 2012. Transforming growth factor-beta inhibits the expression of clock genes. *Ann. N. Y. Acad. Sci.*, 1261, 79–87.

Gatz, M., Reynolds, C.A., Fratiglioni, L., et al., 2006. Role of genes and environments for explaining Alzheimer disease. *Arch. Gen. Psychiatry*, 63, 168–74.

Geller, H.M., Cheng, K.-Y., Goldsmith, N.K., et al., 2001. Oxidative stress mediates neuronal DNA damage and apoptosis in response to cytosine arabinoside. *J. Neurochem.*, 78, 265–275.

Gerlach, R., Demel, G., König, H.-G., et al., 2006. Active secretion of S100B from astrocytes during metabolic stress. *Neuroscience*, 141, 1697–701.

Ghezzo, A., Salvioli, S., Solimando, M.C., et al., 2014. Age-Related Changes of Adaptive and Neuropsychological Features in Persons with Down Syndrome. *PLoS One*, 9, e113111.

Ginhoux, F., Greter, M., Leboeuf, M., et al., 2010. Fate mapping analysis reveals that adult microglia derive from primitive macrophages. *Science*, 330, 841–5.

Glanzer, J.G., Enose, Y., Wang, T., et al., 2007. Genomic and proteomic microglial profiling: pathways for neuroprotective inflammatory responses following nerve fragment clearance and activation. *J. Neurochem.*, 102, 627–45.

Glenner, G.G. and Wong, C.W., 1984a. Alzheimer's disease: initial report of the purification and characterization of a novel cerebrovascular amyloid protein. *Biochem. Biophys. Res. Commun.*, 120, 885–90.

Glenner, G.G. and Wong, C.W., 1984b. Alzheimer's disease and Down's syndrome: sharing of a unique cerebrovascular amyloid fibril protein. *Biochem. Biophys. Res. Commun.*, 122, 1131–5.

Goate, A., Chartier-Harlin, M.C., Mullan, M., et al., 1991. Segregation of a missense mutation in the amyloid precursor protein gene with familial Alzheimer's disease. *Nature*, 349, 704–6.

Goedert, M., Spillantini, M.G., Cairns, N.J., et al., 1992. Tau proteins of Alzheimer paired helical filaments: abnormal phosphorylation of all six brain isoforms. *Neuron*, 8, 159–68.

De Graaf, G., Buckley, F. and Skotko, B.G., 2015. Estimates of the live births, natural losses, and elective terminations with Down syndrome in the United States. *Am. J. Med. Genet. A*, 167, 756–67.

Graeber, M.B. and Streit, W.J., 2010. Microglia: biology and pathology. *Acta Neuropathol.*, 119, 89–105.

Grathwohl, S.A., Kälin, R.E., Bolmont, T., et al., 2009. Formation and maintenance of Alzheimer's disease beta-amyloid plaques in the absence of microglia. *Nat. Neurosci.*, 12, 1361–3.

Gribble, S.M., Wiseman, F.K., Clayton, S., et al., 2013. Massively Parallel Sequencing Reveals the Complex Structure of an Irradiated Human Chromosome on a Mouse Background in the Tc1 Model of Down Syndrome. *PLoS One*, 8, e60482.

Griciuc, A., Serrano-Pozo, A., Parrado, A.R., et al., 2013. Alzheimer's disease risk gene CD33 inhibits microglial uptake of amyloid beta. *Neuron*, 78, 631–43.

Griffin, W.S., Sheng, J.G., McKenzie, J.E., et al., 1998. Life-long overexpression of S100beta in Down's syndrome: implications for Alzheimer pathogenesis. *Neurobiol. Aging*, 19, 401–5.

Griffin, W.S., Stanley, L.C., Ling, C., et al., 1989. Brain interleukin 1 and S-100 immunoreactivity are elevated in Down syndrome and Alzheimer disease. *Proc. Natl. Acad. Sci. U. S. A.*, 86, 7611–5.

Griffin, W.S.T. and Mrak, R.E., 2002. Interleukin-1 in the genesis and progression of and risk for development of neuronal degeneration in Alzheimer's disease. *J. Leukoc. Biol.*, 72, 233–8.

Griffiths-Jones, S., 2004. The microRNA Registry. *Nucleic Acids Res.*, 32, D109–D111.

Guerreiro, R., Wojtas, A., Bras, J., et al., 2013. TREM2 variants in Alzheimer's disease. *NEJM*, 368, 117–27.

Guidi, S., Bonasoni, P., Ceccarelli, C., et al., 2008. Neurogenesis impairment and increased cell death reduce total neuron number in the hippocampal region of fetuses with Down syndrome. *Brain Pathol.*, 18, 180–97.

Guidi, S., Ciani, E., Bonasoni, P., et al., 2011. Widespread proliferation impairment and hypocellularity in the cerebellum of fetuses with down syndrome. *Brain Pathol.*, 21, 361–73.

Guzowski, J.F., McNaughton, B.L., Barnes, C.A., et al., 1999. Environment-specific expression of the immediate-early gene Arc in hippocampal neuronal ensembles. *Nat. Neurosci.*, 2, 1120–4.

Haas, M. a, Bell, D., Slender, A., et al., 2013. Alterations to dendritic spine morphology, but not dendrite patterning, of cortical projection neurons in Tc1 and Ts1Rhr mouse models of Down syndrome. *PLoS One*, 8, e78561.

Haass, C., Hung, A.Y. and Selkoe, D.J., 1991. Processing of beta-amyloid precursor protein in microglia and astrocytes favors an internal localization over constitutive secretion. *J. Neurosci.*, 11, 3783–93.

Haass, C., Kaether, C., Thinakaran, G., et al., 2012. Trafficking and proteolytic processing of APP. *Cold Spring Harb Perspect Med*, 2, a006270.

Haass, C., Lemere, C.A., Capell, A., et al., 1995. The Swedish mutation causes early-onset Alzheimer's disease by β-secretase cleavage within the secretory pathway. *Nat. Med.*, 1, 1291–1296.

Ben Haim, L., Carrillo-de Sauvage, M.-A., Ceyzériat, K., et al., 2015. Elusive roles for reactive astrocytes in neurodegenerative diseases. *Front. Cell. Neurosci.*, 9, 278.

Hall, A.M. and Roberson, E.D., 2012. Mouse models of Alzheimer's disease. *Brain Res. Bull.*, 88, 3–12.

Harbour, V.L., Weigl, Y., Robinson, B., et al., 2013. Comprehensive mapping of regional expression of the clock protein PERIOD2 in rat forebrain across the 24-h day. *PLoS One*, 8, e76391.

Hardy, J. and Selkoe, D.J., 2002. The amyloid hypothesis of Alzheimer's disease: progress and problems on the road to therapeutics. *Science*, 297, 353–356.

Hardy, J.A. and Higgins, G.A., 1992. Alzheimer's disease: the amyloid cascade hypothesis. *Science*, 256, 184–5.

Harrill, J. a, Chen, H., Streifel, K.M., et al., 2015. Ontogeny of biochemical, morphological and functional parameters of synaptogenesis in primary cultures of rat hippocampal and cortical neurons. *Mol. Brain*, 8, 10.

Hartikka, J. and Hefti, F., 1988. Development of septal cholinergic neurons in culture: plating density and glial cells modulate effects of NGF on survival, fiber growth, and expression of transmitter-specific enzymes. *J. Neurosci.*, 8, 2967–85.

Hartley, D., Blumenthal, T., Carrillo, M., et al., 2015. Down syndrome and Alzheimer's disease: Common pathways, common goals. *Alzheimer's Dementia*, 11, 700–9.

Hartzell, A.L., Burke, S.N., Hoang, L.T., et al., 2013. Transcription of the immediate-early gene Arc in CA1 of the hippocampus reveals activity differences along the proximodistal axis that are attenuated by advanced age. *J. Neurosci.*, 33, 3424–33.

Hashioka, S., Miklossy, J., Schwab, C., et al., 2008. Adhesion of exogenous human microglia and THP-1 cells to amyloid plaques of postmortem Alzheimer's disease brain. *J. Alzheimer's Dis.*, 14, 345–52.

Hattori, M., Fujiyama, A., Taylor, T.D., et al., 2000. The DNA sequence of human chromosome 21. *Nature*, 405, 311–9.

Head, E., Doran, E., Nistor, M., et al., 2011. Plasma amyloid-β as a function of age, level of intellectual disability, and presence of dementia in Down syndrome. *J. Alzheimer's Dis.*, 23, 399–409.

Head, E., Garzon-Rodriguez, W., Johnson, J.K., et al., 2001. Oxidation of Abeta and plaque biogenesis in Alzheimer's disease and Down syndrome. *Neurobiol. Dis.*, 8, 792–806.

Hebert, L.E., Weuve, J., Scherr, P.A., et al., 2013. Alzheimer disease in the United States (2010-2050) estimated using the 2010 census. *Neurology*, 80, 1778–83.

Heise, I., Fisher, S.P., Banks, G.T., et al., 2015. Sleep-like behavior and 24-h rhythm disruption in the Tc1 mouse model of Down syndrome. *Genes, Brain Behav.*, 14, 209–16.

Helguera, P., Seiglie, J., Rodriguez, J., et al., 2013. Adaptive downregulation of mitochondrial function in down syndrome. *Cell Metab.*, 17, 132–140.

Hendrickx, A., Pierrot, N., Tasiaux, B., et al., 2014. Epigenetic regulations of immediate early genes expression involved in memory formation by the amyloid precursor protein of alzheimer disease. *PLoS One*, 9, e99467.

Heneka, M.T., Kummer, M.P. and Latz, E., 2014. Innate immune activation in neurodegenerative disease. *Nat. Rev. Immunol.*, 14, 463–77.

Herault, Y., Lopes, P., Magnol, L., et al., 2009. Tackling the complexity of the genotype–phenotype relationship in the Down syndrome with the mouse aneuploidy zoo: a resource of new models to study aneuploidies involving human chromosome 21. In *The American Society of Human Genetics 59th Annual Meeting, Honolulu HI, 20–24 October 2009*.

Herrup, K., 2015. The case for rejecting the amyloid cascade hypothesis. *Nat. Neurosci.*, 18, 794–799.

Heurtaux, T., Michelucci, A., Losciuto, S., et al., 2010. Microglial activation depends on beta-amyloid conformation: role of the formylpeptide receptor 2. *J. Neurochem.*, 114, 576–586.

Hickey, W.F., Vass, K. and Lassmann, H., 1992. Bone marrow-derived elements in the central nervous system: an immunohistochemical and ultrastructural survey of rat chimeras. *J. Neuropathol. Exp. Neurol.*, 51, 246–56.

Hickman, S.E., Allison, E.K. and El Khoury, J., 2008. Microglial dysfunction and defective beta-amyloid clearance pathways in aging Alzheimer's disease mice. *J. Neurosci.*, 28, 8354–60.

Holland, A.J., Hon, J., Huppert, F.A., et al., 1998. Population-based study of the prevalence and presentation of dementia in adults with Down's syndrome. *Br. J. Psychiatry*, 172, 493–8.

Holland, A.J., Hon, J., Huppert, F.A., et al., 2000. Incidence and course of dementia in people with Down's syndrome: findings from a population-based study. *J. Intellect. Disabil. Res.*, 44 (Pt 2), 138–46.

Hollingworth, P., Harold, D., Sims, R., et al., 2011. Common variants at ABCA7, MS4A6A/MS4A4E, EPHA1, CD33 and CD2AP are associated with Alzheimer's disease. *Nat. Genet.*, 43, 429–35.

Holmes, C., Cunningham, C., Zotova, E., et al., 2009. Systemic inflammation and disease progression in Alzheimer disease. *Neurology*, 73, 768–774.

Holtta, M., Hansson, O., Andreasson, U., et al., 2013. Evaluating amyloid-beta oligomers in cerebrospinal fluid as a biomarker for Alzheimer's disease. *PLoS One*, 8, e66381.

Hooli, B. V, Mohapatra, G., Mattheisen, M., et al., 2012. Role of common and rare APP DNA sequence variants in Alzheimer disease. *Neurology*, 78, 1250–7.

Horvath, S., Garagnani, P., Bacalini, M.G., et al., 2015. Accelerated epigenetic aging in Down syndrome. *Aging Cell*, 14, 491–5.

Hosack, D. a, Dennis, G., Sherman, B.T., et al., 2003. Identifying biological themes within lists of genes with EASE. *Genome Biol.*, 4, R70.

Hsia, A.Y., Masliah, E., McConlogue, L., et al., 1999. Plaque-independent disruption of neural circuits in Alzheimer's disease mouse models. *Proc. Natl. Acad. Sci. U. S. A.*, 96, 3228–3233.

Huang, D.W., Sherman, B.T. and Lempicki, R.A., 2009. Systematic and integrative analysis of large gene lists using DAVID bioinformatics resources. *Nat. Protoc.*, 4, 44–57.

Humphries, C., Kohli, M.A., Whitehead, P., et al., 2015. Alzheimer disease (AD) specific transcription, DNA methylation and splicing in twenty AD associated loci. *Mol. Cell. Neurosci.*, 67, 37–45.

Hung, A.Y., Koo, E.H., Haass, C., et al., 1992. Increased expression of beta-amyloid precursor protein during neuronal differentiation is not accompanied by secretory cleavage. *Proc. Natl. Acad. Sci. U. S. A.*, 89, 9439–9443.

Hunter, C.L., Bachman, D. and Granholm, A.-C., 2004. Minocycline prevents cholinergic loss in a mouse model of Down's syndrome. *Ann. Neurol.*, 56, 675–88.

Iliff, J.J. and Nedergaard, M., 2013. Is There a Cerebral Lymphatic System? *Stroke*, 44, S93–S95.

in t' Veld, B.A., Ruitenberg, A., Hofman, A., et al., 2001. Nonsteroidal antiinflammatory drugs and the risk of Alzheimer's disease. *NEJM*, 345, 1515–21.

Iqbal, K., Alonso, A. del C., Chen, S., et al., 2005. Tau pathology in Alzheimer disease and other tauopathies. *Biochim. Biophys. Acta*, 1739, 198–210.

Itagaki, S., McGeer, P.L., Akiyama, H., et al., 1989. Relationship of microglia and astrocytes to amyloid deposits of Alzheimer disease. *J. Neuroimmunol.*, 24, 173–82.

Ito, M., Kodama, M., Masuko, M., et al., 2000. Expression of coxsackievirus and adenovirus receptor in hearts of rats with experimental autoimmune myocarditis. *Circ. Res.*, 86, 275–80.

Ivenshitz, M. and Segal, M., 2010. Neuronal density determines network connectivity and spontaneous activity in cultured hippocampus. *J. Neurophysiol.*, 104, 1052–60.

Iwashyna, T.J., Ely, E.W., Smith, D.M., et al., 2010. Long-term cognitive impairment and functional disability among survivors of severe sepsis. *JAMA*, 304, 1787–94.

Jackson, H.M., Onos, K.D., Pepper, K.W., et al., 2015. DBA/2J genetic background exacerbates spontaneous lethal seizures but lessens amyloid deposition in a mouse model of Alzheimer's disease. *PLoS One*, 10, e0125897.

Jensen, K.M. and Bulova, P.D., 2014. Managing the care of adults with Down's syndrome. *BMJ*, 349, g5596.

Jensen, M.B., Finsen, B. and Zimmer, J., 1997. Morphological and immunophenotypic microglial changes in the denervated fascia dentata of adult rats: correlation with blood-brain barrier damage and astroglial reactions. *Exp. Neurol.*, 143, 103–16.

Jilg, A., Lesny, S., Peruzki, N., et al., 2010. Temporal dynamics of mouse hippocampal clock gene expression support memory processing. *Hippocampus*, 20, 377–88.

Johnston, J.A., Cowburn, R.F., Norgren, S., et al., 1994. Increased beta-amyloid release and levels of amyloid precursor protein (APP) in fibroblast cell lines from family members with the Swedish Alzheimer's disease APP670/671 mutation. *FEBS Lett.*, 354, 274–8.

Jonas, R.A., Yuan, T.-F., Liang, Y.-X., et al., 2012. The Spider Effect: Morphological and Orienting Classification of Microglia in Response to Stimuli in Vivo H. Cai, ed. *PLoS One*, 7, e30763.

Jones, E.L., Hanney, M., Francis, P.T., et al., 2009. Amyloid beta concentrations in older people with Down syndrome and dementia. *Neurosci. Lett.*, 451, 162–4.

Jonsson, T., Stefansson, H., Steinberg, S., et al., 2013. Variant of TREM2 associated with the risk of Alzheimer's disease. *NEJM*, 368, 107–16.

Joshi, P., Benussi, L., Furlan, R., et al., 2015. Extracellular Vesicles in Alzheimer's Disease: Friends or Foes? Focus on Aβ-Vesicle Interaction. *Int. J. Mol. Sci.*, 16, 4800–4813.

Kaech, S. and Banker, G., 2006. Culturing hippocampal neurons. *Nat. Protoc.*, 1, 2406–15.

Kamphuis, W., Orre, M., Kooijman, L., et al., 2012. Differential cell proliferation in the cortex of the APPswePS1dE9 Alzheimer's disease mouse model. *Glia*, 60, 615–29.

Kanaumi, T., Milenkovic, I., Adle-Biassette, H., et al., 2013. Non-neuronal cell responses differ between normal and Down syndrome developing brains. *Int. J. Dev. Neurosci.*, 31, 796–803.

Kang, J., Lemaire, H.G., Unterbeck, A., et al., 1987. The precursor of Alzheimer's disease amyloid A4 protein resembles a cell-surface receptor. *Nature*, 325, 733–6.

Kapuscinski, J., 1995. DAPI: a DNA-specific fluorescent probe. *Biotech. Histochem.*, 70, 220–33.

Karperien, A., Ahammer, H. and Jelinek, H.F., 2013. Quantitating the subtleties of microglial morphology with fractal analysis. *Front. Cell. Neurosci.*, 7, 3.

Kasuga, K., Shimohata, T., Nishimura, A., et al., 2009. Identification of independent APP locus duplication in Japanese patients with early-onset Alzheimer disease. *J. Neurol. Neurosurg. Psychiatry*, 80, 1050–2.

Kester, M.I., Teunissen, C.E., Sutphen, C., et al., 2015. Cerebrospinal fluid VILIP-1 and YKL-40, candidate biomarkers to diagnose, predict and monitor Alzheimer's disease in a memory clinic cohort. *Alzheimers. Res. Ther.*, 7, 59.

Kim, S.H., Cohen, B., Novick, D., et al., 1997. Mammalian type I interferon receptors consists of two subunits: IFNaR1 and IFNaR2. *Gene*, 196, 279–86.

Kim, T., Lim, C.-S. and Kaang, B.-K., 2015. Cell type-specific gene expression profiling in brain tissue: comparison between TRAP, LCM and RNA-seq. *BMB Rep.*, 48, 388–94.

Kligman, D. and Marshak, D.R., 1985. Purification and characterization of a neurite extension factor from bovine brain. *Proc. Natl. Acad. Sci. U. S. A.*, 82, 7136–7139.

Koistinaho, M., Lin, S., Wu, X., et al., 2004. Apolipoprotein E promotes astrocyte colocalization and degradation of deposited amyloid-beta peptides. *Nat Med*, 10, 719–726.

Kokjohn, T. a and Roher, A.E., 2009. Amyloid precursor protein transgenic mouse models and Alzheimer's disease: understanding the paradigms, limitations, and contributions. *Alzheimer's Dementia*, 5, 340–347.

Korb, E. and Finkbeiner, S., 2011. Arc in synaptic plasticity: from gene to behavior. *Trends Neurosci.*, 34, 591–8.

Korbel, J.O., Tirosh-Wagner, T., Urban, A.E., et al., 2009. The genetic architecture of Down syndrome phenotypes revealed by high-resolution analysis of human segmental trisomies. *Proc. Natl. Acad. Sci. U. S. A.*, 106, 12031–12036.

Korenberg, J.R., Chen, X.N., Schipper, R., et al., 1994. Down syndrome phenotypes: the consequences of chromosomal imbalance. *Proc. Natl. Acad. Sci. U. S. A.*, 91, 4997–5001.

Krezowski, J., Knudson, D., Ebeling, C., et al., 2004. Identification of loci determining susceptibility to the lethal effects of amyloid precursor protein transgene overexpression. *Hum Mol Genet*, 13, 1989–1997.

Krinsky-McHale, S.J., Devenny, D.A., Gu, H., et al., 2008. Successful aging in a 70-year-old man with down syndrome: a case study. *Intellect. Dev. Disabil.*, 46, 215–28.

Kuhn, S., Ingham, N., Pearson, S., et al., 2012. Auditory function in the Tc1 mouse model of down syndrome suggests a limited region of human chromosome 21 involved in otitis media. *PLoS One*, 7, e31433.

LaFerla, F.M. and Green, K.N., 2012. Animal models of Alzheimer disease. *Cold Spring Harb. Perspect. Med.*, 2.

Lambert, J.-C., Heath, S., Even, G., et al., 2009. Genome-wide association study identifies variants at CLU and CR1 associated with Alzheimer's disease. *Nat. Genet.*, 41, 1094–1099.

Lambert, J.C., Ibrahim-Verbaas, C.A., Harold, D., et al., 2013. Meta-analysis of 74,046 individuals identifies 11 new susceptibility loci for Alzheimer's disease. *Nat. Genet.*, 45, 1452–8.

Larson, E.B., Wang, L., Bowen, J.D., et al., 2006. Exercise is associated with reduced risk for incident dementia among persons 65 years of age and older. *Ann. Intern. Med.*, 144, 73–81.

Lassalle, J.M., Halley, H., Daumas, S., et al., 2008. Effects of the genetic background on cognitive performances of TG2576 mice. *Behav. Brain Res.*, 191, 104–10.

Lattin, J.E., Schroder, K., Su, A.I., et al., 2008. Expression analysis of G Protein-Coupled Receptors in mouse macrophages. *Immunome Res.*, 4, 5.

Lee, E.B., 2011. Obesity, leptin, and Alzheimer's disease. *Ann. N. Y. Acad. Sci.*, 1243, 15–29.

Lehman, E.J.H., Kulnane, L.S., Gao, Y., et al., 2003. Genetic background regulates beta-amyloid precursor protein processing and beta-amyloid deposition in the mouse. *Hum. Mol. Genet.*, 12, 2949–56.

Lein, E.S., Hawrylycz, M.J., Ao, N., et al., 2007. Genome-wide atlas of gene expression in the adult mouse brain. *Nature*, 445, 168–76.

Leissring, M.A., Farris, W., Chang, A.Y., et al., 2003. Enhanced Proteolysis of β-Amyloid in APP Transgenic Mice Prevents Plaque Formation, Secondary Pathology, and Premature Death. *Neuron*, 40, 1087–1093.

Lejeune, J., Gautier, M. and Turpin, R., 1959. [Study of somatic chromosomes from 9 mongoloid children]. *C. R. Hebd. Seances Acad. Sci.*, 248, 1721–2.

Lepore, A.C., Dejea, C., Carmen, J., et al., 2008. Selective ablation of proliferating astrocytes does not affect disease outcome in either acute or chronic models of motor neuron degeneration. *Exp. Neurol.*, 211, 423–32.

Leslie, J.H. and Nedivi, E., 2011. Activity-regulated genes as mediators of neural circuit plasticity. *Prog. Neurobiol.*, 94, 223–237.

Letourneau, A., Santoni, F.A., Bonilla, X., et al., 2014. Domains of genome-wide gene expression dysregulation in Down's syndrome. *Nature*, 508, 345–50.

Levanon, A., Tarasiuk, A. and Tal, A., 1999. Sleep characteristics in children with Down syndrome. *J. Pediatr.*, 134, 755–760.

Leverenz, J.B. and Raskind, M.A., 1998. Early amyloid deposition in the medial temporal lobe of young Down syndrome patients: a regional quantitative analysis. *Exp. Neurol.*, 150, 296–304.

Li, Y., Liu, L., Barger, S.W., et al., 2003. Interleukin-1 mediates pathological effects of microglia on tau phosphorylation and on synaptophysin synthesis in cortical neurons through a p38-MAPK pathway. *J. Neurosci.*, 23, 1605–11.

Li, Y., Liu, L., Kang, J., et al., 2000. Neuronal-glial interactions mediated by interleukin-1 enhance neuronal acetylcholinesterase activity and mRNA expression. *J. Neurosci.*, 20, 149–55.

Li, Y., Wang, J., Sheng, J.G., et al., 1998. S100 beta increases levels of beta-amyloid precursor protein and its encoding mRNA in rat neuronal cultures. *J. Neurochem.*, 71, 1421–8.

Li, Z., Yu, T., Morishima, M., et al., 2007. Duplication of the entire 22.9 Mb human chromosome 21 syntenic region on mouse chromosome 16 causes cardiovascular and gastrointestinal abnormalities. *Hum. Mol. Genet.*, 16, 1359–66.

Lin, S., Lin, Y., Nery, J.R., et al., 2014. Comparison of the transcriptional landscapes between human and mouse tissues. *Proc. Natl. Acad. Sci. U. S. A.*, 111, 201413624.

Liu, C., Belichenko, P. V, Zhang, L., et al., 2011. Mouse models for Down syndrome-associated developmental cognitive disabilities. *Dev Neurosci*, 33, 404–413.

Liu, C., Morishima, M., Jiang, X., et al., 2014. Engineered chromosome-based genetic mapping establishes a 3.7 Mb critical genomic region for Down syndrome-associated heart defects in mice. *Hum. Genet.*, 133, 743–53.

Lladó, A., Grau-Rivera, O., Sánchez-Valle, R., et al., 2014. Large APP locus duplication in a sporadic case of cerebral haemorrhage. *Neurogenetics*, 15, 145–9.

Loane, M., Morris, J.K., Addor, M.-C., et al., 2013. Twenty-year trends in the prevalence of Down syndrome and other trisomies in Europe: impact of maternal age and prenatal screening. *Eur. J. Hum. Genet.*, 21, 27–33.

Lockstone, H.E., Harris, L.W., Swatton, J.E., et al., 2007. Gene expression profiling in the adult Down syndrome brain. *Genomics*, 90, 647–60.

Loo, L.S., Tang, N., Al-Haddawi, M., et al., 2014. A role for sorting nexin 27 in AMPA receptor trafficking. *Nat. Commun.*, 5, 3176.

Lott, I.T., 2012. Neurological phenotypes for Down syndrome across the life span. *Prog. Brain Res.*, 197, 101–121.

Louveau, A., Smirnov, I., Keyes, T.J., et al., 2015. Structural and functional features of central nervous system lymphatic vessels. *Nature*, 523, 337–341.

Lyle, R., Béna, F., Gagos, S., et al., 2009. Genotype-phenotype correlations in Down syndrome identified by array CGH in 30 cases of partial trisomy and partial monosomy chromosome 21. *Eur. J. Hum. Genet.*, 17, 454–466.

Mably, A.J., Liu, W., Mc Donald, J.M., et al., 2015. Anti-Aβ antibodies incapable of reducing cerebral Aβ oligomers fail to attenuate spatial reference memory deficits in J20 mice. *Neurobiol. Dis.*, 82, 372–384.

Machado, H.B., Vician, L.J. and Herschman, H.R., 2008. The MAPK pathway is required for depolarization-induced “promiscuous” immediate-early gene expression but not for

depolarization-restricted immediate-early gene expression in neurons. *J. Neurosci. Res.*, 86, 593–602.

Maier, T., Güell, M. and Serrano, L., 2009. Correlation of mRNA and protein in complex biological samples. *FEBS Lett.*, 583, 3966–73.

Malarkey, E.B. and Parpura, V., 2008. Mechanisms of glutamate release from astrocytes. *Neurochem. Int.*, 52, 142–54.

Mann, D.M., 1988a. Alzheimer's disease and Down's syndrome. *Histopathology*, 13, 125–137.

Mann, D.M., 1988b. The pathological association between Down syndrome and Alzheimer disease. *Mech. Ageing Dev.*, 43, 99–136.

Mann, D.M. and Esiri, M.M., 1989. The pattern of acquisition of plaques and tangles in the brains of patients under 50 years of age with Down's syndrome. *J. Neurol. Sci.*, 89, 169–79.

Mann, D.M., Yates, P.O., Marcyniuk, B., et al., 1987. Loss of neurones from cortical and subcortical areas in Down's syndrome patients at middle age. Quantitative comparisons with younger Down's patients and patients with Alzheimer's disease. *J. Neurol. Sci.*, 80, 79–89.

Mao, R., Wang, X., Spitznagel, E.L., et al., 2005. Primary and secondary transcriptional effects in the developing human Down syndrome brain and heart. *Genome Biol.*, 6, R107.

Margallo-Lana, M.L., Moore, P.B., Kay, D.W.K., et al., 2007. Fifteen-year follow-up of 92 hospitalized adults with Down's syndrome: incidence of cognitive decline, its relationship to age and neuropathology. *J. Intellect. Disabil. Res.*, 51, 463–77.

Marr, R.A., Rockenstein, E., Mukherjee, A., et al., 2003. Neprilysin gene transfer reduces human amyloid pathology in transgenic mice. *J. Neurosci.*, 23, 1992–6.

Marshak, D.R., 1990. S100 beta as a neurotrophic factor. *Prog Brain Res*, 86, 169–181.

Marshak, D.R., Pesce, S.A., Stanley, L.C., et al., 1992. Increased S100 beta neurotrophic activity in Alzheimer's disease temporal lobe. *Neurobiol. Aging*, 13, 1–7.

Masters, M.C., Morris, J.C. and Roe, C.M., 2015. "Noncognitive" symptoms of early Alzheimer disease: a longitudinal analysis. *Neurology*, 84, 617–22.

Matsuoka, Y., Andrews, H.F., Becker, A.G., et al., The relationship of plasma Abeta levels to dementia in aging individuals with Down syndrome. *Alzheimer Dis. Assoc. Disord.*, 23, 315–8.

McCarron, M., McCallion, P., Reilly, E., et al., 2014. A prospective 14-year longitudinal follow-up of dementia in persons with Down syndrome. *J. Intellect. Disabil. Res.*, 58, 61–70.

McCarron, M.O., Nicoll, J.A. and Graham, D.I., 1998. A quartet of Down's syndrome, Alzheimer's disease, cerebral amyloid angiopathy, and cerebral haemorrhage: interacting genetic risk factors. *J. Neurol. Neurosurg. Psychiatry*, 65, 405–6.

McClelland, J.L. and Goddard, N.H., 1996. Considerations arising from a complementary learning systems perspective on hippocampus and neocortex. *Hippocampus*, 6, 654–665.

McNaughton, D., Knight, W., Guerreiro, R., et al., 2012. Duplication of amyloid precursor protein (APP), but not prion protein (PRNP) gene is a significant cause of early onset dementia in a large UK series. *Neurobiol. Aging*, 33, 426.e13–21.

Meda, L., 2001. Glial activation in Alzheimer's disease: the role of Abeta and its associated proteins. *Neurobiol. Aging*, 22, 885–893.

Mehta, P.D., Dalton, A.J., Mehta, S.P., et al., 1998. Increased plasma amyloid beta protein 1-42 levels in Down syndrome. *Neurosci. Lett.*, 241, 13–6.

Mendel, T., Bertrand, E., Szpak, G.M., et al., 2010. Cerebral amyloid angiopathy as a cause of an extensive brain hemorrhage in adult patient with Down's syndrome - a case report. *Folia Neuropathol.*, 48, 206–11.

Mendez, M. and Lim, G., 2003. Seizures in elderly patients with dementia: epidemiology and management. *Drugs Aging*, 20, 791–803.

Mestas, J. and Hughes, C.C.W., 2004. Of Mice and Not Men: Differences between Mouse and Human Immunology. *J. Immunol.*, 172, 2731–2738.

Meylan, E., Martinon, F., Thome, M., et al., 2002. RIP4 (DIK/PKK), a novel member of the RIP kinase family, activates NF-kappa B and is processed during apoptosis. *EMBO Rep.*, 3, 1201–8.

Mills, J.D., Nalpathamkalam, T., Jacobs, H.I.L., et al., 2013. RNA-Seq analysis of the parietal cortex in Alzheimer's disease reveals alternatively spliced isoforms related to lipid metabolism. *Neurosci. Lett.*, 536, 90–5.

Misiak, B., Leszek, J. and Kiejna, A., 2012. Metabolic syndrome, mild cognitive impairment and Alzheimer's disease—The emerging role of systemic low-grade inflammation and adiposity. *Brain Res. Bull.*, 89, 144–149.

Mito, T. and Becker, L.E., 1993. Developmental changes of S-100 protein and glial fibrillary acidic protein in the brain in Down syndrome. *Exp. Neurol.*, 120, 170–6.

Moraga, A., Pradillo, J.M., García-Culebras, A., et al., 2015. Aging increases microglial proliferation, delays cell migration, and decreases cortical neurogenesis after focal cerebral ischemia. *J. Neuroinflammation*, 12, 87.

Morice, E., Andreae, L.C., Cooke, S.F., et al., 2008. Preservation of long-term memory and synaptic plasticity despite short-term impairments in the Tc1 mouse model of Down syndrome. *Learn. Mem.*, 15, 492–500.

Morishima-Kawashima, M., 2014. Molecular mechanism of the intramembrane cleavage of the β-carboxyl terminal fragment of amyloid precursor protein by γ-secretase. *Front. Physiol.*, 5, 463.

Mosher, K.I. and Wyss-Coray, T., 2014. Microglial dysfunction in brain aging and Alzheimer's disease. *Biochem. Pharmacol.*, 88, 594–604.

Mosser, D.M. and Edwards, J.P., 2008. Exploring the full spectrum of macrophage activation. *Nat. Rev. Immunol.*, 8, 958–69.

Mowen, K.A., Tang, J., Zhu, W., et al., 2001. Arginine methylation of STAT1 modulates IFNalpha/beta-induced transcription. *Cell*, 104, 731–41.

Mrak, R.E. and Griffin, W.S., 2001. The role of activated astrocytes and of the neurotrophic cytokine S100B in the pathogenesis of Alzheimer's disease. *Neurobiol. Aging*, 22, 915–922.

Mucke, L., Masliah, E., Yu, G.-Q.Q., et al., 2000. High-Level Neuronal Expression of Abeta 1-42 in Wild-Type Human Amyloid Protein Precursor Transgenic Mice: Synaptotoxicity without Plaque Formation. *J. Neurosci.*, 20, 4050–8.

Mucke, L. and Selkoe, D.J., 2012. Neurotoxicity of amyloid β-protein: synaptic and network dysfunction. *Cold Spring Harb. Perspect. Med.*, 2, a006338.

Mullan, M., Crawford, F., Axelman, K., et al., 1992. A pathogenic mutation for probable Alzheimer's disease in the APP gene at the N-terminus of beta-amyloid. *Nat. Genet.*, 1, 345–7.

Mullen, R.J., Buck, C.R. and Smith, A.M., 1992. NeuN, a neuronal specific nuclear protein in vertebrates. *Development*, 116, 201–11.

Mulugeta, E., Karlsson, E., Islam, A., et al., 2003. Loss of muscarinic M4 receptors in hippocampus of Alzheimer patients. *Brain Res.*, 960, 259–62.

Murray, A., Letourneau, A., Canzonetta, C., et al., 2015. Brief report: isogenic induced pluripotent stem cell lines from an adult with mosaic down syndrome model accelerated neuronal ageing and neurodegeneration. *Stem Cells*, 33, 2077–84.

Murrell, J., Farlow, M., Ghetti, B., et al., 1991. A mutation in the amyloid precursor protein associated with hereditary Alzheimer's disease. *Science*, 254, 97–9.

Musiek, E.S. and Holtzman, D.M., 2015. Three dimensions of the amyloid hypothesis: time, space and "wingmen." *Nat. Neurosci.*, 18, 800–806.

Naito, K.-S., Sekijima, Y. and Ikeda, S.-I., 2008. Cerebral amyloid angiopathy-related hemorrhage in a middle-aged patient with Down's syndrome. *Amyloid*, 15, 275–7.

Naj, A.C., Jun, G., Beecham, G.W., et al., 2011. Common variants at MS4A4/MS4A6E, CD2AP, CD33 and EPHA1 are associated with late-onset Alzheimer's disease. *Nat Genet*, 43, 436–441.

Nedergaard, M., Ransom, B. and Goldman, S.A., 2003. New roles for astrocytes: redefining the functional architecture of the brain. *Trends Neurosci.*, 26, 523–30.

Ness, S., Rafii, M., Aisen, P., et al., 2012. Down's syndrome and Alzheimer's disease: towards secondary prevention. *Nat. Rev. Drug Discov.*, 11, 655–656.

Nguyen, M.D., Julien, J.-P. and Rivest, S., 2002. Innate immunity: the missing link in neuroprotection and neurodegeneration? *Nat. Rev. Neurosci.*, 3, 216–27.

Nhan, H.S., Chiang, K. and Koo, E.H., 2014. The multifaceted nature of amyloid precursor protein and its proteolytic fragments: friends and foes. *Acta Neuropathol.*, 129, 1–19.

Nimmerjahn, A., Kirchhoff, F. and Helmchen, F., 2005. Resting microglial cells are highly dynamic surveillants of brain parenchyma in vivo. *Science*, 308, 1314–8.

Niwa, O., Tange, Y. and Kurabayashi, A., 2006. Growth arrest and chromosome instability in aneuploid yeast. *Yeast*, 23, 937–50.

Njie, E.G., Boelen, E., Stassen, F.R., et al., 2012. Ex vivo cultures of microglia from young and aged rodent brain reveal age-related changes in microglial function. *Neurobiol. Aging*, 33, 195.e1–12.

Noebels, J., 2011. A perfect storm: Converging paths of epilepsy and Alzheimer's dementia intersect in the hippocampal formation. *Epilepsia*, 52 Suppl 1, 39–46.

O'Callaghan, J.P., Sriram, K. and Miller, D.B., 2008. Defining "neuroinflammation". *Ann. N. Y. Acad. Sci.*, 1139, 318–30.

O'Doherty, A., Ruf, S., Mulligan, C., et al., 2005. An aneuploid mouse strain carrying human chromosome 21 with Down syndrome phenotypes. *Science*, 309, 2033–7.

Oberheim, N.A., Takano, T., Han, X., et al., 2009. Uniquely hominid features of adult human astrocytes. *J. Neurosci.*, 29, 3276–87.

Oberheim, N.A., Wang, X., Goldman, S., et al., 2006. Astrocytic complexity distinguishes the human brain. *Trends Neurosci.*, 29, 547–53.

Ogata, K. and Kosaka, T., 2002. Structural and quantitative analysis of astrocytes in the mouse hippocampus. *Neuroscience*, 113, 221–33.

Okoniewski, M. and Miller, C., 2006. Hybridization interactions between probesets in short oligo microarrays lead to spurious correlations. *BMC Bioinformatics*, 7, 276.

Olabarria, M., Noristani, H.N., Verkhratsky, A., et al., 2010. Concomitant astroglial atrophy and astrogliosis in a triple transgenic animal model of Alzheimer's disease. *Glia*, 58, 831–8.

Oliver, C., Kalsy, S., McQuillan, S., et al., 2011. Behavioural Excesses and Deficits Associated with Dementia in Adults who have Down Syndrome. *J. Appl. Res. Intellect. Disabil.*, 24, 208–216.

Olson, L.E., Richtsmeier, J.T., Leszl, J., et al., 2004. A chromosome 21 critical region does not cause specific Down syndrome phenotypes. *Science*, 306, 687–90.

Orr, M.E. and Oddo, S., 2013. Autophagic/lysosomal dysfunction in Alzheimer's disease. *Alzheimers. Res. Ther.*, 5, 53.

Oyama, F., Cairns, N.J., Shimada, H., et al., 1994. Down's syndrome: up-regulation of beta-amyloid protein precursor and tau mRNAs and their defective coordination. *J. Neurochem.*, 62, 1062–6.

Palop, J.J., Chin, J., Bien-Ly, N., et al., 2005. Vulnerability of dentate granule cells to disruption of arc expression in human amyloid precursor protein transgenic mice. *J. Neurosci.*, 25, 9686–93.

Palop, J.J., Jones, B., Kekonius, L., et al., 2003. Neuronal depletion of calcium-dependent proteins in the dentate gyrus is tightly linked to Alzheimer's disease-related cognitive deficits. *Proc. Natl. Acad. Sci. U. S. A.*, 100, 9572–9577.

Parihar, M.S. and Brewer, G.J., 2010. Amyloid-β as a modulator of synaptic plasticity. *J. Alzheimer's Dis.*, 22, 741–63.

Parpura, V., Grubišić, V. and Verkhratsky, A., 2011. Ca(2+) sources for the exocytotic release of glutamate from astrocytes. *Biochim. Biophys. Acta*, 1813, 984–91.

Parpura, V., Heneka, M.T., Montana, V., et al., 2012. Glial cells in (patho)physiology. *J. Neurochem.*, 121, 4–27.

Pavelka, N., Rancati, G., Zhu, J., et al., 2010. Aneuploidy confers quantitative proteome changes and phenotypic variation in budding yeast. *Nature*, 468, 321–5.

Payne, S.H., 2015. The utility of protein and mRNA correlation. *Trends Biochem. Sci.*, 40, 1–3.

Pereira, P.L., Magnol, L., Sahún, I., et al., 2009. A new mouse model for the trisomy of the Abcg1-U2af1 region reveals the complexity of the combinatorial genetic code of down syndrome. *Hum. Mol. Genet.*, 18, 4756–69.

Perlmutter, L.S., Barron, E. and Chui, H.C., 1990. Morphologic association between microglia and senile plaque amyloid in Alzheimer's disease. *Neurosci. Lett.*, 119, 32–6.

Perluigi, M. and Butterfield, D.A., 2012. Oxidative Stress and Down Syndrome: A Route toward Alzheimer-Like Dementia. *Curr. Gerontol. Geriatr. Res.*, 2012, 724904.

Petersen, M.B. and Mikkelsen, M., 2000. Nondisjunction in trisomy 21: origin and mechanisms. *Cytogenet. Cell Genet.*, 91, 199–203.

Piedrahita, D., Hernández, I., López-Tobón, A., et al., 2010. Silencing of CDK5 reduces neurofibrillary tangles in transgenic alzheimer's mice. *J. Neurosci.*, 30, 13966–76.

Pihlaja, R., Koistinaho, J., Kauppinen, R., et al., 2011. Multiple cellular and molecular mechanisms Are involved in human Aβ clearance by transplanted adult astrocytes. *Glia*, 59, 1643–1657.

Pomilio, C., Pavia, P., Gorojod, R.M., et al., 2015. Glial alterations from early to late stages in a model of alzheimer's disease: Evidence of autophagy involvement in Aβ internalization. *Hippocampus*, In press.

Portelius, E., Brinkmalm, G., Tran, A., et al., 2010. Identification of novel N-terminal fragments of amyloid precursor protein in cerebrospinal fluid. *Exp. Neurol.*, 223, 351–358.

Prasher, V.P. and Krishnan, V.H.R., 1993. Age of onset and duration of dementia in people with down syndrome: Integration of 98 reported cases in the literature. *Int. J. Geriatr. Psychiatry*, 8, 915–922.

Previtera, M.L., Langhammer, C.G. and Firestein, B.L., 2010. Effects of substrate stiffness and cell density on primary hippocampal cultures. *J. Biosci. Bioeng.*, 110, 459–70.

Prince, M., Knapp, M., Guerchet, et al., 2014. *Dementia UK: Update*,

Prokop, S., Miller, K.R. and Heppner, F.L., 2013. Microglia actions in Alzheimer's disease. *Acta Neuropathol.*, 126, 461–77.

Pruitt, K.D., Brown, G.R., Hiatt, S.M., et al., 2014. RefSeq: an update on mammalian reference sequences. *Nucleic Acids Res.*, 42, D756–63.

Rafii, M.S., Wishnek, H., Brewer, J.B., et al., 2015. The down syndrome biomarker initiative (DSBI) pilot: proof of concept for deep phenotyping of Alzheimer's disease biomarkers in down syndrome. *Front. Behav. Neurosci.*, 9, 239.

Rao, V.R., Pintchovski, S.A., Chin, J., et al., 2006. AMPA receptors regulate transcription of the plasticity-related immediate-early gene Arc. *Nat. Neurosci.*, 9, 887–95.

Rath, M.F., Rohde, K., Fahrenkrug, J., et al., 2013. Circadian clock components in the rat neocortex: daily dynamics, localization and regulation. *Brain Struct. Funct.*, 218, 551–62.

Rauchs, G., Schabus, M., Parapatics, S., et al., 2008. Is there a link between sleep changes and memory in Alzheimer's disease? *Neuroreport*, 19, 1159–62.

Reed-Geaghan, E.G., Savage, J.C., Hise, A.G., et al., 2009. CD14 and Toll-Like Receptors 2 and 4 Are Required for Fibrillar A -Stimulated Microglial Activation. *J. Neurosci.*, 29, 11982–11992.

Reeves, R.H., 2006. Down syndrome mouse models are looking up. *Trends Mol. Med.*, 12, 237–40.

Reeves, R.H., Irving, N.G., Moran, T.H., et al., 1995. A mouse model for Down syndrome exhibits learning and behaviour deficits. *Nat. Genet.*, 11, 177–84.

Reeves, R.H., Yao, J., Crowley, M.R., et al., 1994. Astrocytosis and axonal proliferation in the hippocampus of S100b transgenic mice. *Proc. Natl. Acad. Sci. U. S. A.*, 91, 5359–63.

Reinholdt, L.G., Ding, Y., Gilbert, G.J., et al., 2011. Molecular characterization of the translocation breakpoints in the Down syndrome mouse model Ts65Dn. *Mamm. Genome*, 22, 685–91.

Reynolds, L.E., Watson, A.R., Baker, M., et al., 2010. Tumour angiogenesis is reduced in the Tc1 mouse model of Down's syndrome. *Nature*, 465, 813–7.

Ribeiro, S., Shi, X., Engelhard, M., et al., 2007. Novel experience induces persistent sleep-dependent plasticity in the cortex but not in the hippocampus. *Front. Neurosci.*, 1, 43–55.

Rietschel, M., Mattheisen, M., Degenhardt, F., et al., 2012. Association between genetic variation in a region on chromosome 11 and schizophrenia in large samples from Europe. *Mol. Psychiatry*, 17, 906–17.

Rincón, E., Santos, T., Avila-Flores, A., et al., 2007. Proteomics identification of sorting nexin 27 as a diacylglycerol kinase zeta-associated protein: new diacylglycerol kinase roles in endocytic recycling. *Mol. Cell. Proteomics*, 6, 1073–87.

Rock, R.B., Hu, S., Deshpande, A., et al., 2005. Transcriptional response of human microglial cells to interferon-gamma. *Genes Immun.*, 6, 712–9.

Rockenstein, E.M., McConlogue, L., Tan, H., et al., 1995. Levels and alternative splicing of amyloid beta protein precursor (APP) transcripts in brains of APP transgenic mice and humans with Alzheimer's disease. *J. Biol. Chem.*, 270, 28257–28267.

Rountree, R.B., Willis, C.R., Dinh, H., et al., 2010. RIP4 regulates epidermal differentiation and cutaneous inflammation. *J. Invest. Dermatol.*, 130, 102–12.

Rovelet-Lecrux, A., Frebourg, T., Tuominen, H., et al., 2007. APP locus duplication in a Finnish family with dementia and intracerebral haemorrhage. *J. Neurol. Neurosurg. Psychiatry*, 78, 1158–9.

Rovelet-Lecrux, A., Hannequin, D., Raux, G., et al., 2006. APP locus duplication causes autosomal dominant early-onset Alzheimer disease with cerebral amyloid angiopathy. *Nat. Genet.*, 38, 24–6.

Royston, M.C., McKenzie, J.E., Gentleman, S.M., et al., 1999. Overexpression of S100beta in Down's syndrome: correlation with patient age and with beta-amyloid deposition. *Neuropathol. Appl. Neurobiol.*, 25, 387–393.

Rubio, S.E., Vega-Flores, G., Martínez, A., et al., 2012. Accelerated aging of the GABAergic septohippocampal pathway and decreased hippocampal rhythms in a mouse model of Alzheimer's disease. *FASEB J.*, 26, 4458–67.

Rumble, B., Retallack, R., Hilbich, C., et al., 1989. Amyloid A4 protein and its precursor in Down's syndrome and Alzheimer's disease. *NEJM*, 320, 1446–52.

Rustay, N.R., Cronin, E.A., Curzon, P., et al., 2010. Mice expressing the Swedish APP mutation on a 129 genetic background demonstrate consistent behavioral deficits and pathological markers of Alzheimer's disease. *Brain Res.*, 1311, 136–47.

Ryan, N.S. and Rossor, M.N., 2010. Correlating familial Alzheimer's disease gene mutations with clinical phenotype. *Biomark. Med.*, 4, 99–112.

Ryman, D.C., Acosta-Baena, N., Aisen, P.S., et al., 2014. Symptom onset in autosomal dominant Alzheimer disease: a systematic review and meta-analysis. *Neurology*, 83, 253–60.

Saganich, M.J., Schroeder, B.E., Galvan, V., et al., 2006. Deficits in synaptic transmission and learning in amyloid precursor protein (APP) transgenic mice require C-terminal cleavage of APP. *J. Neurosci.*, 26, 13428–36.

Sago, H., Carlson, E.J., Smith, D.J., et al., 1998. Ts1Cje, a partial trisomy 16 mouse model for Down syndrome, exhibits learning and behavioral abnormalities. *Proc. Natl. Acad. Sci. U. S. A.*, 95, 6256–61.

Saha, R.N. and Dudek, S.M., 2013. Splitting hares and tortoises: a classification of neuronal immediate early gene transcription based on poised RNA polymerase II. *Neuroscience*, 247, 175–81.

Sahir, N., Brenneman, D.E. and Hill, J.M., 2006. Neonatal mice of the Down syndrome model, Ts65Dn, exhibit upregulated VIP measures and reduced responsiveness of cortical astrocytes to VIP stimulation. *J. Mol. Neurosci.*, 30, 329–40.

Salehi, A., Delcroix, J.-D., Belichenko, P. V, et al., 2006. Increased App expression in a mouse model of Down's syndrome disrupts NGF transport and causes cholinergic neuron degeneration. *Neuron*, 51, 29–42.

Sanderson, D.J., Good, M.A., Skelton, K., et al., 2009. Enhanced long-term and impaired short-term spatial memory in GluA1 AMPA receptor subunit knockout mice: evidence for a dual-process memory model. *Learn Mem*, 16, 379–86.

Sasahara, M., Fries, J.W., Raines, E.W., et al., 1991. PDGF B-chain in neurons of the central nervous system, posterior pituitary, and in a transgenic model. *Cell*, 64, 217–27.

Sastre, M. and Gentleman, S.M., 2010. NSAIDs: How they Work and their Prospects as Therapeutics in Alzheimer's Disease. *Front. Aging Neurosci.*, 2, 20.

Sastre, M., Klockgether, T. and Heneka, M.T., 2006. Contribution of inflammatory processes to Alzheimer's disease: molecular mechanisms. *Int. J. Dev. Neurosci.*, 24, 167–76.

Saud, K., Herrera-Molina, R. and Von Bernhardi, R., 2005. Pro- and anti-inflammatory cytokines regulate the ERK pathway: implication of the timing for the activation of microglial cells. *Neurotox. Res.*, 8, 277–87.

Saunders, A.M., Schmader, K., Breitner, J.C., et al., 1993. Apolipoprotein E epsilon 4 allele distributions in late-onset Alzheimer's disease and in other amyloid-forming diseases. *Lancet*, 342, 710–711.

Scarmeas, N., Luchsinger, J.A., Schupf, N., et al., 2009. Physical activity, diet, and risk of Alzheimer disease. *JAMA*, 302, 627–37.

Scarr, E., Um, J.Y., Cowie, T.F., et al., 2013. Cholinergic muscarinic M4 receptor gene polymorphisms: a potential risk factor and pharmacogenomic marker for schizophrenia. *Schizophr. Res.*, 146, 279–84.

Schroeder, B.E. and Koo, E.H., 2005. To think or not to think: synaptic activity and Abeta release. *Neuron*, 48, 873–5.

Schupf, N., Lee, A., Park, N., et al., 2015. Candidate genes for Alzheimer's disease are associated with individual differences in plasma levels of beta amyloid peptides in adults with Down syndrome. *Neurobiol. Aging*, 36, 2907.e1–2907.e10.

Schupf, N., Patel, B., Pang, D., et al., 2007. Elevated plasma beta-amyloid peptide Abeta(42) levels, incident dementia, and mortality in Down syndrome. *Arch. Neurol.*, 64, 1007–13.

Schupf, N., Patel, B., Silverman, W., et al., 2001. Elevated plasma amyloid β-peptide 1–42 and onset of dementia in adults with Down syndrome. *Neurosci. Lett.*, 301, 199–203.

Schwanhäusser, B., Busse, D., Li, N., et al., 2011. Global quantification of mammalian gene expression control. *Nature*, 473, 337–42.

Sebastià, J., Cristòfol, R., Pertusa, M., et al., 2004. Down's syndrome astrocytes have greater antioxidant capacity than euploid astrocytes. *Eur. J. Neurosci.*, 20, 2355–2366.

Selenica, M.-L.B., Alvarez, J.A., Nash, K.R., et al., 2013. Diverse activation of microglia by chemokine (C-C motif) ligand 2 overexpression in brain. *J. Neuroinflammation*, 10, 86.

Seo, H. and Isacson, O., 2005. Abnormal APP, cholinergic and cognitive function in Ts65Dn Down's model mice. *Exp. Neurol.*, 193, 469–80.

Seo, M.S., Scarr, E. and Dean, B., 2014. An investigation of the factors that regulate muscarinic receptor expression in schizophrenia. *Schizophr. Res.*, 158, 247–54.

Seok, J., Warren, H.S., Cuenca, A.G., et al., 2013. Genomic responses in mouse models poorly mimic human inflammatory diseases. *Proc. Natl. Acad. Sci. U. S. A.*, 110, 3507–12.

Serrano-Pozo, A., Frosch, M.P., Masliah, E., et al., 2011. Neuropathological alterations in Alzheimer disease. *Cold Spring Harb. Perspect. Med.*, 1, a006189.

Serrano-Pozo, A., Gómez-Isla, T., Growdon, J.H., et al., 2013. A phenotypic change but not proliferation underlies glial responses in Alzheimer disease. *Am. J. Pathol.*, 182, 2332–44.

Seyhan, A.A., 2011. RNAi: a potential new class of therapeutic for human genetic disease. *Hum. Genet.*, 130, 583–605.

Shankar, G.M., Leissring, M.A., Adame, A., et al., 2009. Biochemical and immunohistochemical analysis of an Alzheimer's disease mouse model reveals the presence of multiple cerebral Abeta assembly forms throughout life. *Neurobiol Dis*, 36, 293–302.

Sharova, L. V, Sharov, A.A., Nedorezov, T., et al., 2009. Database for mRNA half-life of 19 977 genes obtained by DNA microarray analysis of pluripotent and differentiating mouse embryonic stem cells. *DNA Res.*, 16, 45–58.

Sheng, J.G., Ito, K., Skinner, R.D., et al., 1996. In vivo and in vitro evidence supporting a role for the inflammatory cytokine interleukin-1 as a driving force in Alzheimer pathogenesis. *Neurobiol. Aging*, 17, 761–6.

Sheng, J.G., Jones, R.A., Zhou, X.Q., et al., 2001. Interleukin-1 promotion of MAPK-p38 overexpression in experimental animals and in Alzheimer's disease: potential significance for tau protein phosphorylation. *Neurochem. Int.*, 39, 341–8.

Sheng, J.G., Mrak, R.E. and Griffin, W.S., 1998. Enlarged and phagocytic, but not primed, interleukin-1 alpha-immunoreactive microglia increase with age in normal human brain. *Acta Neuropathol.*, 95, 229–34.

Sheng, J.G., Mrak, R.E. and Griffin, W.S., 1997. Neuritic plaque evolution in Alzheimer's disease is accompanied by transition of activated microglia from primed to enlarged to phagocytic forms. *Acta Neuropathol.*, 94, 1–5.

Sheng, J.G., Zhu, S.G., Jones, R.A., et al., 2000. Interleukin-1 promotes expression and phosphorylation of neurofilament and tau proteins in vivo. *Exp. Neurol.*, 163, 388–91.

Sheppard, O., Plattner, F., Rubin, A., et al., 2012. Altered regulation of tau phosphorylation in a mouse model of down syndrome aging. *Neurobiol. Aging*, 33, 828.e31–44.

Sherman, B.T., Huang, D.W., Tan, Q., et al., 2007. DAVID Knowledgebase: a gene-centered database integrating heterogeneous gene annotation resources to facilitate high-throughput gene functional analysis. *BMC Bioinformatics*, 8, 426.

Sherman, S.L., Allen, E.G., Bean, L.H., et al., 2007. Epidemiology of Down syndrome. *Ment. Retard. Dev. Disabil. Res. Rev.*, 13, 221–227.

Shi, Y., Kirwan, P., Smith, J., et al., 2012. A human stem cell model of early Alzheimer's disease pathology in Down syndrome. *Sci. Transl. Med.*, 4, 124ra29.

Siegel, J.J. and Amon, A., 2012. New insights into the troubles of aneuploidy. *Annu. Rev. Cell Dev. Biol.*, 28, 189–214.

De Simone, R., Puig, X.S., Gelisse, P., et al., 2010. Senile myoclonic epilepsy: delineation of a common condition associated with Alzheimer's disease in Down syndrome. *Seizure*, 19, 383–389.

Simons, M. and Raposo, G., 2009. Exosomes--vesicular carriers for intercellular communication. *Curr. Opin. Cell Biol.*, 21, 575–81.

Simons, M., de Strooper, B., Multhaup, G., et al., 1996. Amyloidogenic processing of the human amyloid precursor protein in primary cultures of rat hippocampal neurons. *J. Neurosci.*, 16, 899–908.

Simpson, J.E., Ince, P.G., Lace, G., et al., 2010. Astrocyte phenotype in relation to Alzheimer-type pathology in the ageing brain. *Neurobiol. Aging*, 31, 578–90.

Singh, P., Schimenti, J.C. and Bolcun-Filas, E., 2014. A Mouse Geneticist's Practical Guide to CRISPR Applications. *Genetics*, 199, 1–15.

Sirko, S., Behrendt, G., Johansson, P.A., et al., 2013. Reactive glia in the injured brain acquire stem cell properties in response to sonic hedgehog. [corrected]. *Cell Stem Cell*, 12, 426–39.

Sleegers, K., Brouwers, N., Gijselinck, I., et al., 2006. APP duplication is sufficient to cause early onset Alzheimer's dementia with cerebral amyloid angiopathy. *Brain*, 129, 2977–83.

Sofroniew, M. V, 2009. Molecular dissection of reactive astrogliosis and glial scar formation. *Trends Neurosci.*, 32, 638–47.

Solito, E. and Sastre, M., 2012. Microglia Function in Alzheimer's Disease. *Front. Pharmacol.*, 3, 14.

Soltani, M.H., Pichardo, R., Song, Z., et al., 2005. Microtubule-associated protein 2, a marker of neuronal differentiation, induces mitotic defects, inhibits growth of melanoma cells, and predicts metastatic potential of cutaneous melanoma. *Am. J. Pathol.*, 166, 1841–50.

De Sousa Abreu, R., Penalva, L.O., Marcotte, E.M., et al., 2009. Global signatures of protein and mRNA expression levels. *Mol. Biosyst.*, 5, 1512–1526.

Spires-Jones, T.L. and Hyman, B.T., 2014. The intersection of amyloid beta and tau at synapses in Alzheimer's disease. *Neuron*, 82, 756–71.

Stence, N., Waite, M. and Dailey, M.E., 2001. Dynamics of microglial activation: a confocal time-lapse analysis in hippocampal slices. *Glia*, 33, 256–66.

Steuble, M., Diep, T.-M., Schätzle, P., et al., 2012. Calsyntenin-1 shelters APP from proteolytic processing during anterograde axonal transport. *Biol. Open*, 1, 761–74.

Steward, O. and Worley, P.F., 2001. Selective targeting of newly synthesized Arc mRNA to active synapses requires NMDA receptor activation. *Neuron*, 30, 227–40.

Stilling, R.M., Benito, E., Gertig, M., et al., 2014. De-regulation of gene expression and alternative splicing affects distinct cellular pathways in the aging hippocampus. *Front. Cell. Neurosci.*, 8, 373.

Streit, W.J., 2010. Microglial activation and neuroinflammation in Alzheimer's disease: a critical examination of recent history. *Front. Aging Neurosci.*, 2, 22.

Streit, W.J., Braak, H., Xue, Q.-S., et al., 2009. Dystrophic (senescent) rather than activated microglial cells are associated with tau pathology and likely precede neurodegeneration in Alzheimer's disease. *Acta Neuropathol.*, 118, 475–85.

Streit, W.J., Xue, Q.-S., Tischer, J., et al., 2014. Microglial pathology. *Acta Neuropathol. Commun.*, 2, 142.

De Strooper, B., Simons, M., Multhaup, G., et al., 1995. Production of intracellular amyloid-containing fragments in hippocampal neurons expressing human amyloid precursor protein and protection against amyloidogenesis by subtle amino acid substitutions in the rodent sequence. *EMBO J.*, 14, 4932–4938.

Strydom, A., Shooshtari, S., Lee, L., et al., 2010. Dementia in Older Adults With Intellectual Disabilities-Epidemiology, Presentation, and Diagnosis. *J. Policy Pract. Intellect. Disabil.*, 7, 96–110.

Su, Z., Łabaj, P.P., Li, S., et al., 2014. A comprehensive assessment of RNA-seq accuracy, reproducibility and information content by the Sequencing Quality Control Consortium. *Nat. Biotechnol.*, 32, 903–914.

Sudduth, T.L., Greenstein, A. and Wilcock, D.M., 2013. Intracranial Injection of Gammagard, a Human IVIg, Modulates the Inflammatory Response of the Brain and Lowers A in APP/PS1 Mice Along a Different Time Course than Anti-A Antibodies. *J. Neurosci.*, 33, 9684–9692.

Sutherland, G.T., Janitz, M. and Kril, J.J., 2011. Understanding the pathogenesis of Alzheimer's disease: will RNA-Seq realize the promise of transcriptomics? *J. Neurochem.*, 116, 937–46.

Suzuki, N., Cheung, T.T., Cai, X.D., et al., 1994. An increased percentage of long amyloid beta protein secreted by familial amyloid beta protein precursor (beta APP717) mutants. *Science*, 264, 1336–40.

Swaminathan, S., Huentelman, M.J., Corneveaux, J.J., et al., 2012. Analysis of copy number variation in Alzheimer's disease in a cohort of clinically characterized and neuropathologically verified individuals. *PLoS One*, 7, e50640.

Swaminathan, S., Shen, L., Kim, S., et al., 2012. Analysis of copy number variation in Alzheimer's disease: the NIALOAD/ NCRAD Family Study. *Curr. Alzheimer Res.*, 9, 801–14.

Tamaoka, A., Odaka, A., Ishibashi, Y., et al., 1994. APP717 missense mutation affects the ratio of amyloid beta protein species (A beta 1-42/43 and a beta 1-40) in familial Alzheimer's disease brain. *J. Biol. Chem.*, 269, 32721–4.

Tampellini, D. and Gouras, G.K., 2011. *Analysis of vesicular trafficking in primary neurons by live imaging.* G. Manfredi & H. Kawamata, eds., Totowa, NJ: Humana Press.

Taylor, S.C., Berkelman, T., Yadav, G., et al., 2013. A defined methodology for reliable quantification of Western blot data. *Mol. Biotechnol.*, 55, 217–26.

Teber, I., Köhling, R., Speckmann, E.-J., et al., 2004. Muscarinic acetylcholine receptor stimulation induces expression of the activity-regulated cytoskeleton-associated gene (ARC). *Brain Res. Mol. Brain Res.*, 121, 131–6.

Teller, J.K., Russo, C., DeBusk, L.M., et al., 1996. Presence of soluble amyloid beta-peptide precedes amyloid plaque formation in Down's syndrome. *Nat. Med.*, 2, 93–5.

Thies, W. and Bleiler, L., 2013. 2013 Alzheimer's disease facts and figures. *Alzheimer's Dementia*, 9, 208–45.

Thonberg, H., Fallström, M., Björkström, J., et al., 2011. Mutation screening of patients with Alzheimer disease identifies APP locus duplication in a Swedish patient. *BMC Res. Notes*, 4, 476.

Tischfield, M.A., Baris, H.N., Wu, C., et al., 2010. Human TUBB3 mutations perturb microtubule dynamics, kinesin interactions, and axon guidance. *Cell*, 140, 74–87.

Tiu, S.C., Chan, W.Y., Heizmann, C.W., et al., 2000. Differential expression of S100B and S100A6(1) in the human fetal and aged cerebral cortex. *Brain Res. Dev. Brain Res.*, 119, 159–68.

Tokuda, T., Fukushima, T., Ikeda, S., et al., 1997. Plasma levels of amyloid beta proteins Abeta1-40 and Abeta1-42(43) are elevated in Down's syndrome. *Ann. Neurol.*, 41, 271–3.

Toro, J. De, Herschlik, L., Waldner, C., et al., 2015. Emerging roles of exosomes in normal and pathological conditions : new insights for diagnosis and. *Front. Immunol.*, 6, 1–12.

Torres, E.M., Sokolsky, T., Tucker, C.M., et al., 2007. Effects of aneuploidy on cellular physiology and cell division in haploid yeast. *Science*, 317, 916–24.

Torres-Platas, S.G., Comeau, S., Rachalski, A., et al., 2014. Morphometric characterization of microglial phenotypes in human cerebral cortex. *J. Neuroinflammation*, 11, 12.

Trazzi, S., Fuchs, C., Valli, E., et al., 2013. The amyloid precursor protein (APP) triplicated gene impairs neuronal precursor differentiation and neurite development through two different domains in the Ts65Dn mouse model for Down syndrome. *J. Biol. Chem.*, 288, 20817–29.

Trousdale, C. and Kim, K., 2015. Retromer: Structure, function, and roles in mammalian disease. *Eur. J. Cell Biol.*, S0171-9335, 00071–0.

Truett, G.E., Heeger, P., Mynatt, R.L., et al., 2000. Preparation of PCR-quality mouse genomic DNA with hot sodium hydroxide and tris (HotSHOT). *Biotechniques*, 29, 52–54.

Twine, N.A., Janitz, K., Wilkins, M.R., et al., 2011. Whole transcriptome sequencing reveals gene expression and splicing differences in brain regions affected by Alzheimer's disease. *PLoS One*, 6, e16266.

Tybulewicz, V.L.J. and Fisher, E.M.C., 2006. New techniques to understand chromosome dosage: mouse models of aneuploidy. *Hum. Mol. Genet.*, 15 Spec No, R103–9.

Tyrrell, J., Cosgrave, M., McCarron, M., et al., 2001. Dementia in people with Down's syndrome. *Int. J. Geriatr. Psychiatry*, 16, 1168–74.

Vacík, T., Ort, M., Gregorová, S., et al., 2005. Segmental trisomy of chromosome 17: a mouse model of human aneuploidy syndromes. *Proc. Natl. Acad. Sci. U. S. A.*, 102, 4500–5.

van der Kant, R. and Goldstein, L.S.B., 2015. Cellular Functions of the Amyloid Precursor Protein from Development to Dementia. *Dev. Cell*, 32, 502–515.

Vandesompele, J., De Preter, K., Pattyn, F., et al., 2002. Accurate normalization of real-time quantitative RT-PCR data by geometric averaging of multiple internal control genes. *Genome Biol.*, 3, research0034.1–research0034.11.

Vazdarjanova, A., Ramirez-Amaya, V., Insel, N., et al., 2006. Spatial exploration induces ARC, a plasticity-related immediate-early gene, only in calcium/calmodulin-dependent protein kinase II-positive principal excitatory and inhibitory neurons of the rat forebrain. *J. Comp. Neurol.*, 498, 317–29.

Veerappan, C.S., Sleiman, S. and Coppola, G., 2013. Epigenetics of Alzheimer's disease and frontotemporal dementia. *Neurotherapeutics*, 10, 709–21.

Vella, L.J. and Cappai, R., 2012. Identification of a novel amyloid precursor protein processing pathway that generates secreted N-terminal fragments. *FASEB J.*, 26, 2930–40.

Verkhratsky, A. and Nedergaard, M., 2014. Astroglial cradle in the life of the synapse. *Philos. Trans. R. Soc. B Biol. Sci.*, 369, 20130595–20130595.

Verkhratsky, A., Olabarria, M., Noristani, H.N., et al., 2010. Astrocytes in Alzheimer's disease. *Neurotherapeutics*, 7, 399–412.

Vilardell, M., Rasche, A., Thormann, A., et al., 2011. Meta-analysis of heterogeneous Down Syndrome data reveals consistent genome-wide dosage effects related to neurological processes. *BMC Genomics*, 12, 229.

Vingtdeux, V., Giliberto, L., Zhao, H., et al., 2010. AMP-activated protein kinase signaling activation by resveratrol modulates amyloid-beta peptide metabolism. *J. Biol. Chem.*, 285, 9100–13.

Vlad, S.C., Miller, D.R., Kowall, N.W., et al., 2008. Protective effects of NSAIDs on the development of Alzheimer disease. *Neurology*, 70, 1672–7.

Vogel, C. and Marcotte, E.M., 2012. Insights into the regulation of protein abundance from proteomic and transcriptomic analyses. *Nat. Rev. Genet.*, 13, 227–32.

Wagenaar, D.A., Pine, J. and Potter, S.M., 2006. An extremely rich repertoire of bursting patterns during the development of cortical cultures. *BMC Neurosci.*, 7, 11.

Wake, H., Moorhouse, A.J., Jinno, S., et al., 2009. Resting microglia directly monitor the functional state of synapses in vivo and determine the fate of ischemic terminals. *J. Neurosci.*, 29, 3974–80.

Wallon, D., Rousseau, S., Rovelet-Lecrux, A., et al., 2012. The French series of autosomal dominant early onset Alzheimer's disease cases: mutation spectrum and cerebrospinal fluid biomarkers. *J. Alzheimer's Dis.*, 30, 847–56.

Wang, C., Gong, B., Bushel, P.R., et al., 2014. The concordance between RNA-seq and microarray data depends on chemical treatment and transcript abundance. *Nat. Biotechnol.*, 32, 926–32.

Wang, D.-C., Chen, S.-S., Lee, Y.-C., et al., 2006. Amyloid-beta at sublethal level impairs BDNF-induced arc expression in cortical neurons. *Neurosci. Lett.*, 398, 78–82.

Wang, D.D. and Bordey, A., 2008. The astrocyte odyssey. *Prog. Neurobiol.*, 86, 342–67.

Wang, X., Huang, T., Zhao, Y., et al., 2014. Sorting nexin 27 regulates Aβ production through modulating γ-secretase activity. *Cell Rep.*, 9, 1023–33.

Wang, X., Zhao, Y., Zhang, X., et al., 2013. Loss of sorting nexin 27 contributes to excitatory synaptic dysfunction by modulating glutamate receptor recycling in Down's syndrome. *Nat Med*, 19, 473–80.

Wang, Z., Gerstein, M. and Snyder, M., 2009. RNA-Seq: a revolutionary tool for transcriptomics. *Nat. Rev. Genet.*, 10, 57–63.

Waung, M.W., Pfeiffer, B.E., Nosyreva, E.D., et al., 2008. Rapid translation of Arc/Arg3.1 selectively mediates mGluR-dependent LTD through persistent increases in AMPAR endocytosis rate. *Neuron*, 59, 84–97.

Webster, S.J., Bachstetter, A.D., Nelson, P.T., et al., 2014. Using mice to model Alzheimer's dementia: an overview of the clinical disease and the preclinical behavioral changes in 10 mouse models. *Front. Genet.*, 5, 88.

Weggen, S., Eriksen, J.L., Das, P., et al., 2001. A subset of NSAIDs lower amyloidogenic Abeta42 independently of cyclooxygenase activity. *Nature*, 414, 212–6.

Weldemichael, D.A. and Grossberg, G.T., 2010. Circadian rhythm disturbances in patients with Alzheimer's disease: a review. *Int. J. Alzheimers. Dis.*, 716453, 1–9.

Wertkin, A.M., Turner, R.S., Pleasure, S.J., et al., 1993. Human neurons derived from a teratocarcinoma cell line express solely the 695-amino acid amyloid precursor protein and produce intracellular beta-amyloid or A4 peptides. *Proc. Natl. Acad. Sci. U. S. A.*, 90, 9513–9517.

Wharton, S.B., O'Callaghan, J.P., Savva, G.M., et al., 2009. Population variation in glial fibrillary acidic protein levels in brain ageing: relationship to Alzheimer-type pathology and dementia. *Dement. Geriatr. Cogn. Disord.*, 27, 465–73.

Wilcock, D.M. and Griffin, W.S.T., 2013. Down's syndrome, neuroinflammation, and Alzheimer neuropathogenesis. *J. Neuroinflammation*, 10, 84.

Wilcock, D.M., Hurban, J., Helman, A.M., et al., 2015. Down syndrome individuals with Alzheimer's disease have a distinct neuroinflammatory phenotype compared to sporadic Alzheimer's disease. *Neurobiol. Aging*, 36, 2468–74.

Wilhelmsson, U., Bushong, E.A., Price, D.L., et al., 2006. Redefining the concept of reactive astrocytes as cells that remain within their unique domains upon reaction to injury. *Proc. Natl. Acad. Sci. U. S. A.*, 103, 17513–8.

Williams, B.R., Prabhu, V.R., Hunter, K.E., et al., 2008. Aneuploidy affects proliferation and spontaneous immortalization in mammalian cells. *Science*, 322, 703–9.

Wiseman, F.K., Al-Janabi, T., Hardy, J., et al., 2015. A genetic cause of Alzheimer disease: mechanistic insights from Down syndrome. *Nat. Rev. Neurosci.*, 16, 564–574.

Wiseman, F.K., Sheppard, O., Linehan, J.M., et al., 2010. Generation of a panel of antibodies against proteins encoded on human chromosome 21. *J. Negat. Results Biomed.*, 9, 7.

Wisniewski, H.M. and Rabe, A., 1986. Discrepancy between Alzheimer-type neuropathology and dementia in persons with Down's syndrome. *Ann. N. Y. Acad. Sci.*, 477, 247–60.

Wisniewski, K.E., Wisniewski, H.M. and Wen, G.Y., 1985. Occurrence of neuropathological changes and dementia of Alzheimer's disease in Down's syndrome. *Ann. Neurol.*, 17, 278–82.

Witton, J., Padmashri, R., Zinyuk, L.E., et al., 2015. Hippocampal circuit dysfunction in the Tc1 mouse model of Down syndrome. *Nat. Neurosci.*, 18, 1291–1298.

Wright, A.L., Zinn, R., Hohensinn, B., et al., 2013. Neuroinflammation and neuronal loss precede Abeta plaque deposition in the hAPP-J20 mouse model of Alzheimer's disease. *PLoS One*, 8, e59586.

Wu, C., Macleod, I. and Su, A.I., 2013. BioGPS and MyGene.info: organizing online, gene-centric information. *Nucleic Acids Res.*, 41, D561–5.

Wu, J. and Morris, J.K., 2013. The population prevalence of Down's syndrome in England and Wales in 2011. *Eur. J. Hum. Genet.*, 21, 1016–9.

Wu, J., Petralia, R.S., Kurushima, H., et al., 2011. Arc/Arg3.1 regulates an endosomal pathway essential for activity-dependent β-amyloid generation. *Cell*, 147, 615–28.

Wu, Y.-H., Fischer, D.F., Kalsbeek, A., et al., 2006. Pineal clock gene oscillation is disturbed in Alzheimer's disease, due to functional disconnection from the "master clock". *FASEB J.*, 20, 1874–6.

Wyss-Coray, T. and Mucke, L., 2002. Inflammation in neurodegenerative disease--a double-edged sword. *Neuron*, 35, 419–32.

Xie, H., Liu, Y., Zhu, Y., et al., 2014. In vivo imaging of immediate early gene expression reveals layer-specific memory traces in the mammalian brain. *Proc. Natl. Acad. Sci. U. S. A.*, 111, 2788–93.

Xue, Q.-S. and Streit, W.J., 2011. Microglial pathology in Down syndrome. *Acta Neuropathol.*, 122, 455–66.

Yang, D.-S.S., Stavrides, P., Mohan, P.S., et al., 2011. Reversal of autophagy dysfunction in the TgCRND8 mouse model of Alzheimer's disease ameliorates amyloid pathologies and memory deficits. *Brain*, 134, 258–277.

Yang, Q., Rasmussen, S.A. and Friedman, J.M., 2002. Mortality associated with Down's syndrome in the USA from 1983 to 1997: a population-based study. *Lancet*, 359, 1019–25.

Yasuno, F., Kosaka, J., Ota, M., et al., 2012. Increased binding of peripheral benzodiazepine receptor in mild cognitive impairment-dementia converters measured by positron emission tomography with [^{11}C]DAA1106. *Psychiatry Res.*, 203, 67–74.

Yeh, C.-Y., Vadhwana, B., Verkhratsky, A., et al., 2011. Early astrocytic atrophy in the entorhinal cortex of a triple transgenic animal model of Alzheimer's disease. *ASN Neuro*, 3, 271–9.

Yin, K.-J., Cirrito, J.R., Yan, P., et al., 2006. Matrix Metalloproteinases Expressed by Astrocytes Mediate Extracellular Amyloid-beta Peptide Catabolism. *J. Neurosci.*, 26, 10939–10948.

Ying, S.-W., Futter, M., Rosenblum, K., et al., 2002. Brain-derived neurotrophic factor induces long-term potentiation in intact adult hippocampus: requirement for ERK activation coupled to CREB and upregulation of Arc synthesis. *J. Neurosci.*, 22, 1532–40.

Yu, T., Li, Z., Jia, Z., et al., 2010. A mouse model of Down syndrome trisomic for all human chromosome 21 syntenic regions. *Hum. Mol. Genet.*, 19, 2780–91.

Yu, T., Liu, C., Belichenko, P., et al., 2010. Effects of individual segmental trisomies of human chromosome 21 syntenic regions on hippocampal long-term potentiation and cognitive behaviors in mice. *Brain Res.*, 1366, 162–71.

Zeisel, A., Manchado, A.B.M., Codeluppi, S., et al., 2015. Cell types in the mouse cortex and hippocampus revealed by single-cell RNA-seq. *Science*, 347, 1138–1142.

Zhang, B., Gaiteri, C., Bodea, L.-G., et al., 2013. Integrated systems approach identifies genetic nodes and networks in late-onset Alzheimer's disease. *Cell*, 153, 707–20.

Zhao, J., Paganini, L., Mucke, L., et al., 1996. Beta-secretase processing of the beta-amyloid precursor protein in transgenic mice is efficient in neurons but inefficient in astrocytes. *J. Biol. Chem.*, 271, 31407–11.

Zigman, W.B., 2013. Atypical aging in Down syndrome. *Dev. Disabil. Res. Rev.*, 18, 51–67.

frontiers in Behavioral Neuroscience

REVIEW
published: 13 October 2015
doi: 10.3389/fnbeh.2015.00268

Dissecting Alzheimer disease in Down syndrome using mouse models

Xun Yu Choong[1,2], *Justin L. Tosh*[1,2], *Laura J. Pulford*[1,2] *and Elizabeth M. C. Fisher*[1,2]*

[1] *Department of Neurodegenerative Disease, Institute of Neurology, University College London, London, UK,* [2] *The LonDownS Consortium, London, UK*

Down syndrome (DS) is a common genetic condition caused by the presence of three copies of chromosome 21 (trisomy 21). This greatly increases the risk of Alzheimer disease (AD), but although virtually all people with DS have AD neuropathology by 40 years of age, not all develop dementia. To dissect the genetic contribution of trisomy 21 to DS phenotypes including those relevant to AD, a range of DS mouse models has been generated which are trisomic for chromosome segments syntenic to human chromosome 21. Here, we consider key characteristics of human AD in DS (AD-DS), and our current state of knowledge on related phenotypes in AD and DS mouse models. We go on to review important features needed in future models of AD-DS, to understand this type of dementia and so highlight pathogenic mechanisms relevant to all populations at risk of AD.

Keywords: Alzheimer disease, APP, Down syndrome, mouse models, trisomy 21

OPEN ACCESS

Edited by:
Roger H. Reeves, Johns Hopkins University, USA

Reviewed by:
Sebastian Herbert Scharf, F. Hoffmann-La Roche Ltd, Switzerland
Yann Herault, Centre National de la Recherche Scientifique, France
Alexander M. Kleschevnikov, University of California, San Diego, USA

***Correspondence:**
Elizabeth M. C. Fisher, Department of Neurodegenerative Disease, UCL Institute of Neurology, Queen Square, London WC1N 3BG, UK
e.fisher@prion.ucl.ac.uk

Received: *22 May 2015*
Accepted: *21 September 2015*
Published: *13 October 2015*

Citation:
Choong XY, Tosh JL, Pulford LJ and Fisher EMC (2015) Dissecting Alzheimer disease in Down syndrome using mouse models. Front. Behav. Neurosci. 9:268. doi: 10.3389/fnbeh.2015.00268

Introduction: AD-DS, the Most Common Genetic Form of AD

Down syndrome (DS) is a complex, heterogeneous disorder caused by the presence of an extra copy of human chromosome 21. Trisomy 21 is a common condition, with an incidence of 1 in 750 live births (Parker et al., 2010). Prevalence in many countries is growing due to increasing maternal age, the greatest risk factor for DS (Loane et al., 2013), together with rises in DS life expectancy (Yang et al., 2002; Bittles and Glasson, 2004). In Northern Europe, for example, the number of people aged over 40 years with DS is approximately double what it was in 1990, and in the UK this age group accounts for a third of the estimated 40,000 people with DS (Wu and Morris, 2013).

The clinical presentation of DS varies extensively and includes features present in all individuals, such as cognitive deficits, and those seen in only some people, such as heart defects (Zigman, 2013; Jensen and Bulova, 2014). Alzheimer disease (AD) pathology is found in the brains of virtually all people with DS by 40 years of age (Wisniewski et al., 1985; Mann and Esiri, 1989), and trisomy 21 causes an increased risk of dementia such that approximately one third of the DS population has AD ("AD-DS") by the age of 60, with an estimated lifetime prevalence of 90% for all people with DS (Prasher and Krishnan, 1993; Holland et al., 1998; Coppus et al., 2006; Margallo-Lana et al., 2007; McCarron et al., 2014). However, while AD-DS is one of the largest contributors to morbidity and mortality in DS (Coppus et al., 2008), not all individuals develop dementia, even by 70 years of age (Krinsky-McHale et al., 2008; Ghezzo et al., 2014). Thus, the DS population has the most common genetic form of early-onset AD, caused by trisomy 21. Studying AD-DS allows investigation of the initial pathogenic events leading to AD and the development of dementia, relevant to both people with DS and to the general population.

One approach to dissecting human disease is through studying mouse models, and a large number of transgenic strains have been generated to understand specific aspects of AD

pathology, most of which have human gene mutations that give rise to rare early-onset familial Alzheimer disease (FAD; Braidy et al., 2012; Webster et al., 2014). In the last decade, chromosome engineering techniques have enabled the generation of an array of DS mouse models that will allow us to dissect the genetic contribution of chromosome 21 (Hsa21), or regions of the mouse genome syntenic to Hsa21, to DS phenotypes. These models recapitulate a wide range of DS features, including neurobiological, behavioral and aging-related aspects (Zhang et al., 2012b; Ruparelia et al., 2013). Thus, in the study of AD-DS, mouse models of DS offer an increasingly important approach to understanding pathogenic mechanisms, so informing us about pathways and networks relevant to all populations at risk of dementia.

Here, we present an overview of clinical features of AD-DS, compared to other genetic forms of AD, to highlight human phenotypes that may be assessed in mechanistic studies of mouse models. We then give examples of data from DS mouse models compared to transgenic mice modeling aspects of AD pathology, to illustrate informative findings from both types of model. We also offer examples of potentially helpful data for investigating AD-DS from the outcomes of overexpressing single genes from Hsa21. Finally, we consider the important features for mouse models to enhance our understanding of AD-DS, and therefore the pathogenetic mechanisms relevant to all AD. For brevity, citations may not necessarily be the original papers, but useful reviews or later references.

Genetic Forms of AD, Including AD-DS

The *APP* gene lies on Hsa21 and encodes the amyloid precursor protein that is at the heart of the amyloid cascade hypothesis of Alzheimer disease (Glenner and Wong, 1984; Hardy and Higgins, 1992; Hardy and Selkoe, 2002). This hypothesis was generated partly from the observation that extracellular plaques in brains of people with AD are composed of Aβ peptides that are products of APP metabolism. The hypothesis suggests that abnormal APP metabolism initiates AD pathogenesis by triggering a set of events that result in Aβ aggregation, particularly of the Aβ42 peptide, in these extracellular plaques. This leads to the formation of intracellular neurofibrillary tangles, primarily composed of the protein tau, and eventually loss of synapses and neurons. The relationship between the histopathological features of AD and dementia is not yet clear (Castellani and Perry, 2014).

The amyloid cascade hypothesis is currently the most widely-accepted paradigm guiding investigations of AD pathogenesis, and is supported at least in part by the rare cases of FAD caused by different mutations in *APP*, and in the presenilin genes *PSEN1* and *PSEN2* that affect APP processing. *APP* mutations may, for example, result in an increase in total Aβ production, or a relative increase in Aβ species associated with pathogenicity (Ryan and Rossor, 2010).

Importantly for understanding AD-DS, the link between *APP* and AD also extends to gene dose: in rare forms of FAD, duplication of the wildtype *APP* locus alone ("Dup-APP") is sufficient to cause highly penetrant early-onset AD (Rovelet-Lecrux et al., 2006; Sleegers et al., 2006). Dup-APP cases demonstrate that the three doses of *APP* arising from trisomy 21 are likely to be causative for AD-DS. Conversely, although very rare, partial trisomy 21 excluding *APP* (i.e., with two "doses" of *APP*) does not appear to lead to AD (Prasher et al., 1998; Korbel et al., 2009).

While people with DS and Dup-APP are at high risk of dementia, presumably in both cases because of *APP* triplication, there are some intriguing differences in their AD-related clinical features (Wiseman et al., 2015). Examining the effects of different *APP* genotypes may therefore provide insights into the modulation of *APP* pathogenesis. **Table 1** shows key examples of phenotypes in AD-DS and how these compare with Dup-APP, FAD due to other *APP* mutations (primarily point mutations) and late-onset sporadic AD (SAD). Mutations in *PSEN1* and *PSEN2*, which do not map to Hsa21, are not included.

However, a difficulty in analysing phenotypes is the considerable heterogeneity in clinical presentation within each *APP* genotype, even within families with the same mutation. For example, there is a wide variety of non-cognitive symptoms and behavioral changes across all four AD genotypes, including personality changes (Nelson et al., 2001; Ball et al., 2008), hallucinations (Sleegers et al., 2006; Basun et al., 2008; Guyant-Marechal et al., 2008), paranoia (Sleegers et al., 2006; Pilotto et al., 2013), and delusions (Burns et al., 1990), some of which are associated with cognitive decline (Adams and Oliver, 2010). Another important issue in diagnosing AD in AD-DS is that dementia is an additional cognitive deficit acquired on top of the baseline cognitive impairment found in people with DS: distinguishing between cognitive deficits due to intellectual disability, and decline at early stages of AD, is therefore an important challenge. However, diagnosis of dementia by experienced clinicians has been shown to be accurate in DS, and even more reliable than recent operational dementia criteria (Sheehan et al., 2015). Further, a few clinical features stand out in AD-DS—a striking example, albeit one of unknown relevance to AD, is seizure susceptibility in adulthood, which appears heightened by *APP* duplication, as both AD-DS (84%) and Dup-APP (57%) have significantly higher rates of seizures than SAD (10–20%). This may indicate specific pathways that are progressively disrupted by *APP* duplication, resulting in damaging electrical activity in the brain.

Dup-APP and FAD caused by *APP* mutations are relatively rare, and much information about these conditions remains to be gathered, for example, on synaptic dysfunction, oxidative stress and neuroinflammation. In contrast, AD-DS arises in a population with a well-defined genetic basis and a sizeable prevalence, which means it is of great value for investigating AD pathogenesis for everyone at risk of dementia.

Modeling DS, Including AD-DS, in Mice

Human chromosome 21 has synteny with the mouse genome, such that its ortholog genes are found in three blocks with conserved order and gene orientation on mouse chromosomes 10 (Mmu10), Mmu16, and Mmu17 (Hattori et al., 2000; Dierssen et al., 2009); the mouse *App* gene lies on Mmu16 (**Figure 1**).

TABLE 1 | Comparison of phenotypes from different genetic forms of human Alzheimer disease.

Phenotype		AD-DS: three copies of wildtype *APP*	FAD (Dup-APP): three copies of wildtype *APP*	FAD (*APP* mutations): Usually heterozygous for a mutant *APP* allele. ***N.B. these mutations do not necessarily act by the same mechanisms***	SAD: two copies of wildtype *APP*
CLINICAL SYMPTOMS					
Cognition	Incidence and age of onset of dementia	Less than 40 years of age, <5% people with DS have dementia but prevalence doubles every 5 years; by 55–60 years, 50–70% of DS have AD (Tyrrell et al., 2001; Hartley et al., 2015) Total prevalence across lifespan estimated at ∼90% (McCarron et al., 2014)	Dementia onset ∼42–59 years of age (Cabrejo et al., 2006)	Dementia onset ∼45–60 years of age (Ryan and Rossor, 2010)	Dementia onset usually >65 years of age (Querfurth and LaFerla, 2010)
	Pre-clinical cognitive symptoms	Pre-existing cognitive impairments complicate diagnosis of AD in DS (Zigman, 2013) Memory deficits may occur up to 3 years before dementia diagnosis (Krinsky-McHale et al., 2002)	No apparent pre-symptomatic cognitive impairment (Cabrejo et al., 2006; Rovelet-Lecrux et al., 2006)	Pre-symptomatic impairment of verbal memory and IQ; early progressive impairment of episodic memory (Rovelet-Lecrux et al., 2006; Hooli et al., 2012)	Mild cognitive impairment (cognitive symptoms, notably memory problems, which do not significantly affect function) precedes dementia (Albert et al., 2011), although only 5–20% go on to develop dementia
	Clinical presentation of dementia	Amnestic presentation similar to AD after taking into account pre-existing baseline intellectual deficits However, changes in behavior and personality are more common than SAD (Krinsky-McHale et al., 2000; Devenny et al., 2002; Ball et al., 2008)	Slow and progressive memory impairment and loss of cognition (Sleegers et al., 2006)	Most cases have similar amnestic presentation to SAD (Pilotto et al., 2013)	Progressive deficits in episodic memory, semantic knowledge, working memory, and attention (Weintraub et al., 2012)
	Sex differences	No difference between sexes (Coppus et al., 2006)	Not reported	Not reported	Women at higher risk (Musicco, 2009)
Epilepsy		Up to 84% AD-DS experience seizures (Mendez and Lim, 2003; De Simone et al., 2010)	Up to 57% exhibit seizures (Rovelet-Lecrux et al., 2006)	Seizures described in at least four different APP mutations (Kumar-Singh et al., 2000; Murrell et al., 2000; Grabowski et al., 2001; Pasalar et al., 2002)	Up to 10–20% of patients exhibit seizures (Mendez and Lim, 2003; Palop, 2009)
CLASSICAL AD NEUROPATHOLOGY: Aβ AND TAU					
Aβ accumulation and deposition	Intracellular Aβ	Intraneuronal accumulation of Aβ42 has been seen at 3 years of age. Levels decline as diffuse and dense core plaques develop (Mori et al., 2002)	Intraneuronal accumulation of Aβ40 in post mortem brain. No intraneuronal Aβ42 detected (Cabrejo et al., 2006)	Not reported	Intracellular staining found in post mortem SAD tissue (LaFerla et al., 2007)

(Continued)

TABLE 1 | Continued

Phenotype		AD-DS: three copies of wildtype *APP*	FAD (Dup-APP): three copies of wildtype *APP*	FAD (*APP* mutations): Usually heterozygous for a mutant *APP* allele. *N.B. these mutations do not necessarily act by the same mechanisms*	SAD: two copies of wildtype *APP*
	Extracellular Aβ	Earliest extracellular deposition found at 8 years of age (Leverenz and Raskind, 1998) Aβ40 undetectable in plaques in DS brain <50 years of age. Proportion of Aβ40 in plaques gradually increases until =50 years of age 42% of dense-core plaques comprise of Aβ40 (Iwatsubo et al., 1995) Amyloid plaques universal in DS people by age 31 (Leverenz and Raskind, 1998; Hartley et al., 2015)	Parenchymal lesions predominantly composed of Aβ42. Vascular amyloid predominantly Aβ40 (Cabrejo et al., 2006; Rovelet-Lecrux et al., 2006) Abundant parenchymal and vascular lesions as both dense-core and diffuse plaques (Cabrejo et al., 2006; Guyant-Marechal et al., 2008)	Increased Aβ42/Aβ40 ratio and/or increased Aβ production (Tanzi, 2012). Rare APP A673T mutant confers protection against AD pathology (Peacock et al., 1993; Hashimoto and Matsuoka, 2014) Pattern and progression of amyloid plaque deposition is largely identical to SAD. However, mutations within the Aβ sequence can cause increased deposition in the vasculature (Pilotto et al., 2013)	Accumulation of Aβ42 and Aβ40 into amyloid plaques. Aβ42 is more abundant in plaques (Serrano-Pozo et al., 2011) Amyloid plaque deposition progresses in a stereotypical fashion characterized by Thal phases I-V (Thal et al., 2002) Highest accumulation of plaques found in layers II–IV of the isocortex (Braak and Braak, 1991; Serrano-Pozo et al., 2011)
	Cerebral Amyloid Angiopathy (CAA) and Intra-cranial Hemorrhage (ICH)	CAA pathology common in DS. ICH is rare (Mann, 1988a; McCarron et al., 1998; Naito et al., 2008)	CAA is ubiquitous (Cabrejo et al., 2006; Sleegers et al., 2006; Rovelet-Lecrux et al., 2007; Kasuga et al., 2009) ICH in 20–50% of cases (Cabrejo et al., 2006; Rovelet-Lecrux et al., 2007; Guyant-Marechal et al., 2008; Kasuga et al., 2009)	CAA is in a large number of FAD mutations but not all (Ryan and Rossor, 2010) Arctic and Dutch APP mutations both affect residue 693 but only patients with Dutch mutation develop CAA and ICH (Basun et al., 2008; Ryan and Rossor, 2010)	∼50–80% of cases have CAA, deposits primarily composed of Aβ40 (Jellinger et al., 2007; Serrano-Pozo et al., 2011) ICH in ∼3% of SAD cases, possibly related to hypertension (Jellinger et al., 2007)
Neurofibrillary tangles		NFTs present in almost all people with DS by age 45. Density of NFTs triples between age 40–50 (Wisniewski et al., 1985; Goedert et al., 1992) NFT density correlates more strongly with clinical dementia rating than Aβ plaque count (Margallo-Lana et al., 2007) NFTs only manifest subsequent to dense-core amyloid plaques (Hartley et al., 2015)	NFTs consistent with late stage AD present at time of death (Rovelet-Lecrux et al., 2006)	Different FAD mutations exert highly variable effects on NFTs, from absence of NFTs in Arctic mutations to severe pathology (Ryan and Rossor, 2010)	Stereotypical spatiotemporal progression of NFTs begins in the allocortex of the medial temporal lobe with six stages of development, distinguished by Braak stages (Braak and Braak, 1991) Increased levels of total tau and phospho-tau correlate with increase in SAD severity (Wallin et al., 2006; Serrano-Pozo et al., 2011)

(Continued)

TABLE 1 | Continued

Phenotype	AD-DS: three copies of wildtype *APP*	FAD (Dup-APP): three copies of wildtype *APP*	FAD (*APP* mutations): Usually heterozygous for a mutant *APP* allele. ***N.B. these mutations do not necessarily act by the same mechanisms***	SAD: two copies of wildtype *APP*
Neuronal loss and brain atrophy	Neuronal atrophy follows SAD pattern but trend for less relative cell loss and atrophy compared to SAD (Mann, 1988b) Selective loss of BFCNs from as early as 5.5 months of age. Progressive loss of neurons in the Nucleus basalis of Meynert during aging (Casanova et al., 1985; McGeer et al., 1985)	Diffuse cortical atrophy with parietal dominance and neuronal loss (Cabrejo et al., 2006; Sleegers et al., 2006; Rovelet-Lecrux et al., 2007; Guyant-Marechal et al., 2008; Kasuga et al., 2009)	Similar neuronal atrophy pattern to SAD with a slightly more severe medial-temporal pattern (Pilotto et al., 2013)	Characteristic loss of neurons and white matter (Querfurth and LaFerla, 2010). Neuronal loss correlates with NFTs (Gómez-Isla et al., 1997; Serrano-Pozo et al., 2011) Basal forebrain atrophy correlates with Aβ burden (Kerbler et al., 2015)
OTHER FEATURES OF AD PATHOLOGY				
Synaptic loss and dysfunction	Synaptic protein expression decreased in aging DS brain (Downes et al., 2008) GABA levels decreased in post-mortem hippocampus and temporal cortex (Reynolds and Warner, 1988; Seidl et al., 2001; Martínez-Cué et al., 2014)	Not reported	Not reported	Synapse loss is best correlate of cognitive decline and precedes neuronal loss (Ingelsson et al., 2004; Scheff et al., 2007) GABA significantly reduced in post mortem cortical but not subcortical brain regions. *In vivo* evidence of GABA loss in parietal cortex (Seidl et al., 2001; Bai et al., 2014)
Oxidative stress and proteostasis	Some proteins oxidatively modified differently in DS and control groups, suggesting DS subjects vulnerable to oxidative damage (Di Domenico et al., 2014)	Not reported	Not reported	Increased levels of oxidative stress are a hallmark of SAD pathology and linked to aging (Madeo, 2013)
Endosomal dysfunction	Endosome enlargement, alterations in morphology and function in young DS (pre-AD) and DS fibroblasts (Jiang et al., 2010)	Not reported	Enlarged endosomes modulated by ApoE status (Cataldo et al., 2001)	Enlarged endosomes detected in preclinical stages (Cataldo et al., 1997, 2000) Aβ accumulates within late endosomes in AD brain (Takahashi et al., 2002)

(Continued)

TABLE 1 | Continued

Phenotype	AD-DS: three copies of wildtype *APP*	FAD (Dup-APP): three copies of wildtype *APP*	FAD (*APP* mutations): Usually heterozygous for a mutant *APP* allele. ***N.B. these mutations do not necessarily act by the same mechanisms***	**SAD: two copies of wildtype *APP***
Neuroinflammation	Dystrophic microglia and absence of activated microglia at 40 years of age, coincident with tau pathology (Xue and Streit, 2011) Increased astrocytic activation in early DS, increases with age and correlates with amyloid deposition (Royston et al., 1999)	Not reported	Not reported	Hyper-reactive, dystrophic microglia associated with dense-core plaques and NFTs (McGeer et al., 1987; Streit et al., 2009) Reactive astrocytes locate early to dense-core plaques, triggered by Aβ (Itagaki et al., 1989; Pike et al., 1995) Higher neuroinflammation in younger (<80) compared to older patients with SAD, suggesting importance in early stages of disease (Hoozemans et al., 2011)

Down syndrome (AD-DS), familial AD due to APP duplications (Dup-APP), familial AD due to APP mutations (FAD), and sporadic Alzheimer disease (SAD) Abbreviations: BFCNs, basal forebrain cholinergic neurons; CAA, cerebral amyloid angiopathy; GABA, γ-Aminobutyric acid; ICH, intra-cranial hemorrhage; ID, intellectual disability; NFT, neurofibrillary tangles.

Mice with precisely-defined trisomies (or monosomies) have been generated, now usually by chromosome engineering (Brault et al., 2006; Tybulewicz and Fisher, 2006), to provide a set of models that are segmentally trisomic for regions orthologous to Hsa21 (Davisson et al., 1993; Sago et al., 1998; Olson et al., 2004; Li et al., 2007; Herault et al., 2009; Pereira et al., 2009; Yu et al., 2010a; Liu et al., 2011, 2014; Brault et al., 2015).

Generating many models with different partial trisomies creates a mapping panel in which individual phenotypes may be assessed in several strains, and so assigned to specific trisomic chromosomal region(s). As all DS phenotypes presumably arise from abnormal gene dosage, candidate genes that when present in three copies give rise to all or part of the phenotype, can be chosen from the trisomic critical region. Individual candidate genes can then be studied, for example, in overexpression or knockout models, to assess the effects of different copy numbers of the gene. **Figure 1** is an overview of DS mouse models and the chromosomal segments for which they are trisomic. **Table 2** details the gene content for each DS mouse model shown, including protein-coding and non-protein-coding genes relevant to human trisomy 21.

The most complete mouse model to date, *Dp(10)1Yey/+;Dp(16)1Yey/+;Dp(17)1Yey/+*, is trisomic for all Hsa21 syntenic regions and was generated by crossing three DS mouse models, each carrying duplications of the respective Hsa21 orthologous regions on Mmu10, Mmu16 and Mmu17 (Li et al., 2007; Yu et al., 2010a,b; **Figure 1**). However, the vast majority of studies relating to AD-DS have been performed on the Ts65Dn mouse, as this has been an extremely important "standard model" of DS for many years, prior to the development of newer strains by chromosome engineering (Davisson et al., 1993; Reeves et al., 1995; **Table 2**). The Ts65Dn mouse carries a Robertsonian translocation resulting in trisomy of ∼42% of the protein-coding genes orthologous to Hsa21, but it also has 79 additional genes (including long non-coding sequences) from Mmu17 that are outside the Hsa21 region of synteny, and these need to be taken into account when analysing phenotypes (Duchon et al., 2011; Reinholdt et al., 2011). These extra triplicated genes that do not relate to DS happen to include non-Hsa21 genes, such as *SYNJ2* and *TIAM2* that have Hsa21/Mmu16 paralogues (*SYNJ1*, *TIAM1*), which may complicate phenotype-genotype correlations (Duchon et al., 2011). Other triplicated genes in Ts65Dn irrelevant to DS include several genes encoding dynein light chains that may influence endosomal trafficking, and so potentially affect neuronal phenotypes (Hartley et al., 2015).

A different type of mouse model of DS is the "humanized" transchromosomic "Tc1" mouse that carries a freely-segregating Hsa21 (O'Doherty et al., 2005), which is functionally trisomic for ∼75% of Hsa21 protein-coding genes (Gribble et al., 2013). However, this extra chromosome is rearranged, and lost stochastically at different rates in different mouse tissues—thus, Tc1 mice are mosaic for the human chromosome. With respect to AD research, the *APP* gene is not functionally trisomic in Tc1 mice because of a rearrangement that has occurred by chance, so this animal expresses just the two endogenous copies of mouse *App* (Sheppard et al., 2012).

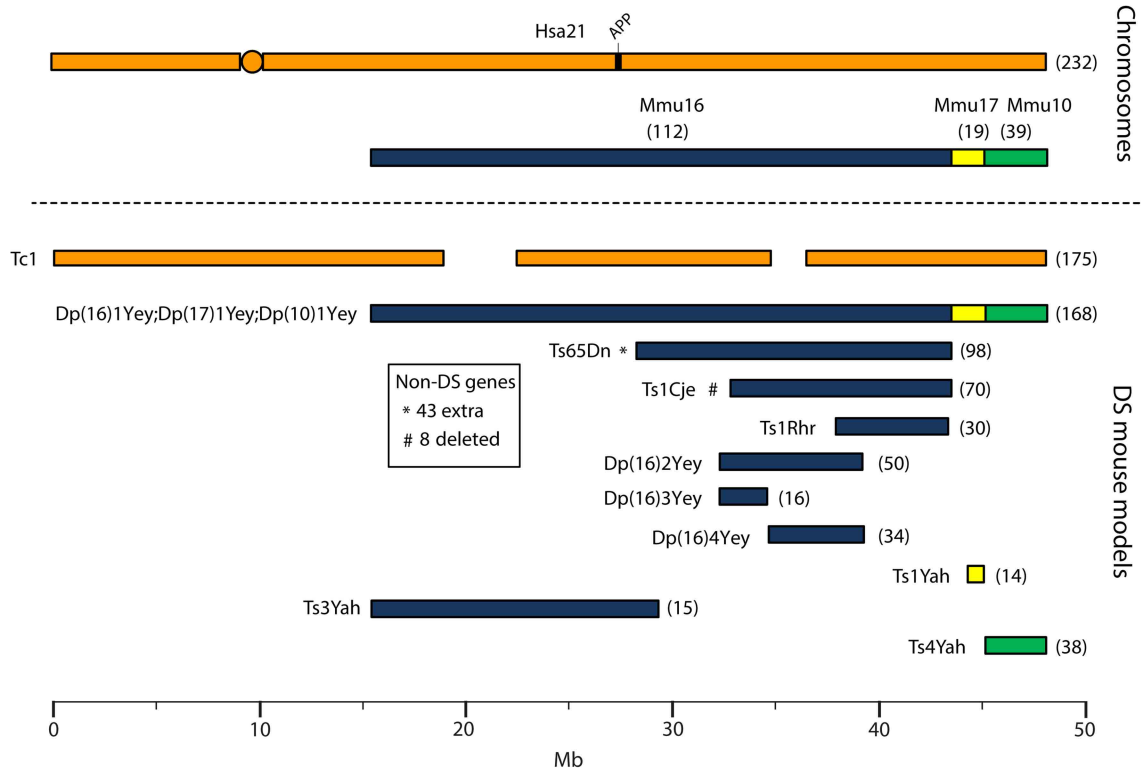

FIGURE 1 | Human chromosome 21 (Hsa21), orthologous mouse chromosomes (Mmu), and key mouse models of Down syndrome. Diagram representing Hsa21 and its alignment with syntenic regions on Mmus 16, 17, and 10. The orange circle represents the human centromere and mouse models are color-coded and aligned according to the chromosomal segment for which they are trisomic. Numbers in brackets represent the number of protein-coding Hsa21 orthologous genes within each region or mouse model, according to Ensembl release 79 and the breakpoints published in papers referenced here. The Tc1 mouse is the only model which carries Hsa21, though genomic rearrangements and deletions (indicated by breaks in the chromosome) mean the mouse is functionally trisomic for only ~75% of Hsa21 genes (Gribble et al., 2013). All other mouse models carry duplications of mouse orthologues. The Dp1(16)Yey;Dp1(17)Yey;Dp1(10)Yey (or Ts1Yey;Ts3Yey;Ts2Yey) mouse was generated by crossing together three partial trisomy models (Yu et al., 2010a) and spans the entirety of the Hsa21-syntenic regions. The Ts65Dn mouse (Davisson et al., 1993) contains a freely segregating segment of Mmu16, however it is also trisomic for 43 extra protein-coding genes on the centromeric section of Mmu17 that are not relevant to DS (indicated by an asterisk (*) and accompanying text box; Duchon et al., 2011; Reinholdt et al., 2011). The Ts1Cje mouse (Sago et al., 1998) also contains a monosomy of eight protein-coding genes on Mmu12, irrelevant to the DS phenotype (indicated by "#" and accompanying text box. Gene numbers are based on Ensembl release 79, compared to the original seven monosomic genes detailed in Duchon et al., 2011). Other mice are Ts1Rhr or Dp1(16)Rhr mice (Olson et al., 2004); Ts1Yah mice (Pereira et al., 2009); Ts3Yah (previously published as Ts2Yah; Brault et al., 2015); and Ts4Yah mice (previously published as Ts3Yah mice; Herault et al., 2009). Other useful examples of mouse models include the Ts43H model (not shown) which is partially trisomic for Mmu17 including some genes with ortholog on Hsa21 (Vacík et al., 2005). The scale is in megabase pairs (Mb).

While many DS mouse models have been published, there is no single complete model, and the usefulness of these strains lies in their comparative and complementary use in studying genotype-phenotype relationships, including AD-related phenotypes (**Table 3**). These studies enable us to map critical dosage-sensitive genes because each locus is likely expressed at trisomic levels, mimicking human DS transcription. We can also study the interactions of Hsa21 dosage-sensitive genes with the rest of the genome (Hsa21 and non-Hsa21), as well as effects exerted by aneuploidy *per se*.

Modeling Amyloid Deposition in Mice

In contrast to the segmental duplication of tens of endogenous wildtype genes in DS mouse strains, AD models are primarily transgenic lines that overexpress one or more of the human mutant genes that cause FAD. These transgenes usually insert at random sites in the genome and may be driven by artificial promoters (see examples in **Table 4**), which vary in terms of their spatial and temporal expression patterns, and result in expression at often 5–10 fold compared to endogenous mouse orthologue (Balducci and Forloni, 2011; Hall and Roberson, 2012). Overexpressing wildtype human *APP* or mouse *App* does not result in amyloid deposition (Elder et al., 2010); hence the need to use known AD-causative mutant sequences in transgenic mice.

In general, while mutant *APP* transgenic mice develop robust amyloid deposition, synaptotoxic features and memory impairments, none of them reproduces tau-containing neurofibrillary tangles, the hallmark pathology of AD which most

TABLE 2 | Trisomic region and triplicated gene content in Down syndrome mouse models shown in Figure 1 compared with Hsa21 (Ensembl release 79).

		Protein-coding genes		Non-protein-coding genes		Total genes		% Protein-coding genes from Hsa21
	Hsa21	232		648		880		
DS mouse model	Official MGI name*	Mouse genes	Hsa21 genes	Mouse genes	Hsa21 genes	Mouse genes	Hsa21 genes	
Tc1	B6;129S-Tc(Hsa21)1TybEmcf/J	–	175	–	Undetermined	–	N/A	75
Dp(16)1Yey	B6.129S7-Dp(16Lipi-Zbtb21)1Yey/J	149	112	112	6	261	118	48
Dp(17)1Yey	B6;129S7-Dp(17Abcg1-Rrp1b)3Yey/J	19	18	6	0	25	18	8
Dp(10)1Yey	B6;129S7-Dp(10Prmt2-Pdxk)2Yey/J	55	39	20	1	75	40	17
Ts65Dn**	B6EiC3Sn a/A-Ts(1716)65Dn	133	98	71	3	204	101	42
Ts1Cje***	B6.Cg-T(12;16)1Cje/CjeDnJ	76	70	51	1	127	71	30
Ts1Rhr	B6.129S6-Dp(16Cbr1-Fam3b)1Rhr/J	32	30	20	0	52	30	13
Dp(16)2Yey	129-Dp(16Tiam1-Kcnj6)6Yey/J	53	50	37	1	90	51	22
Dp(16)3Yey	129-Dp(16Tiam1-Il10rb)8Yey/J	18	16	12	0	30	16	7
Dp(16)4Yey	129-Dp(16Ifnar1-Kcnj6)10Yey/J	35	34	24	1	59	35	15
Ts1Yah	B6;129P2-Dp(17Abcg1-Cbs)1Yah/Orl	15	14	4	0	19	14	6
Ts3Yah (previously Ts2Yah)	B6;129P2-Dp(16Hspa13-App)2Yah/Orl	19	15	45	5	64	20	6
Ts4Yah (previously Ts3Yah)	B6.Cg-Dp(10Prmt2-Cstb)3Yah/Orl	54	38	20	1	74	39	16
TRISOMIC/MONOSOMIC REGIONS AND GENE CONTENT IRRELEVANT TO Hsa21 AND ITS SYNTENIC REGIONS IN MICE								
Ts65Dn**	B6EiC3Sn a/A-Ts(1716)65Dn	43	–	36	–	79	–	
Ts1Cje***	B6.Cg-T(12;16)1Cje/CjeDnJ	8	–	4	–	12	–	

Mouse genome informatics site that includes the official mouse strain names www.informatics.jax.org; the shaded line shows number of Hsa21 genes.

***indicates gene content of Ts65Dn and ***indicates gene content of Ts1Cje mice.*

TABLE 3 | Examples of AD phenotypes studied in DS mouse models, and related findings in *APP* transgenic strains described in Table 4.

Phenotype	DS models		*APP* transgenic models
Cognitive deficits	Learning and memory deficits widely demonstrated, mostly in young mice (Das and Reeves, 2011) Differentiating between early cognitive impairment and neurodegeneration in old age is a challenge (Ruparelia et al., 2013). One study suggests learning deficits in Ts65Dn worsen with age, but due to lack of motivation or motor impairment rather than neurodegeneration (Sanders et al., 2009)		Working memory, episodic memory, executive function, and attention deficits in *APP* transgenic mice from young ages (3–5 months; Webster et al., 2014) Memory impairments linked to neurotoxicity as a result of Aβ oligomers (Lesné et al., 2006) or insoluble Aβ deposits (Westerman et al., 2002) Behavioral deficits deteriorate with age in some *APP* transgenic mice (Hsiao et al., 1996; Van Dam et al., 2003)
Long-term potentiation (LTP)	Hippocampal LTP deficits reported in all models trisomic for Mmu16 regions syntenic to Hsa21, apart from Ts2Yah for which no LTP data is available (Das and Reeves, 2011) LTP increased in Dp1(17)Yey and unaltered in Dp1(10)Yey (Yu et al., 2010b) LTP deficits observed in Tc1 suggest compromised entorhinal cortex input into the dentate gyrus, contributing to impaired CA3 and CA1 function (Witton et al., 2015)		LTP studies have produced often contradictory measurements within the same mouse models (Pozueta et al., 2013) Aberrant neuronal activity is a prominent feature; restoring inhibitory synaptic activity may rescue network hypersynchrony, memory deficits and early mortality (Sanchez et al., 2011; Verret et al., 2012; Stargardt et al., 2015)
Aβ accumulation and deposition	APP protein and mRNA expression	In Ts65Dn, APP protein increases to trisomic levels from 6 months in the striatum (Hunter et al., 2003), and from 10 months in cortex and hippocampus (Seo and Isacson, 2005; Contestabile et al., 2006) APP mRNA in Ts65Dn remains similar to disomic levels at 5 months but increases at 12 months (Choi et al., 2009)	*APP* transgenic mice generally overexpress human *APP* with FAD mutations at levels at least 5x endogenous mouse *App*. *APP* transgene transcription is directed by artificial promoters (**Table 4**) allowing expression in the central nervous system, usually from embryonic or early postnatal age (Crews et al., 2010; Balducci and Forloni, 2011; Hall and Roberson, 2012)
	APP metabolism	In Ts65Dn, total APP CTF levels increased in hippocampus, enriched in synaptosomes and early endosomes from 6 months (Salehi et al., 2006; Lockrow et al., 2009) In Ts65Dn no difference in Aβ42/40 ratios, low levels of larger (~115 kDa) SDS-stable Aβ oligomers (Salehi et al., 2006; Choi et al., 2009; Peng et al., 2009)	In line with the overexpression of *APP*, Aβ levels are generally overexpressed, with some models expressing FAD mutations driving an increase in Aβ42/40 ratios (Crews et al., 2010)
Tau	Neurofibrillary pathology	In aged Ts65Dn mice increased tau and reelin detected in granules in hippocampus and olfactory bulb (Kern et al., 2011) No tau neurofibrillary tangles detectable in Tc1 and Ts1Cje brains (O'Doherty et al., 2005; Shukkur et al., 2006; Sheppard et al., 2012)	*APP* transgenic mice fail to produce neurofibrillary tangles without additional mutations introduced in presenilin or tau (Kokjohn and Roher, 2009)
	Tau hyper-phosphorylation	In Ts65Dn, Ts1Cje and Tc1, increased tau phosphorylation in hippocampus and cortex at various phosphorylation sites (Shukkur et al., 2006; Liu et al., 2008; Sheppard et al., 2012) In Tc1 this was detected in old (20 months) but not young (2 months) mice (Sheppard et al., 2012) Unphosphorylated tau decreased in Ts1Cje mice (Shukkur et al., 2006)	Hyperphosphorylation of tau and its regulation have primarily been studied in *APP* transgenic mice with additional mutations in presenilin and/or tau Hyperphosphorylated tau is detectable in some *APP* transgenic mouse models (Kokjohn and Roher, 2009; Crews et al., 2010)

(Continued)

TABLE 3 | Continued

Phenotype		DS models	*APP* transgenic models
	Regulation of tau phosphorylation	Increased phosphorylation of GSK-3β in Tc1 and Ts1Cje (Shukkur et al., 2006; Sheppard et al., 2012). Increased phosphorylation of AKT in Tc1 and Ts65Dn (Siarey et al., 2006; Sheppard et al., 2012) CDK5 expression upregulated in Ts65Dn but not in Tc1 (Pollonini et al., 2008; Sheppard et al., 2012). No difference in CDK5 activators p25/p35 levels detected in both Ts1Cje and Tc1 (Shukkur et al., 2006; Sheppard et al., 2012)	
Neuronal loss and dysfunction	Loss and dysfunction of Basal Forebrain Cholinergic Neurons (BFCNs)	Reduced BFCN numbers and cell size in Ts65Dn mice from 12 months (Cooper et al., 2001; Salehi et al., 2006) ChAT activity increased in 10-month but no different from control in 19-month Ts65Dn (Contestabile et al., 2006) Distribution of cholinergic neurons in dentate gyrus altered in Ts65Dn (Cooper et al., 2001; Salehi et al., 2006) All above alterations not observed in Ts1Cje and Ts65Dn:App$^{+/+/-}$ mice, both of which are disomic for *App* (Salehi et al., 2006)	Loss of BFCNs observed in APP23 and APP(V717I; Choi et al., 2013). No loss of BFCNs observed in APP23 (Boncristiano et al., 2002) and Tg2576 (Apelt et al., 2002) Decreased ChAT and AChE activity in basal forebrain nuclei of APP23 (Van Dam et al., 2005)
	Loss and dysfunction of noradrenergic neurons	Degenerative morphology and loss of noradrenergic neurons in rostral LC in Ts65Dn at 12 months but not 4 months (Lockrow et al., 2011b; Fortress et al., 2015)	Noradrenaline levels declined with aging in TgCRND8 hippocampus (Francis et al., 2012). No overt cell loss in LC in old APP23 and PDAPP mice, although neurons decreased in size in PDAPP (Szot et al., 2009; Francis et al., 2012)
OTHER FEATURES POTENTIALLY RELEVANT TO AD			
Epilepsy	5–10x increased rates of audiogenic seizures and seizure-related death in 21-day old Ts65Dn mice, attenuated by mGluR5 antagonists (Westmark et al., 2010)		Epileptiform activity and spontaneous non-convulsive seizures frequently observed in *APP* transgenic mice, from young ages (Born, 2015). Whether this is caused by overproduction of Aβ (Palop, 2009) or is an artifact of *APP* overexpression during development (Born et al., 2014) is unclear
Synaptic loss and dysfunction	Synaptic and dendritic abnormalities	In Ts65Dn, increased average synapse size with no change in synaptic number or density (Hernández-González et al., 2015) In Ts65Dn, dendritic spines are enlarged, less dense, and redistributed on principal neurons; arborizations are poorly developed. Similar but less severe observations in Ts1Cje (Dierssen et al., 2003; Belichenko et al., 2004) In Tc1, reduced synaptic size, complexity and density observed in hippocampus (Witton et al., 2015); decreased dendritic mushroom spines (associated with memory) at 3 months and increase in stubby spines (Haas et al., 2013) Ts1Rhr fewer thin spines (associated with learning) at 3 weeks of age (Haas et al., 2013)	Loss and alterations in dendritic spines and synapses are early features of neuronal pathology in *APP* transgenic mice models, before onset of plaque deposition and cognitive deficits. Synaptic deficits correlate well with soluble Aβ (Pozueta et al., 2013) Reduced density of mushroom-type spines of CA1 hippocampal region in two *APP* transgenic mouse models (Perez-Cruz et al., 2011)

(Continued)

TABLE 3 | Continued

Phenotype	DS models	*APP* transgenic models
Oxidative stress and proteostasis	Oxidative stress markers increased in young and old Ts65Dn mice (Lockrow et al., 2009; Shichiri et al., 2011; Di Domenico et al., 2015) Impaired mitochondrial function and increased ROS production in Ts1Cje cortical astrocyte and hippocampal neuronal cultures (Shukkur et al., 2006)	Oxidative stress increased and precedes Aβ deposition in *APP* transgenic mice. Increased Aβ levels lead to mitochondrial impairments (Eckert et al., 2010; Ye et al., 2012; Meraz-Ríos et al., 2014)
Endosomal dysfunction	Enlarged EEs in BFCNs and expression of EE proteins detected from 6 months in Ts65Dn, increasing in number with age (Cataldo et al., 2003; Salehi et al., 2006) EEs not enlarged in Ts1Cje and Ts65Dn-App$^{+/+/-}$ mice, both of which are disomic for *App* (Cataldo et al., 2003) Axonal transport disruption selectively impaired for endosomal cargo in Ts65Dn mice (Salehi et al., 2006)	No enlargement of EEs observed in APP22 and APP23 mice (Cataldo et al., 2003). Enlarged EEs found in APP23 (Choi et al., 2013) Aβ42 accumulates in endosomal compartments in Tg2576 mice before plaque deposition, and increases with age (Takahashi et al., 2002)
Neuroinflammation and glial phenotypes	Increased astrocytic protein expression and metabolic activity in old Ts65Dn mice (Holtzman et al., 1996; Contestabile et al., 2006) Increased microglial activation in basal forebrain and hippocampus of old Ts65Dn mice (Hunter et al., 2004; Lockrow et al., 2011a)	Astrocytic changes in morphology and increased calcium signaling in *APP* transgenic mice (Takano et al., 2007; Beauquis et al., 2013; Rodríguez-Arellano et al., 2015) Impairments in microglia phagocytosis and increased microglia proliferation around plaques in APP23 and Tg2576 (Frautschy et al., 1998; Krabbe et al., 2013)

Abbreviations: AChE, acetylcholinesterase; AKT, protein kinase B; BFCN, basal forebrain cholinergic neuron; CA1, Cornu Ammonis area 1; CDK5, cyclin-dependent kinase 5; ChAT, choline acetyltransferase; CTF, C-terminal fragment; EE, early endosome; GSK-3β, glycogen synthase kinase 3β; LC, locus coeruleus; LTP, long-term potentiation; mGluR5, metabotropic glutamate receptor 5; ROS, reactive oxygen species; SDS, sodium-dodecyl sulfate.

TABLE 4 | Human *APP* overexpressing transgenic mice referred to in this review (information obtained from Alzforum.org).

Mouse	Mutation	Promoter	Genetic Background	References
APP22	APP751 KM670/671NL (Swedish), V717I (London)	Human THY1	C57BL/6	Sturchler-Pierrat et al., 1997
APP23	APP751 KM670/671NL (Swedish)	Mouse Thy1	C57BL/6	Sturchler-Pierrat et al., 1997
APP(V717I)	APP695 V717I (London)	Mouse Thy1	Originally generated on FVB/N background; available at reMYND as C57BL/6xFVB/N	Moechars et al., 1999
Tg2576	APP695 KM670/671NL (Swedish)	Hamster prion protein	C57BL/6;SJL mixed background	Hsiao et al., 1996
TgCRND8	APP KM670/671NL (Swedish), V717F (Indiana)	Hamster prion protein	C3H/He-C57BL/6 mixed background	Chishti et al., 2001
PDAPP	APP V717F (Indiana)	Human PDGF	C57BL/6 x DBA2	Games et al., 1995

closely correlates with dementia (Hall and Roberson, 2012). The combined overexpression of mutant *APP* and mutant human tau is required to reproduce both amyloid and tau pathology, although these tau mutations in humans do not alone cause AD but another form of neurodegeneration, frontotemporal dementia. Mutant *APP* transgenics may be best considered models of APP/Aβ pathology (amyloid deposition) rather than full AD.

Studying AD-DS Phenotypes in Mice

In **Table 3**, we summarize examples of findings that may be informative for AD-DS from different DS (mainly Ts65Dn) mice and examples of AD models (**Table 4**). With respect to AD, a wide range of mutant *APP* transgenic strains are available in the literature, so we have chosen a few well-known examples [APP22, APP23, APP (V717I), PDAPP, Tg2576, TgCRND8] to illustrate some potential phenotypes of interest. We note that the expression of wildtype mouse APP, and wildtype or mutant human APP protein in these different models can influence amyloid pathology (Kokjohn and Roher, 2009). For example, because of amino acid differences between the two species, mouse APP may be processed with little BACE1 cleavage and so may yield three times less Aβ than wildtype human APP (De Strooper et al., 1995). In addition, the genetic background of AD mouse strains affects a range of APP/Aβ phenotypes, including plaque deposition, APP metabolism, survival, and seizure rates (Carlson et al., 1997; Lehman et al., 2003; Krezowski et al., 2004; Lassalle et al., 2008; Rustay et al., 2010; Jackson et al., 2015). Similarly, phenotypes observed in DS mice may be influenced by genetic background (O'Doherty et al., 2005; Galante et al., 2009; Costa et al., 2010; Deitz and Roper, 2011; Haydar and Reeves, 2012). We consider only *APP* transgenic models of AD, as the other genes used in such models (*PSEN1, PSEN2*, and *MAPT*) are not encoded on Hsa21, and therefore are not directly relevant to AD-DS.

In studying mouse phenotypes to understand AD-DS, we are presented with two key issues. Firstly, we need to test longitudinally DS models to look for changes in older mice that are not apparent early on, and so may indicate aging or neurodegenerative processes rather than neurodevelopmental deficits. Secondly, we need to separate normal aging processes in DS from those connected specifically to AD-DS. The thoughtful use of the increasing range of different mouse models is enabling us to dissect these issues to further our understanding of AD-DS.

A study that has addressed both (1) neurodegenerative vs. neurodevelopmental and (2) normal aging vs. AD phenotypes has been performed in the Ts65Dn mouse. This study concerned the neurodegenerative phenotype loss of basal forebrain cholinergic neurons (BFCNs), and was carried out through an experimental design involving optimal crossing of different mouse models and assessment of the genetically-distinct progeny (Salehi et al., 2006). Firstly, Salehi and colleagues quantified the known loss of BFCNs in Ts65Dn mice, and showed this loss to be progressive, thus an aging or an AD-related phenotype in this DS mouse model. The authors then compared BFCN loss in Ts65Dn and Ts1Cje DS mouse models (**Figure 1**), and were able to map a dosage-sensitive critical region that had to contain a candidate gene for this phenotype: Ts65Dn mice lose BFCNs but Ts1Cje mice turned out to have no loss compared to wildtype mice. Therefore, the dosage-sensitive gene(s), that when present in three copies is responsible for BFCN loss, must map within the region of trisomy present in Ts65Dn but not in Ts1Cje. A key candidate in this region was the *App* gene. By crossing Ts65Dn mice to heterozygous *App* knockout mice, the authors generated cohorts of progeny that carried the trisomic region with either two or three copies of wildtype *App*. Assessing BFCN loss in these cohorts led to the conclusion that the phenotype arises mainly from having three copies of *App* and, further, that it is associated with impairments in nerve growth factor retrograde transport, linked to early endosomes, which are enlarged (Salehi et al., 2006).

Given the role of *APP* triplication in this phenotype, there is likely a strong link to AD and AD-DS. In people with early AD pathology or mild cognitive impairment, neurofibrillary pathology has been detected in BFCNs (Mesulam et al., 2004; Grudzien et al., 2007), while their loss has been observed in patients with SAD (and other neurodegenerative disorders; Zarow et al., 2003). Interestingly, enlarged early endosomes have been detected in cortical tissues from cognitively intact individuals with mild AD pathology, and in young individuals

with DS (under 12 years old), suggesting that endosome enlargement is an early feature in AD pathogenesis (Cataldo et al., 2000).

DS Models in the Study of Candidate Genes Influencing AD

As illustrated in **Table 1**, while people with DS have three copies of *APP* and develop early AD neuropathology, their clinical presentation is variable, suggesting that other genetic and environmental factors influence pathogenesis. In addition to *APP*, many genes on Hsa21 have been studied in the context of neurodegeneration and/or AD, and it is conceivable that a three-copy dose of any of these genes could contribute to disease and dysfunction.

Single gene overexpressing transgenics do not model DS, or AD-DS, but may provide some insights if carefully considered. For example, seizures and neuronal network abnormalities remain challenging areas to investigate but important phenotypes to be explored in DS, AD-DS, and *APP* overexpression models of AD (i.e., which are single gene transgenic models). In SAD, seizures have been associated with early cognitive decline (Vossel et al., 2013), while the incidence of seizures in AD-DS is high and is associated with increased risk of dementia (for example, McCarron et al., 2014). To date, seizure phenotypes and epileptiform activity have been characterized across numerous *APP* transgenic mice (Born, 2015), but it is unclear whether these phenotypes are primarily driven by amyloid overproduction (Mucke and Selkoe, 2012) or are an effect of unphysiological *APP* overexpression during development (Born et al., 2014). Antiepileptic drugs, such as levetiracetam, which improve seizures in DS (Sangani et al., 2010) and in AD (Cumbo and Ligori, 2010), also ameliorate synaptic and memory dysfunctions in APP transgenic mice by suppressing neuronal network dysfunction (Sanchez et al., 2012; Devi and Ohno, 2013).

So, while single gene transgenic models do not model human trisomy 21 or AD because they usually express the gene by many-fold, from ectopic promoters, they offer insights into some of the functional consequences of overexpression, albeit at non-trisomic levels. **Table 5** presents a list of Hsa21 gene candidates, in chromosomal order, that have been investigated for overexpression-related phenotypes linked with AD across different mouse, fruitfly, and cellular models. We also compare, where data are available, how related changes in these genes have been explored in humans with AD and/or DS. Making optimal use of mouse genetics, some of the single-gene-overexpressing mouse transgenics have been crossed with AD models, to look for changes in phenotypes that may be informative. For example, crossing an *S100β* overexpression model with the Tg2576 *APP* transgenic mouse generates double mutant progeny with exacerbated cerebral amyloidosis and reactive gliosis. This suggests that increased expression of *S100β* could contribute to AD pathogenesis possibly by promoting amyloidogenic APP processing (Mori et al., 2010).

Other key Hsa21 gene candidates *DYRK1A* and *RCAN1* have been linked to AD pathogenesis through their effects on tau. The toxic neurofibrillary tangles (NFTs) that accumulate in AD are formed of hyperphosphorylated tau protein. Overexpression of *DYRK1A* in transgenic mice resulted in tau hyperphosphorylation (Ryoo et al., 2007, 2008), and DYRK1A has been shown to co-localize with NFTs more frequently in AD-DS brain compared to SAD (Wegiel et al., 2008). Similarly, overexpression of *RCAN1* in a mouse model resulted in abnormal tau hyperphosphorylation (Wegiel et al., 2011). This suggests that the increased expression of *DYRK1A* and *RCAN1* in DS could promote the formation of NFTs, a hallmark feature of AD pathology.

Triplication of Hsa21 genes in DS does not necessarily lead to a 1.5-fold increase (compared to euploid individuals) in their RNA or protein expression. For example, a study in DS fetal cortical tissue revealed multiple Hsa21 proteins in fact expressed at similar or lower levels than in disomic controls (Cheon et al., 2003a,b,c,d). Assessments at transcriptomic and proteomic levels, together with meta-analysis across these studies, provide useful resources for understanding patterns of alteration in gene expression (for example, see Vilardell et al., 2011). As a few of the studies in **Table 5** have demonstrated, it is important to verify the effect of trisomy on candidate gene expression, in relevant tissues and contexts, before further characterization of any potential downstream effects of trisomy.

Prospects for Research

Individuals with DS manifest the most common genetic form of AD, and this undoubtedly largely arises from expressing three copies of *APP* (Ness et al., 2012; Hartley et al., 2015). Therefore, studying and modeling this population will assist in understanding the contribution of APP to AD pathogenesis, and evaluating the amyloid cascade hypothesis. However, the variation in clinical presentation of AD-DS shows that many other genetic and environmental factors contribute, almost certainly including protective factors. The thoughtful use of models will thus provide insight into these factors.

To study mouse models of AD-DS, it is critical to dissect neurodevelopmental from neurodegenerative effects (Bothwell and Giniger, 2000; Contestabile et al., 2010). To be of interest for AD-DS, such phenotypes should differ from normal aging in the mouse strain of interest, although this can be difficult to determine, particularly as DS has been characterized as a syndrome of accelerated aging in both clinical (Lott, 2012; Zigman, 2013) and epigenetic terms (Horvath et al., 2015), and because aging remains the clearest non-genetic risk factor for all forms of AD (Fratiglioni, 1996; Bush and Beail, 2004). The longitudinal study of cognitive decline in DS mice poses similar challenges to those in people with DS, and tests need to distinguish between dysfunction due to dementia, as opposed to aging or baseline learning deficits. For example, variations of a learning procedure involving incremental repeated acquisition tasks suggest that declining performances by Ts65Dn mice with age may be due to motor impairments and/or decreased motivation, rather than neurodegenerative-related effects (Sanders et al., 2009). To improve behavioral testing in mouse models of AD-DS, a potential avenue to explore

TABLE 5 | Single gene overexpression models from Hsa21, with relevance to AD phenotypes. Genes are listed in order from centromere to Hsa21q telomere.

Hsa21 gene	Phenotypes studied in models	Phenotypes studied in humans
APP	Please refer to **Table 3**.	Please refer to **Table 1**
SOD1	*SOD1* overexpression protects against APP-induced lethality in transgenic mice (Carlson et al., 1997)	SOD1 activity positively correlates with levels of memory functioning in DS adults (Zis et al., 2012)
ITSN1	Overexpression of *ITSN1* homolog *nla* in combination with *SYNJ1* and *RCAN1* homologs causes impaired vesicle recycling in *Drosophila* (Chang and Min, 2009)	ITSN1 protein (Hunter et al., 2011) and mRNA (Pucharcos et al., 1999) elevated in DS *ITSN1* highly expressed in AD brain (Blalock et al., 2004; Wilmot et al., 2008)
SYNJ1	Mice overexpressing *SYNJ1* have deficits in synaptic transmission (Voronov et al., 2008) *SYNJ1* transgenic mice display enlarged endosomes (Cossec et al., 2012)	SYNJ1 levels higher in DS brain tissue compared to controls, and elevated in AD-DS cases (Martin et al., 2014)
OLIG2	Neural progenitors from *Olig2*-overexpressing mice exhibit impairments in neural progenitor proliferation (Lu et al., 2012)	SNPs in *OLIG2* associated with psychotic symptoms in AD (Sims et al., 2009)
RCAN1	*RCAN1* overexpression in a mouse model causes abnormal tau phosphorylation (Wegiel et al., 2011) In cell models, *RCAN1* overexpression leads to deficits in synaptic transmission (Martin et al., 2012) and promotes neuronal apoptosis (Sun et al., 2011, 2014)	*RCAN1* chronically elevated in AD and DS (Ermak et al., 2001)
DYRK1A	*DYRK1A* overexpression linked to tau hyperphosphorylation and increased Aβ production in transgenic mice (Ryoo et al., 2007, 2008) and cellular models (Park et al., 2007; Coutadeur et al., 2015) *Dyrk1a* overexpression causes phosphorylation of PS1, increasing γ-secretase activity in cells and stabilizing γ-secretase complex in mice (Ryu et al., 2010) Mouse *Dyrk1a* overexpression in TgDyrk1A mice results in a significant reduction of *Rest* mRNA (Canzonetta et al., 2008)	DYRK1A increased in the brains of patients with AD (Kimura et al., 2007) and DS (Ryoo et al., 2008) DYRK1A expression in DS brain correlates with 3-repeat tau levels (Shi et al., 2008; Wegiel et al., 2011) Plasma DYRK1A positively correlates with cerebrospinal fluid tau and phospho-tau in AD patients (Janel et al., 2014) Co-localization of DYRK1A with NFTs greater in AD-DS than SAD (Wegiel et al., 2008) REST levels correlate with cognitive preservation and longevity in aging and are downregulated in AD (Lu et al., 2014)
DSCAM	Trisomy of *Dscam* in *Drosophila* results in synaptic targeting errors (Cvetkovska et al., 2013)	DSCAM overexpressed in a DS patient, and DSCAM immunoreactivity associated with Aβ plaques in demented DS patients (Saito et al., 2000)
ETS2	*Ets2* transgenic mice and fibroblasts overexpressing ETS2 have elevated APP, presenilin1 protein and increased Aβ production (Wolvetang et al., 2003b) *Ets2* overexpression causes apoptosis via caspase 3 activation in primary neuronal cultures (Wolvetang et al., 2003a) and in DS cortical neurons (Helguera et al., 2005)	ETS2 immunoreactivity associated with intracellular Aβ and hyperphosphorylated tau in both AD-DS and sporadic AD brain tissue (Helguera et al., 2005)
BACE2	*BACE2* overexpression *in vitro* reduces Aβ levels (Sun et al., 2006) In a mouse model, overexpression of *BACE2* has no effect on Aβ production (Azkona et al., 2010a,b)	*BACE2* polymorphisms may predict age of onset of dementia in DS (Myllykangas et al., 2005; Mok et al., 2014)
ABCG1	*ABCG1* overexpression stimulates cholesterol efflux *in vitro* (Kim et al., 2007; Tansley et al., 2007) and either reduces (Kim et al., 2007) or increases Aβ production (Tansley et al., 2007), the latter through an increase in APP processing *ABCG1* overexpression in a mouse model has no effect on reference or working memory or synaptic plasticity (Parkinson et al., 2009), nor alters Aβ, APOE nor cholesterol efflux *in vivo* (Burgess et al., 2008)	*ABCG1* gene upregulated in patients with DS (Tansley et al., 2007; Kong et al., 2015) *ABCG1* gene expression unaltered in AD (Tansley et al., 2007)
CSTB	*Cstb* overexpression in a mouse model does not induce epileptic activity or a myoclonic seizure phenotype (Brault et al., 2011)	CSTB protein unaltered in DS fetal cerebral cortex (Cheon et al., 2003b).

(Continued)

TABLE 5 | Continued

Hsa21 gene	Phenotypes studied in models	Phenotypes studied in humans
SUMO3	*SUMO3* overexpression in cell culture systems shown to both increase (Dorval et al., 2007) and reduce (Zhang and Sarge, 2008) Aβ levels *SUMO3* overexpression modulates APP processing, increasing the CTF/APP ratio *in vitro* (Dorval et al., 2007)	High molecular weight SUMO3 conjugates decreased in AD brain tissue (Lee et al., 2014)
S100β	S100β application results in tau hyperphosphorylation in cultured neural stem cells (Esposito et al., 2008) *S100β* overexpression increases neuronal death and reduces neuronal production in DS stem cells (Lu et al., 2011) *S100β* overexpression in Tg2576 AD mice increases Aβ deposition and BACE1 activity (Mori et al., 2010) Mice overexpressing *S100β* show accelerated signs of aging (Shapiro and Whitaker-Azmitia, 2004) neuropathology (Shapiro et al., 2004) and behavioral deficits (Borella et al., 2003)	*S100β* upregulated in DS and AD (Griffin et al., 1989; Sheng et al., 1994) *S100β* overexpression positively correlates with age in DS patients (Royston et al., 1999)

SOD1, superoxide dismutase1; ITSN1, intersectin 1; SYNJ1, synaptojanin 1; OLIG2, oligodendrocyte transcription factor 2; RCAN1, regulator of calcineurin 1; DYRK1A, Dual specificity tyrosine-phosphorylation-regulated kinase 1A; DSCAM, Down syndrome cell adhesion molecule; ETS2, V-Ets Avian Erythroblastosis Virus E26 Oncogene Homolog 2; BACE2, beta-site APP cleaving enzyme 2; ABCG1, ATP-binding cassette sub-family G member 1; CSTB, cystatin B; SUMO3, small ubiquitin-like modifier 3; S100β, S100 calcium binding protein β; REST, repressor element-1 silencing transcription factor.

capitalizes on the association of dementia with deficits in episodic memory. The development of tests based on, for example, visuo-spatial data, should therefore highlight age-dependent, dementia-related deficits in mouse models, because they rely on the encoding and binding of information spontaneously, and do not challenge other cognitive domains (Iordanova et al., 2009).

As well as the hypothesis-driven study of AD-DS phenotypes, one of the greatest strengths of working with mouse models is our ability to undertake unbiased hypothesis-generating research, by mapping phenotypes to genomic critical regions using the range of strains now available. These include chromosome-engineered panels of partially trisomic mice (**Figure 1**) as well as single gene knockout animals, such as the $App^{+/-}$ heterozygous mice, which may be crossed to partially trisomic strains, to generate progeny with altered single gene copy numbers on different trisomic region backgrounds. The cohorts of progeny from these crosses provide ideal groups for testing the contributions of single Hsa21 genes to AD-DS.

Mouse genome engineering continues to offer new models and approaches for teasing apart AD-DS relevant phenotypes, and new strains are being published regularly to help refine experimental strategies. For example, the recent genomically humanized NLF mouse (Saito et al., 2014), which has human amino acid residues at key sites within APP that affect its processing, may yield new insights into the biology of both AD and AD-DS, partly through expressing mutant *APP* at physiological levels. The strategic breeding of new *APP* models with DS segmental trisomies will contribute to determining which phenotypes are downstream of an amyloid cascade. Furthermore, independent study of partial trisomies without three copies of *App* may help tease out effects of other factors, for example oxidative stress, cholesterol metabolism or immune system dysfunction, in the development of dementia (Wiseman et al., 2015).

DS mouse models also give us the flexibility to investigate the effects of potentially dosage-sensitive non-coding regions. For example, microRNAs (miRs)—short (20–23 nucleotide) RNAs that downregulate the transcription of target genes—have increasingly been investigated in AD pathogenesis due to their differential regulation in molecular pathways associated with AD (Veerappan et al., 2013). Hsa21 encodes 29 miRs (MirBase release 21, Griffiths-Jones, 2004), and their potential overexpression in trisomy may contribute to genetic dysregulation relevant to AD-DS. Overexpression of the Hsa21-encoded miR-155 in DS has been reported to increase Aβ production via the downregulation of sorting nexin 27, a membrane-trafficking component found in early endosomes, that modulates γ-secretase activity (Wang et al., 2013, 2014).

Hsa21 also encodes genes involved in post-translational histone modification, including *DYRK1A*, *ETS2*, *HMGN1*, *BRWD1,* and *RUNX1* (Dekker et al., 2014), which may be investigated for their potential roles leading to the aberrant histone modifications observed in AD (Zhang et al., 2012a; Narayan et al., 2015). Histone methylation (specifically H3K4me3) has been shown to correlate highly with genome-wide domains of dysregulated gene expression in DS, which are highly conserved between humans and Ts65Dn mice (Letourneau et al., 2014). DS mouse models therefore model epigenetic structures in humans and may be used to study the effects of its dysregulation in AD-DS.

Finally, mouse model research must be undertaken in parallel with other rapid advances in the AD-DS field. The advent of human induced pluripotent stem (iPS) cells (Hunsberger et al., 2015) for DS provides for the first time a trisomic human *in vitro* model that recapitulates hallmarks of some AD pathology (Shi et al., 2012; Chang et al., 2015; Moore et al., 2015; Murray et al., 2015). The further development of this technology (Hunsberger et al., 2015) will prove valuable to phenotyping and drug target discovery, alongside *in vivo* research

and *in vitro* primary cultures from DS mice. An increasing call is being made for partnerships to build up large cohorts of, and biobanks from, people with DS for the systematic longitudinal study of AD-DS progression (Hartley et al., 2015). In-depth phenotypic studies across development with infants and adults with DS are already underway (Wiseman et al., 2015). These will allow greater power to identify biomarkers for the prediction of AD in this large, genetically well-defined population, for example, through plasma (Dekker et al., 2015; Schupf et al., 2015), cerebrospinal fluid (Portelius et al., 2014a,b), and neuroimaging studies (Beacher et al., 2009; Landt et al., 2011; Powell et al., 2014; Sabbagh et al., 2015). Biomarker studies are also being performed in AD models, including at very early phases of Aβ deposition (Maia et al., 2015). Extending these studies to mouse models of DS and AD-DS will contribute to elucidating the genotype-phenotype relationships that ultimately lead to dementia.

Acknowledgments

We would like to thank members of the London Down Syndrome Consortium (LonDownS) for their constructive feedback to this review, in particular Annette Karmiloff-Smith, Carla Startin, Andre Strydom, Victor Tybulewicz, Frances Wiseman, as well as Veronique Brault, Mark Good, Eva Lana-Elola and Sheona Watson-Scales for their generous comments and advice. XYC is funded by the Brain Research Trust, JT is funded by the Alzheimer's Society, LP is funded by Alzheimer's Research UK, EF is funded by the Wellcome Trust.

References

Adams, D., and Oliver, C. (2010). The relationship between acquired impairments of executive function and behaviour change in adults with Down syndrome. *J. Intellect. Disabil. Res.* 54, 393–405. doi: 10.1111/j.1365-2788.2010.01271.x

Albert, M. S., DeKosky, S. T., Dickson, D., Dubois, B., Feldman, H. H., Fox, N. C., et al. (2011). The diagnosis of mild cognitive impairment due to Alzheimer's disease: recommendations from the National Institute on Aging-Alzheimer's Association workgroups on diagnostic guidelines for Alzheimer's disease. *Alzheimer's Dementia* 7, 270–279. doi: 10.1016/j.jalz.2011.03.008

Apelt, J., Kumar, A., and Schliebs, R. (2002). Impairment of cholinergic neurotransmission in adult and aged transgenic Tg2576 mouse brain expressing the Swedish mutation of human beta-amyloid precursor protein. *Brain Res.* 953, 17–30. doi: 10.1016/S0006-8993(02)03262-6

Azkona, G., Amador-Arjona, A., Obradors-Tarragó, C., Varea, E., Arqué, G., Pinacho, R., et al. (2010a). Characterization of a mouse model overexpressing beta-site APP-cleaving enzyme 2 reveals a new role for BACE2. *Genes Brain Behav.* 9, 160–172. doi: 10.1111/j.1601-183X.2009.00538.x

Azkona, G., Levannon, D., Groner, Y., and Dierssen, M. (2010b). *In vivo* effects of APP are not exacerbated by BACE2 co-overexpression: behavioural characterization of a double transgenic mouse model. *Amino Acids* 39, 1571–1580. doi: 10.1007/s00726-010-0662-8

Bai, X., Edden, R. A. E., Gao, F., Wang, G., Wu, L., Zhao, B., et al. (2014). Decreased γ-aminobutyric acid levels in the parietal region of patients with Alzheimer's disease. *Magn. Reson. Imaging* 41, 1326–1331. doi: 10.1002/jmri.24665

Balducci, C., and Forloni, G. (2011). APP transgenic mice: their use and limitations. *NeuroMol. Med.* 13, 117–137. doi: 10.1007/s12017-010-8141-7

Ball, S. L., Holland, A. J., Treppner, P., Watson, P. C., and Huppert, F. A. (2008). Executive dysfunction and its association with personality and behaviour changes in the development of Alzheimer's disease in adults with Down syndrome and mild to moderate learning disabilities. *Br. J. Clin. Psychol.* 47, 1–29. doi: 10.1348/014466507X230967

Basun, H., Bogdanovic, N., Ingelsson, M., Almkvist, O., Näslund, J., Axelman, K., et al. (2008). Clinical and neuropathological features of the arctic APP gene mutation causing early-onset Alzheimer disease. *Arch. Neurol.* 65, 499–505. doi: 10.1001/archneur.65.4.499

Beacher, F., Daly, E., Simmons, A., Prasher, V., Morris, R., Robinson, C., et al. (2009). Alzheimer's disease and Down's syndrome: an *in vivo* MRI study. *Psychol. Med.* 39, 675–684. doi: 10.1017/S0033291708004054

Beauquis, J., Pavía, P., Pomilio, C., Vinuesa, A., Podlutskaya, N., Galvan, V., et al. (2013). Environmental enrichment prevents astroglial pathological changes in the hippocampus of APP transgenic mice, model of Alzheimer's disease. *Exp. Neurol.* 239, 28–37. doi: 10.1016/j.expneurol.2012.09.009

Belichenko, P. V., Masliah, E., Kleschevnikov, A. M., Villar, A. J., Epstein, C. J., Salehi, A., et al. (2004). Synaptic structural abnormalities in the Ts65Dn mouse model of Down Syndrome. *J. Comp. Neurol.* 480, 281–298. doi: 10.1002/cne.20337

Bittles, A. H., and Glasson, E. J. (2004). Clinical, social, and ethical implications of changing life expectancy in Down syndrome. *Dev. Med. Child Neurol.* 46, 282–286. doi: 10.1111/j.1469-8749.2004.tb00483.x

Blalock, E. M., Geddes, J. W., Chen, K. C., Porter, N. M., Markesbery, W. R., and Landfield, P. W. (2004). Incipient Alzheimer's disease: microarray correlation analyses reveal major transcriptional and tumor suppressor responses. *Proc. Natl. Acad. Sci. U.S.A.* 101, 2173–2178. doi: 10.1073/pnas.0308512100

Boncristiano, S., Calhoun, M. E., Kelly, P. H., Pfeifer, M., Bondolfi, L., Stalder, M., et al. (2002). Cholinergic changes in the APP23 transgenic mouse model of cerebral amyloidosis. *J. Neurosci.* 22, 3234–3243.

Borella, A., Sumangali, R., Ko, J., and Whitaker-Azmitia, P. M. (2003). Characterization of social behaviors and oxytocinergic neurons in the S-100 beta overexpressing mouse model of Down Syndrome. *Behav. Brain Res.* 141, 229–236. doi: 10.1016/S0166-4328(02)00373-X

Born, H. A., Kim, J. Y., Savjani, R. R., Das, P., Dabaghian, Y. A., Guo, Q., et al. (2014). Genetic suppression of transgenic APP rescues Hypersynchronous network activity in a mouse model of Alzeimer's disease. *J. Neurosci.* 34, 3826–3840. doi: 10.1523/jneurosci.5171-13.2014

Born, H. A. (2015). Seizures in Alzheimer's disease. *Neuroscience* 286C, 251–263. doi: 10.1016/j.neuroscience.2014.11.051

Bothwell, M., and Giniger, E. (2000). Alzheimer's Disease. *Cell* 102, 271–273. doi: 10.1016/S0092-8674(00)00032-5

Braak, H., and Braak, E. (1991). Neuropathological stageing of Alzheimer-related changes. *Acta Neuropathol.* 82, 239–259. doi: 10.1007/BF00308809

Braidy, N., Muñoz, P., Palacios, A. G., Castellano-Gonzalez, G., Inestrosa, N. C., Chung, R. S., et al. (2012). Recent rodent models for Alzheimer's disease: clinical implications and basic research. *J. Neural Transm.* 119, 173–195. doi: 10.1007/s00702-011-0731-5

Brault, V., Duchon, A., Romestaing, C., Sahun, I., Pothion, S., Karout, M., et al. (2015). Opposite phenotypes of muscle strength and locomotor function in mouse models of partial trisomy and monosomy 21 for the proximal Hspa13-App region. *PLoS Genet.* 11:e1005062. doi: 10.1371/journal.pgen.1005062

Brault, V., Martin, B., Costet, N., Bizot, J. C., and Hérault, Y. (2011). Characterization of PTZ-induced seizure susceptibility in a down syndrome mouse model that overexpresses CSTB. *PLoS ONE* 6:e27845. doi: 10.1371/journal.pone.0027845

Brault, V., Pereira, P., Duchon, A., and Hérault, Y. (2006). Modeling chromosomes in mouse to explore the function of genes, genomic disorders, and chromosomal organization. *PLoS Genet.* 2:e86. doi: 10.1371/journal.pgen.0020086

Burgess, B. L., Parkinson, P. F., Racke, M. M., Hirsch-Reinshagen, V., Fan, J., Wong, C., et al. (2008). ABCG1 influences the brain cholesterol biosynthetic pathway but does not affect amyloid precursor protein or apolipoprotein E metabolism *in vivo*. *J. Lipid Res.* 49, 1254–1267. doi: 10.1194/jlr.M700481-JLR200

Burns, A., Jacoby, R., and Levy, R. (1990). Psychiatric phenomena in Alzheimer's disease. I Disorders of thought content. *Br. J. Psychiatry* 157, 72–76. doi: 10.1192/bjp.157.1.72

Bush, A., and Beail, N. (2004). Risk factors for dementia in people with down syndrome: issues in assessment and diagnosis. *Am. J. Ment. Retard.* 109, 83–97. doi: 10.1352/0895-8017(2004)109<83:RFFDIP>2.0.CO;2

Cabrejo, L., Guyant-Maréchal, L., Laquerrière, A., Vercelletto, M., De la Fournière, F., Thomas-Antérion, C., et al. (2006). Phenotype associated with APP duplication in five families. *Brain* 129, 2966–2976. doi: 10.1093/brain/awl237

Canzonetta, C., Mulligan, C., Deutsch, S., Ruf, S., O'Doherty, A., Lyle, R., et al. (2008). DYRK1A-dosage imbalance perturbs NRSF/REST levels, deregulating pluripotency and embryonic stem cell fate in Down syndrome. *Am. J. Hum. Genet.* 83, 388–400. doi: 10.1016/j.ajhg.2008.08.012

Carlson, G. A., Borchelt, D. R., Dake, A., Turner, S., Danielson, V., Coffin, J. D., et al. (1997). Genetic modification of the phenotypes produced by amyloid precursor protein overexpression in transgenic mice. *Hum. Mol. Genet.* 6, 1951–1959. doi: 10.1093/hmg/6.11.1951

Casanova, M. F., Walker, L. C., Whitehouse, P. J., and Price, D. L. (1985). Abnormalities of the nucleus basalis in Down's syndrome. *Ann. Neurol.* 18, 310–313. doi: 10.1002/ana.410180306

Castellani, R. J., and Perry, G. (2014). The complexities of the pathology-pathogenesis relationship in Alzheimer disease. *Biochem. Pharmacol.* 88, 671–676. doi: 10.1016/j.bcp.2014.01.009

Cataldo, A., Rebeck, G. W., Ghetri, B., Hulette, C., Lippa, C., Van Broeckhoven, C., et al. (2001). Endocytic disturbances distinguish among subtypes of Alzheimer's disease and related disorders. *Ann. Neurol.* 50, 661–665. doi: 10.1002/ana.1254

Cataldo, A. M., Barnett, J. L., Pieroni, C., and Nixon, R. A. (1997). Increased Neuronal Endocytosis and Protease Delivery to Early Endosomes in Sporadic Alzheimer's Disease: neuropathologic Evidence for a Mechanism of Increased beta -Amyloidogenesis. *J. Neurosci.* 17, 6142–6151.

Cataldo, A. M., Petanceska, S., Peterhoff, C. M., Terio, N. B., Epstein, C. J., Villar, A., et al. (2003). App Gene dosage modulates endosomal abnormalities of Alzheimer's Disease in a segmental Trisomy 16 mouse model of down syndrome. *J. Neurosci.* 23, 6788–6792.

Cataldo, A. M., Peterhoff, C. M., Troncoso, J. C., Gomez-Isla, T., Hyman, B. T., and Nixon, R. A. (2000). Endocytic pathway abnormalities precede amyloid beta deposition in sporadic Alzheimer's disease and Down syndrome: differential effects of APOE genotype and presenilin mutations. *Am. J. Pathol.* 157, 277–286. doi: 10.1016/S0002-9440(10)64538-5

Chang, C.-Y., Chen, S.-M., Lu, H.-E., Lai, S.-M., Lai, P.-S., Shen, P.-W., et al. (2015). N-butylidenephthalide attenuates Alzheimer's Disease-like Cytopathy in down syndrome induced pluripotent stem cell-derived neurons. *Sci. Rep.* 5, 8744. doi: 10.1038/srep08744

Chang, K. T., and Min, K. T. (2009). Upregulation of three Drosophila homologs of human chromosome 21 genes alters synaptic function: implications for Down syndrome. *Proc. Natl. Acad. Sci. U.S.A.* 106, 17117–17122. doi: 10.1073/pnas.0904397106

Cheon, M. S., Bajo, M., Kim, S. H., Claudio, J. O., Stewart, A. K., Patterson, D., et al. (2003a). Protein levels of genes encoded on chromosome 21 in fetal Down syndrome brain: challenging the gene dosage effect hypothesis (Part II). *Amino Acids* 24, 119–125. doi: 10.1007/s00726-002-0337-1

Cheon, M. S., Kim, S. H., Ovod, V., Kopitar Jerala, N., Morgan, J. I., Hatefi, Y., et al. (2003b). Protein levels of genes encoded on chromosome 21 in fetal Down syndrome brain: challenging the gene dosage effect hypothesis (Part III). *Amino Acids* 24, 127–134. doi: 10.1007/s00726-002-0340-6

Cheon, M. S., Kim, S. H., Yaspo, M.-L., Blasi, F., Aoki, Y., Melen, K., et al. (2003c). Protein levels of genes encoded on chromosome 21 in fetal Down syndrome brain: challenging the gene dosage effect hypothesis (Part I). *Amino Acids* 24, 111–117. doi: 10.1007/s00726-002-0336-2

Cheon, M. S., Shim, K. S., Kim, S. H., Hara, A., and Lubec, G. (2003d). Protein levels of genes encoded on chromosome 21 in fetal Down syndrome brain: challenging the gene dosage effect hypothesis (Part IV). *Amino Acids* 25, 41–47. doi: 10.1007/s00726-003-0009-9

Chishti, M. A., Yang, D. S., Janus, C., Phinney, A. L., Horne, P., Pearson, J., et al. (2001). Early-onset amyloid deposition and cognitive deficits in transgenic mice expressing a double mutant form of amyloid precursor protein 695. *J. Biol. Chem.* 276, 21562–21570. doi: 10.1074/jbc.M100710200

Choi, J. H. K., Berger, J. D., Mazzella, M. J., Morales-Corraliza, J., Cataldo, A. M., Nixon, R. A., et al. (2009). Age-dependent dysregulation of brain amyloid precursor protein in the Ts65Dn Down syndrome mouse model. *J. Neurochem.* 110, 1818–1827. doi: 10.1111/j.1471-4159.2009.06277.x

Choi, J. H. K., Kaur, G., Mazzella, M. J., Morales-Corraliza, J., Levy, E., and Mathews, P. M. (2013). Early endosomal abnormalities and cholinergic neuron degeneration in Amyloid-β protein precursor transgenic mice. *J. Alzheimers Dis.* 34, 691–700. doi: 10.3233/JAD-122143

Contestabile, A., Benfenati, F., and Gasparini, L. (2010). Communication breaks-Down: from neurodevelopment defects to cognitive disabilities in Down syndrome. *Prog. Neurobiol.* 91, 1–22. doi: 10.1016/j.pneurobio.2010.01.003

Contestabile, A., Fila, T., Bartesaghi, R., Contestabile, A., and Ciani, E. (2006). Choline acetyltransferase activity at different ages in brain of Ts65Dn mice, an animal model for Down's syndrome and related neurodegenerative diseases. *J. Neurochem.* 97, 515–526. doi: 10.1111/j.1471-4159.2006.03769.x

Cooper, J. D., Salehi, A., Delcroix, J. D., Howe, C. L., Belichenko, P. V., Chua-Couzens, J., et al. (2001). Failed retrograde transport of NGF in a mouse model of Down's syndrome: reversal of cholinergic neurodegenerative phenotypes following NGF infusion. *Proc. Natl. Acad. Sci. U.S.A.* 98, 10439–10444. doi: 10.1073/pnas.181219298

Coppus, A., Evenhuis, H., Verberne, G.-J., Visser, F., van Gool, P., Eikelenboom, P., et al. (2006). Dementia and mortality in persons with Down's syndrome. *J. Intellect. Disabil. Res.* 50, 768–777. doi: 10.1111/j.1365-2788.2006.00842.x

Coppus, A. M. W., Evenhuis, H. M., Verberne, G.-J., Visser, F. E., Oostra, B. A., Eikelenboom, P., et al. (2008). Survival in elderly persons with Down syndrome. *J. Am. Geriatr. Soc.* 56, 2311–2316. doi: 10.1111/j.1532-5415.2008.01999.x

Cossec, J. C., Lavaur, J., Berman, D. E., Rivals, I., Hoischen, A., Stora, S., et al. (2012). Trisomy for synaptojanin1 in down syndrome is functionally linked to the enlargement of early endosomes. *Hum. Mol. Genet.* 21, 3156–3172. doi: 10.1093/hmg/dds142

Costa, A. C. S., Stasko, M. R., Schmidt, C., and Davisson, M. T. (2010). Behavioral validation of the Ts65Dn mouse model for Down syndrome of a genetic background free of the retinal degeneration mutation Pde6brd1. *Behav. Brain Res.* 206, 52–62. doi: 10.1016/j.bbr.2009.08.034

Coutadeur, S., Benyamine, H., Delalonde, L., de Oliveira, C., Leblond, B., Foucourt, A., et al. (2015). A novel DYRK1A (Dual specificity tyrosine phosphorylation-regulated kinase 1A) inhibitor for the treatment of Alzheimer's disease: effect on Tau and amyloid pathologies *in vitro*. *J. Neurochem.* 133, 440–451. doi: 10.1111/jnc.13018

Crews, L., Rockenstein, E., and Masliah, E. (2010). APP transgenic modeling of Alzheimer's disease: mechanisms of neurodegeneration and aberrant neurogenesis. *Brain Struct. Funct.* 214, 111–126. doi: 10.1007/s00429-009-0232-6

Cumbo, E., and Ligori, L. D. (2010). Levetiracetam, lamotrigine, and phenobarbital in patients with epileptic seizures and Alzheimer's disease. *Epilepsy Behav.* 17, 461–466. doi: 10.1016/j.yebeh.2010.01.015

Cvetkovska, V., Hibbert, A. D., Emran, F., and Chen, B. E. (2013). Overexpression of Down syndrome cell adhesion molecule impairs precise synaptic targeting. *Nat. Neurosci.* 16, 677–682. doi: 10.1038/nn.3396

Das, I., and Reeves, R. H. (2011). The use of mouse models to understand and improve cognitive deficits in Down syndrome. *Dis. Model. Mech.* 4, 596–606. doi: 10.1242/dmm.007716

Davisson, M. T., Schmidt, C., Reeves, R. H., Irving, N. G., Akeson, E. C., Harris, B. S., et al. (1993). Segmental trisomy as a mouse model for Down syndrome. *Prog. Clin. Biol. Res.* 384, 117–133.

De Simone, R., Puig, X. S., Gelisse, P., Crespel, A., Genton, P., and Gélisse, P. (2010). Senile myoclonic epilepsy: delineation of a common condition associated with Alzheimer's disease in Down syndrome. *Seizure* 19, 383–389. doi: 10.1016/j.seizure.2010.04.008

De Strooper, B., Simons, M., Multhaup, G., Van Leuven, F., Beyreuther, K., and Dotti, C. G. (1995). Production of intracellular amyloid-containing fragments in hippocampal neurons expressing human amyloid precursor protein and protection against amyloidogenesis by subtle amino acid substitutions in the rodent sequence. *EMBO J.* 14, 4932–4938.

Deitz, S. L., and Roper, R. J. (2011). Trisomic and allelic differences influence phenotypic variability during development of Down syndrome mice. *Genetics* 189, 1487–1495. doi: 10.1534/genetics.111.131391

Dekker, A. D., Coppus, A. M. W., Vermeiren, Y., Aerts, T., van Duijn, C. M., Kremer, B. P., et al. (2015). Serum MHPG strongly predicts conversion to Alzheimer's disease in behaviorally characterized subjects with Down syndrome. *J. Alzheimers Dis.* 43, 871–891. doi: 10.3233/JAD-140783

Dekker, A. D., De Deyn, P. P., and Rots, M. G. (2014). Epigenetics: the neglected key to minimize learning and memory deficits in Down syndrome. *Neurosci. Biobehav. Rev.* 45, 72–84. doi: 10.1016/j.neubiorev.2014.05.004

Devenny, D. A., Zimmerli, E. J., Kittler, P., and Krinsky-McHale, S. J. (2002). Cued recall in early-stage dementia in adults with Down's syndrome. *J. Intellect. Disabil. Res.* 46, 472–483. doi: 10.1046/j.1365-2788.2002.00417.x

Devi, L., and Ohno, M. (2013). Effects of levetiracetam, an antiepileptic drug, on memory impairments associated with aging and Alzheimer's disease in mice. *Neurobiol. Learn. Mem.* 102, 7–11. doi: 10.1016/j.nlm.2013.02.001

Di Domenico, F., Pupo, G., Mancuso, C., Barone, E., Paolini, F., Arena, A., et al. (2015). Bach1 overexpression in Down syndrome correlates with the alteration of the HO-1/BVR-a system: insights for transition to Alzheimer's disease. *J. Alzheimers Dis.* 44, 1107–1120. doi: 10.3233/JAD-141254

Di Domenico, F., Pupo, G., Tramutola, A., Giorgi, A., Schininà, M. E., Coccia, R., et al. (2014). Redox proteomics analysis of HNE-modified proteins in Down syndrome brain: clues for understanding the development of Alzheimer disease. *Free Radic. Biol. Med.* 71, 270–280. doi: 10.1016/j.freeradbiomed.2014.03.027

Dierssen, M., Benavides-Piccione, R., Martínez-Cué, C., Estivill, X., Flórez, J., Elston, G. N., et al. (2003). Alterations of neocortical pyramidal cell phenotype in the Ts65Dn mouse model of Down syndrome: effects of environmental enrichment. *Cereb. Cortex* 13, 758–764. doi: 10.1093/cercor/13.7.758

Dierssen, M., Herault, Y., and Estivill, X. (2009). Aneuploidy: from a physiological mechanism of variance to Down syndrome. *Physiol. Rev.* 89, 887–920. doi: 10.1152/physrev.00032.2007

Dorval, V., Mazzella, M. J., Mathews, P. M., Hay, R. T., and Fraser, P. E. (2007). Modulation of Abeta generation by small ubiquitin-like modifiers does not require conjugation to target proteins. *Biochem. J.* 404, 309–316. doi: 10.1042/bj20061451

Downes, E. C., Robson, J., Grailly, E., Abdel-All, Z., Xuereb, J., Brayne, C., et al. (2008). Loss of synaptophysin and synaptosomal-associated protein 25-kDa (SNAP-25) in elderly Down syndrome individuals. *Neuropathol. Appl. Neurobiol.* 34, 12–22. doi: 10.1111/j.1365-2990.2007.00899.x

Duchon, A., Raveau, M., Chevalier, C., Nalesso, V., Sharp, A. J., and Herault, Y. (2011). Identification of the translocation breakpoints in the Ts65Dn and Ts1Cje mouse lines: relevance for modeling Down syndrome. *Mamm. Genome* 22, 674–684. doi: 10.1007/s00335-011-9356-0

Eckert, A., Schulz, K. L., Rhein, V., and Götz, J. (2010). Convergence of amyloid-β and tau pathologies on mitochondria *in vivo*. *Mol. Neurobiol.* 41, 107–114. doi: 10.1007/s12035-010-8109-5

Elder, G. A., Gama Sosa, M. A., and De Gasperi, R. (2010). Transgenic mouse models of Alzheimer's disease. *Mt. Sinai J. Med.* 77, 69–81. doi: 10.1002/msj.20159

Ermak, G., Morgan, T. E., and Davies, K. J. (2001). Chronic overexpression of the calcineurin inhibitory gene DSCR1 (Adapt78) is associated with Alzheimer's disease. *J. Biol. Chem.* 276, 38787–38794. doi: 10.1074/jbc.M102829200

Esposito, G., Scuderi, C., Lu, J., Savani, C., De Filippis, D., Iuvone, T., et al. (2008). S100B induces tau protein hyperphosphorylation *via* Dickopff-1 up-regulation and disrupts the Wnt pathway in human neural stem cells. *J. Cell. Mol. Med.* 12, 914–927. doi: 10.1111/j.1582-4934.2008.00159.x

Fortress, A. M., Hamlett, E. D., Vazey, E. M., Aston-Jones, G., Cass, W. A., Boger, H. A., et al. (2015). Designer receptors enhance memory in a mouse model of down syndrome. *J. Neurosci.* 35, 1343–1353. doi: 10.1523/JNEUROSCI.2658-14.2015

Francis, B. M., Yang, J., Hajderi, E., Brown, M. E., Michalski, B., McLaurin, J., et al. (2012). Reduced Tissue Levels of Noradrenaline Are Associated with Behavioral Phenotypes of the TgCRND8 Mouse Model of Alzheimer's Disease. *Neuropsychopharmacology* 37, 1934–1944. doi: 10.1038/npp.2012.40

Fratiglioni, L. (1996). Epidemiology of Alzheimer's disease and current possibilities for prevention. *Acta Neurol. Scand. Suppl.* 165, 33–40. doi: 10.1111/j.1600-0404.1996.tb05870.x

Frautschy, S. A., Yang, F., Irrizarry, M., Hyman, B., Saido, T. C., Hsiao, K., et al. (1998). Microglial response to amyloid plaques in APPsw transgenic mice. *Am. J. Pathol.* 152, 307–317.

Galante, M., Jani, H., Vanes, L., Daniel, H., Fisher, E. M. C., Tybulewicz, V. L. J., et al. (2009). Impairments in motor coordination without major changes in cerebellar plasticity in the Tc1 mouse model of Down syndrome. *Hum. Mol. Genet.* 18, 1449–1463. doi: 10.1093/hmg/ddp055

Games, D., Adams, D., Alessandrini, R., Barbour, R., Berthelette, P., Blackwell, C., et al. (1995). Alzheimer-type neuropathology in transgenic mice overexpressing V717F beta-amyloid precursor protein. *Nature* 373, 523–527. doi: 10.1038/373523a0

Ghezzo, A., Salvioli, S., Solimando, M. C., Palmieri, A., Chiostergi, C., Scurti, M., et al. (2014). Age-related changes of adaptive and neuropsychological features in persons with Down Syndrome. *PLoS ONE* 9:e113111. doi: 10.1371/journal.pone.0113111

Glenner, G. G., and Wong, C. W. (1984). Alzheimer's disease: initial report of the purification and characterization of a novel cerebrovascular amyloid protein. *Biochem. Biophys. Res. Commun.* 120, 885–890.

Goedert, M., Spillantini, M. G., Cairns, N. J., and Crowther, R. A. (1992). Tau proteins of Alzheimer paired helical filaments: abnormal phosphorylation of all six brain isoforms. *Neuron* 8, 159–168. doi: 10.1016/0896-6273(92)90117-V

Gómez-Isla, T., Hollister, R., West, H., Mui, S., Growdon, J. H., Petersen, R. C., et al. (1997). Neuronal loss correlates with but exceeds neurofibrillary tangles in Alzheimer's disease. *Ann. Neurol.* 41, 17–24. doi: 10.1002/ana.410410106

Grabowski, T. J., Cho, H. S., Vonsattel, J. P., Rebeck, G. W., and Greenberg, S. M. (2001). Novel amyloid precursor protein mutation in an Iowa family with dementia and severe cerebral amyloid angiopathy. *Ann. Neurol.* 49, 697–705. doi: 10.1002/ana.1009

Gribble, S. M., Wiseman, F. K., Clayton, S., Prigmore, E., Langley, E., Yang, F., et al. (2013). Massively parallel sequencing reveals the complex structure of an irradiated human chromosome on a mouse background in the Tc1 model of Down syndrome. *PLoS ONE* 8:e60482. doi: 10.1371/journal.pone.0060482

Griffin, W. S., Stanley, L. C., Ling, C., White, L., MacLeod, V., Perrot, L. J., et al. (1989). Brain interleukin 1 and S-100 immunoreactivity are elevated in Down syndrome and Alzheimer disease. *Proc. Natl. Acad. Sci. U.S.A.* 86, 7611–7615. doi: 10.1073/pnas.86.19.7611

Griffiths-Jones, S. (2004). The microRNA Registry. *Nucleic Acids Res.* 32, D109–D111. doi: 10.1093/nar/gkh023

Grudzien, A., Shaw, P., Weintraub, S., Bigio, E., Mash, D. C., and Mesulam, M. M. (2007). Locus coeruleus neurofibrillary degeneration in aging, mild cognitive impairment and early Alzheimer's disease. *Neurobiol. Aging* 28, 327–335. doi: 10.1016/j.neurobiolaging.2006.02.007

Guyant-Marechal, I., Berger, E., Laquerrière, A., Rovelet-Lecrux, A., Viennet, G., Frebourg, T., et al. (2008). Intrafamilial diversity of phenotype associated with app duplication. *Neurology* 71, 1925–1926. doi: 10.1212/01.wnl.0000339400.64213.56

Haas, M. A., Bell, D., Slender, A., Lana-Elola, E., Watson-Scales, S., Fisher, E. M. C., et al. (2013). Alterations to dendritic spine morphology, but not dendrite patterning, of cortical projection neurons in Tc1 and Ts1Rhr mouse models of Down syndrome. *PLoS ONE* 8:e78561. doi: 10.1371/journal.pone.0078561

Hall, A. M., and Roberson, E. D. (2012). Mouse models of Alzheimer's disease. *Brain Res. Bull.* 88, 3–12. doi: 10.1016/j.brainresbull.2011.11.017

Hardy, J., and Selkoe, D. J. (2002). The amyloid hypothesis of Alzheimer's disease: progress and problems on the road to therapeutics. *Science* 297, 353–356. doi: 10.1126/science.1072994

Hardy, J. A., and Higgins, G. A. (1992). Alzheimer's disease: the amyloid cascade hypothesis. *Science* 256, 184–185. doi: 10.1126/science.1566067

Hartley, D., Blumenthal, T., Carrillo, M., DiPaolo, G., Esralew, L., Gardiner, K., et al. (2015). Down syndrome and Alzheimer's disease: common pathways, common goals. *Alzheimers Dementia* 11, 700–709. doi: 10.1016/j.jalz.2014.10.007

Hashimoto, Y., and Matsuoka, M. (2014). A mutation protective against Alzheimer's disease renders amyloid β precursor protein incapable of mediating neurotoxicity. *J. Neurochem.* 130, 291–300. doi: 10.1111/jnc.12717

Hattori, M., Fujiyama, A., Taylor, T. D., Watanabe, H., Yada, T., Park, H. S., et al. (2000). The DNA sequence of human chromosome 21. *Nature* 405, 311–319. doi: 10.1038/35012518

Haydar, T. F., and Reeves, R. H. (2012). Trisomy 21 and early brain development. *Trends Neurosci.* 35, 81–91. doi: 10.1016/j.tins.2011.11.001

Helguera, P., Pelsman, A., Pigino, G., Wolvetang, E., Head, E., and Busciglio, J. (2005). ets-2 promotes the activation of a mitochondrial death pathway in Down's syndrome neurons. *J. Neurosci*. 25, 2295–2303. doi: 10.1523/jneurosci.5107-04.2005

Herault, Y., Lopes, P. P., Magnol, L., Sahun, I., Duchon, A., Prandini, P., et al. (2009). "Tackling the complexity of the genotype–phenotype relationship in the Down syndrome with the mouse aneuploidy zoo: a resource of new models to study aneuploidies involving human chromosome 21," in *The American Society of Human Genetics 59th Annual Meeting*. (Honolulu HI).

Hernández-González, S., Ballestín, R., López-Hidalgo, R., Gilabert-Juan, J., Blasco-Ibáñez, J. M., Crespo, C., et al. (2015). Altered distribution of hippocampal interneurons in the murine Down Syndrome Model Ts65Dn. *Neurochem. Res.* 40, 151–164. doi: 10.1007/s11064-014-1479-8

Holland, A. J., Hon, J., Huppert, F. A., Stevens, F., and Watson, P. (1998). Population-based study of the prevalence and presentation of dementia in adults with Down's syndrome. *Br. J. Psychiatry* 172, 493–498.

Holtzman, D. M., Santucci, D., Kilbridge, J., Chua-Couzens, J., Fontana, D. J., Daniels, S. E., et al. (1996). Developmental abnormalities and age-related neurodegeneration in a mouse model of Down syndrome. *Proc. Natl. Acad. Sci. U.S.A.* 93, 13333–13338. doi: 10.1073/pnas.93.23.13333

Hooli, B. V., Mohapatra, G., Mattheisen, M., Parrado, A. R., Roehr, J. T., Shen, Y., et al. (2012). Role of common and rare APP DNA sequence variants in Alzheimer disease. *Neurology* 78, 1250–1257. doi: 10.1212/WNL.0b013e3182515972

Hoozemans, J. J. M., Rozemuller, A. J. M., van Haastert, E. S., Eikelenboom, P., and van Gool, W. A. (2011). Neuroinflammation in Alzheimer's disease wanes with age. *J. Neuroinflammation* 8:171. doi: 10.1186/1742-2094-8-171

Horvath, S., Garagnani, P., Bacalini, M. G., Pirazzini, C., Salvioli, S., Gentilini, D., et al. (2015). Accelerated epigenetic aging in Down syndrome. *Aging Cell* 14, 491–495. doi: 10.1111/acel.12325

Hsiao, K., Chapman, P., Nilsen, S., Eckman, C., Harigaya, Y., Younkin, S., et al. (1996). Correlative memory deficits, Abeta elevation, and amyloid plaques in transgenic mice. *Science* 274, 99–102.

Hunsberger, J., Efthymiou, A. G., Malik, N., Behl, M., Mead, I. L., Zeng, X., et al. (2015). Induced pluripotent stem cell models to enable *in vitro* models for screening in the CNS. *Stem Cells Dev*. 24, 1852–1864. doi: 10.1089/scd.2014.0531

Hunter, C. L., Bimonte-Nelson, H. A., Nelson, M., Eckman, C. B., and Granholm, A.-C. (2004). Behavioral and neurobiological markers of Alzheimer's disease in Ts65Dn mice: effects of estrogen. *Neurobiol. Aging* 25, 873–884. doi: 10.1016/j.neurobiolaging.2003.10.010

Hunter, C. L., Isacson, O., Nelson, M., Bimonte-Nelson, H., Seo, H., Lin, L., et al. (2003). Regional alterations in amyloid precursor protein and nerve growth factor across age in a mouse model of Down's syndrome. *Neurosci. Res.* 45, 437–445. doi: 10.1016/S0168-0102(03)00005-1

Hunter, M. P., Nelson, M., Kurzer, M., Wang, X., Kryscio, R. J., Head, E., et al. (2011). Intersectin 1 contributes to phenotypes *in vivo*: implications for Down's syndrome. *Neuroreport* 22, 767–772. doi: 10.1097/WNR.0b013e32834ae348

Ingelsson, M., Fukumoto, H., Newell, K. L., Growdon, J. H., Hedley-Whyte, E. T., Frosch, M. P., et al. (2004). Early Abeta accumulation and progressive synaptic loss, gliosis, and tangle formation in AD brain. *Neurology* 62, 925–931. doi: 10.1212/01.WNL.0000115115.98960.37

Iordanova, M. D., Burnett, D. J., Aggleton, J. P., Good, M., and Honey, R. C. (2009). The role of the hippocampus in mnemonic integration and retrieval: complementary evidence from lesion and inactivation studies. *Eur. J. Neurosci.* 30, 2177–2189. doi: 10.1111/j.1460-9568.2009.07010.x

Itagaki, S., McGeer, P. L., Akiyama, H., Zhu, S., and Selkoe, D. (1989). Relationship of microglia and astrocytes to amyloid deposits of Alzheimer disease. *J. Neuroimmunol.* 24, 173–182. doi: 10.1016/0165-5728(89)90115-X

Iwatsubo, T., Mann, D. M., Odaka, A., Suzuki, N., and Ihara, Y. (1995). Amyloid beta protein (A beta) deposition: a beta 42(43) precedes A beta 40 in Down syndrome. *Ann. Neurol.* 37, 294–299. doi: 10.1002/ana.410370305

Jackson, H. M., Onos, K. D., Pepper, K. W., Graham, L. C., Akeson, E. C., Byers, C., et al. (2015). DBA/2J genetic background exacerbates spontaneous lethal seizures but lessens amyloid deposition in a mouse model of Alzheimer's disease. *PLoS ONE* 10:e0125897. doi: 10.1371/journal.pone.0125897

Janel, N., Sarazin, M., Corlier, F., Corne, H., de Souza, L. C., Hamelin, L., et al. (2014). Plasma DYRK1A as a novel risk factor for Alzheimer's disease. *Transl. Psychiatry* 4:e425. doi: 10.1038/tp.2014.61

Jellinger, K. A., Lauda, F., and Attems, J. (2007). Sporadic cerebral amyloid angiopathy is not a frequent cause of spontaneous brain hemorrhage. *Eur. J. Neurol.* 14, 923–928. doi: 10.1111/j.1468-1331.2007.01880.x

Jensen, K. M., and Bulova, P. D. (2014). Managing the care of adults with Down's syndrome. *BMJ* 349:g5596. doi: 10.1136/bmj.g5596

Jiang, Y., Mullaney, K. A., Peterhoff, C. M., Che, S., Schmidt, S. D., Boyer-Boiteau, A., et al. (2010). Alzheimer's-related endosome dysfunction in Down syndrome is Abeta-independent but requires APP and is reversed by BACE-1 inhibition. *Proc. Natl. Acad. Sci. U.S.A.* 107, 1630–1635. doi: 10.1073/pnas.0908953107

Kasuga, K., Shimohata, T., Nishimura, A., Shiga, A., Mizuguchi, T., Tokunaga, J., et al. (2009). Identification of independent APP locus duplication in Japanese patients with early-onset Alzheimer disease. *J. Neurol. Neurosurg. Psychiatry* 80, 1050–1052. doi: 10.1136/jnnp.2008.161703

Kerbler, G. M., Fripp, J., Rowe, C. C., Villemagne, V. L., Salvado, O., Rose, S., et al. (2015). Basal forebrain atrophy correlates with amyloid β burden in Alzheimer's disease. *NeuroImage Clin.* 7, 105–113. doi: 10.1016/j.nicl.2014.11.015

Kern, D. S., Maclean, K. N., Jiang, H., Synder, E. Y., Sladek, J. R., and Bjugstad, K. B. (2011). Neural stem cells reduce hippocampal tau and reelin accumulation in aged Ts65Dn Down syndrome mice. *Cell Transplant.* 20, 371–379. doi: 10.3727/096368910X528085

Kim, W. S., Rahmanto, A. S., Kamili, A., Rye, K. A., Guillemin, G. J., Gelissen, I. C., et al. (2007). Role of ABCG1 and ABCA1 in regulation of neuronal cholesterol efflux to apolipoprotein E discs and suppression of amyloid-beta peptide generation. *J. Biol. Chem.* 282, 2851–2861. doi: 10.1074/jbc.M607831200

Kimura, R., Kamino, K., Yamamoto, M., Nuripa, A., Kida, T., Kazui, H., et al. (2007). The DYRK1A gene, encoded in chromosome 21 Down syndrome critical region, bridges between beta-amyloid production and tau phosphorylation in Alzheimer disease. *Hum Mol Genet*. 16, 15–23. doi: 10.1093/hmg/ddl437

Kokjohn, T. A., and Roher, A. E. (2009). Amyloid precursor protein transgenic mouse models and Alzheimer's disease: understanding the paradigms, limitations, and contributions. *Alzheimers Dementia* 5, 340–347. doi: 10.1016/j.jalz.2009.03.002

Kong, X. D., Liu, N., Xu, X. J., Zhao, Z. H., and Jiang, M. (2015). Screening of human chromosome 21 genes in the dorsolateral prefrontal cortex of individuals with Down syndrome. *Mol. Med. Rep*. 11, 1235–1239. doi: 10.3892/mmr.2014.2855

Korbel, J. O., Tirosh-Wagner, T., Urban, A. E., Chen, X.-N., Kasowski, M., Dai, L., et al. (2009). The genetic architecture of Down syndrome phenotypes revealed by high-resolution analysis of human segmental trisomies. *Proc. Natl. Acad. Sci. U.S.A.* 106, 12031–12036. doi: 10.1073/pnas.0813248106

Krabbe, G., Halle, A., Matyash, V., Rinnenthal, J. L., Eom, G. D., Bernhardt, U., et al. (2013). Functional impairment of microglia coincides with Beta-amyloid deposition in mice with Alzheimer-like pathology. *PLoS ONE* 8:e60921. doi: 10.1371/journal.pone.0060921

Krezowski, J., Knudson, D., Ebeling, C., Pitstick, R., Giri, R. K., Schenk, D., et al. (2004). Identification of loci determining susceptibility to the lethal effects of amyloid precursor protein transgene overexpression. *Hum. Mol. Genet.* 13, 1989–1997. doi: 10.1093/hmg/ddh210

Krinsky-McHale, S. J., Devenny, D. A., Gu, H., Jenkins, E. C., Kittler, P., Murty, V. V., et al. (2008). Successful aging in a 70-year-old man with down syndrome: a case study. *Intellect. Dev. Disabil.* 46, 215–228. doi: 10.1352/2008.46:215-228

Krinsky-McHale, S. J., Devenny, D. A., and Silverman, W. P. (2002). Changes in explicit memory associated with early dementia in adults with Down's syndrome. *J. Intellect. Disabil. Res.* 46, 198–208. doi: 10.1046/j.1365-2788.2002.00365.x

Krinsky-McHale, S. J., Devenny, D. A., Sersen, G., and Silverman, W. P. (2000). Sequence of cognitive decline in dementia in adults with Down's syndrome. *J. Intellect. Disabil. Res.* 44, 654–665. doi: 10.1111/j.1365-2788.2000.00305.x

Kumar-Singh, S., De Jonghe, C., Cruts, M., Kleinert, R., Wang, R., Mercken, M., et al. (2000). Nonfibrillar diffuse amyloid deposition due to a gamma(42)-secretase site mutation points to an essential role for N-truncated A beta(42) in Alzheimer's disease. *Hum. Mol. Genet.* 9, 2589–2598. doi: 10.1093/hmg/9.18.2589

LaFerla, F. M., Green, K. N., and Oddo, S. (2007). Intracellular amyloid-beta in Alzheimer's disease. *Nat. Rev. Neurosci.* 8, 499–509. doi: 10.1038/nrn2168

Landt, J., D'Abrera, J. C., Holland, A. J., Aigbirhio, F. I., Fryer, T. D., Canales, R., et al. (2011). Using positron emission tomography and Carbon 11-labeled Pittsburgh Compound B to image brain Fibrillar β-amyloid in adults with down syndrome: safety, acceptability, and feasibility. *Arch. Neurol.* 68, 890–896. doi: 10.1001/archneurol.2011.36

Lassalle, J. M., Halley, H., Daumas, S., Verret, L., and Francés, B. (2008). Effects of the genetic background on cognitive performances of TG2576 mice. *Behav. Brain Res.* 191, 104–110. doi: 10.1016/j.bbr.2008.03.017

Lee, L., Dale, E., Staniszewski, A., Zhang, H., Saeed, F., Sakurai, M., et al. (2014). Regulation of synaptic plasticity and cognition by SUMO in normal physiology and Alzheimer's disease. *Sci. Rep.* 4:7190. doi: 10.1038/srep07190

Lehman, E. J. H., Kulnane, L. S., Gao, Y., Petriello, M. C., Pimpis, K. M., Younkin, L., et al. (2003). Genetic background regulates beta-amyloid precursor protein processing and beta-amyloid deposition in the mouse. *Hum. Mol. Genet.* 12, 2949–2956. doi: 10.1093/hmg/ddg322

Lesné, S., Koh, M. T., Kotilinek, L., Kayed, R., Glabe, C. G., Yang, A., et al. (2006). A specific amyloid-beta protein assembly in the brain impairs memory. *Nature* 440, 352–357. doi: 10.1038/nature04533

Letourneau, A., Santoni, F. A., Bonilla, X., Sailani, M. R., Gonzalez, D., Kind, J., et al. (2014). Domains of genome-wide gene expression dysregulation in Down's syndrome. *Nature* 508, 345–350. doi: 10.1038/nature13200

Leverenz, J. B., and Raskind, M. A. (1998). Early amyloid deposition in the medial temporal lobe of young Down syndrome patients: a regional quantitative analysis. *Exp. Neurol.* 150, 296–304. doi: 10.1006/exnr.1997.6777

Li, Z., Yu, T., Morishima, M., Pao, A., LaDuca, J., Conroy, J., et al. (2007). Duplication of the entire 22.9 Mb human chromosome 21 syntenic region on mouse chromosome 16 causes cardiovascular and gastrointestinal abnormalities. *Hum. Mol. Genet.* 16, 1359–1366. doi: 10.1093/hmg/ddm086

Liu, C., Belichenko, P. V., Zhang, L., Fu, D., Kleschevnikov, A. M., Baldini, A., et al. (2011). Mouse models for Down syndrome-associated developmental cognitive disabilities. *Dev. Neurosci.* 33, 404–413. doi: 10.1159/000329422

Liu, C., Morishima, M., Jiang, X., Yu, T., Meng, K., Ray, D., et al. (2014). Engineered chromosome-based genetic mapping establishes a 3.7 Mb critical genomic region for Down syndrome-associated heart defects in mice. *Hum. Genet.* 133, 743–753. doi: 10.1007/s00439-013-1407-z

Liu, F., Liang, Z., Wegiel, J., Hwang, Y.-W., Iqbal, K., Grundke-Iqbal, I., et al. (2008). Overexpression of Dyrk1A contributes to neurofibrillary degeneration in Down syndrome. *FASEB J.* 22, 3224–3233. doi: 10.1096/fj.07-104539

Loane, M., Morris, J. K., Addor, M.-C., Arriola, L., Budd, J., Doray, B., et al. (2013). Twenty-year trends in the prevalence of Down syndrome and other trisomies in Europe: impact of maternal age and prenatal screening. *Eur. J. Hum. Genet.* 21, 27–33. doi: 10.1038/ejhg.2012.94

Lockrow, J., Boger, H., Bimonte-Nelson, H., and Granholm, A. C. (2011a). Effects of long-term memantine on memory and neuropathology in Ts65Dn mice, a model for Down syndrome. *Behav. Brain Res.* 221, 610–622. doi: 10.1016/j.bbr.2010.03.036

Lockrow, J., Boger, H., Gerhardt, G., Aston-Jones, G., Bachman, D., and Granholm, A. C. (2011b). A noradrenergic lesion exacerbates neurodegeneration in a down syndrome mouse model. *J. Alzheimers Dis.* 23, 471–489. doi: 10.3233/JAD-2010-101218

Lockrow, J., Prakasam, A., Huang, P., Bimonte-Nelson, H., Sambamurti, K., and Granholm, A. C. (2009). Cholinergic degeneration and memory loss delayed by vitamin E in a Down syndrome mouse model. *Exp. Neurol.* 216, 278–289. doi: 10.1016/j.expneurol.2008.11.021

Lott, I. T. (2012). Neurological phenotypes for Down syndrome across the life span. *Prog. Brain Res.* 197, 101–121. doi: 10.1016/B978-0-444-54299-1.00006-6

Lu, J., Esposito, G., Scuderi, C., Steardo, L., Delli-Bovi, L. C., Hecht, J. L., et al. (2011). S100B and APP promote a gliocentric shift and impaired neurogenesis in down syndrome neural progenitors. *PLoS ONE* 6:e22126. doi: 10.1371/journal.pone.0022126

Lu, J., Lian, G., Zhou, H., Esposito, G., Steardo, L., Delli-Bovi, L. C., et al. (2012). OLIG2 over-expression impairs proliferation of human Down syndrome neural progenitors. *Hum. Mol. Genet.* 21, 2330–2340. doi: 10.1093/hmg/dds052

Lu, T., Aron, L., Zullo, J., Pan, Y., Kim, H., Chen, Y., et al. (2014). REST and stress resistance in ageing and Alzheimer disease. *Nature* 507, 448–454. doi: 10.1038/nature13163

Madeo, J. (2013). The Role of Oxidative Stress in Alzheimer's Disease. *J. Alzheimers Dis. Park.* 03:116. doi: 10.4172/2161-0460.1000116

Maia, L. F., Kaeser, S. A., Reichwald, J., Lambert, M., Obermüller, U., Schelle, J., et al. (2015). Increased CSF Aβ during the very early phase of cerebral Aβ deposition in mouse models. *EMBO Mol. Med.* 7, 895–903. doi: 10.15252/emmm.201505026

Mann, D. M., and Esiri, M. M. (1989). The pattern of acquisition of plaques and tangles in the brains of patients under 50 years of age with Down's syndrome. *J. Neurol. Sci.* 89, 169–179.

Mann, D. M. (1988a). The pathological association between Down syndrome and Alzheimer disease. *Mech. Ageing Dev.* 43, 99–136. doi: 10.1016/0047-6374(88)90041-3

Mann, D. M. (1988b). Alzheimer's disease and Down's syndrome. *Histopathology* 13, 125–137. doi: 10.1111/j.1365-2559.1988.tb02018.x

Margallo-Lana, M. L., Moore, P. B., Kay, D. W. K., Perry, R. H., Reid, B. E., Berney, T. P., et al. (2007). Fifteen-year follow-up of 92 hospitalized adults with Down's syndrome: incidence of cognitive decline, its relationship to age and neuropathology. *J. Intellect. Disabil. Res.* 51, 463–477. doi: 10.1111/j.1365-2788.2006.00902.x

Martin, K. R., Corlett, A., Dubach, D., Mustafa, T., Coleman, H. A., Parkington, H. C., et al. (2012). Over-expression of RCAN1 causes Down syndrome-like hippocampal deficits that alter learning and memory. *Hum. Mol. Genet.* 21, 3025–3041. doi: 10.1093/hmg/dds134

Martin, S. B., Dowling, A. L., Lianekhammy, J., Lott, I. T., Doran, E., Murphy, M. P., et al. (2014). Synaptophysin and Synaptojanin-1 in Down Syndrome are Differentially Affected by Alzheimer's Disease. *J. Alzheimers Dis.* 42, 767–775. doi: 10.3233/jad-140795

Martínez-Cué, C., Delatour, B., and Potier, M.-C. (2014). Treating enhanced GABAergic inhibition in Down syndrome: use of GABA α5-selective inverse agonists. *Neurosci. Biobehav. Rev.* 46, 218–227. doi: 10.1016/j.neubiorev.2013.12.008

McCarron, M., McCallion, P., Reilly, E., and Mulryan, N. (2014). A prospective 14-year longitudinal follow-up of dementia in persons with Down syndrome. *J. Intellect. Disabil. Res.* 58, 61–70. doi: 10.1111/jir.12074

McCarron, M. O., Nicoll, J. A., and Graham, D. I. (1998). A quartet of Down's syndrome, Alzheimer's disease, cerebral amyloid angiopathy, and cerebral haemorrhage: interacting genetic risk factors. *J. Neurol. Neurosurg. Psychiatry* 65, 405–406. doi: 10.1136/jnnp.65.3.405

McGeer, E. G., Norman, M., Boyes, B., O'Kusky, J., Suzuki, J., and McGeer, P. L. (1985). Acetylcholine and aromatic amine systems in postmortem brain of an infant with Down's syndrome. *Exp. Neurol.* 87, 557–570. doi: 10.1016/0014-4886(85)90184-0

McGeer, P. L., Itagaki, S., Tago, H., and McGeer, E. G. (1987). Reactive microglia in patients with senile dementia of the Alzheimer type are positive for the histocompatibility glycoprotein HLA-DR. *Neurosci. Lett.* 79, 195–200. doi: 10.1016/0304-3940(87)90696-3

Mendez, M., and Lim, G. (2003). Seizures in elderly patients with dementia: epidemiology and management. *Drugs Aging* 20, 791–803. doi: 10.2165/00002512-200320110-00001

Meraz-Ríos, M. A., Franco-Bocanegra, D., Toral Rios, D., and Campos-Peña, V. (2014). Early onset Alzheimer's disease and oxidative stress. *Oxid. Med. Cell. Longev.* 2014, 375968. doi: 10.1155/2014/375968

Mesulam, M., Shaw, P., Mash, D., and Weintraub, S. (2004). Cholinergic nucleus basalis tauopathy emerges early in the aging-MCI-AD continuum. *Ann. Neurol.* 55, 815–828. doi: 10.1002/ana.20100

Moechars, D., Dewachter, I., Lorent, K., Reversé, D., Baekelandt, V., Naidu, A., et al. (1999). Early phenotypic changes in transgenic mice that overexpress different mutants of amyloid precursor protein in brain. *J. Biol. Chem.* 274, 6483–6492.

Mok, K. Y., Jones, E. L., Hanney, M., Harold, D., Sims, R., Williams, J., et al. (2014). Polymorphisms in BACE2 may affect the age of onset Alzheimer's dementia in Down syndrome. *Neurobiol. Aging* 35, e1–e5. doi: 10.1016/j.neurobiolaging.2013.12.022

Moore, S., Evans, L. D. B., Andersson, T., Portelius, E., Smith, J., Dias, T. B., et al. (2015). APP Metabolism Regulates Tau Proteostasis in Human Cerebral Cortex Neurons. *Cell Rep.* 11, 689–696. doi: 10.1016/j.celrep.2015.03.068

Mori, C., Spooner, E. T., Wisniewsk, K. E., Wisniewski, T. M., Yamaguch, H., Saido, T. C., et al. (2002). Intraneuronal Abeta42 accumulation in Down syndrome brain. *Amyloid* 9, 88–102.

Mori, T., Koyama, N., Arendash, G. W., Horikoshi-Sakuraba, Y., Tan, J., and Town, T. (2010). Overexpression of human S100B exacerbates cerebral amyloidosis and gliosis in the Tg2576 mouse model of Alzheimer's disease. *Glia* 58, 300–314. doi: 10.1002/glia.20924

Mucke, L., and Selkoe, D. J. (2012). Neurotoxicity of amyloid β-protein: synaptic and network dysfunction. *Cold Spring Harb. Perspect. Med.* 2, a006338. doi: 10.1101/cshperspect.a006338

Murray, A., Letourneau, A., Canzonetta, C., Stathaki, E., Gimelli, S., Sloan-Bena, F., et al. (2015). Brief report: isogenic induced pluripotent stem cell lines from an adult with mosaic down syndrome model accelerated neuronal ageing and neurodegeneration. *Stem Cells* 33, 2077–2084. doi: 10.1002/stem.1968

Murrell, J. R., Hake, A. M., Quaid, K. A., Farlow, M. R., and Ghetti, B. (2000). Early-onset Alzheimer disease caused by a new mutation (V717L) in the amyloid precursor protein gene. *Arch. Neurol.* 57, 885–887. doi: 10.1001/archneur.57.6.885

Musicco, M. (2009). Gender differences in the occurrence of Alzheimer's disease. *Funct. Neurol.* 24, 89–92.

Myllykangas, L., Wavrant-De Vrieze, F., Polvikoski, T., Notkola, I. L., Sulkava, R., Niinisto, L., et al. (2005). Chromosome 21 BACE2 haplotype associates with Alzheimer's disease: a two-stage study. *J. Neurol. Sci.* 236, 17–24. doi: 10.1016/j.jns.2005.04.008

Naito, K.-S., Sekijima, Y., and Ikeda, S.-I. (2008). Cerebral amyloid angiopathy-related hemorrhage in a middle-aged patient with Down's syndrome. *Amyloid* 15, 275–277. doi: 10.1080/13506120802524981

Narayan, P. J., Lill, C., Faull, R., Curtis, M. A., and Dragunow, M. (2015). Increased acetyl and total histone levels in post-mortem Alzheimer's disease brain. *Neurobiol. Dis.* 74, 281–294. doi: 10.1016/j.nbd.2014.11.023

Nelson, L. D., Orme, D., Osann, K., and Lott, I. T. (2001). Neurological changes and emotional functioning in adults with Down Syndrome. *J. Intellect. Disabil. Res.* 45, 450–456. doi: 10.1046/j.1365-2788.2001.00379.x

Ness, S., Rafii, M., Aisen, P., Krams, M., Silverman, W., and Manji, H. (2012). Down's syndrome and Alzheimer's disease: towards secondary prevention. *Nat. Rev. Drug Discov.* 11, 655–656. doi: 10.1038/nrd3822

O'Doherty, A., Ruf, S., Mulligan, C., Hildreth, V., Errington, M. L., Cooke, S., et al. (2005). An aneuploid mouse strain carrying human chromosome 21 with Down syndrome phenotypes. *Science* 309, 2033–2037. doi: 10.1126/science.1114535

Olson, L. E., Richtsmeier, J. T., Leszl, J., and Reeves, R. H. (2004). A chromosome 21 critical region does not cause specific Down syndrome phenotypes. *Science* 306, 687–690. doi: 10.1126/science.1098992

Palop, J. J. (2009). Epilepsy and Cognitive Impairments in Alzheimer Disease. *Arch. Neurol.* 66, 435. doi: 10.1001/archneurol.2009.15

Park, J., Yang, E. J., Yoon, J. H., and Chung, K. C. (2007). Dyrk1A overexpression in immortalized hippocampal cells produces the neuropathological features of Down syndrome. *Mol. Cell Neurosci.* 36, 270–279. doi: 10.1016/j.mcn.2007.07.007

Parker, S. E., Mai, C. T., Canfield, M. A., Rickard, R., Wang, Y., Meyer, R. E., et al. (2010). Updated National Birth Prevalence estimates for selected birth defects in the United States, 2004-2006. *Birth Defects Res. A. Clin. Mol. Teratol.* 88, 1008–1016. doi: 10.1002/bdra.20735

Parkinson, P. F., Kannangara, T. S., Eadie, B. D., Burgess, B. L., Wellington, C. L., and Christie, B. R. (2009). Cognition, learning behaviour and hippocampal synaptic plasticity are not disrupted in mice over-expressing the cholesterol transporter ABCG1. *Lipids Heal. Dis.* 8:5. doi: 10.1186/1476-511x-8-5

Pasalar, P., Najmabadi, H., Noorian, A. R., Moghimi, B., Jannati, A., Soltanzadeh, A., et al. (2002). An Iranian family with Alzheimer's disease caused by a novel APP mutation (Thr714Ala). *Neurology* 58, 1574–1575. doi: 10.1212/WNL.58.10.1574

Peacock, M. L., Warren, J. T., Roses, A. D., and Fink, J. K. (1993). Novel polymorphism in the A4 region of the amyloid precursor protein gene in a patient without Alzheimer's disease. *Neurology* 43, 1254–1256. doi: 10.1212/WNL.43.6.1254

Peng, S., Garzon, D. J., Marchese, M., Klein, W., Ginsberg, S. D., Francis, B. M., et al. (2009). Decreased brain-derived neurotrophic factor depends on amyloid aggregation state in transgenic mouse models of Alzheimer's disease. *J. Neurosci.* 29, 9321–9329. doi: 10.1523/JNEUROSCI.4736-08.2009

Pereira, P. L., Magnol, L., Sahún, I., Brault, V., Duchon, A., Prandini, P., et al. (2009). A new mouse model for the trisomy of the Abcg1-U2af1 region reveals the complexity of the combinatorial genetic code of down syndrome. *Hum. Mol. Genet.* 18, 4756–4769. doi: 10.1093/hmg/ddp438

Perez-Cruz, C., Nolte, M. W., van Gaalen, M. M., Rustay, N. R., Termont, A., Tanghe, A., et al. (2011). Reduced spine density in specific regions of CA1 pyramidal neurons in two transgenic mouse models of Alzheimer's disease. *J. Neurosci.* 31, 3926–3934. doi: 10.1523/JNEUROSCI.6142-10.2011

Pike, C. J., Cummings, B. J., and Cotman, C. W. (1995). Early association of reactive astrocytes with senile plaques in Alzheimer's disease. *Exp. Neurol.* 132, 172–179. doi: 10.1016/0014-4886(95)90022-5

Pilotto, A., Padovani, A., and Borroni, B. (2013). Clinical, biological, and imaging features of monogenic Alzheimer's Disease. *Biomed. Res. Int.* 2013:689591. doi: 10.1155/2013/689591

Pollonini, G., Gao, V., Rabe, A., Palminiello, S., Albertini, G., and Alberini, C. M. (2008). Abnormal expression of synaptic proteins and neurotrophin-3 in the Down syndrome mouse model Ts65Dn. *Neuroscience* 156, 99–106. doi: 10.1016/j.neuroscience.2008.07.025

Portelius, E., Hölttä, M., Soininen, H., Bjerke, M., Zetterberg, H., Westerlund, A., et al. (2014a). Altered cerebrospinal fluid levels of amyloid β and amyloid precursor-like protein 1 peptides in Down's syndrome. *NeuroMol. Med.* 16, 510–516. doi: 10.1007/s12017-014-8302-1

Portelius, E., Soininen, H., Andreasson, U., Zetterberg, H., Persson, R., Karlsson, G., et al. (2014b). Exploring Alzheimer molecular pathology in Down's syndrome cerebrospinal fluid. *Neurodegener. Dis.* 14, 98–106. doi: 10.1159/000358800

Powell, D., Caban-Holt, A., Jicha, G., Robertson, W., Davis, R., Gold, B. T., et al. (2014). Frontal white matter integrity in adults with Down syndrome with and without dementia. *Neurobiol. Aging* 35, 1562–1569. doi: 10.1016/j.neurobiolaging.2014.01.137

Pozueta, J., Lefort, R., and Shelanski, M. L. (2013). Synaptic changes in Alzheimer's disease and its models. *Neuroscience* 251, 51–65. doi: 10.1016/j.neuroscience.2012.05.050

Prasher, V. P., Farrer, M. J., Kessling, A. M., Fisher, E. M., West, R. J., Barber, P. C., et al. (1998). Molecular mapping of Alzheimer-type dementia in Down's syndrome. *Ann. Neurol.* 43, 380–383. doi: 10.1002/ana.410430316

Prasher, V. P., and Krishnan, V. H. R. (1993). Age of onset and duration of dementia in people with down syndrome: integration of 98 reported cases in the literature. *Int. J. Geriatr. Psychiatry* 8, 915–922. doi: 10.1002/gps.930081105

Pucharcos, C., Fuentes, J. J., Casas, C., de la Luna, S., Alcantara, S., Arbones, M. L., et al. (1999). Alu-splice cloning of human Intersectin (ITSN), a putative multivalent binding protein expressed in proliferating and differentiating neurons and overexpressed in Down syndrome. *Eur. J. Hum. Genet.* 7, 704–712. doi: 10.1038/sj.ejhg.5200356

Querfurth, H. W., and LaFerla, F. M. (2010). Alzheimer's disease. *N. Engl. J. Med.* 362, 329–344. doi: 10.1056/NEJMra0909142

Reeves, R. H., Irving, N. G., Moran, T. H., Wohn, A., Kitt, C., Sisodia, S. S., et al. (1995). A mouse model for Down syndrome exhibits learning and behaviour deficits. *Nat. Genet.* 11, 177–184. doi: 10.1038/ng1095-177

Reinholdt, L. G., Ding, Y., Gilbert, G. J., Gilbert, G. T., Czechanski, A., Solzak, J. P., et al. (2011). Molecular characterization of the translocation breakpoints in the Down syndrome mouse model Ts65Dn. *Mamm. Genome* 22, 685–691. doi: 10.1007/s00335-011-9357-z

Reynolds, G. P., and Warner, C. E. J. (1988). Amino acid neurotransmitter deficits in adult Down's syndrome brain tissue. *Neurosci. Lett.* 94, 224–227. doi: 10.1016/0304-3940(88)90299-6

Rodríguez-Arellano, J. J., Parpura, V., Zorec, R., and Verkhratsky, A. (2015). Astrocytes in physiological aging and Alzheimer's disease. *Neuroscience*. doi: 10.1016/j.neuroscience.2015.01.007. [Epub ahead of print].

Rovelet-Lecrux, A., Frebourg, T., Tuominen, H., Majamaa, K., Campion, D., and Remes, A. M. (2007). APP locus duplication in a Finnish family with dementia and intracerebral haemorrhage. *J. Neurol. Neurosurg. Psychiatry* 78, 1158–1159. doi: 10.1136/jnnp.2006.113514

Rovelet-Lecrux, A., Hannequin, D., Raux, G., Le Meur, N., Laquerrière, A., Vital, A., et al. (2006). APP locus duplication causes autosomal dominant early-onset Alzheimer disease with cerebral amyloid angiopathy. *Nat. Genet.* 38, 24–26. doi: 10.1038/ng1718

Royston, M. C., McKenzie, J. E., Gentleman, S. M., Sheng, J. G., Mann, D. M., Griffin, W. S., et al. (1999). Overexpression of S100beta in Down's syndrome:

correlation with patient age and with beta-amyloid deposition. *Neuropathol. Appl. Neurobiol.* 25, 387–393. doi: 10.1046/j.1365-2990.1999.00196.x

Ruparelia, A., Pearn, M. L., and Mobley, W. C. (2013). Aging and intellectual disability: insights from mouse models of Down syndrome. *Dev. Disabil. Res. Rev.* 18, 43–50. doi: 10.1002/ddrr.1127

Rustay, N. R., Cronin, E. A., Curzon, P., Markosyan, S., Bitner, R. S., Ellis, T. A., et al. (2010). Mice expressing the Swedish APP mutation on a 129 genetic background demonstrate consistent behavioral deficits and pathological markers of Alzheimer's disease. *Brain Res.* 1311, 136–147. doi: 10.1016/j.brainres.2009.11.040

Ryan, N. S., and Rossor, M. N. (2010). Correlating familial Alzheimer's disease gene mutations with clinical phenotype. *Biomark. Med.* 4, 99–112. doi: 10.2217/bmm.09.92

Ryoo, S. R., Cho, H. J., Lee, H. W., Jeong, H. K., Radnaabazar, C., Kim, Y. S., et al. (2008). Dual-specificity tyrosine(Y)-phosphorylation regulated kinase 1A-mediated phosphorylation of amyloid precursor protein: evidence for a functional link between Down syndrome and Alzheimer's disease. *J. Neurochem.* 104, 1333–1344. doi: 10.1111/j.1471-4159.2007.05075.x

Ryoo, S. R., Jeong, H. K., Radnaabazar, C., Yoo, J. J., Cho, H. J., Lee, H. W., et al. (2007). DYRK1A-mediated hyperphosphorylation of Tau. A functional link between Down syndrome and Alzheimer disease. *J. Biol. Chem.* 282, 34850–34857. doi: 10.1074/jbc.M707358200

Ryu, Y. S., Park, S. Y., Jung, M. S., Yoon, S. H., Kwen, M. Y., Lee, S. Y., et al. (2010). Dyrk1A-mediated phosphorylation of Presenilin 1: a functional link between Down syndrome and Alzheimer's disease. *J. Neurochem.* 115, 574–584. doi: 10.1111/j.1471-4159.2010.06769.x

Sabbagh, M. N., Chen, K., Rogers, J., Fleisher, A. S., Liebsack, C., Bandy, D., et al. (2015). Florbetapir PET, FDG PET, and MRI in Down syndrome individuals with and without Alzheimer's dementia. *Alzheimers Dementia* 11, 994–1004. doi: 10.1016/j.jalz.2015.01.006

Sago, H., Carlson, E. J., Smith, D. J., Kilbridge, J., Rubin, E. M., Mobley, W. C., et al. (1998). Ts1Cje, a partial trisomy 16 mouse model for Down syndrome, exhibits learning and behavioral abnormalities. *Proc. Natl. Acad. Sci. U.S.A.* 95, 6256–6261. doi: 10.1073/pnas.95.11.6256

Saito, T., Matsuba, Y., Mihira, N., Takano, J., Nilsson, P., Itohara, S., et al. (2014). Single App knock-in mouse models of Alzheimer's disease. *Nat. Neurosci.* 17, 661–663. doi: 10.1038/nn.3697

Saito, Y., Oka, A., Mizuguchi, M., Motonaga, K., Mori, Y., Becker, L. E., et al. (2000). The developmental and aging changes of Down's syndrome cell adhesion molecule expression in normal and Down's syndrome brains. *Acta Neuropathol.* 100, 654–664. doi: 10.1007/s004010000230

Salehi, A., Delcroix, J.-D., Belichenko, P. V., Zhan, K., Wu, C., Valletta, J. S., et al. (2006). Increased App expression in a mouse model of Down's syndrome disrupts NGF transport and causes cholinergic neuron degeneration. *Neuron* 51, 29–42. doi: 10.1016/j.neuron.2006.05.022

Sanchez, M. M., Moghadam, S., Naik, P., Martin, K. J., and Salehi, A. (2011). Hippocampal network alterations in Alzheimer's disease and Down syndrome: from structure to therapy. *J. Alzheimers Dis.* 26(Suppl 3), 29–47. doi: 10.3233/JAD-2011-0050

Sanchez, P. E., Zhu, L., Verret, L., Vossel, K. A., Orr, A. G., Cirrito, J. R., et al. (2012). Levetiracetam suppresses neuronal network dysfunction and reverses synaptic and cognitive deficits in an Alzheimer's disease model. *Proc. Natl. Acad. Sci. U.S.A.* 109, E2895–E2903. doi: 10.1073/pnas.11210 81109

Sanders, N. C., Williams, D. K., and Wenger, G. R. (2009). Does the learning deficit observed under an incremental repeated acquisition schedule of reinforcement in Ts65Dn mice, a model for Down syndrome, change as they age? *Behav. Brain Res.* 203, 137–142. doi: 10.1016/j.bbr.2009.04.031

Sangani, M., Shahid, A., Amina, S., and Koubeissi, M. (2010). Improvement of myoclonic epilepsy in Down syndrome treated with levetiracetam. *Epileptic Disord.* 12, 151–154. doi: 10.1684/epd.2010.0306

Scheff, S. W., Price, D. A., Schmitt, F. A., DeKosky, S. T., and Mufson, E. J. (2007). Synaptic alterations in CA1 in mild Alzheimer disease and mild cognitive impairment. *Neurology* 68, 1501–1508. doi: 10.1212/01.wnl.0000260698.46517.8f

Schupf, N., Lee, A., Park, N., Dang, L.-H., Pang, D., Yale, A., et al. (2015). Candidate genes for Alzheimer's disease are associated with individual differences in plasma levels of beta amyloid peptides in adults with Down syndrome. *Neurobiol. Aging* 36, 2907.e1–2907.e10. doi: 10.1016/j.neurobiolaging.2015.06.020

Seidl, R., Cairns, N., Singewald, N., Kaehler, S. T., and Lubec, G. (2001). Differences between GABA levels in Alzheimer's disease and Down syndrome with Alzheimer-like neuropathology. *Naunyn. Schmiedebergs. Arch. Pharmacol.* 363, 139–145. doi: 10.1007/s002100000346

Seo, H., and Isacson, O. (2005). Abnormal APP, cholinergic and cognitive function in Ts65Dn Down's model mice. *Exp. Neurol.* 193, 469–480. doi: 10.1016/j.expneurol.2004.11.017

Serrano-Pozo, A., Frosch, M. P., Masliah, E., and Hyman, B. T. (2011). Neuropathological alterations in Alzheimer disease. *Cold Spring Harb. Perspect. Med.* 1:a006189. doi: 10.1101/cshperspect.a006189

Shapiro, L. A., Marks, A., and Whitaker-Azmitia, P. M. (2004). Increased clusterin expression in old but not young adult S100B transgenic mice: evidence of neuropathological aging in a model of Down Syndrome. *Brain Res.* 1010, 17–21. doi: 10.1016/j.brainres.2003.12.057

Shapiro, L. A., and Whitaker-Azmitia, P. M. (2004). Expression levels of cytoskeletal proteins indicate pathological aging of S100B transgenic mice: an immunohistochemical study of MAP-2, drebrin and GAP-43. *Brain Res.* 1019, 39–46. doi: 10.1016/j.brainres.2004.05.100

Sheehan, R., Sinai, A., Bass, N., Blatchford, P., Bohnen, I., Bonell, S., et al. (2015). Dementia diagnostic criteria in Down syndrome. *Int. J. Geriatr. Psychiatry* 30, 857–863. doi: 10.1002/gps.4228

Sheng, J. G., Mrak, R. E., and Griffin, W. S. (1994). S100 beta protein expression in Alzheimer disease: potential role in the pathogenesis of neuritic plaques. *J. Neurosci. Res.* 39, 398–404. doi: 10.1002/jnr.490390406

Sheppard, O., Plattner, F., Rubin, A., Slender, A., Linehan, J. M., Brandner, S., et al. (2012). Altered regulation of tau phosphorylation in a mouse model of down syndrome aging. *Neurobiol. Aging* 33, e31–e44. doi: 10.1016/j.neurobiolaging.2011.06.025

Shi, J., Zhang, T., Zhou, C., Chohan, M. O., Gu, X., Wegiel, J., et al. (2008). Increased dosage of Dyrk1A alters alternative splicing factor (ASF)-regulated alternative splicing of tau in Down syndrome. *J. Biol. Chem.* 283, 28660–28669. doi: 10.1074/jbc.M802645200

Shi, Y., Kirwan, P., Smith, J., MacLean, G., Orkin, S. H., and Livesey, F. J. (2012). A human stem cell model of early Alzheimer's disease pathology in Down syndrome. *Sci. Transl. Med.* 4, 124ra29. doi: 10.1126/scitranslmed. 3003771

Shichiri, M., Yoshida, Y., Ishida, N., Hagihara, Y., Iwahashi, H., Tamai, H., et al. (2011). α-Tocopherol suppresses lipid peroxidation and behavioral and cognitive impairments in the Ts65Dn mouse model of Down syndrome. *Free Radic. Biol. Med.* 50, 1801–1811. doi: 10.1016/j.freeradbiomed.2011.03.023

Shukkur, E. A., Shimohata, A., Akagi, T., Yu, W., Yamaguchi, M., Murayama, M., et al. (2006). Mitochondrial dysfunction and tau hyperphosphorylation in Ts1Cje, a mouse model for Down syndrome. *Hum. Mol. Genet.* 15, 2752–2762. doi: 10.1093/hmg/ddl211

Siarey, R. J., Kline-Burgess, A., Cho, M., Balbo, A., Best, T. K., Harashima, C., et al. (2006). Altered signaling pathways underlying abnormal hippocampal synaptic plasticity in the Ts65Dn mouse model of Down syndrome. *J. Neurochem.* 98, 1266–1277. doi: 10.1111/j.1471-4159.2006.03971.x

Sims, R., Hollingworth, P., Moskvina, V., Dowzell, K., O'Donovan, M. C., Powell, J., et al. (2009). Evidence that variation in the oligodendrocyte lineage transcription factor 2 (OLIG2) gene is associated with psychosis in Alzheimer's disease. *Neurosci. Lett.* 461, 54–59. doi: 10.1016/j.neulet.2009.05.051

Sleegers, K., Brouwers, N., Gijselinck, I., Theuns, J., Goossens, D., Wauters, J., et al. (2006). APP duplication is sufficient to cause early onset Alzheimer's dementia with cerebral amyloid angiopathy. *Brain* 129, 2977–2983. doi: 10.1093/brain/awl203

Stargardt, A., Swaab, D. F., and Bossers, K. (2015). The storm before the quiet: neuronal hyperactivity and Aβ in the presymptomatic stages of Alzheimer's disease. *Neurobiol. Aging* 36, 1–11. doi: 10.1016/j.neurobiolaging.2014. 08.014

Streit, W. J., Braak, H., Xue, Q.-S., and Bechmann, I. (2009). Dystrophic (senescent) rather than activated microglial cells are associated with tau pathology and likely precede neurodegeneration in Alzheimer's disease. *Acta Neuropathol.* 118, 475–485. doi: 10.1007/s00401-009-0556-6

Sturchler-Pierrat, C., Abramowski, D., Duke, M., Wiederhold, K. H., Mistl, C., Rothacher, S., et al. (1997). Two amyloid precursor protein transgenic mouse

models with Alzheimer disease-like pathology. *Proc. Natl. Acad. Sci. U.S.A.* 94, 13287–13292. doi: 10.1073/pnas.94.24.13287

Sun, X., He, G., and Song, W. (2006). BACE2, as a novel APP theta-secretase, is not responsible for the pathogenesis of Alzheimer's disease in Down syndrome. *FASEB J.* 20, 1369–1376. doi: 10.1096/fj.05-5632com

Sun, X., Wu, Y., Chen, B., Zhang, Z., Zhou, W., Tong, Y., et al. (2011). Regulator of calcineurin 1 (RCAN1) facilitates neuronal apoptosis through caspase-3 activation. *J. Biol. Chem.* 286, 9049–9062. doi: 10.1074/jbc.M110.177519

Sun, X., Wu, Y., Herculano, B., and Song, W. (2014). RCAN1 Overexpression exacerbates calcium overloading-induced neuronal apoptosis. *PLoS ONE* 9:e95471. doi: 10.1371/journal.pone.0095471

Szot, P., Van Dam, D., White, S. S., Franklin, A., Staufenbiel, M., and De Deyn, P. P. (2009). Age-dependent changes in noradrenergic locus coeruleus system in wild-type and APP23 transgenic mice. *Neurosci. Lett.* 463, 93–97. doi: 10.1016/j.neulet.2009.07.055

Takahashi, R. H., Milner, T. A., Li, F., Nam, E. E., Edgar, M. A., Yamaguchi, H., et al. (2002). Intraneuronal Alzheimer abeta42 accumulates in multivesicular bodies and is associated with synaptic pathology. *Am. J. Pathol.* 161, 1869–1879. doi: 10.1016/S0002-9440(10)64463-X

Takano, T., Han, X., Deane, R., Zlokovic, B., and Nedergaard, M. (2007). Two-photon imaging of astrocytic Ca2+ signaling and the microvasculature in experimental mice models of Alzheimer's disease. *Ann. N. Y. Acad. Sci.* 1097, 40–50. doi: 10.1196/annals.1379.004

Tansley, G. H., Burgess, B. L., Bryan, M. T., Su, Y., Hirsch-Reinshagen, V., Pearce, J., et al. (2007). The cholesterol transporter ABCG1 modulates the subcellular distribution and proteolytic processing of beta-amyloid precursor protein. *J. Lipid Res.* 48, 1022–1034. doi: 10.1194/jlr.M600542-JLR200

Tanzi, R. E. (2012). The genetics of Alzheimer disease. *Cold Spring Harb. Perspect. Med.* 2:a006296. doi: 10.1101/cshperspect.a006296

Thal, D. R., Rüb, U., Orantes, M., and Braak, H. (2002). Phases of A β-deposition in the human brain and its relevance for the development of AD. *Neurology* 58, 1791–1800. doi: 10.1212/WNL.58.12.1791

Tybulewicz, V. L. J., and Fisher, E. M. C. (2006). New techniques to understand chromosome dosage: mouse models of aneuploidy. *Hum. Mol. Genet.* 15, R103–R109. doi: 10.1093/hmg/ddl179

Tyrrell, J., Cosgrave, M., McCarron, M., McPherson, J., Calvert, J., Kelly, A., et al. (2001). Dementia in people with Down's syndrome. *Int. J. Geriatr. Psychiatry* 16, 1168–1174. doi: 10.1002/gps.502

Vacík, T., Ort, M., Gregorová, S., Strnad, P., Blatny, R., Conte, N., et al. (2005). Segmental trisomy of chromosome 17: a mouse model of human aneuploidy syndromes. *Proc. Natl. Acad. Sci. U.S.A.* 102, 4500–4505. doi: 10.1073/pnas.0500802102

Van Dam, D., D'Hooge, R., Staufenbiel, M., Van Ginneken, C., Van Meir, F., and De Deyn, P. P. (2003). Age-dependent cognitive decline in the APP23 model precedes amyloid deposition. *Eur. J. Neurosci.* 17, 388–396. doi: 10.1046/j.1460-9568.2003.02444.x

Van Dam, D., Marescau, B., Engelborghs, S., Cremers, T., Mulder, J., Staufenbiel, M., et al. (2005). Analysis of cholinergic markers, biogenic amines, and amino acids in the CNS of two APP overexpression mouse models. *Neurochem. Int.* 46, 409–422. doi: 10.1016/j.neuint.2004.11.005

Veerappan, C. S., Sleiman, S., and Coppola, G. (2013). Epigenetics of Alzheimer's disease and frontotemporal dementia. *Neurotherapeutics* 10, 709–721. doi: 10.1007/s13311-013-0219-0

Verret, L., Mann, E. O., Hang, G. B., Barth, A. M. I., Cobos, I., Ho, K., et al. (2012). Inhibitory interneuron deficit links altered network activity and cognitive dysfunction in Alzheimer model. *Cell* 149, 708–721. doi: 10.1016/j.cell.2012.02.046

Vilardell, M., Rasche, A., Thormann, A., Maschke-Dutz, E., Pérez-Jurado, L. A., Lehrach, H., et al. (2011). Meta-analysis of heterogeneous Down Syndrome data reveals consistent genome-wide dosage effects related to neurological processes. *BMC Genomics* 12:229. doi: 10.1186/1471-2164-12-229

Voronov, S. V., Frere, S. G., Giovedi, S., Pollina, E. A., Borel, C., Zhang, H., et al. (2008). Synaptojanin 1-linked phosphoinositide dyshomeostasis and cognitive deficits in mouse models of Down's syndrome. *Proc. Natl. Acad. Sci. U.S.A.* 105, 9415–9420. doi: 10.1073/pnas.0803756105

Vossel, K. A., Beagle, A. J., Rabinovici, G. D., Shu, H., Lee, S. E., Naasan, G., et al. (2013). Seizures and epileptiform activity in the early stages of Alzheimer disease. *JAMA Neurol.* 70, 1158–1166. doi: 10.1001/jamaneurol.2013.136

Wallin, A. K., Blennow, K., Andreasen, N., and Minthon, L. (2006). CSF biomarkers for Alzheimer's Disease: levels of beta-amyloid, tau, phosphorylated tau relate to clinical symptoms and survival. *Dement. Geriatr. Cogn. Disord.* 21, 131–138. doi: 10.1159/000090631

Wang, X., Huang, T., Zhao, Y., Zheng, Q., Thompson, R. C., Bu, G., et al. (2014). Sorting nexin 27 regulates Abeta production through modulating gamma-secretase activity. *Cell Rep.* 9, 1023–1033. doi: 10.1016/j.celrep.2014.09.037

Wang, X., Zhao, Y., Zhang, X., Badie, H., Zhou, Y., Mu, Y., et al. (2013). Loss of sorting nexin 27 contributes to excitatory synaptic dysfunction by modulating glutamate receptor recycling in Down's syndrome. *Nat. Med.* 19, 473–480. doi: 10.1038/nm.3117

Webster, S. J., Bachstetter, A. D., Nelson, P. T., Schmitt, F. A., and Van Eldik, L. J. (2014). Using mice to model Alzheimer's dementia: an overview of the clinical disease and the preclinical behavioral changes in 10 mouse models. *Front. Genet.* 5:88. doi: 10.3389/fgene.2014.00088

Wegiel, J., Dowjat, K., Kaczmarski, W., Kuchna, I., Nowicki, K., Frackowiak, J., et al. (2008). The role of overexpressed DYRK1A protein in the early onset of neurofibrillary degeneration in Down syndrome. *Acta Neuropathol.* 116, 391–407. doi: 10.1007/s00401-008-0419-6

Wegiel, J., Kaczmarski, W., Barua, M., Kuchna, I., Nowicki, K., Wang, K. C., et al. (2011). Link between DYRK1A overexpression and several-fold enhancement of neurofibrillary degeneration with 3-repeat tau protein in Down syndrome. *J. Neuropathol. Exp. Neurol.* 70, 36–50. doi: 10.1097/NEN.0b013e318202bfa1

Weintraub, S., Wicklund, A. H., and Salmon, D. P. (2012). The neuropsychological profile of Alzheimer disease. *Cold Spring Harb. Perspect. Med.* 2, a006171. doi: 10.1101/cshperspect.a006171

Westerman, M. A., Cooper-Blacketer, D., Mariash, A., Kotilinek, L., Kawarabayashi, T., Younkin, L. H., et al. (2002). The relationship between Abeta and memory in the Tg2576 mouse model of Alzheimer's disease. *J. Neurosci.* 22, 1858–1867.

Westmark, C. J., Westmark, P. R., and Malter, J. S. (2010). Alzheimer's disease and Down syndrome rodent models exhibit audiogenic seizures. *J. Alzheimer's Dis.* 20, 1009–1013. doi: 10.3233/JAD-2010-100087

Wilmot, B., McWeeney, S. K., Nixon, R. R., Montine, T. J., Laut, J., Harrington, C. A., et al. (2008). Translational gene mapping of cognitive decline. *Neurobiol. Aging* 29, 524–541. doi: 10.1016/j.neurobiolaging.2006.11.008

Wiseman, F. K., Al-Janabi, T., Hardy, J., Karmiloff-Smith, A., Nizetic, D., Tybulewicz, V. L. J., et al. (2015). A genetic cause of Alzheimer disease: mechanistic insights from Down syndrome. *Nat. Rev. Neurosci.* 16, 564–574. doi: 10.1038/nrn3983

Wisniewski, K. E., Wisniewski, H. M., and Wen, G. Y. (1985). Occurrence of neuropathological changes and dementia of Alzheimer's disease in Down's syndrome. *Ann. Neurol.* 17, 278–282. doi: 10.1002/ana.410170310

Witton, J., Padmashri, R., Zinyuk, L. E., Popov, V. I., Kraev, I., Line, S. J., et al. (2015). Hippocampal circuit dysfunction in the Tc1 mouse model of Down syndrome. *Nat. Neurosci.* 18, 1291–1298. doi: 10.1038/nn.4072

Wolvetang, E. J., Wilson, T. J., Sanij, E., Busciglio, J., Hatzistavrou, T., Seth, A., et al. (2003a). ETS2 overexpression in transgenic models and in Down syndrome predisposes to apoptosis via the p53 pathway. *Hum. Mol. Genet.* 12, 247–255. doi: 10.1093/hmg/ddg015

Wolvetang, E. W., Bradfield, O. M., Tymms, M., Zavarsek, S., Hatzistavrou, T., Kola, I., et al. (2003b). The chromosome 21 transcription factor ETS2 transactivates the beta-APP promoter: implications for Down syndrome. *Biochim. Biophys. Acta* 1628, 105–110. doi: 10.1016/S0167-4781(03)00121-0

Wu, J., and Morris, J. K. (2013). The population prevalence of Down's syndrome in England and Wales in 2011. *Eur. J. Hum. Genet.* 21, 1016–1019. doi: 10.1038/ejhg.2012.294

Xue, Q.-S., and Streit, W. J. (2011). Microglial pathology in Down syndrome. *Acta Neuropathol.* 122, 455–466. doi: 10.1007/s00401-011-0864-5

Yang, Q., Rasmussen, S. A., and Friedman, J. M. (2002). Mortality associated with Down's syndrome in the USA from 1983 to 1997: a population-based study. *Lancet* 359, 1019–1025. doi: 10.1016/S0140-6736(02)08092-3

Ye, X., Tai, W., and Zhang, D. (2012). The early events of Alzheimer's disease pathology: from mitochondrial dysfunction to BDNF axonal transport deficits. *Neurobiol. Aging* 33, e1–e10. doi: 10.1016/j.neurobiolaging.2011.11.004

Yu, T., Liu, C., Belichenko, P., Clapcote, S. J., Li, S., Pao, A., et al. (2010b). Effects of individual segmental trisomies of human chromosome

21 syntenic regions on hippocampal long-term potentiation and cognitive behaviors in mice. *Brain Res.* 1366, 162–171. doi: 10.1016/j.brainres.2010.09.107

Yu, T., Li, Z., Jia, Z., Clapcote, S. J., Liu, C., Li, S., et al. (2010a). A mouse model of Down syndrome trisomic for all human chromosome 21 syntenic regions. *Hum. Mol. Genet.* 19, 2780–2791. doi: 10.1093/hmg/ddq179

Zarow, C., Lyness, S. A., Mortimer, J. A., and Chui, H. C. (2003). Neuronal Loss Is Greater in the Locus Coeruleus Than Nucleus Basalis and Substantia Nigra in Alzheimer and Parkinson Diseases. *Arch. Neurol.* 60, 337. doi: 10.1001/archneur.60.3.337

Zhang, K., Schrag, M., Crofton, A., Trivedi, R., Vinters, H., and Kirsch, W. (2012a). Targeted proteomics for quantification of histone acetylation in Alzheimer's disease. *Proteomics* 12, 1261–1268. doi: 10.1002/pmic.201200010

Zhang, L., Fu, D., Belichenko, P. V., Liu, C., Kleschevnikov, A. M., Pao, A., et al. (2012b). Genetic analysis of Down syndrome facilitated by mouse chromosome engineering. *Bioeng. Bugs* 3, 8–12. doi: 10.4161/bbug.3.1.17696

Zhang, Y. Q., and Sarge, K. D. (2008). Sumoylation of amyloid precursor protein negatively regulates Abeta aggregate levels. *Biochem. Biophys. Res. Commun.* 374, 673–678. doi: 10.1016/j.bbrc.2008.07.109

Zigman, W. B. (2013). Atypical aging in Down syndrome. *Dev. Disabil. Res. Rev.* 18, 51–67. doi: 10.1002/ddrr.1128

Zis, P., Dickinson, M., Shende, S., Walker, Z., and Strydom, A. (2012). Oxidative stress and memory decline in adults with Down syndrome: longitudinal study. *J. Alzheimer's Dis.* 31, 277–283. doi: 10.3233/JAD-2012-120073

Conflict of Interest Statement: The authors declare that the research was conducted in the absence of any commercial or financial relationships that could be construed as a potential conflict of interest.